NRL Report 6409

Systematic Errors in Ultrasonic Propagation Parameter Measurements

Part 3 - Sound Speed by Iterative Reflection-Interferometry

V. A. Del Grosso

Propagation Branch
Sound Division

August 9, 1966

NAVAL RESEARCH LABORATORY
Washington, D.C.

DISTRIBUTION OF THIS REPORT IS UNLIMITED

PREVIOUS REPORTS IN THIS SERIES

"Part 1 – Effect of Free-Field Diffraction," V. A. Del Grosso, NRL Report 6026, Jan. 1964.

"Part 2 – Effects of Guided Cylindrical Modes," V. A. Del Grosso, NRL Report 6133, Jan. 1965.

CONTENTS

Abstract 1
Problem Status 1
Authorization 1

INTRODUCTION 1

FORMULATION OF ITERATIVE REFLECTION 2

INTRODUCTION OF ATTENUATION IN FLUID 7

DEGENERATE CASE OF PLANE WAVES 8

PROCEDURE FOR NONORTHOGONAL MODES 11

EQUATIONS FOR CALCULATION OF MODES 19

STANDARD REFERENCE PARAMETERS 21

ORTHOGONALITY CHECKS 21

PLANE WAVE RESULTS AND DISCUSSION 22

DIFFRACTED WAVE
Results 38
Discussion 39

APPARENT SOUND SPEEDS 43

CONCLUSIONS 43

FUTURE WORK 44

ACKNOWLEDGMENTS 45

REFERENCES 45

FIGURES 16 – 37 47

TABLES 2 – 82 164

Systematic Errors in Ultrasonic Propagation Parameter Measurement

Part 3 – Sound Speed by Iterative Reflection – Interferometry

This report shows, that, although the free-field diffraction and guided mode dispersion errors detailed in Parts 1 and 2 of this series do carry over to the case of iterative reflection (accomplished by adding a termination to the liquid cylinder), the errors for a given geometrical configuration are smaller for interferometry than for nonterminated or pulsing situations. Indeed, the approach with improved parameters is toward plane wave results for interferometry rather than toward free-field results as is the case for pulsing.

Other advantages accruing to interferometry are (a) the use of differential instead of total, acoustic paths, (b) the simplified determination of these paths by the use of parallel source and reflector, (c) the simple measurement of frequency rather than small time intervals, and (d) the suitability of the method for determinations of chemical concentration (salinity) and pressure coefficients, as well as the temperature coefficient.

This report includes many impedance circle plots as well as the more usual reaction plots for ultrasonic interferometers with walls that are either infinitely flexible, absolutely rigid, liquid, or elastic. Various parameters including tube size, source size, source-to-reflector separation, frequency, and attenuation coefficients are included along with several imposed characteristics. The plot readings, and apparent sound speeds calculated from them, are tabulated. Errors may be as large as a few percent or as small as 6 parts per million (0.01 m/s).

INTRODUCTION

Earlier reports in this series were concerned with the effects of free-field diffraction from a piston source (1) and the effects of guided mode propagation along cylinders (2). These reports demonstrated that appreciable errors in both sound speed and sound absorption can be attributed to the neglect of these effects. It was also indicated that for nonterminated situations or those for which one can utilize time separation of responses (as in some pulsing methods), piston sources with a radius a of 10 wavelengths (corresponding to $ka = 20\pi$ where $\kappa = 2\pi/\lambda_1$) result in almost identical plots up to $z\lambda_1/a^2 = 10$ for the respective magnitudes and phases relative to plane wave values. This is true irrespective of whether the lateral boundary conditions are those pertinent to a cylindrical enclosure with absolutely rigid walls, infinitely flexible walls, liquid walls, or elastic solid walls, provided that the ratio of the fluid cylinder radius b to the crystal radius a is greater than 2. For $b/a \geq 10$, all boundary conditions considered coincided with the free-field calculations for the same piston up to a range of $z\lambda_1/a^2 = 10$ where z is the distance from the piston measured perpendicular to its face. The impossibility of obtaining uniform piston motion when $b/a = 1$ was noted, and the ineptness of such a choice was indicated by both the drastic changes for absolutely rigid boundary conditions when this ratio is slightly greater than unity, and the larger anomalies at $b/a = 1$ for the more realistic consideration of elastic solid boundary conditions.

A much earlier report (3) indicated that a deliberate attempt to destroy cylindrical symmetry could in fact result in close approximation to the conditions of free-field propagation for continuous waves in a terminated enclosure. But the experimental finding also indicated that although the anomalies could be found at predicted distances, they were damped appreciably and the final result closely approximated a plane wave. (Also see Ref. 1.)

This report adds to the two earlier ones in this series a termination to the liquid cylinder. The references contained in the first three references herein are considered to comprise a comprehensive introduction to ultrasonic interferometry.

The procedure utilized in this report will be to discuss the interferometer situation from the standpoint of the formulation pertinent to propagation in a right-circular cylindrical cavity, that is, from the standpoint of guided cylinder modes. Free-field conditions can then be approached

NRL Problem S01–02; Project RF 101–03–45–5251. This is an interim report on the problem; work is continuing. Manuscript submitted March 16, 1966.

by letting the tube diameter b increase without limit (proceeding from the Fourier series of the discrete set to the Fourier integral of the continuum).

FORMULATION OF ITERATIVE REFLECTION

The configuration we assume is again a right-circular cylinder of fluid I (see Fig. 1) of finite radius b and length ℓ, terminated at one end by a piston transducer of radius a ($< b$) which is set in an infinite baffle, and closed at the other end by a plane-parallel reflector III of radius b and extending to ∞ for $z > \ell$. Both source and reflector are centered on and normal to the cylinder axis. The cylinder of fluid is otherwise enclosed by another medium II.

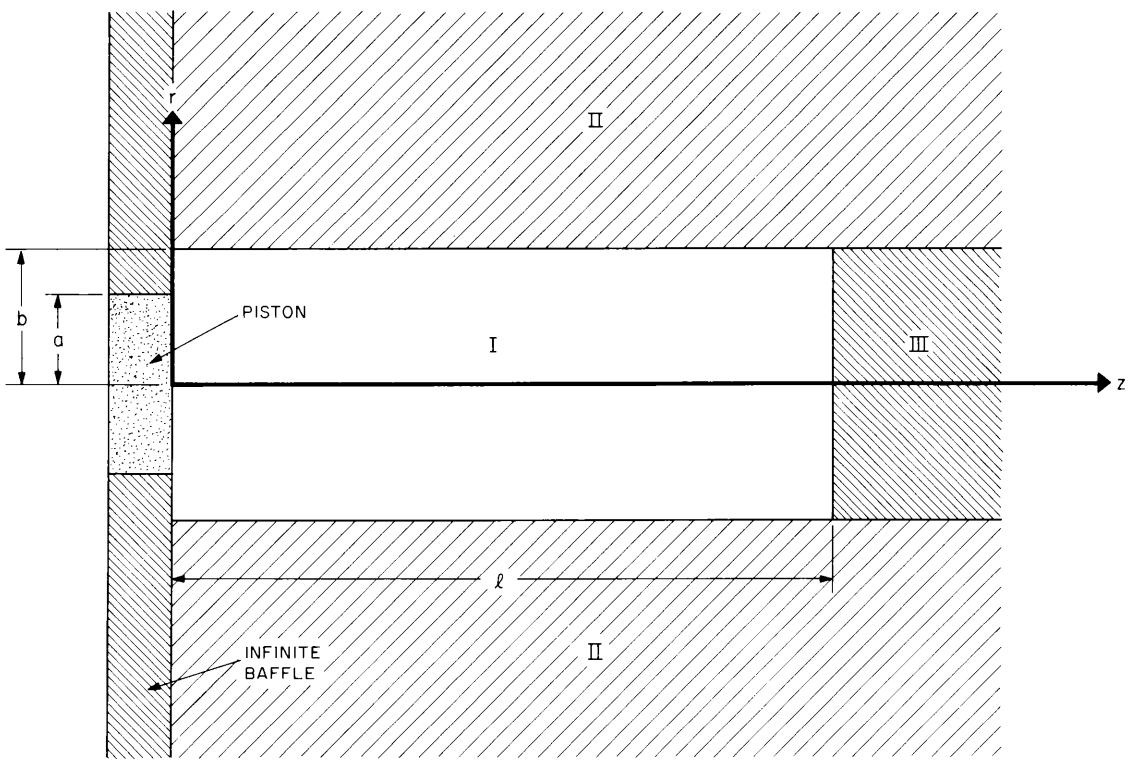

Fig. 1 — A right-circular, cylindrical cavity of liquid medium I capped on one end by a driving source of radius a in a baffle and on the other end by a reflector medium III of cavity radius b. The cylindrical cavity is otherwise surrounded by a medium II

Separating the harmonic time dependence from the ordinary wave equation

$$\nabla^2 \Psi + \frac{1}{c^2} \frac{\partial^2 \Psi}{\partial t^2} = 0, \tag{1}$$

where $\Psi = \Psi(r, \theta, z, t)$, yields the time-independent Helmholtz equation

$$\nabla^2 \varphi + k^2 \varphi = 0, \tag{2}$$

where $\phi = \phi(r, \theta, z)$. The solution of Eq. (2), for both incoming and outgoing waves, is given by

$$\varphi_{nm} = \left(C_{nm} \cos n\theta + D_{nm} \sin n\theta\right) \times \left(G_{nm} \mathcal{J}_n\left(r\sqrt{k^2 - q_{nm}^2}\right)\right) \times \left(E_{nm} e^{iq_{nm} z} + F_{nm} e^{-iq_{nm} z}\right). \tag{3}$$

Invoking circular (axial) symmetry restricts n to 0, whereby

$$\begin{aligned} \varphi_{0m} &= C_{0m} G_{0m} \mathcal{J}_0\left(r\sqrt{k^2 - q_{0m}^2}\right)\left(E_{0m} e^{iq_{0m} z} + F_{0m} e^{-iq_{0m} z}\right) \\ &= \mathcal{J}_0\left(r\sqrt{k^2 - q_{0m}^2}\right)\left(K_{0m} e^{iq_{0m} z} + L_{0m} e^{-iq_{0m} z}\right) \end{aligned} \tag{4}$$

The characteristic value

$$X_{0m} \equiv b\sqrt{k^2 - q_{0m}^2} \tag{5}$$

is determined by the characteristic equation appropriate to a given lateral boundary condition; from Eq. (5), we obtain

$$q_{0m} = \sqrt{k^2 - \left(\frac{X_{0m}}{b}\right)^2}. \tag{6}$$

We again assume that the time-independent field inside the cylinder may be expanded in terms of the natural modes φ_{0m} as

$$\varphi(r, z) = \sum_m \mathcal{J}_0\left(r\frac{X_{0m}}{b}\right)\left(K_{0m} e^{iq_{0m} z} + L_{0m} e^{-iq_{0m} z}\right) \tag{7}$$

where, as justified in Ref. (2) for all boundary conditions considered herein, we consider the φ_{0m} to form a complete orthogonal set.*

At $z = 0$ we have

$$\varphi(r, 0) = \sum_m \mathcal{J}_0\left(r\frac{X_{0m}}{b}\right)\left(K_{0m} + L_{0m}\right) \tag{8}$$

and, invoking orthogonality,*

$$\sum_m \left(K_{0m} + L_{0m}\right)\frac{b^2}{2}\left[\mathcal{J}_0^2\left(X_{0m}\right) + \mathcal{J}_1^2\left(X_{0m}\right)\right] = \int_0^b \varphi(r, 0)\, \mathcal{J}_0\left(r\frac{X_{0m}}{b}\right) r dr. \tag{9}$$

For a piston vibrator of radius $a < b$, the function $\varphi(r, 0) \to \varphi_0$ (a constant), and the limits of the integral are from 0 to a (rather than b). Then

$$K_{0m} + L_{0m} = \frac{2a\, \varphi_0\, \mathcal{J}_1\left(X_{0m}\frac{a}{b}\right)}{b\, X_{0m}\left[\mathcal{J}_0^2\left(X_{0m}\right) + \mathcal{J}_1^2\left(X_{0m}\right)\right]}. \tag{10}$$

* This restriction is later removed and is in fact valid only for $b/a \geq 2$. (See section on "Procedure for Nonorthogonal Modes.")

To calculate the impedance at the reflector end we restore the time dependence ($e^{-i\omega t}$ for outward-going waves)

$$\varphi_{0m}(r, z, t) = \mathcal{J}_0\left(r\frac{X_{0m}}{b}\right)\left(K_{0m}e^{i(q_{0m}z - \omega t)} + L_{0m}e^{i(-q_{0m}z - \omega t)}\right) \tag{11}$$

and, using the relation for the pressure p given by

$$p = -\rho\,\frac{\partial\varphi}{\partial t},$$

we obtain

$$p_{0m}(z) = P\left(K_{0m}e^{iq_{0m}z} + L_{0m}e^{-iq_{0m}z}\right)\left(= i\omega\rho_1\phi_{0m}\right) \tag{12}$$

where

$$P \equiv i\omega\rho_1\,\mathcal{J}_0\left(r\,\frac{X_{0m}}{b}\right)e^{-i\omega t} \tag{13}$$

and ρ_1 is the density in medium I. Similarly, from the relation for the particle velocity u in the z direction, given by

$$u(z) = \partial\varphi/\partial z,$$

we obtain

$$u_{0m}(z) = \frac{q_{0m}P}{\omega\rho_1}\left(K_{0m}e^{iq_{0m}z} - L_{0m}e^{-iq_{0m}z}\right) \tag{14}$$

with P defined as previously.

Now, the impedance in the z direction is defined as

$$\mathrm{Imp}(z) = \frac{p}{u(z)},$$

and we shall denote the impedance of the reflector material as $\rho_3 C_3$ where ρ_3 is the density and C_3 the wave velocity associated with the reflector (medium III). So,

$$[\mathrm{Imp}(z)]_{z=\ell} = \rho_3 C_3$$

and

$$\rho_3 C_3 = \frac{\omega\rho_1}{q_{0m}}\left(\frac{K_{0m}e^{iq_{0m}\ell} + L_{0m}e^{-iq_{0m}\ell}}{K_{0m}e^{iq_{0m}\ell} - L_{0m}e^{-iq_{0m}\ell}}\right), \tag{15}$$

which can be directly transformed to

$$K_{0m}\left(1 + \frac{q_{0m}\rho_3 C_3}{k_1\ \rho_1 C_1}\right)e^{iq_{0m}\ell} + L_{0m}\left(1 - \frac{q_{0m}\rho_3 C_3}{k_1\ \rho_1 C_1}\right)e^{iq_{0m}\ell} = 0. \tag{16}$$

Considering the source as a receiver ($r = a$), the average time-independent velocity potential becomes

$$\langle \varphi \rangle = \frac{1}{\pi a^2} \int_0^a \varphi(r, z)\, 2\pi\, r dr, \tag{17}$$

and utilizing Eq. (7) we obtain, after some manipulation,

$$\langle \varphi \rangle = \sum_m \left(K_{0m} e^{iq_{0m} z} + L_{0m} e^{-iq_{0m} z} \right) \frac{2\mathcal{J}_1\left(X_{0m} \frac{a}{b}\right)}{\left(X_{0m} \frac{a}{b}\right)}. \tag{18}$$

From $p = -\rho\, (\partial \varphi / \partial t) = i\rho\omega\, \varphi$ we have

$$\langle p \rangle_0 = i\rho\omega \sum_m \left(K_{0m} + L_{0m} \right) \frac{2\mathcal{J}_1\left(X_{0m} \frac{a}{b}\right)}{\left(X_{0m} \frac{a}{b}\right)}. \tag{19}$$

Similarly, from $u = \partial \varphi / \partial z$ we could write

$$\langle u \rangle_{z=0} = \left[\frac{\partial \langle \varphi \rangle}{\partial z} \right]_{z=0}$$

and obtain from Eq. (18)

$$\langle u \rangle_0 = \sum_m iq_{0m} \left(K_{0m} - L_{0m} \right) \frac{2\mathcal{J}_1\left(X_{0m} \frac{a}{b}\right)}{\left(X_{0m} \frac{a}{b}\right)}. \tag{20}$$

However, we *do not* use Eq. (20) to calculate the impedance at the crystal but rather use the nonaveraged U_0 at source ($z = 0$) as a piston, that is,

$$\left(\frac{\partial \varphi}{\partial z} \right)_{z=0} = U_0 \text{ (a constant)},$$

which leads directly, invoking orthogonality,* to

$$K_{0m} - L_{0m} = \frac{2iU_0\, a\mathcal{J}_1\left(X_{0m} \frac{a}{b}\right)}{b\, q_{0m}\, X_{0m} \left[\mathcal{J}_0^2 (X_{0m}) + \mathcal{J}_1^2 (X_{0m}) \right]}. \tag{21}$$

*See preceding footnote.

The radiation impedance of the crystal is defined as the quotient of the force exerted by the piston on the medium (negative of the force exerted by the medium on the crystal) to the velocity of the piston or

$$\frac{\langle p \rangle_0}{U_0} \equiv Z_0 \tag{22}$$

Thus,

$$Z_0 = -\rho\omega \sum_m \frac{1}{q_{0m}} \frac{(K_{0m} + L_{0m})\, 4\mathcal{J}_1^2\left(X_{0m}\frac{a}{b}\right)}{(K_{0m} - L_{0m})\, X_{0m}^2 \left[\mathcal{J}_0^2(X_{0m}) + \mathcal{J}_1^2(X_{0m})\right]} . \tag{23}$$

We may rewrite Eq. (16) by defining

$$A \equiv \frac{q_{0m}}{k_1} \frac{\rho_3 C_3}{\rho_1 C_1} \tag{24}$$

so

$$K_{0m} = \frac{(A-1)\, e^{-iq_{0m}\ell}}{(A+1)\, e^{iq_{0m}\ell}} L_{0m} \tag{25}$$

and

$$\frac{K_{0m} + L_{0m}}{K_{0m} - L_{0m}} = \frac{e^{-iq_{0m}\ell} - \left(\frac{1+A}{1-A}\right) e^{iq_{0m}\ell}}{e^{-iq_{0m}\ell} + \left(\frac{1+A}{1-A}\right) e^{iq_{0m}\ell}} . \tag{26}$$

By further defining

$$\frac{1+A}{1-A} \equiv S_{0m}, \tag{27}$$

we obtain

$$Z_0 = -\rho\omega \sum_m \frac{4\mathcal{J}_1^2\left(X_{0m}\frac{a}{b}\right)\left[\frac{e^{-iq_{0m}\ell} - S_{0m}\, e^{iq_{0m}\ell}}{e^{-iq_{0m}\ell} + S_{0m}\, e^{iq_{0m}\ell}}\right]}{q_{0m}\, X_{0m}^2 \left[\mathcal{J}_0^2(X_{0m}) + \mathcal{J}_1^2(X_{0m})\right]} \tag{28}$$

We note that it may be easily shown that

$$\sum_{m=0}^{\infty} \frac{4\mathcal{J}_1^2\left(X_{0m}\frac{a}{b}\right)}{X_{0m}^2 \left[\mathcal{J}_0^2(X_{0m}) + \mathcal{J}_1^2(X_{0m})\right]} \equiv 1, \tag{29}$$

but we also note from p. 8 of Ref. 2 that m is summed, at most, to $X_{0m} \leq kb$. For this case, Eq. (29) is not equal to 1.

If we now define

$$\theta \equiv \coth^{-1} A \tag{30}$$

we find that

$$S_{0m} = \frac{1 + \coth\theta}{1 - \coth\theta} = -e^{2\theta}, \tag{31}$$

and finally

$$Z_0 = \sum_m \frac{\rho_1 C_1 k_1 \, 4\mathcal{J}_1^2\left(X_{0m}\dfrac{a}{b}\right)}{q_{0m} X_{0m}^2 \left[\mathcal{J}_0^2\left(X_{0m}\right) + \mathcal{J}_1^2\left(X_{0m}\right)\right]} \coth\left(iq_{0m}\ell + \theta\right) \tag{32}$$

which is in the form

$$Z_0 = z \coth\left(iq_{0m}\ell + \theta\right) \tag{33}$$

used, for example, on p. 14 of Ref. 3.

INTRODUCTION OF ATTENUATION IN FLUID

As mentioned earlier, the X_{0m} are the characteristic values determined from the characteristic equations appropriate to given lateral boundary conditions. As detailed in Ref. 2, the X_{0m} are taken to be pure real numbers, even when a complex propagation number is introduced. Thus the characteristic values themselves are not modified by attenuation, and the effect is restricted to propagation in the modes. We recall that there is no approximation involved in this procedure for the limiting boundary conditions of absolutely rigid and infinitely flexible walls. In this report then, we also introduce absorption by letting*

$$\begin{aligned}
C_1 \to C_1^\star &= \frac{C_{00}}{1 - i\dfrac{\alpha_{00}}{k_{00}}} \\
k_1 \to k_1^\star &= k_{00} - i\alpha_{00} \\
q_{0m} \to q_{0m}^\star &= q_{0m}^M - i\alpha_{0m} \\
\theta \to \theta^\star &= \coth^{-1}\frac{\rho_3 C_3^\star q_{0m}^\star}{\rho_1 C_1^\star k_1^\star} = \coth^{-1}\frac{k_3\rho_3 C_3\left(q_{0m}^M - i\alpha_{0m}\right)}{k_{00}\rho_1 C_{00}\left(k_3 - i\alpha_3\right)} \\
&= \coth^{-1}\frac{\rho_3\left(q_{0m}^M - i\alpha_{0m}\right)}{\rho_1\left(k_3 - i\alpha_3\right)}.
\end{aligned} \tag{34}$$

*This notation follows that in the earlier reports in that the star superscript refers only to a complex value of a previously real number.

We find as before (2) that

$$\alpha_{0m} = \frac{\alpha_{00}\, k_{00}}{q_{0m}^{M}} \tag{35}$$

and

$$2\left(q_{0m}^{M}\right)^2 = k_{00}^2 - \alpha_{00}^2 - \left(\frac{X_{0m}}{b}\right)^2 + \left[\begin{array}{l} \left(\frac{X_{0m}}{b}\right)^4 + k_{00}^4 + \alpha_{00}^4 \\ + 2k_{00}^2\ \alpha_{00}^2 \\ + 2\left(\frac{X_{0m}}{b}\right)^2\ \alpha_{00}^2 \\ - 2\left(\frac{X_{0m}}{b}\right)^2\ k_{00}^2 \end{array}\right]^{1/2} \tag{36}$$

Equation (32) may then be written as

$$Z_0 = \sum_m \frac{k_{00}\rho_1 C_{00}\left(q_{0m}^{M} + i\,\frac{\alpha_{00}k_{00}}{q_{0m}^{M}}\right) 4\mathcal{J}_1^2\left(X_{0m}\,\frac{a}{b}\right)}{\left[\left(q_{0m}^{M}\right)^2 + \frac{\alpha_{00}^2 k_{00}^2}{\left(q_{0m}^{M}\right)^2}\right] X_{0m}^2\left[\mathcal{J}_0^2\left(X_{0m}\right) + \mathcal{J}_1^2\left(X_{0m}\right)\right]} \times \coth\left[i q_{0m}^{M}\ell + \frac{\alpha_{00}k_{00}}{q_{0m}^{M}} + \coth^{-1}(u+iv)\right] \tag{37}$$

where $\coth^{-1}(u+iv) \equiv \theta^{\star}$.

DEGENERATE CASE OF PLANE WAVES

Equation (32) may be written as

$$Z_0 = Z \coth\left(i q_{0m}\ell + \theta\right) \tag{38}$$

where

$$Z = \sum_m \frac{\rho_1 C_1 k_1\ 4\mathcal{J}_1^2\left(X_{0m}\,\frac{a}{b}\right)}{q_{0m} X_{0m}^2\left[\mathcal{J}_0^2\left(X_{0m}\right) + \mathcal{J}_1^2\left(X_{0m}\right)\right]}$$

and

$$\theta \equiv \coth^{-1}\frac{\rho_3 C_3}{\rho_1 C_1}\ \frac{q_{0m}}{k_1}$$

with

$$X_{0m} \equiv b\sqrt{k^2 - q_{0m}^2}.$$

We could also write

$$\coth(iq_{0m}\ell+\theta) = \frac{\sinh 2\theta - i\sin 2q_{0m}\ell}{\cosh 2\theta - \cos 2q_{0m}\ell}. \tag{39}$$

For plane waves only, we note that

$$q_{0m} \to k_{00} \quad \text{and} \quad X_{0m} \to 0,$$

so we find directly that

$$Z_{0P} = \rho_1 C_1 \coth(ik\ell+\theta') \tag{40}$$

with

$$\theta' \equiv \coth^{-1}\frac{\rho_3 C_3}{\rho_1 C_1},$$

and we could then write

$$\frac{Z_{0P}}{\rho_1 C_1} = \frac{\sinh 2\theta' - i\sin 2k\ell}{\cosh 2\theta' - \cos 2k\ell} \tag{41}$$

for plane waves in a medium with no attenuation. We note that $Z_{0P}/\rho_1 C_1$ is real when either

$$2k\ell = (2n-1)\pi \tag{42a}$$

or

$$2k\ell = 2n\pi. \tag{43a}$$

Equation (42a) signifies the minimum R since, for this case,

$$\frac{Z_{0P}}{\rho_1 C_1} \to \frac{R_{0P}}{\rho_1 C_1} \tag{42b}$$

for

$$\ell = \left(n - \frac{1}{2}\right)\frac{\lambda_1}{2} \tag{42c}$$

and

$$\frac{R_{0P}}{\rho_1 C_1} = \frac{\sinh 2\theta'}{\cosh 2\theta' + 1} = \tanh\theta' = \frac{\rho_1 C_1}{\rho_3 C_3}. \tag{42d}$$

Equation (43a) implies the maximum R since then

$$\frac{Z_{0P}}{\rho_1 C_1} \to \frac{R_{0P}}{\rho_1 C_1} \tag{43b}$$

for

$$\ell = \frac{n\lambda_1}{2} \tag{43c}$$

and

$$\frac{R_{0P}}{\rho_1 C_1} = \coth \theta' = \frac{\rho_3 C_3}{\rho_1 C_1}. \tag{43d}$$

We thus note that for plane waves in a nonabsorbing medium both max R and min R coincide with zero X (reactance) and are thus points of zero phase.

To allow for intrinsic absorption of plane waves by the medium, we find that the appropriate equations are modified to

$$\frac{Z_{0P}}{\rho_1 C_1} = \frac{k_{00}}{k_{00} - i\alpha_{00}} \coth \left[i\left(k_{00} - i\alpha_{00}\right)\ell + \theta'^{\star} \right] \tag{44}$$

where

$$\theta'^{\star} \equiv \coth^{-1} \frac{\rho_3 C_3 k_3 \left(k_1 - i\alpha_1\right)}{\rho_1 C_1 k_1 \left(k_3 - i\alpha_3\right)} = \coth^{-1} \frac{\rho_3 \left(k_1 - i\alpha_1\right)}{\rho_1 \left(k_3 - i\alpha_3\right)}$$

$$= \coth^{-1} \left[U' + iV'\right] \equiv D' + iE'.$$

So we may write

$$\frac{Z_{0P}}{\rho_1 C_1} = \left(\frac{k}{k - i\alpha}\right) \frac{\sinh 2\left(D' + \alpha\ell\right) - i \sin 2\left(k\ell - E'\right)}{\cosh 2\left(D' + \alpha\ell\right) - \cos 2\left(k\ell - E'\right)}. \tag{45}$$

We note that, if $\alpha \ll k$,

$$\frac{Z_{0P}}{\rho_1 C_1} = \frac{\sinh 2\left(D' + \alpha\ell\right) - i \sin 2\left(k\ell - E'\right)}{\cosh 2\left(D' + \alpha\ell\right) - \cos 2\left(k\ell - E'\right)}. \tag{46}$$

Again we note that $Z_{0P}/\rho_1 C_1$ is real for either

$$2k\ell - 2E' = (2n - 1)\pi \tag{47a}$$

or

$$2k\ell - 2E' = 2n\pi. \tag{48a}$$

Equation (47a) implies, for

$$\ell = \left(n - \frac{1}{2}\right)\frac{\lambda_1}{2} + \frac{E'}{k}, \tag{47b}$$

that

$$\frac{Z_{0P}}{\rho_1 C_1} \to \frac{R_{0P}}{\rho_1 C_1} = \tanh\left(D' + \alpha\ell\right) \tag{47c}$$

which corresponds to the minimum R. Similarly, Eq. (48a) implies, for

$$\ell = \frac{n\lambda_1}{2} + \frac{E'}{k}, \tag{48b}$$

that

$$\frac{Z_{0P}}{\rho_1 C_1} \to \frac{R_{0P}}{\rho_1 C_1} = \coth\left(D' + \alpha\ell\right) \tag{48c}$$

which corresponds to the maximum R.

So we note even with an attenuating medium that both max R and min R occur very close to points of zero phase for the plane wave case.

PROCEDURE FOR NONORTHOGONAL MODES

Equation (21) was obtained by invoking orthogonality in the usual manner. In a previous report (2) we found that the modes for liquid and elastic solid boundary conditions were nonorthogonal but that the errors attributable to the erroneous (but simplifying) assumption of orthogonality were insignificant in the nonterminated situation, except for $b \simeq a$ (and then only for elastic solid walls). We will now detail the procedure and the resulting formulation so that we may calculate results both ways for this reflection situation and determine where, and indeed whether, the orthogonal simplification may be used.

Again using

$$\left(\frac{\partial\varphi}{\partial z}\right)_{z=0} = U_0 \text{ (a constant)}$$

with Eq. (7), we obtain, after multiplying by

$$r\mathcal{J}_0\left(r\frac{X_{0\ell}}{b}\right)$$

and integrating with respect to r over the limits 0 to b,

$$\int_0^b \sum_m iq_{0m}\left(K_{0m} - L_{0m}\right)\mathcal{J}_0\left(r\frac{X_{0m}}{b}\right)\mathcal{J}_0\left(r\frac{X_{0\ell}}{b}\right)rdr = \int_0^b U_0\,\mathcal{J}_0\left(r\frac{X_{0\ell}}{b}\right)rdr. \tag{49}$$

Since U_0 extends only to a, the right-hand side of Eq. (49) becomes

$$\text{right-hand side} = U_0 \, \mathcal{J}_1\left(X_{0\ell} \frac{a}{b}\right) \frac{ba}{X_{0\ell}}. \tag{50}$$

Here we simplify the notation by defining

$$R_{nm} \equiv \mathcal{J}_n\left(r \frac{X_{0m}}{b}\right) \tag{51}$$

and obtain

$$U_0 \frac{ab}{X_{0\ell}} \mathcal{J}_1\left(X_{0\ell} \frac{a}{b}\right) = \int_0^b \sum_m iq_{0m} \left(K_{0m} - L_{0m}\right) R_{0m} R_{0\ell} \, rdr \tag{52}$$

which expands to

$$U_0 \frac{ab}{X_{01}} \mathcal{J}_1\left(X_{01} \frac{a}{b}\right) = iq_{01}\left(K_{01} - L_{01}\right)\int_0^b R_{01}^2 \, rdr + iq_{02}\left[K_{02} - L_{02}\right] \int_0^b R_{02} R_{01} \, rdr$$

$$+ iq_{03}\left(K_{03} - L_{03}\right) \int_0^b R_{03} R_{01} \, rdr + \cdots$$

$$U_0 \frac{ab}{X_{02}} \mathcal{J}_1\left(X_{02} \frac{a}{b}\right) = iq_{01}\left(K_{01} - L_{01}\right) \int_0^b R_{01} R_{02} \, rdr + iq_{02}\left(K_{02} - L_{02}\right) \int_0^b R_{02}^2 \, rdr$$

$$+ iq_{03}\left(K_{03} - L_{03}\right)\int_0^b R_{03} R_{02} \, rdr + \cdots$$

$$U_0 \frac{ab}{X_{03}} \mathcal{J}_1\left(X_{03} \frac{a}{b}\right) = iq_{01}\left(K_{01} - L_{01}\right) \int_0^b R_{01} R_{03} \, rdr + iq_{02}\left(K_{02} - L_{02}\right) \int_0^b R_{02} R_{03} \, rdr$$

$$+ iq_{03}\left(K_{03} - L_{03}\right) \int_0^b R_{03}^2 \, \mathrm{rdr} + \cdots \tag{53}$$

We recall that

$$\int_0^b R_{0m}^2 \, rdr = \frac{b^2}{2}\left[\mathcal{J}_0^2\left(X_{0m}\right) + \mathcal{J}_1^2\left(X_{0m}\right)\right] \tag{54}$$

and

$$iq_{0m}\left(K_{0m}-L_{0m}\right)\int_a^b \mathcal{J}_0\left(r\frac{X_{0m}}{b}\right)\mathcal{J}_0\left(r\frac{X_{0\ell}}{b}\right)rdr$$

$$= iq_{0m}\left(K_{0m}-L_{0m}\right)\left(\frac{b^2}{X_{0\ell}^2-X_{0m}^2}\right)\left[\begin{array}{l} X_{0\ell}\,\mathcal{J}_0\left(X_{0m}\right)\,\mathcal{J}_1\left(X_{0\ell}\right) \\ -X_{0m}\,\mathcal{J}_0\left(X_{0\ell}\right)\,\mathcal{J}_1\left(X_{0m}\right)\end{array}\right] \tag{55}$$

and we solve this finite set of simultaneous equations (m is summed up to $X_{0m} \leq kb$) for the various $K_{0m}-L_{0m}$. We note that, for example,

$$K_{01}-L_{01} = N_1U_0$$

$$K_{02}-L_{02} = N_2U_0 \quad \text{etc,}$$

and

$$\sum_m \frac{K_{0m}-L_{0m}}{N_m} = U_0 \tag{56}$$

where the N_m are numerical constants, so we may, combining this with Eq. (19), write

$$\frac{\langle p\rangle_0}{U_0} \equiv Z_0 = i\omega\rho\sum_m\left(\frac{K_{0m}+L_{0m}}{K_{0m}-L_{0m}}\right)\frac{2\mathcal{J}_1\left(X_{0m}\frac{a}{b}\right)}{X_{0m}\frac{a}{b}}N_m. \tag{57}$$

Relating this to the previous orthogonal form, we find that

$$N_m \xrightarrow[\text{(for orthogonality)}]{} \frac{-2ia\,\mathcal{J}_1\left(X_{0m}\frac{a}{b}\right)}{bq_{0m}X_{0m}\left[\mathcal{J}_0^2\left(X_{0m}\right)+\mathcal{J}_1^2\left(X_{0m}\right)\right]}. \tag{58}$$

Continuing the development then we obtain Eq. (32) in the form

$$Z_0 = \sum_m \frac{2i\rho_1C_1k_1\,\mathcal{J}_1\left(X_{0m}\frac{a}{b}\right)N_m}{X_{0m}\frac{a}{b}}\coth\left(iq_{0m}\ell+\theta\right) \tag{59}$$

where again

$$\theta \equiv \coth^{-1}A$$

and

$$A \equiv \frac{q_{0m}\,\rho_3 C_3}{k_1\,\rho_1 C_1}$$

and the N_m are obtained as solutions to the simultaneous equations.

Besides these two alternatives of either (a) assuming orthogonality of our expansion functions (which assumption we have previously found to be generally erroneous, although permissable within certain limits) or (b) solving the set of simultaneous equations just detailed to obtain the correct expansion coefficients, we have a third possibility, namely, (c) orthogonalizing the nonorthogonal set of functions we generate from the roots of the various characteristic equations appropriate to the four boundary conditions considered. We now detail this third alternative.

First, for simplicity of formulation we return to the subject of the immediately preceding report (2) involving no termination of the cylinder. To reiterate, we obtained a set of characteristic values X_{0m} from the several boundary condition characteristic equations. The characteristic functions R_{0m} are then formed as

$$R_{0m} = \mathcal{J}_0\left(r\,\frac{X_{0m}}{b}\right), \tag{60}$$

and the expansion for velocity potential is

$$\phi(r, z) = \sum_m K_{0m}\,R_{0m}\,e^{iq_{0m}z} \tag{61}$$

with the individual modes designated by ϕ_{0m} and the expansion coefficients by K_{0m}. The coefficients are obtained in the usual manner by writing $\phi\,(r, z)$ at the origin ($z=0$), multiplying by $rR_{0\ell}$, and integrating with respect to r over the limits 0 to b. With the assumption that $\phi\,(r, 0) \to \phi_0$ (a constant) over the radius a, the above yields

$$\phi_0\,\frac{ab}{X_{0\ell}}\,\mathcal{J}_1\left(X_{0\ell}\,\frac{a}{b}\right) = \int_0^b \sum_m K_{0m}\,R_{0m}\,R_{0\ell}\,rdr. \tag{62}$$

This set of simultaneous equations can be written in matrix notation as

$$\phi_0 ab\begin{pmatrix} \dfrac{\mathcal{J}_1\left(X_{00}\,\dfrac{a}{b}\right)}{X_{00}} \\ \vdots \\ \dfrac{\mathcal{J}_1\left(X_{0m}\,\dfrac{a}{b}\right)}{X_{0m}} \end{pmatrix} = \begin{pmatrix} \displaystyle\int_0^b R_{00}^2\,rdr & \displaystyle\int_0^b R_{00}\,R_{01}\,rdr \ldots \\ \vdots & \vdots \\ \displaystyle\int_0^b R_{0m}\,R_{00}\,rdr & \displaystyle\int_0^b R_{0m}\,R_{01}\,rdr \ldots \end{pmatrix} \begin{pmatrix} K_{00} \\ \vdots \\ K_{0m} \end{pmatrix} \tag{63}$$

If the R_{0m} form an orthogonal set, the matrix containing these terms becomes a diagonal matrix, all other terms being identically zero by the definition of orthogonality. Then separate equations

are immediately obtained as

$$\phi_0 \frac{ab}{X_{0m}} \mathcal{J}_1\left(X_{0m} \frac{a}{b}\right) = K_{0m} \int_0^b R_{0m}^2 \, rdr \tag{64}$$

which, using Eq. (54) yields the coefficients directly as

$$K_{0m} = \phi_0 \frac{2a \, \mathcal{J}_1\left(X_{0m} \frac{a}{b}\right)}{bX_{0m} \left[\mathcal{J}_0^2(X_{0m}) + \mathcal{J}_1^2(X_{0m})\right]} . \tag{65}$$

If, however, the functions R_{0m} are not orthogonal, and they generally are not for our realistic cases, the off-diagonal elements of the matrix do not vanish and the determinantal solution must be obtained. We then made use of the relation

$$\int_0^b R_{0m} R_{0\ell} \, rdr = \frac{b^2}{X_{0m}^2 - X_{0\ell}^2} \begin{bmatrix} X_{0m} \mathcal{J}_0(X_{0\ell}) \mathcal{J}_1(X_{0m}) \\ -X_{0\ell} \mathcal{J}_0(X_{0m}) \mathcal{J}_1(X_{0\ell}) \end{bmatrix} \tag{66}$$

and solved the complete equations for the K_{0m} to obtain what we called the *actual* coefficients as opposed to those derived from the orthogonal assumption. The third procedure we may utilize is to develop modified characteristic functions R_{0m}^N such that they form an orthogonal set. We again beg the question of completeness, which may even be an improper question here since our expansion is a finite series analogous to box normalization employed in quantum theory and questions of least-squares fit or convergence in the mean may not be germane. However, as a purely mechanical method of orthogonalizing our nonorthogonal set, we employ the Gram-Schmidt technique. This is usually found to yield characteristic functions which could have been obtained directly from some Liouville equation with specified boundary conditions. The technique yields the normalization integrals directly and can be summarized by the following equations in our notation

$$R_{00}^N \equiv R_{00}$$

$$R_{01}^N \equiv R_{01} - \frac{R_{00}^N \int_0^b R_{00}^N R_{01} \, rdr}{N_0}$$

$$R_{02}^N \equiv R_{02} - \frac{R_{01}^N \int_0^b R_{01}^N R_{02} \, rdr}{N_1} - \frac{R_{00}^N \int_0^b R_{00}^N R_{02} \, rdr}{N_0}$$

etc., where

$$N_0 \equiv \int_0^b R_{00}^2 \, rdr \tag{67}$$

$$N_1 \equiv \int_0^b R_{01}^2\, rdr - \frac{\left|\int_0^b R_{00}^N R_{01}\, rdr\right|^2}{N_0}$$

$$N_2 \equiv \int_0^b R_{02}^2\, rdr - \frac{\left|\int_0^b R_{01}^N R_{02}\, rdr\right|^2}{N_1} - \frac{\left|\int_0^b R_{00}^N R_{02}\, rdr\right|^2}{N_0} \tag{67 cont.}$$

etc. However, these R_{0m}^N cannot be simply substituted with the middle matrix of Eq. (63) (which is a diagonal matrix for these orthogonal functions). It is instead necessary to go back to the beginning of the development. Following this line, then, we finally obtain

$$\phi_0 \begin{pmatrix} \int_0^a R_{00}^N\, rdr \\ \int_0^a R_{01}^N\, rdr \\ \int_0^a R_{02}^N\, rdr \\ \vdots \\ \int_0^a R_{0m}^N\, rdr \end{pmatrix} = \begin{pmatrix} \int_0^b \left(R_{00}^N\right)^2 rdr & 0 & 0 \ldots & 0 \\ 0 & \int_0^b \left(R_{01}^N\right)^2 rdr & 0 \ldots & 0 \\ 0 & 0 & \int_0^b \left(R_{02}^N\right)^2 rdr \ldots & 0 \\ \vdots & \vdots & \vdots & \vdots \\ 0 & 0 & 0 \ldots & \int_0^b \left(R_{0m}^N\right)^2 rdr \end{pmatrix} \begin{pmatrix} K_{00} \\ K_{01} \\ K_{02} \\ \vdots \\ K_{0m} \end{pmatrix} \tag{68}$$

which reduces to separate equations

$$\phi_0 \int_0^a R_{0m}^N\, rdr = K_{0m} \int_0^b \left(R_{0m}^N\right)^2 rdr. \tag{69}$$

This may be directly solved for the coefficients K_{0m} and leads to

$$\langle\phi\rangle_{\text{rel}} = \sum_m \left(\frac{2}{a^2} e^{-i(k-q_{0m}z)}\right) \frac{\left[\int_0^a R_{0m}^N\, rdr\right]^2}{\int_0^b \left(R_{0m}^N\right)^2 rdr}$$

where we used

$$\langle\phi\rangle = \sum_m \frac{2}{a^2} \int_0^a K_{0m}^N R_{0m}^N e^{iq_{0m}z}\, rdr$$

and

$$\langle\phi\rangle_{\text{rel}} = \langle\phi\rangle \frac{e^{-ikz}}{\phi_0}.$$

But the equations for the present iterative reflection situation are not as simple as those obtained for the nonterminated case just detailed. We note for this that Eq. (7) may be written

$$\phi(r,z) = \sum_m R_{0m}^N \left(K_{0m}\, e^{iq_{0m}z} + L_{0m}\, e^{-iq_{0m}z}\right). \tag{70}$$

Equation (8) then is, using $\phi(r,0) \to \phi_0$,

$$\phi_0 = \sum_m R_{0m}^N \left(K_{0m} + L_{0m}\right), \tag{71}$$

and Eq. (10) becomes

$$\sum_m \left(K_{0m} + L_{0m}\right) = \frac{\phi_0 \int_0^a R_{0\ell}^N\, rdr}{\int_0^b \sum_m R_{0m}^N R_{0\ell}^N\, rdr}. \tag{72}$$

The development through Eq. (16) remains unchanged and continues from Eq. (24) through (27), and also Eq. (31). Equation (18) becomes

$$\langle\phi\rangle = \sum_m \left(K_{0m} e^{iq_{0m}z} + L_{0m} e^{-iq_{0m}z}\right) \frac{2}{a^2} \int_0^a R_{0m}^N\, rdr, \tag{73}$$

and Eq. (19) becomes

$$\langle p\rangle_0 = \frac{2i\omega\rho}{a^2} \sum_m \left(K_{0m} + L_{0m}\right) \int_0^a R_{0m}^N\, rdr. \tag{74}$$

Using $U_0 = \left(\partial\phi/\partial z\right)_{z=0}$, we obtain instead of Eq. (21)

$$\sum_m \left(K_{0m} - L_{0m}\right) = \sum_m \frac{iU_0}{q_{0m}} \frac{\int_0^a R_{0\ell}^N\, rdr}{\int_0^b R_{0m}^N R_{0\ell}^N\, rdr}, \tag{75}$$

and finally for Eq. (23) we obtain

$$Z_0 = -\frac{2\rho\omega}{a^2}\sum_m \frac{1}{q_{0m}}\left(\frac{K_{0m}+L_{0m}}{K_{0m}-L_{0m}}\right)\frac{\int_0^a R_{0m}^N\, rdr \int_0^a R_{0\ell}^N\, rdr}{\int_0^b R_{0m}^N R_{0\ell}^N\, rdr} \tag{76}$$

or, eventually, for Eq. (32)

$$Z_0 = -\sum_m \frac{2\rho_1 C_1 k_1}{a^2 q_{0m}} \frac{\int_0^a R_{0m}^N\, rdr \int_0^a R_{0\ell}^N\, rdr}{\int_0^b R_{0m}^N R_{0\ell}^N\, rdr} \coth\left(iq_{0m}\ell+\theta\right) \tag{77}$$

where θ is defined by Eqs. (30) and (24). Equation (76) is easily checked for the case of the R_{0m} themselves being orthogonal, in which case we delete the superscript N's in using the above and directly find, using

$$R_{0m} \equiv \mathcal{J}_0\left(r\frac{X_{0m}}{b}\right)$$

$$\int_0^a R_{0m}\, rdr = \frac{ab}{X_{0m}}\mathcal{J}_1\left(X_{0m}\frac{a}{b}\right)$$

$$\int_0^b R_{0m}^2\, rdr = \frac{b^2}{2}\left[\mathcal{J}_0^2\left(X_{0m}\right) + \mathcal{J}_1^2\left(X_{0m}\right)\right],$$

that

$$Z_0 = -\rho_1 C_1 k_1 \sum_m \frac{1}{q_{0m}}\left(\frac{K_{0m}+L_{0m}}{K_{0m}-L_{0m}}\right)\frac{4\mathcal{J}_1^2\left(X_{0m}\frac{a}{b}\right)}{X_{0m}^2\left[\mathcal{J}_0^2\left(X_{0m}\right)+\mathcal{J}_1^2\left(X_{0m}\right)\right]}\,. \tag{23 repeated}$$

In summary, then, for orthogonal R_{0m} written as R_{0m}^N, we have

$$Z_0 = \sum_m \frac{2i\rho_1 C_1 k_1}{a^2} N_m^N \coth\left(iq_{0m}\ell+\theta\right)\int_0^a R_{0m}^N\, rdr$$

where

$$N_m^N = \frac{-i\int_0^a R_{0m}^N\, rdr}{q_{0m}\int_0^b \left(R_{0m}^N\right)^2 rdr} \equiv \frac{K_{0m}-L_{0m}}{U_0}.$$

And, if $R^N_{0m} \equiv \mathcal{J}_0\left[r\left(X_{0m}/b\right)\right]$, we have

$$N^N_m = \frac{-iab2\mathcal{J}_1\left(X_{0m}\dfrac{a}{b}\right)}{q_{0m}X_{0m}\,b^2\left[\mathcal{J}_0^2\left(X_{0m}\right) + \mathcal{J}_1^2\left(X_{0m}\right)\right]},$$

and thus

$$Z_0 = \sum_m \frac{4\rho_1 C_1 k_1\,\mathcal{J}_1^2\left(X_{0m}\dfrac{a}{b}\right)\coth\left(iq_{0m}\ell + \theta\right)}{q_{0m}X^2_{0m}\left[\mathcal{J}_0^2\left(X_{0m}\right) + \mathcal{J}_1^2\left(X_{0m}\right)\right]}. \qquad \text{(32 repeated)}$$

If the R_{0m} are not orthogonal, we still have, for $R_{0m} = \mathcal{J}_0\left[r\left(X_{0m}/b\right)\right]$,

$$\int_0^a R_{0m}\,rdr = \frac{ab}{X_{0m}}\,\mathcal{J}_1\left(X_{0m}\frac{a}{b}\right).$$

But now instead of the simplification

$$\int_0^b \left(R^N_{0m}\right)^2 rdr = \frac{b^2}{2}\left[\mathcal{J}_0^2\left(X_{0m}\right) + \mathcal{J}_1^2\left(X_{0m}\right)\right],$$

we have

$$\int_0^a R_{0\ell}\,rdr = \int_0^b \sum_m iq_{0m}N_m R_{0m}R_{0\ell}\,rdr$$

which is just the simultaneous equations (53).

EQUATIONS FOR CALCULATION OF MODES

In Ref. 2 the appropriate characteristic equation for an inviscid liquid cylinder surrounded by an elastic solid was found to be

$$\begin{aligned}\frac{\mathcal{J}_0\left(X_{0m}\right)\rho_1}{X_{0m}\,\mathcal{J}_1\left(X_{0m}\right)\rho_2} = &-\frac{2}{b^2k_s^2}\\ &-\frac{4q_{0m}^2}{bk_s^4}\sqrt{Y_s^2 - X_{0m}^2}\;\frac{\mathcal{K}_0\left(\sqrt{Y_s^2 - X_{0m}^2}\right)}{\mathcal{K}_1\left(\sqrt{Y_s^2 - X_{0m}^2}\right)}\\ &+\frac{\left(2q_{0m}^2 - k_s^2\right)^2}{k_s^4\sqrt{Y_c^2 - X_{0m}^2}}\;\frac{\mathcal{K}_0\left(\sqrt{Y_c^2 - X_{0m}^2}\right)}{\mathcal{K}_1\left(\sqrt{Y_c^2 - X_{0m}^2}\right)}\end{aligned} \qquad (78)$$

where $\mathcal{J}_m$ is a Bessel function of the 1st kind, $\mathcal{K}_m$ is a modified Bessel function of the second kind, ρ_1 is the guide liquid density, ρ_2 is the wall material density, b is the tube radius, k is the media wave number (with the subscripts c and s referring to compressional and shear waves, respectively), q_{0m} is the mode wavenumber, and we have defined

$$X_{0m} \equiv b\sqrt{k^2 - q_{0m}^2}$$

$$Y_c \equiv b\sqrt{k^2 - k_c^2}$$

$$Y_s \equiv b\sqrt{k^2 - k_s^2}.$$

The roots of this characteristic equation [Eq. (78)] are the characteristic values and are denoted by X_{Em}.

To consider inviscid liquid boundary conditions, it is sufficient to allow $k_s \to \infty \left(c_s \to 0\right)$ in Eq. (59), whereby we obtain

$$\frac{\mathcal{J}_0\left(X_{0m}\right)}{X_{0m}\mathcal{J}_1\left(X_{0m}\right)} = \frac{\rho_2}{\rho_1}\,\frac{\mathcal{K}_0\left(\sqrt{Y^2 - X_{0m}^2}\right)}{\sqrt{Y^2 - X_{0m}^2}\,\mathcal{K}_1\left(\sqrt{Y^2 - X_{0m}^2}\right)} \tag{79}$$

where we noted $Y_c \to Y$. From the identities

$$\mathcal{H}_0^{(1)}\left(iX\right) = \frac{2}{\pi i}\,\mathcal{K}_0\left(X\right)$$

$$\mathcal{H}_1^{(1)}\left(iX\right) = -\frac{2}{\pi}\,\mathcal{K}_1\left(X\right)$$

we may write Eq. (79) as

$$\frac{\mathcal{J}_0\left(X_{0m}\right)}{X_{0m}\mathcal{J}_1\left(X_{0m}\right)} = \frac{\rho_2}{\rho_1}\,\frac{\mathcal{H}_0^{(1)}\left(i\sqrt{Y^2 - X_{0m}^2}\right)}{i\sqrt{Y^2 - X_{0m}^2}\,\mathcal{H}_1^{(1)}\left(i\sqrt{Y^2 - X_{0m}^2}\right)} \tag{80}$$

where we further note the definition

$$\mathcal{H}_n^{(1)}\left(X\right) = \mathcal{J}_n\left(X\right) + i\mathcal{N}_n\left(X\right)$$

where $\mathcal{H}_n$ is a Bessel function of the third kind and $\mathcal{N}_n$ a Bessel function of the second kind. $\mathcal{K}_n$ is sometimes called the hyperbolic Bessel function and is related directly to $\mathcal{J}_n$ and $\mathcal{N}_n$ by

$$\mathcal{K}_n\left(X\right) = \frac{1}{2}\pi i^{n+1}\left[\mathcal{J}_n\left(iX\right) + i\mathcal{N}_n\left(iX\right)\right].$$

The characteristic values for inviscid liquid boundary conditions will again be designated by X_{Lm}. The foregoing equations are essentially a statement of equality of acoustic impedance at the boundary.

If we allow the boundary material to become infinitely flexible, then the equation becomes

$$\frac{\mathcal{J}_0(X_{0m})}{X_{0m}\,\mathcal{J}_1(X_{0m})} = 0$$

or

$$\mathcal{J}_0(X_{Fm}) = 0 \tag{81}$$

where the flexible boundary characteristic values are denoted X_{Fm}.

Similarly, if the boundary material becomes absolutely rigid then

$$\frac{\mathcal{J}_0(X_{0m})}{X_{0m}\,\mathcal{J}_1(X_{0m})} = \infty$$

or

$$\mathcal{J}_1(X_{Rm}) = 0 \tag{82}$$

is the characteristic equation for rigid boundary conditions with the roots designated X_{Rm}.

In the preceding we have obviously chosen a time dependence $e^{-i\omega t}$ and a corresponding space dependence $e^{iq_{0m}z}$ for an outgoing wave.

STANDARD REFERENCE PARAMETERS

As in the immediately previous report (2) we will standardize our parameters as shown in Table 1. Again, the reference ratio b/a is equal to 2, and this will be varied between 1 and 10 later in the report. The density ratio and wave number ratio are chosen, as before, to yield an impedance ratio of 28; together with the Poisson's ratio of 0.325, these values correspond to a good nickel steel. The latter three parameters are not varied in this report as they were sufficiently investigated in Ref. 2. The absorption coefficient of the guide liquid again has the initial reference value of zero, but it will later be varied up to 1 cm^{-1} (nepers).

Because the results of this report are not immediately transformable to other wave numbers, as are those of Parts 1 and 2 of this series of reports [here the actual reflector crystal separation ℓ is used rather than the previous parameter $z(\lambda/a^2)$], the superscripts I, III, and V have been added to k_1 and to the guide λ. For the given $a = 1.5$ cm the superscripts refer to the particular frequencies 1, 3, and 5 MHz which yield ka values, respectively, of 20π, 60π, and 100π.

This report adds a third propagation medium, as compared to only two media discussed in the previous reports in this series. We arbitrarily select $\rho_3 = \rho_2$ and $k_3 = k_2$. The absorption coefficient α_3 is given the reference value of zero, but some results are also shown for $\alpha_3 = 0.001$ cm^{-1}.

ORTHOGONALITY CHECKS

From the previous report we note that the characteristic functions for both liquid and elastic solid boundary conditions were not orthogonal. Also, although the actual and orthogonal assumption expansion coefficients differed, the final results of average pressure and average phase did not differ except for $b/a = 1$ with elastic solid boundaries. We note here that the modes for these iterative reflection calculations are the same as those calculated in Part 2, although the expansion coefficients here are obviously changed. We will in this report dispense with any

Table 1

Standard Reference Parameters Used in Calculations of Radiation Impedance Leading to Sound Speed Values

$\lambda_1^{\mathrm{I}} = 0.15$ cm (sound wavelength in medium I at freq. I)

$a = 10\lambda_1^{\mathrm{I}} = 1.5$ cm (Radius of acoustic source)

$b = 2a = 20\lambda_1^{\mathrm{I}} = 3.0$ cm (radius of liquid cylinder)*

$k_1^{\mathrm{I}} = 2\pi/\lambda_1^{\mathrm{I}} = 20\pi/a$ (wave number of medium I at freq. I)†

$\rho_2/\rho_1 = 7$ (density ratio of outer to inner cylinder media)

$k_1/k_2 = 4$ (wave number ratio of inner to outer cylinder media)

$k_1/k_2 = \lambda_2/\lambda_1 = C_2/C_1$ (C is sound speed in indicated medium)

$\rho_3 = \rho_2$ (ρ_3 is density of termination)

$k_3 = k_2$ (k_3 is wave number of termination)

$\nu_2 = 0.325$ (Poisson's ratio)

$\alpha_1 = 0$ (absorption coefficient in liquid cylinder medium I)

$\alpha_3 = 0$ (absorption coefficient in termination medium III)

$\ell = n(\lambda_1^{\mathrm{I}}/2) \pm 0.005$ cm (separation of acoustic source from reflector)‡

*The later variations in b/a from the value of 2 are obtained by changing b only.

†The later variations in $k_1 a$ from the value 20π are obtained by changing k_1 only. Thus $k_1^{\mathrm{I}} a = 20\pi$, $k_1^{\mathrm{III}} a = 60\pi$, and $k_1^{\mathrm{V}} a = 100\pi$ indicate that $\lambda_1^{\mathrm{I}} = 3\lambda_1^{\mathrm{III}} = 5\lambda_1^{\mathrm{V}}$, or $\lambda_1^{\mathrm{III}} = 0.05$ cm and $\lambda_1^{\mathrm{V}} = 0.03$ cm.

‡Note that n, the number of half wavelenghts, is consistenly chosen so that ℓ represents respective median distances of 0, 0.15, 0.75, 1.5, 7.5, 15, and 22.5 cm; that is, the $n(\lambda_1/2)$ correspond to these separations. So the n for λ_1^{I} are 0, 1, 5, 10, 50, 100, and 150, respectively; the n for λ_1^{III} are 0, 3, 15, 30, 150, 300, and 450, respectively; and the respective n for λ_1^{V} are 0, 5, 25, 50, 250, 500, and 750. Reflecting the increased sharpness of the imposed characteristic indication, the usual variation of ± 0.005 cm for λ_1^{I} is decreased to 1/3 for λ_1^{III} and to 1/5 for λ_1^{V} (± 0.001 cm for the latter). All calculations were made with 100 discrete points in these intervals, so the $k_1^{\mathrm{V}} a = 100\pi$ calculations were made for 0.2-micron steps. Additional points were calculated to extend the circle diagrams for those cases with large aberrations.

preliminary checks of orthogonal assumption vs actual calculations, and we will check only the final results of sound speed errors attributable to diffraction, which will be calculated using both methods.

PLANE WAVE RESULTS AND DISCUSSION

Using the degenerate form of Eq. (32) expressed by Eq. (41), we calculated $Z_{0P}/\rho_1 C_1$ for the pertinent standard parameters in Table 1. Noting that $Z_{0P} \equiv R_{0P} + iX_{0P}$, we plot in Fig. 2

R and X vs ℓ. Obviously, for plane waves these curves repeat every $n(\lambda/2)$, and the maximum value of R_{0P} remains at $\rho_3 C_3/\rho_1 C_1 = 28$ for each successive $n(\lambda/2)$ (for the standard parameters) in the absence of intrinsic absorption in medium I. The most noticeable feature of these

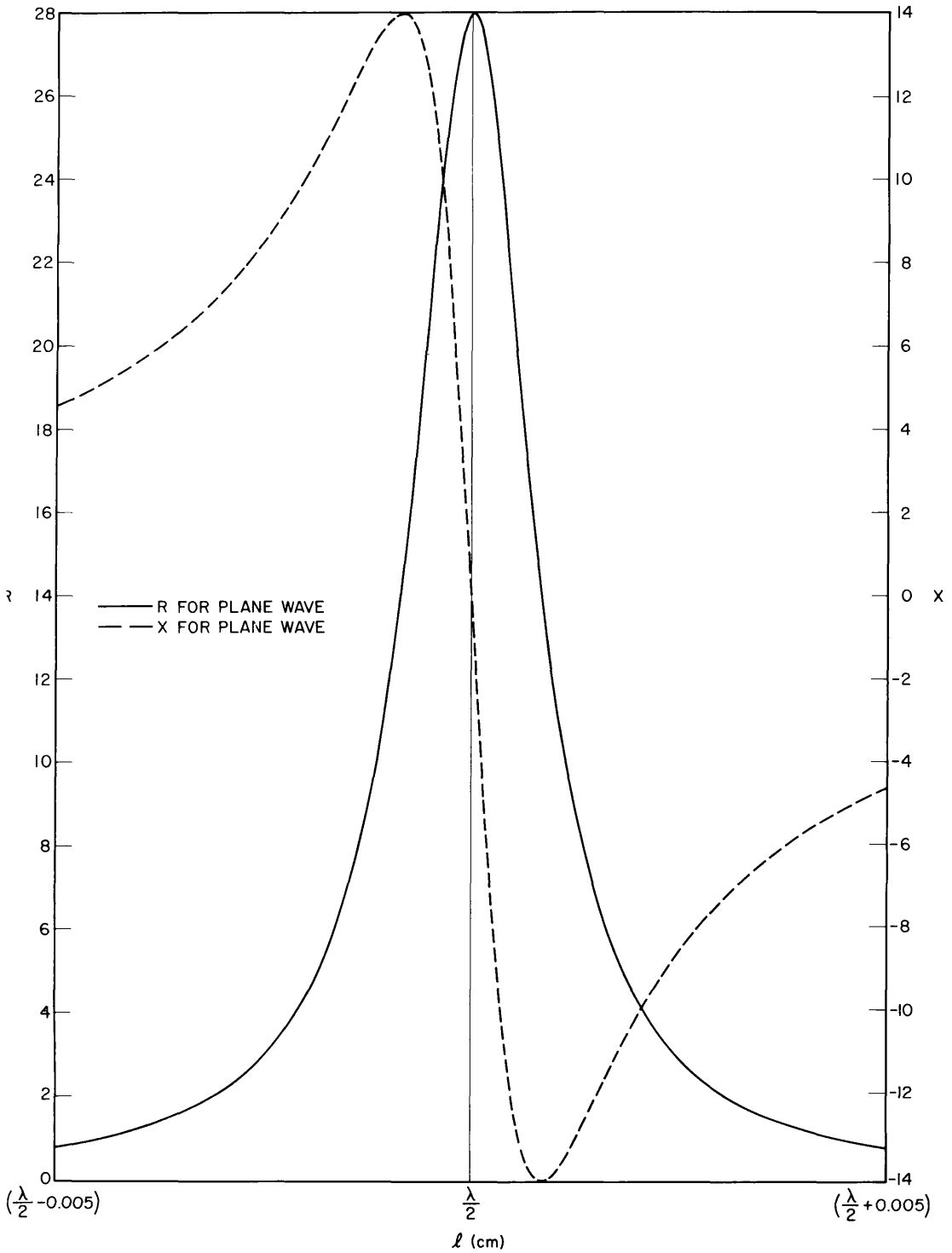

Fig. 2 – Real and imaginary parts of impedance ($Z = R + iX$) vs source-to-reflector separation $\ell \sim \lambda_1/2$ for the standard reference parameters of Table 1 and plane wave simplification

curves is that the maximum R occurs at the same ℓ as does the zero of X, namely at $\lambda/2$, and thus this distance also corresponds to a point of zero phase.

A more informative manner of indicating this data is to plot the impedance directly in the complex plane, that is, plot R vs X for specified values of the parameter ℓ. This is done in Fig. 3. The points indicate values of ℓ differing by 0.0001 cm and the plot is for a range of the parameter $\ell = (\lambda_1/2) \pm 0.005$ cm. The $\lambda_1/2$ point is indicated by a larger circle. Obviously this circle repeats in $n(\lambda/2)$. As discussed more fully in Ref. 3, and as is obvious from Fig. 3, the nature of the circle is such that the variation with ℓ is compressed for small R and expanded for large R, which results in maximum delineation of ℓ about the $n(\lambda_1/2)$ point.

Referring to Eq. (43d) we note that if we allow the reflector impedance to become infinite, that is, if we assume an absolutely rigid reflector, the result is that the maximum R points occurring

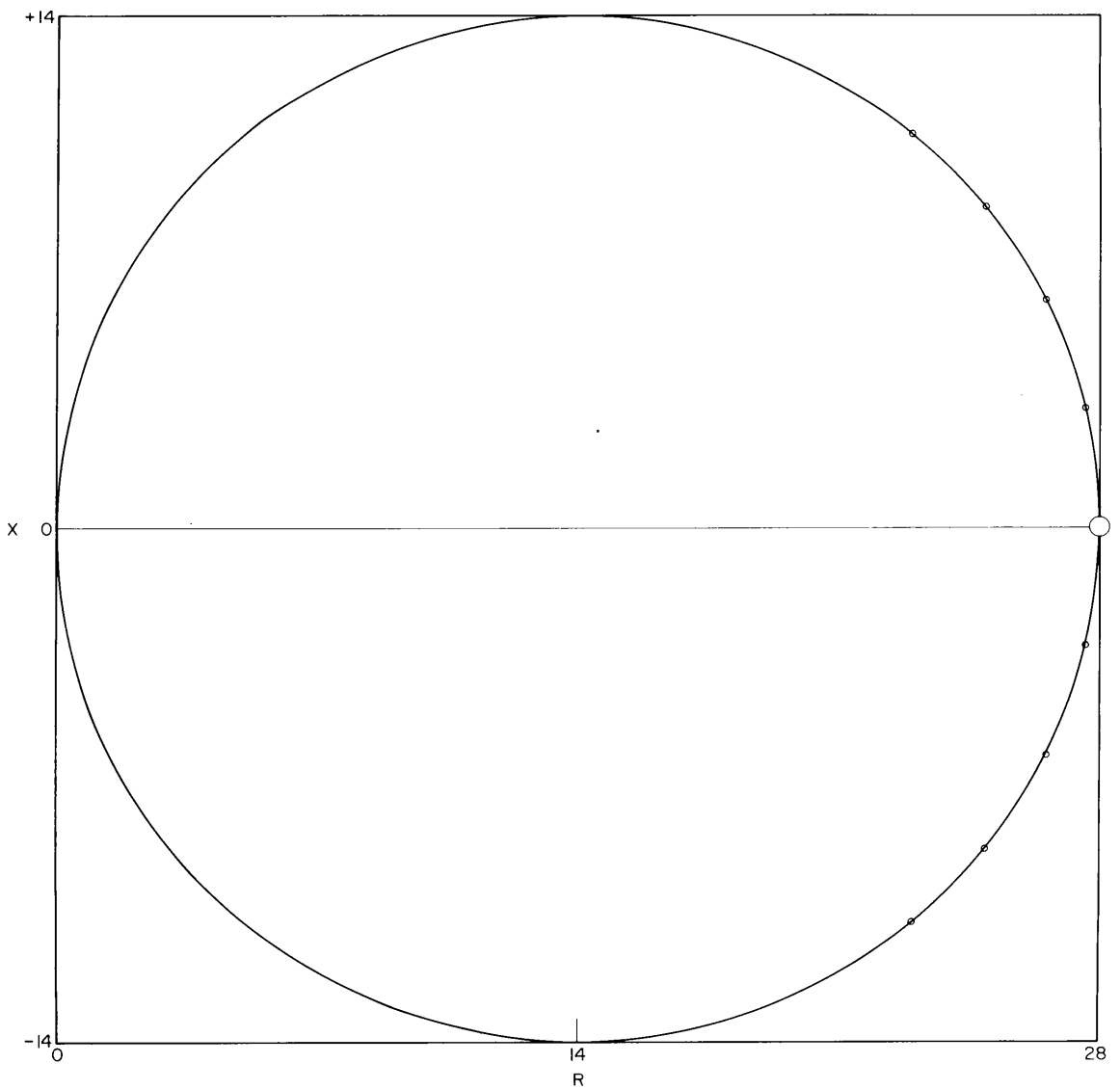

Fig. 3 – Circle diagram of real vs imaginary parts of impedance for parameter $\ell \sim \lambda_1/2$ for the standard reference parameters of Table 1 and plane wave simplification

at $n(\lambda_1/2)$ now became infinite. From Eq. (41) we obtain, for $\rho_3 C_3 = \infty$,

$$\frac{Z_{0P}}{\rho_1 C_1} \equiv \frac{R_{0P}}{\rho_1 C_1} + i\frac{X_{0P}}{\rho_1 C_1} = \frac{0}{1 - \cos 2k\ell} - i\,\frac{\sin 2k\ell}{1 - \cos 2k\ell} = \frac{0}{1 - \cos 2k\ell} - i \cot k\ell.$$

Obviously $R_{0P}/\rho_1 C_1$ is zero, except at $\ell = n(\lambda_1/2)$ where $2k\ell = 2n\pi$ and R_{0P} is infinite. Similarly, $X_{0P}/\rho_1 C_1 = -\cot k\ell$ is intermediate to $-\infty$ and $+\infty$ at these same values of ℓ, taking on the value zero. $R_{0P}/\rho_1 C_1$ is plotted in Fig. 4 for both $\rho_3 C_3/\rho_1 C_1 = 28$ and $\rho_3 C_3/\rho_1 C_1 = \infty$. Similarly, $X_{0P}/\rho_1 C_1$ or $-\cot k\ell$ is plotted in Fig. 5 for the same two values of $\rho_3 C_3/\rho_1 C_1$. It appears that a reflector with the largest acoustic impedance $\rho_3 C_3$ is desirable. But actually the impedance ratio is the primary consideration. If we allow the reflector impedance to become zero, that is, if we assume an infinitely flexible reflector, such as a vacuum, we obtain maximum R points of infinity at $(n - 1/2)(\lambda_1/2)$ values of ℓ. In other words, these maxima now occur at the odd quarter-wavelength values of ℓ as opposed to their occurrence at the even quarter-wavelength (or half-wavelength) values of ℓ for an absolutely rigid reflector.

Again using Eq. (41) we obtain for $\rho_3 C_3/\rho_1 C_1 = 0$

$$\frac{Z_{0P}}{\rho_1 C_1} = \frac{0}{-1 - \cos 2k\ell} + i\,\frac{\sin 2k\ell}{1 + \cos 2k\ell} = \frac{0}{-1 - \cos 2k\ell} + i \tan k\ell.$$

In this case obviously $R_{0P}/\rho_1 C_1$ is zero, except at $\ell = (2n + 1)(\lambda/4)$ where $2k\ell = (2n + 1)\pi$ and R_{0P} is infinite. Similarly $X_{0P}/\rho_1 C_1 = \tan k\ell$ is again zero at the corresponding points. Figures 6 and 7 show, respectively, $R_{0P}/\rho_1 C_1$ and $X_{0P}/\rho_1 C_1$ for $\rho_3 C_3/\rho_1 C_1 = 0$ as compared to their values for $\rho_3 C_3/\rho_1 C_1 = 28$, and we again note that the infinite (or zero) impedance ratio is apparently preferable.

At this point we recall that the standard parameter $\rho_3 C_3/\rho_1 C_1 = 28$ corresponds quite closely to the impedance ratio between a good nickel steel and water, and hence adequately represents an attainable elastic solid reflector. However, if we consider an air reflector with water medium, then $\rho_3/\rho_1 = 0.001$ and $C_3/C_1 = 0.2$, so that $\rho_3 C_3/\rho_1 C_1 = 0.0002$ or $\rho_1 C_1/\rho_3 C_3 = 5000$. This ratio of these impedances is greater than that between steel and water, and hence we would anticipate increased sensitivity for an air reflector as opposed to a metal reflector. Such has been tried, but the problems associated with nonplanarity and nonquiescence of the interface render this technique undesirable. However, the major reason for eliminating an air reflector is its obvious unsuitability or unadaptability to the determination of the hydrostatic pressure coefficient of the acoustic parameters of liquids.

We now investigate the effect of absorption in the liquid cylinder. Figures 8 through 11 are plane wave impedance plots for a reflector to guide liquid impedance ratio of 28. Unlike the case of zero absorption in the liquid, where the circle in Fig. 3 is repeated endlessly with parameter ℓ, we find that absorption results in a shrinking of the circle diameter for half-wavelength variations at increasing values of ℓ. Actually, the plot, as detailed in Ref. 3, is a spiral, here converging on the point (1, 0). As is immediately obvious from Figs. 8 through 11, which are for absorption coefficients of 10^{-3}, 10^{-2}, 10^{-1}, and 1 cm^{-1}, respectively, the effect of increasing absorption for this plane wave situation is merely an increased rate of shrinkage of the circles, which in these impedance plots and all succeeding ones for frequency I (1 MHz) are for the specific values of $n = 0, 1, 5, 10, 50, 100$, and 150 where n is the number of the particular half wavelength in the guide medium for the standard reference condition $k_1^I a = 20\pi$, or $\lambda_1^I = 0.15$ cm ($C_1 = 1500$ m/s).

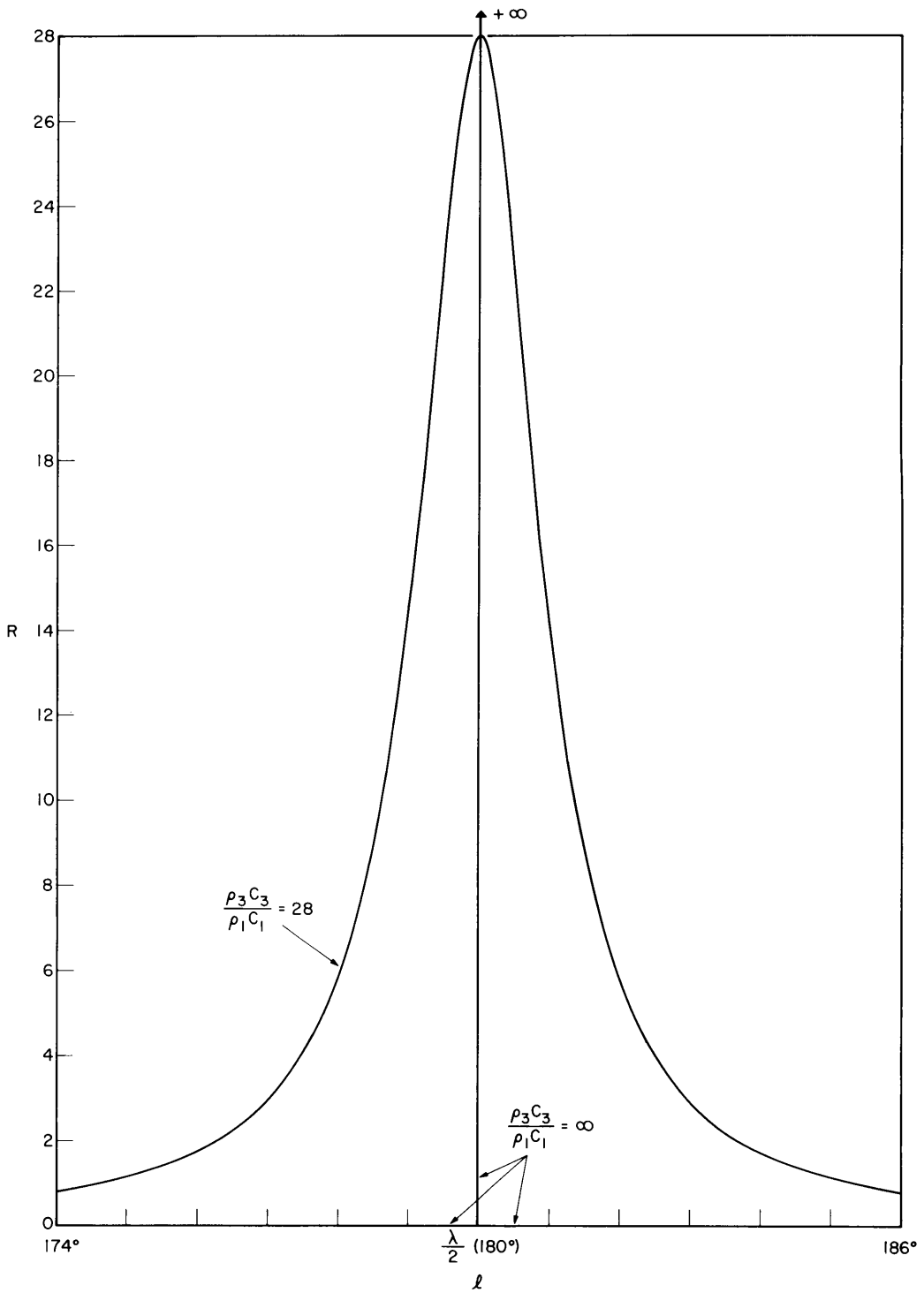

Fig. 4 – Real part of impedance vs $\ell \sim \lambda_1/2$ for the standard reference parameters of Table 1 (and also for $\rho_3 = \infty$) and plane wave simplification

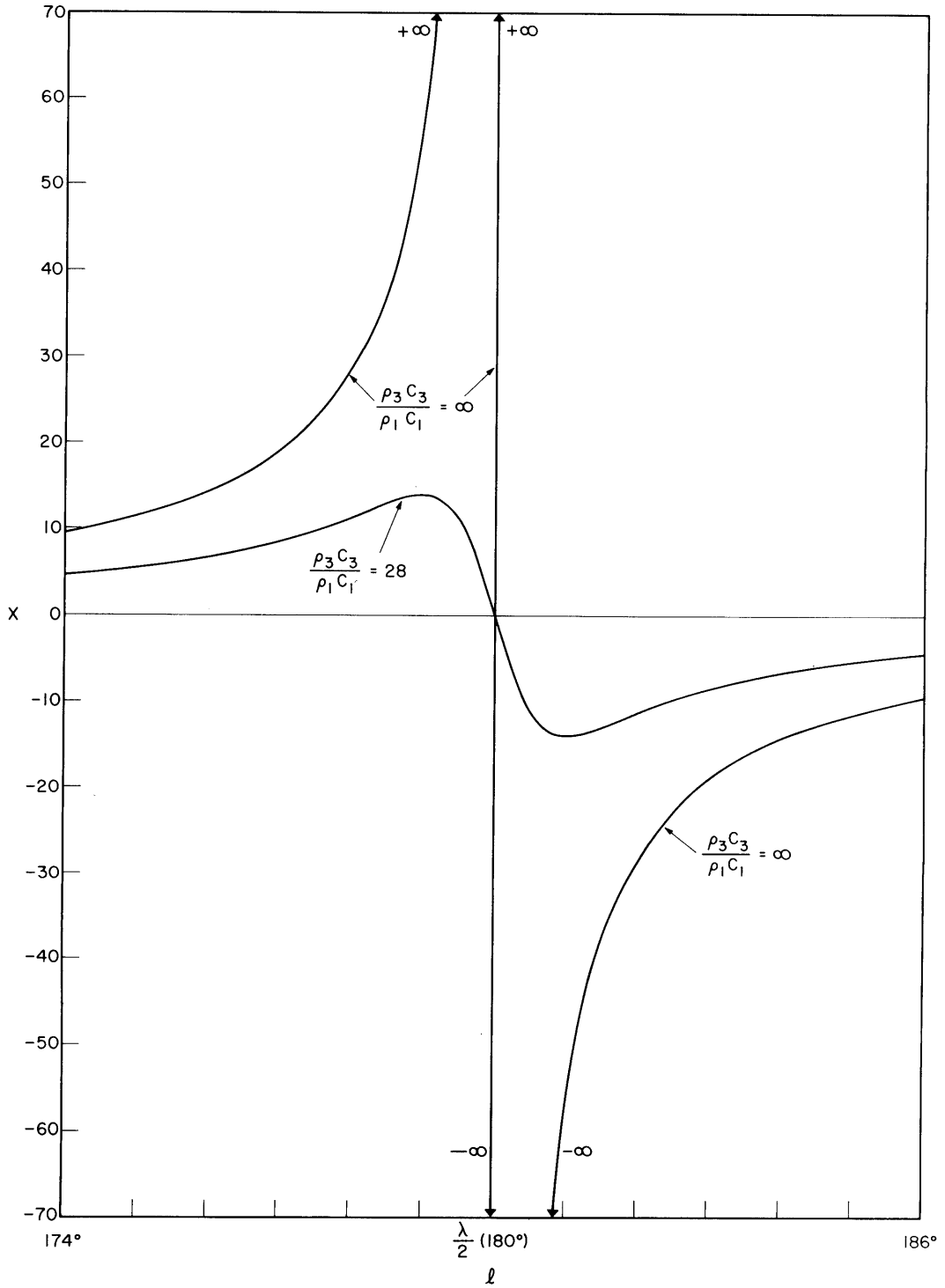

Fig. 5 – Imaginary part of impedance vs $\ell \sim \lambda_1/2$ for the standard reference parameters of Table 1 (and also for $\rho_3 = \infty$) and plane wave simplification

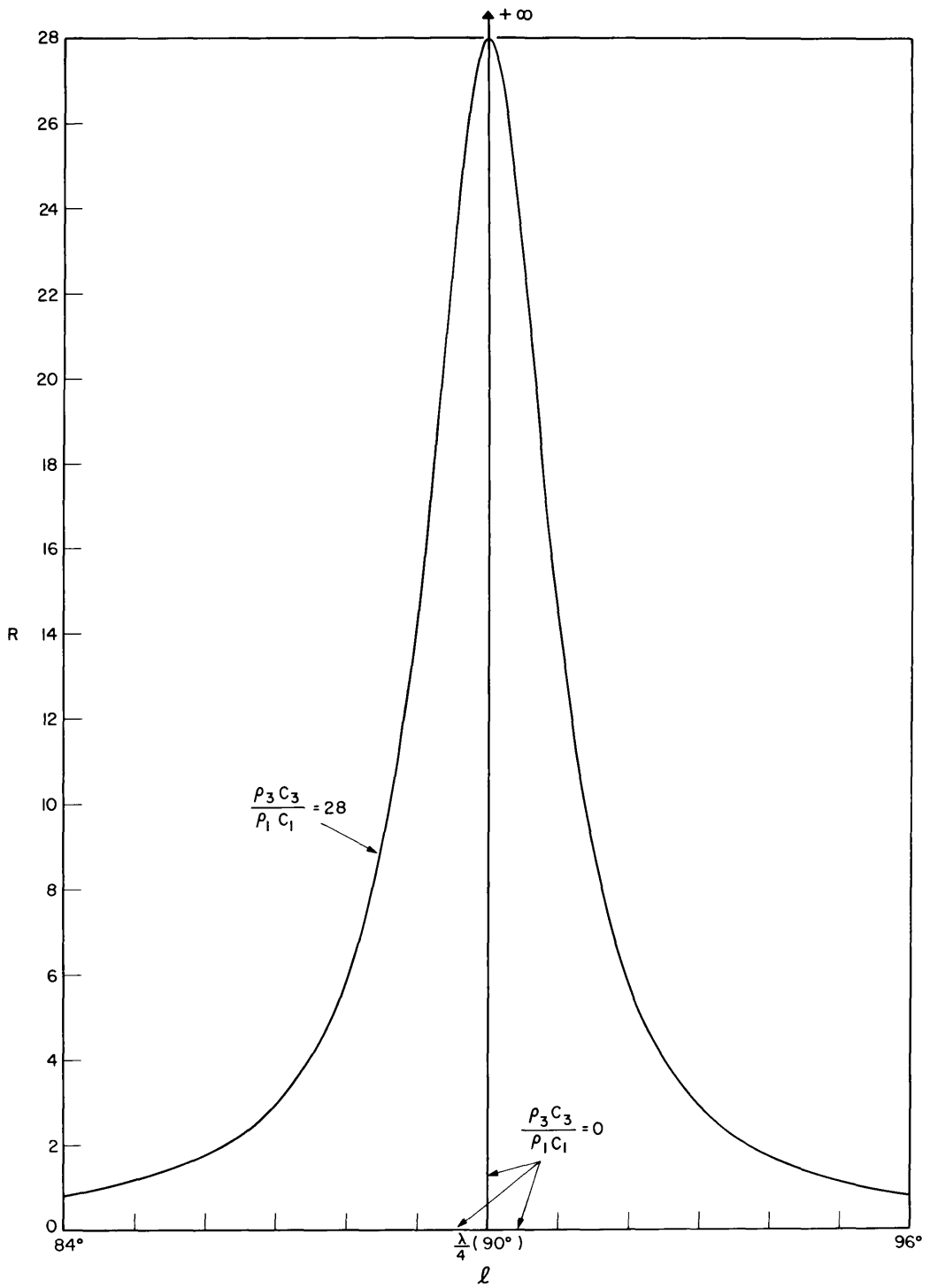

Fig. 6 – Real part of impedance vs $\ell \sim \lambda_l/4$ for the standard reference parameters of Table 1 (and also for $\rho_3 = 0$) and plane wave simplification

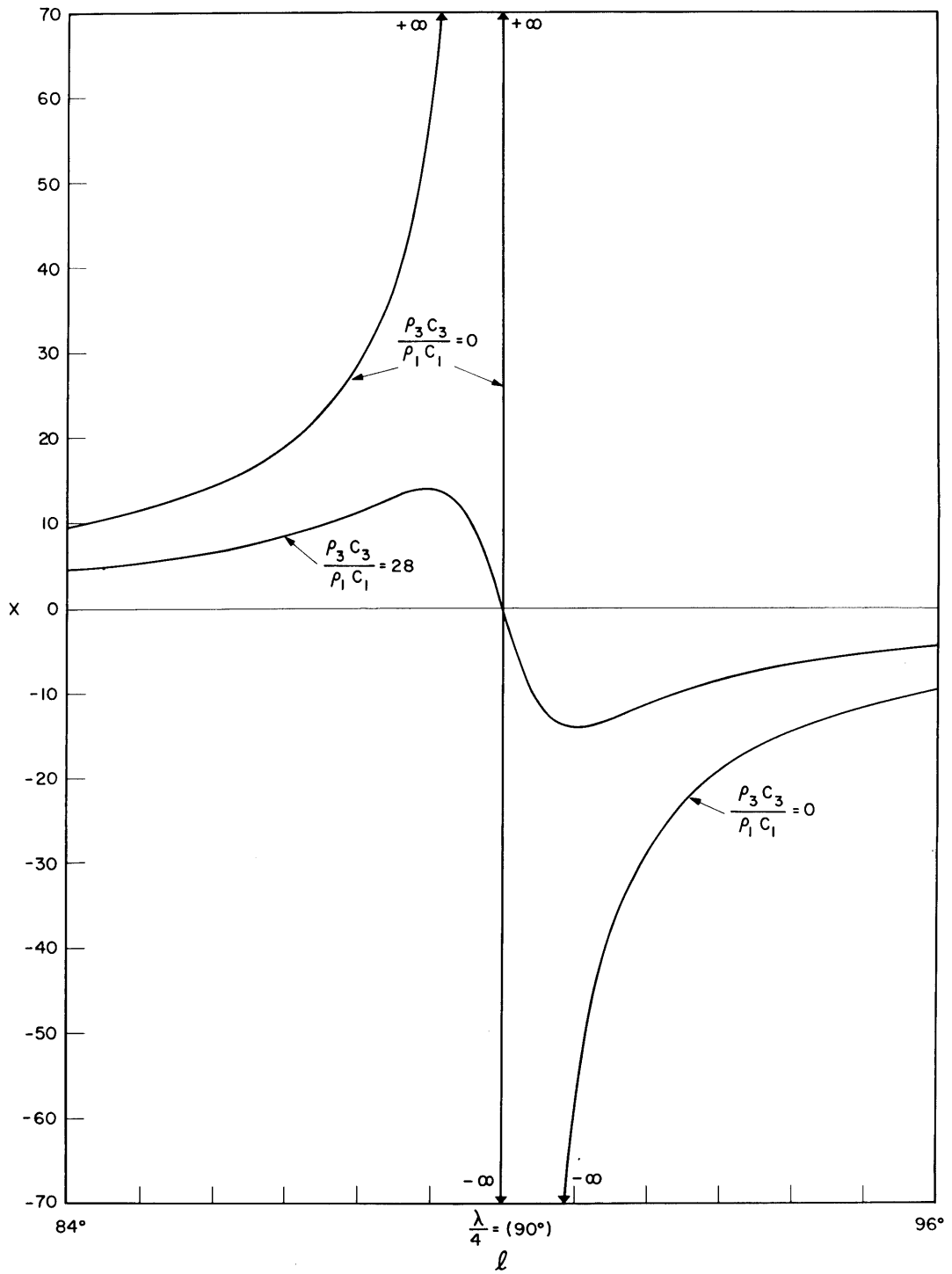

Fig. 7—Imaginary part of impedance vs $\ell \sim \lambda_1/4$ for the standard reference parameters of Table 1 (and also for $\rho_3 = 0$) and plane wave simplification

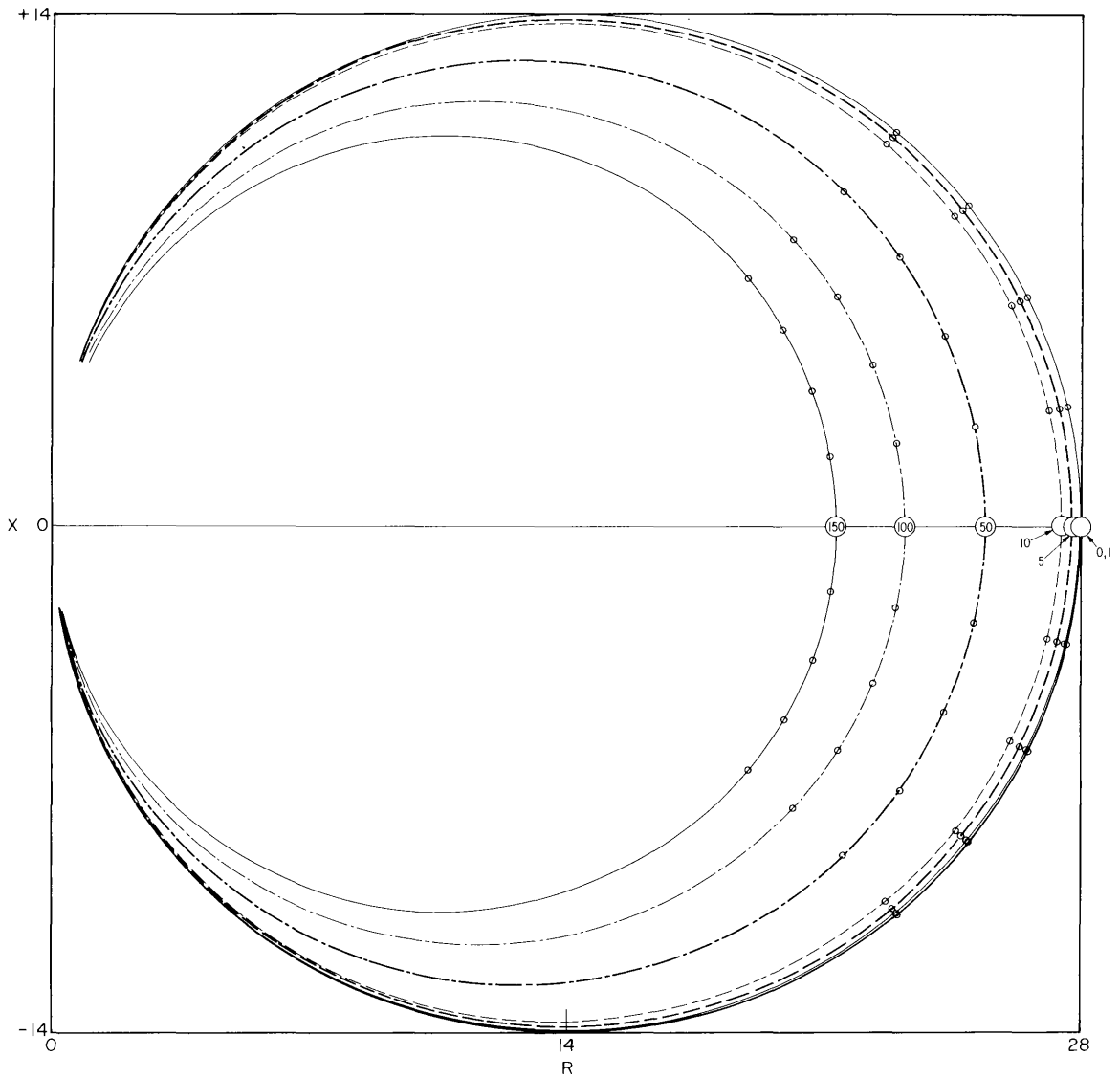

Fig. 8 – Plane wave circle diagram–real vs imaginary parts of impedance for parameter $\ell = n(\lambda_1/2) \pm 0.005$ cm with $n = 0, 1, 5, 10, 50, 100$, and 150 for the standard reference parameters of Table 1 (except $\alpha_1 = 10^{-3}$ cm^{-1}) and plane wave simplification

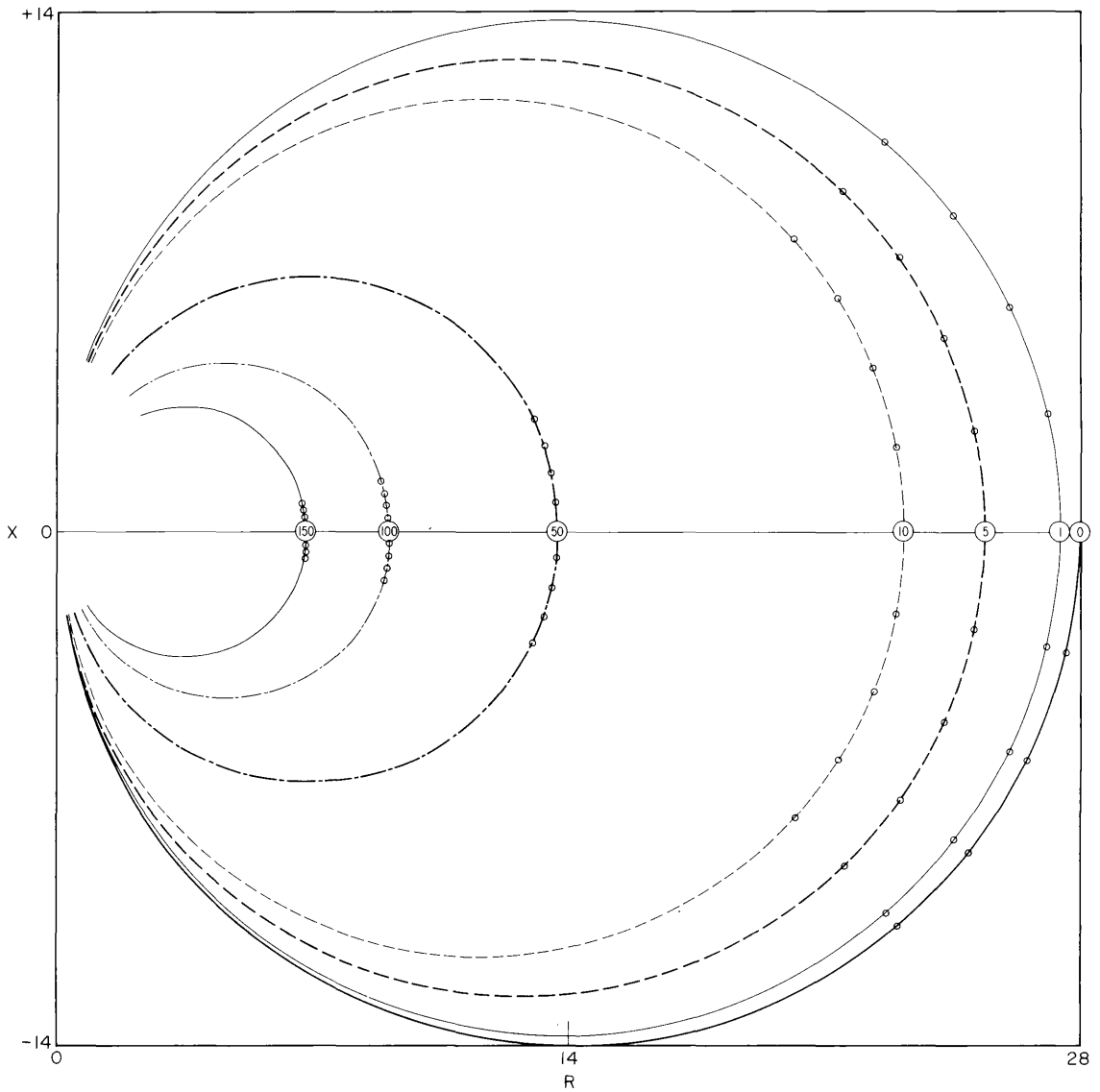

Fig. 9 – Plane wave circle diagram–real vs imaginary parts of impedance for parameter $\ell = n(\lambda_1/2) \pm 0.005$ cm with n = 0, 1, 5, 10, 50, 100, and 150 for the standard reference parameters of Table 1 (except $\alpha_1 = 10^{-2}$ cm^{-1}) and plane wave simplification

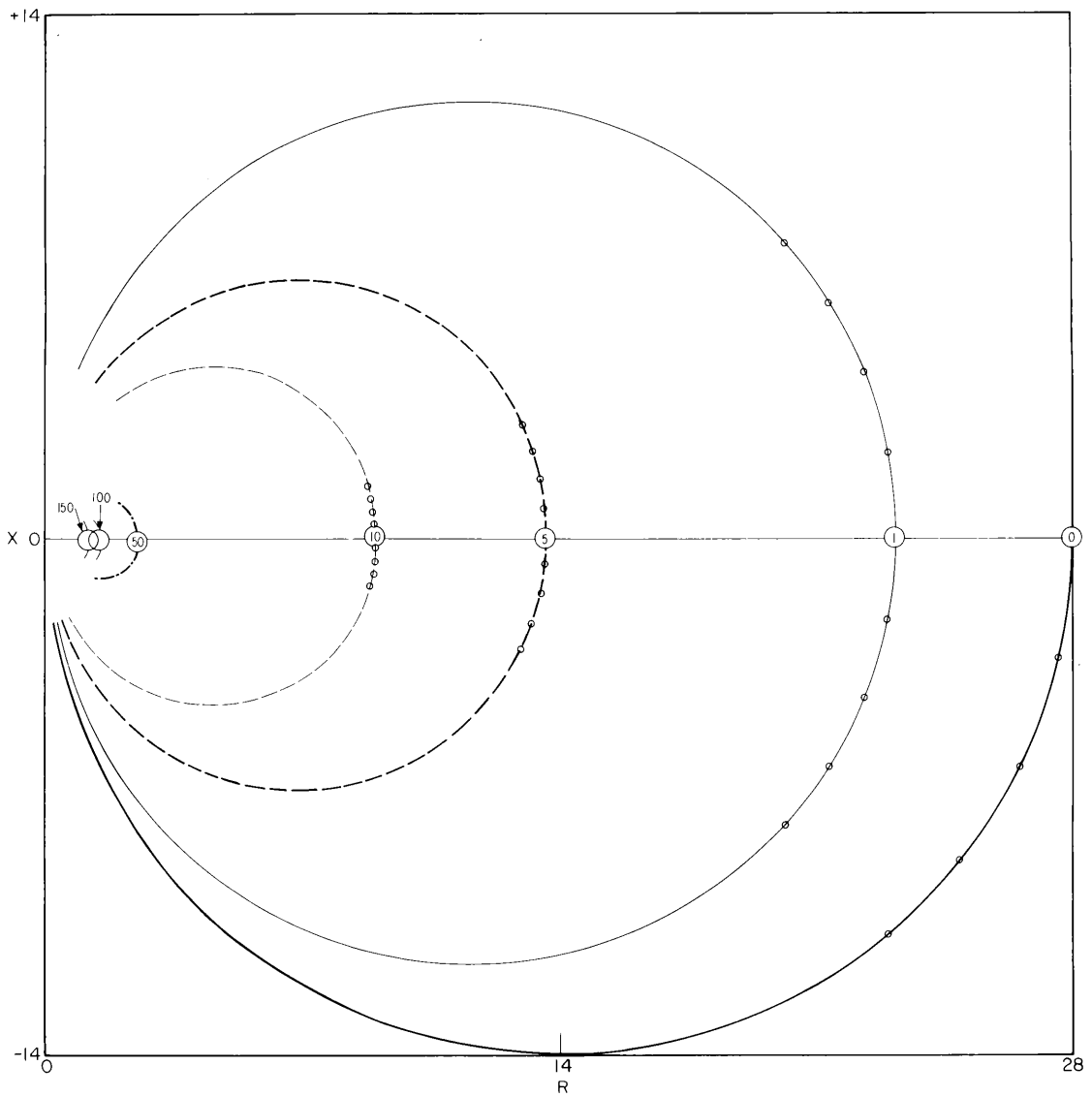

Fig. 10 – Plane wave circle diagram–real vs imaginary parts of impedance for parameter $\ell = n(\lambda_1/2) \pm 0.005$ cm with n = 0, 1, 5, 10, 50, 100, and 150 for the standard reference parameters of Table 1 (except $\alpha_1 = 10^{-1}$ cm^{-1}) and plane wave simplification

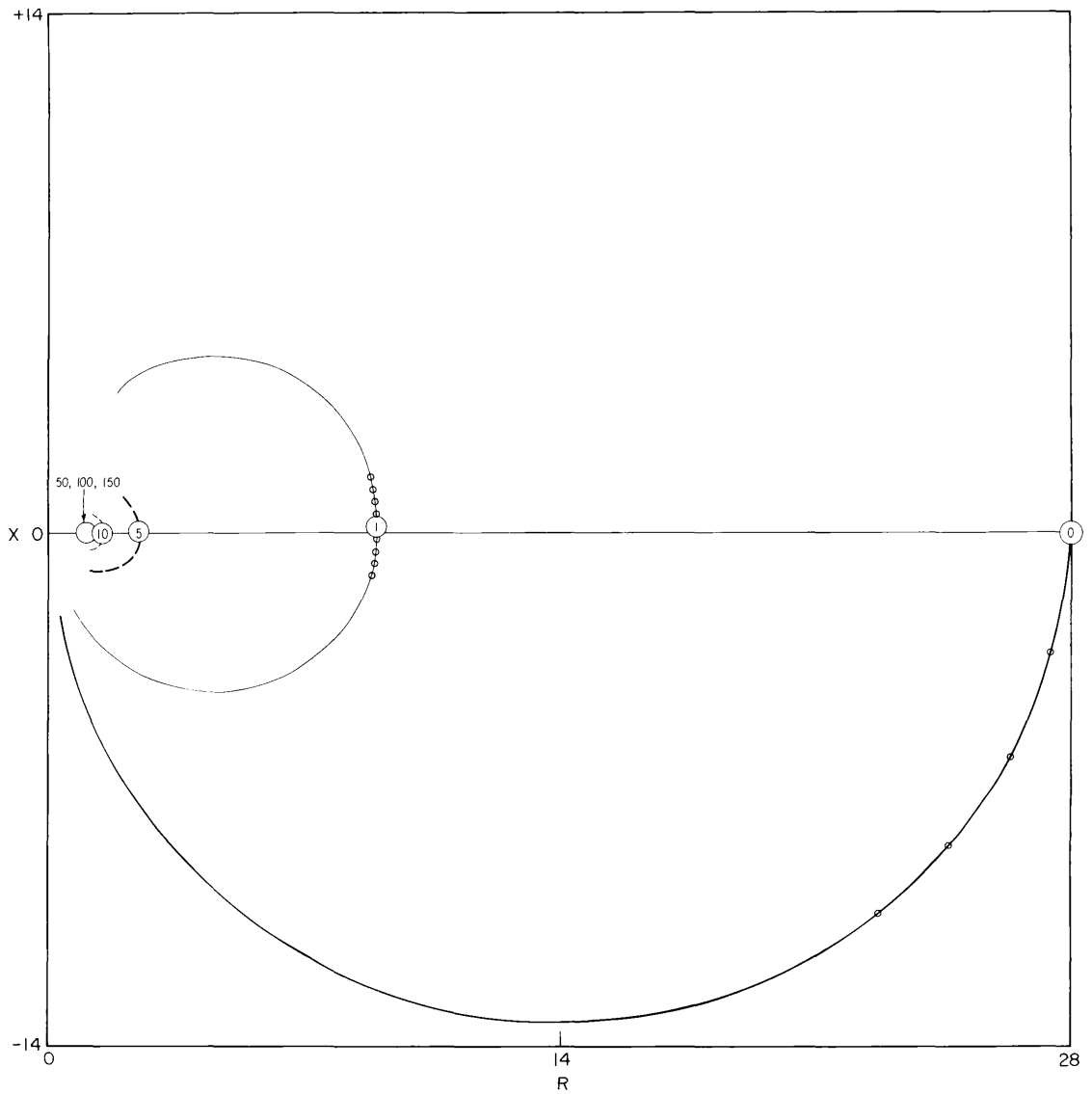

Fig. 11 – Plane wave circle diagram—real vs imaginary parts of impedance for parameter $\ell = n(\lambda_1/2) \pm 0.005$ cm with n = 0, 1, 5, 10, 50, 100, and 150 for the standard reference parameters of Table 1 (except α_1 = 1 cm^{-1}) and plane wave simplification

Figures 12 through 15 are similar to the previous four except that a realistic absorption coefficient of 10^{-3} cm^{-1} has been attributed to the reflector material. A perusal of these four figures shows that they are indeed individually similar to Figs. 8 through 11, respectively. So the attribution of either zero absorption or a coefficient of 10^{-3} cm^{-1} to the reflector material results in virtually identical plots for common values of guide liquid absorption coefficients. It is almost immediately obvious that, as predicted in a previous section titled "Degenerate Case of Plane Waves", the $n(\lambda_1/2)$ points almost precisely coincide, even with a realistic absorption attributed to the medium, with points of zero phase, maximum R, and maximum Z simultaneously. It should be noted, however, that the fiducial $n(\lambda_1/2)$ point indicated for the unrealistic case of $\alpha_1 = 1$ cm^{-1} are slightly displaced in the positive X direction from the $X = 0$ axis. The effect of this on calculated sound speeds will be shown later in the section titled "Discussion" under "Diffracted Wave."

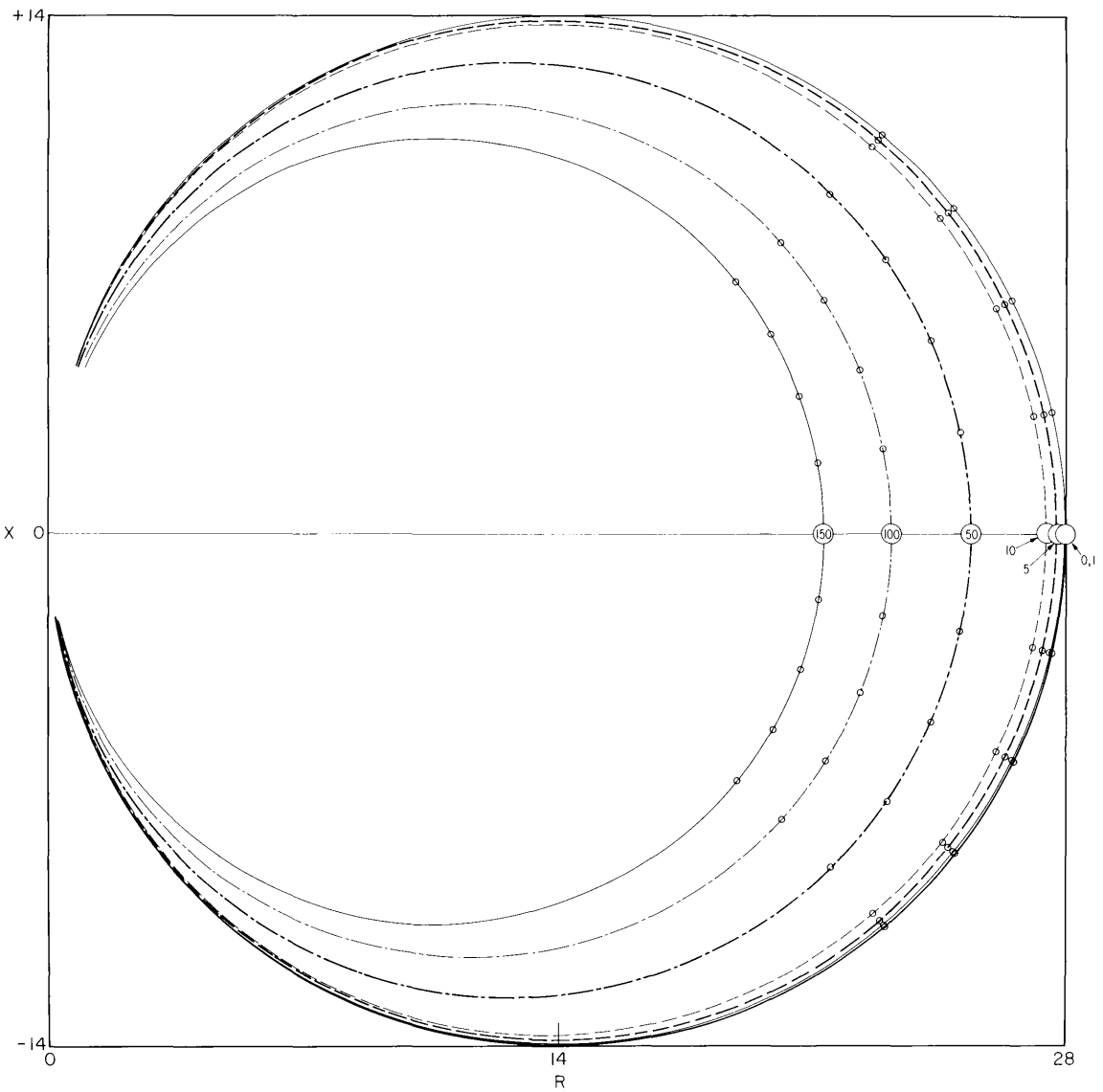

Fig. 12—Plane wave circle diagram—real vs imaginary parts of impedance for parameter $\ell = n(\lambda_1/2) \pm 0.005$ cm with n = 0, 1, 5, 10, 50, 100, and 150 for the standard reference parameters of Table 1 (except $\alpha_1 = 10^{-3}$ cm^{-1} and $\alpha_3 = 10^{-3}$ cm^{-1}) and plane wave simplification

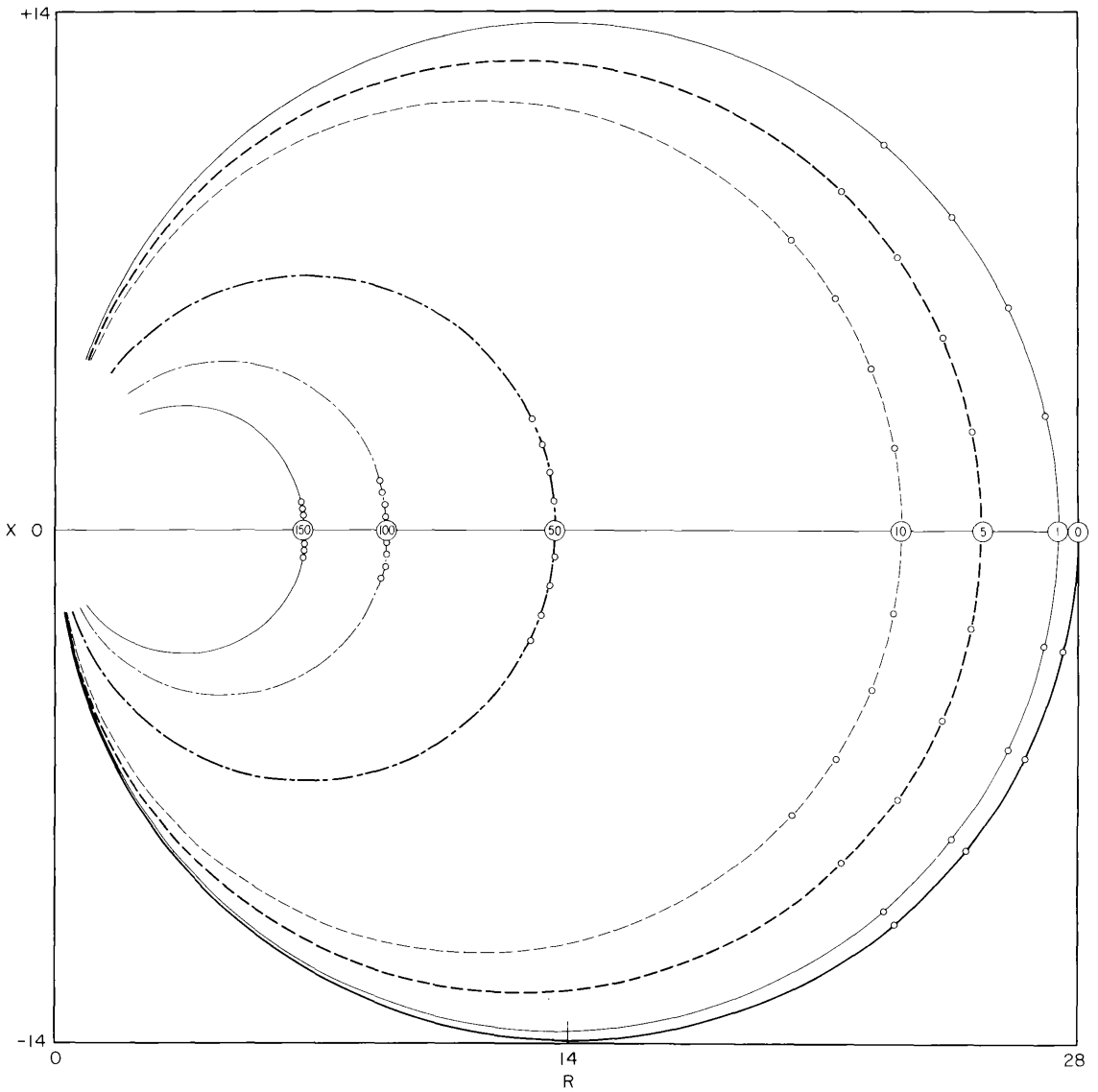

Fig. 13 – Plane wave circle diagram–real vs imaginary parts of impedance for parameter $\ell = n(\lambda_1/2) \pm 0.005$ cm with n = 0, 1, 5, 10, 50, 100, and 150 for the standard reference parameters of Table 1 (except $\alpha_1 = 10^{-2}$ cm^{-1} and $\alpha_3 = 10^{-3}$ cm^{-1}) and plane wave simplification

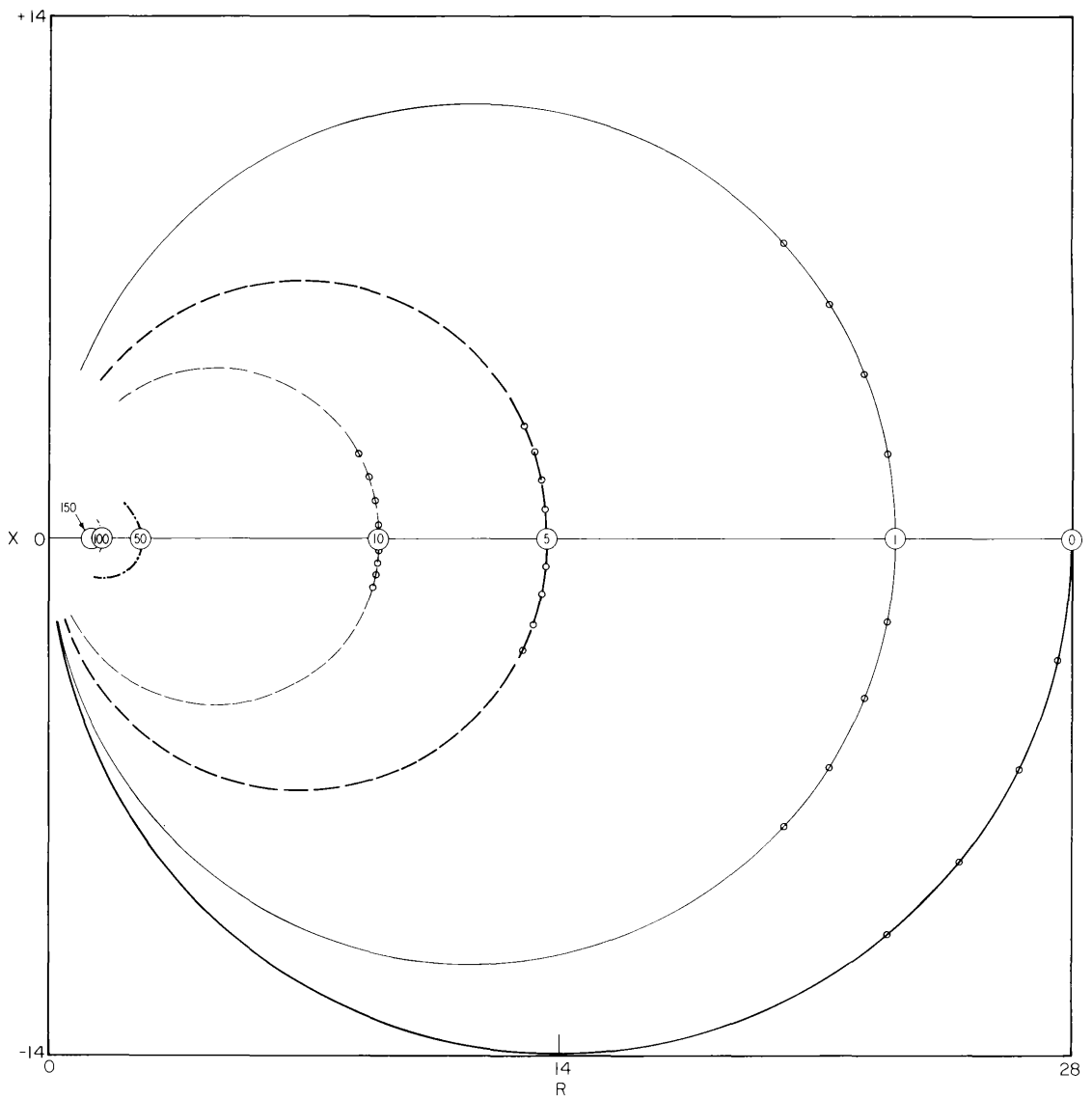

Fig. 14 – Plane wave circle diagram–real vs imaginary parts of impedance for parameter $\ell = n(\lambda_1/2) \pm 0.005$ cm with n = 0, 1, 5, 10, 50, 100, and 150 for the standard reference parameters of Table 1 (except $\alpha_1 = 10^{-1}$ cm^{-1} and $\alpha_3 = 10^{-3}$ cm^{-1}) and plane wave simplification

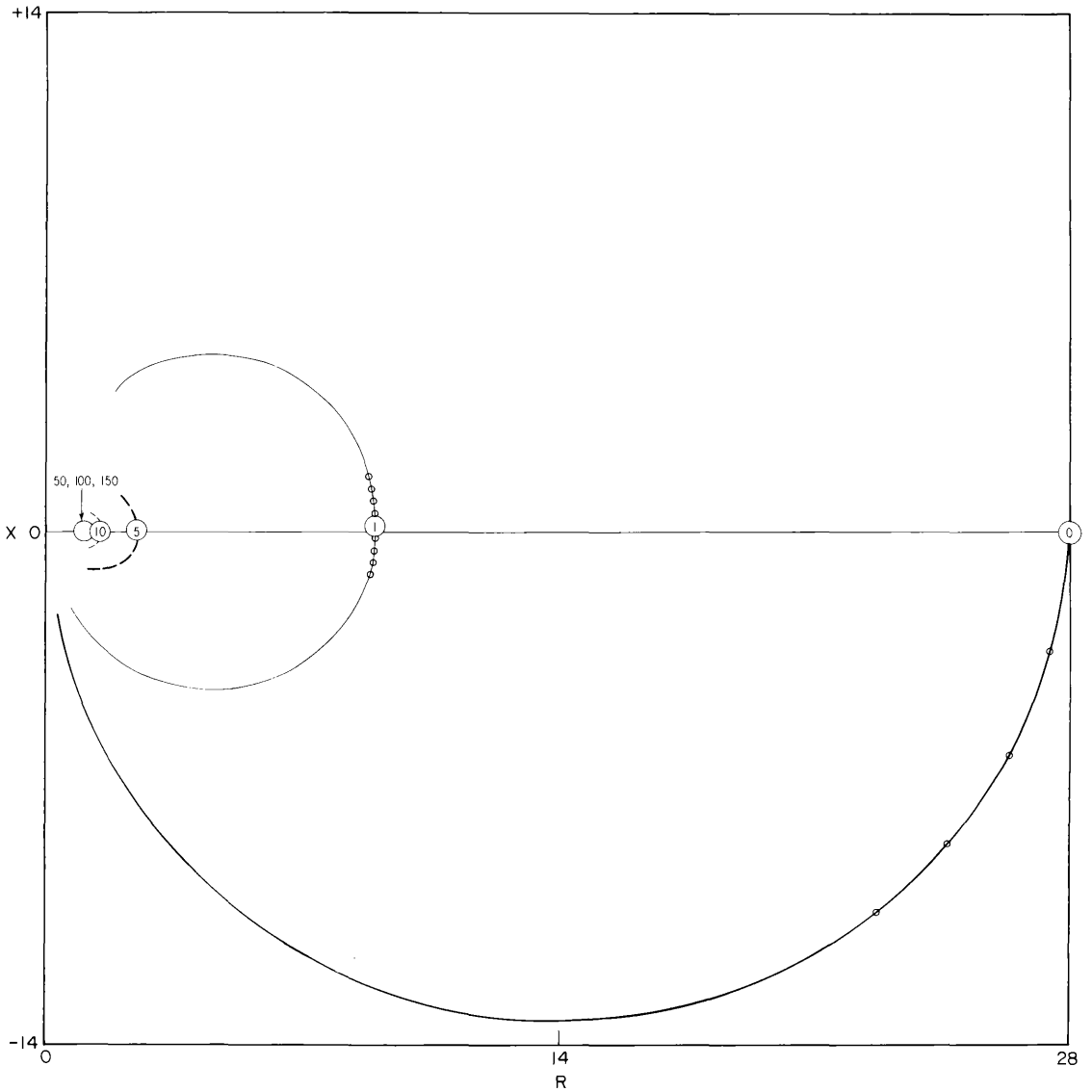

Fig. 15 – Plane wave circle diagram—real vs imaginary parts of impedance for parameter $\ell = n(\lambda_1/2) \pm 0.005$ cm with n = 0, 1, 5, 10, 50, 100, and 150 for the standard reference parameters of Table 1 (except α_1 = 1 cm^{-1} and $\alpha_3 = 10^{-3}$ cm^{-1}) and plane wave simplification

DIFFRACTED WAVE

Results

A number of impedance calculations have been made on the NAREC computer for various geometric parameters, frequencies, and radial boundary conditions. These will be detailed in the order of their appearance.

Figures 16* through 21 are plots of impedance versus the separation distance $\ell = n(\lambda_1^I/2) \pm 0.005$ cm, with separate plots for $n = 1, 5, 10, 50, 100$, and 150. These figures compare the parameter b/a values of 1 and 2 and otherwise are for the standard reference parameters of Table 1. Figures 16a-f are for the boundary condition of absolute rigidity and Figs. 17a-f are for infinitely flexible boundary conditions. Figures 18 and 19 are for liquid boundary conditions with the orthogonal assumption and the actual calculations, respectively, and Figs. 20 and 21 are likewise with the orthogonal assumption and the actual calculations for elastic solid boundary conditions.

Figures 22 through 25 are circle diagrams, that is, plots of the real vs the imaginary parts of the radiation impedance for the parameter $\ell = n(\lambda_1^I/2) \pm 0.005$ cm with $n = 0, 1, 5, 10, 50, 100$, and 150. Separate plots are given for individual values of b/a for specified boundary conditions and otherwise the standard reference parameters of Table 1 are used. Figures 22a-e are circle diagrams for absolutely rigid boundary conditions and present separate plots for $b/a = 1, 1.1, 2, 5$, and 10. Figures 23a-d are circle diagrams for infinitely flexible boundary conditions and include plots for $b/a = 1, 2, 5$, and 10. Figures 24a-f are circle diagrams for liquid boundary conditions with plots for $b/a = 1, 2, 5$, and 10 and include both orthogonal assumption and actual results for the values $b/a = 1$ and 2. Figures 25a-j are circle diagrams for elastic solid boundary conditions with b/a values of 1, 1.1, 2, 5, 10, 20, and 50, including plots for both orthogonal assumption and actual calculations with $b/a = 1, 1.1$, and 2.

Figures 26 through 29 are the same sort of circle diagrams as the previous figures but now for $k_1^{III}a = 60\pi$ instead of $k_1^I a = 20\pi$ as was true for Figs. 22 through 25. Because the same values of ℓ were used, the plots are now for $\ell = n(\lambda_1^{III}/2) \pm 0.005/3$ cm with $n = 0, 3, 15, 30, 150, 300$, and 450. Figures 26a-d are for rigid boundary conditions with $b/a = 1.1, 2, 5$, and 10. Figures 27a-d are for flexible boundary conditions with $b/a = 1, 2, 5$, and 10. Similarly, Figs. 28a-e are for liquid boundary conditions with $b/a = 1, 2, 5$, and 10; included here are orthogonal assumption and actual function plots for $b/a = 1$ only as machine storage space limitation prevented higher comparisons. Figures 29a-g are similarly for elastic solid boundary conditions with $b/a = 1, 1.1, 2, 5$, and 10, including the actual and orthogonal assumption results for $b/a = 1$ and 1.1 only.

Figures 30 through 33 again are the same sort of circle diagrams, but now for $k_1^V a = 100\pi$ with the same $\ell = n(\lambda_1^V/2) \pm 0.001$ cm so that $n = 0, 5, 25, 50, 250, 500$, and 750. Figures 30 are for absolutely rigid boundary conditions with $b/a = 1.1, 2, 5$, and 10. Figures 31 are for infinitely flexible boundary conditions with $b/a = 1, 2, 5$, and 10. Figures 32 are liquid boundary condition plots for $b/a = 1, 2, 5$, and 10 and Figures 33 are $b/a = 1, 1.1, 2, 5$, and 10 for elastic solid boundary conditions. The latter two figures are from orthogonal assumption calculations only because of machine storage limitations.

Figures 34 through 37 are circle diagrams for $b/a = 2$ and the four boundary conditions considered with the introduction of attenuation into both the guide medium (medium I) and the reflector medium (medium III). A realistic attenuation coefficient of $\alpha_3 = 10^{-3}$ cm^{-1} has been attributed to the reflector material, and attenuation coefficients considered for the guide medium include $\alpha_1 = 10^{-3}, 10^{-2}, 10^{-1}$, and 1 cm^{-1}. Figures 34 through 37 are for boundary conditions, respectively, of absolute rigidity, infinite flexibility, liquid, and elastic solid, all with $k_1^I a = 20\pi$.

*Figures 16 through 37 are located at the end of this report.

Discussion

Obviously the results for a plane wave in a nonattenuating medium are such that the fiducial $n(\lambda/2)$ points correspond exactly to the standard imposed characteristics of zero phase, maximum resistance, and maximum impedance. In fact the correspondence is to all three imposed characteristics simultaneously. As we have pointed out previously, and as readily seen from Figs. 8 through 15, the attribution of nominal absorption coefficients to the guide liquid and the reflector medium do not change this observation, and the only effect is the replacement of the single circle in the z plane by a spiral converging on the point 1, 0. Each loop of the spiral corresponds to a single value of $n(\lambda/2)$, and the nature of the variation of ℓ along the loop is such that the points are compressed for small R and expanded for large R. We also note that the curves comparing reflector medium absorption coefficients α_3 of zero and 10^{-3} cm^{-1} are identical. But for the somewhat unrealistic guide liquid medium attenuation coefficient of 1 cm^{-1}, which for $ka = 20\pi$ corresponds to an absorption per wavelength $\alpha\lambda = 0.15$, we note that the fiducial $n(\lambda/2)$ points have been pushed above the real axis. That is, the fiducial $n(\lambda/2)$ points occur at a value of ℓ smaller than that which the imposed characteristic of zero phase yields. Turning this about, the values of ℓ given by the imposed characteristic of zero phase are greater than the ℓ for the corresponding $n(\lambda/2)$ points, and thus the apparent wavelengths or sound speeds calculated for this condition would be greater than the true specified value. Since the three imposed characteristics of zero phase, maximum R, and maximum Z coincide for the perfect circle obtained for a plane wave in a nonattenuating medium, we might expect them to occur reasonably together even with attenuation, and thus obtain apparent wavelengths greater than the plane wave value specified for all three imposed characteristics. However, even though the fiducial $n(\lambda/2)$ points are pushed above the real axis, while zero phase by definition occurs on the axis, we find that the extremely rapid shrinking of the spiral for the larger guide liquid attenuation coefficient has resulted in a pushing up by an even greater amount of the "center" of the circle which is approximated by an individual loop of the spiral. Thus there is an opposing effect, which may cancel or even dominate, resulting in apparent wavelengths greater than the plane wave defined value for the imposed characteristics of maximum R and maximum Z. In particular by referring to the actual calculations and/or to enlarged figures corresponding to 10-ft-diam plots, although most of the circle diagrams were originally drawn on 30-in. square sheets, we find that the following apparent sound speeds (in m/s) are calculated in the n intervals of 0 to 1, 1 to 5, and 5 to 10, respectively: for zero phase, 1500.860, 1500.990, and 1501.584; for maximum R, 1500.000, 1499.840, and 1499.980; and for maximum Z, 1500.000, 1498.820, and 1499.904. These results appear to indicate that the extremum, rather than zero phase, are the preferred imposed characteristics. But it is well to note that the effect of absorption on a plane wave, which can be considered a single mode, should not be the result expected as the effect of absorption on diffracted waves, which are the result of a summation of several, often very many, modes. Since absorption acts to preferentially attenuate the higher order, more complex modes, a net result of accentuation of the lower order, more plane, modes should be expected, and increased planarity of the wavefronts with increasing ℓ should be observed. The results of actual calculations concerning this point will be detailed later. For now we return to the figures as numbered. Figures 16a-b show graphically the coincidence of maximum R and zero X at the same, in fact the fiducial, $n(\lambda/2)$ point for the unrealistic case of absolutely rigid boundary conditions with $b/a = 1$. The individual figures demonstrate how this observation for $b/a = 1$ is unchanged for larger values of n, but they also indicate the manner in which the often-referred-to "satellite" peaks appear at greater distances when $b > a$, or here specifically for $b/a = 2$. An interesting observation, which is apparently at variance with the concept that each successively higher mode is monotonically excited less, is that the smaller peak remains centered about the fiducial $n(\lambda/2)$ point for each n while the larger peak moves to greater separations in the positive ℓ direction from the fiducial point. But this observation is misleading and is an accident here because of the specified parameters.

Other graphs, for larger b/a ratios, do show a peeling off of satellite peaks in increasing number and an increasing shift in the positive ℓ direction; also, the amplitude decreases for increasing n. This behavior is also obvious in the circle diagrams, which will be discussed later. These peak figures are presented not only because of their historical interest, but because some features (not the most important, however) of the imposed characteristic variations can be seen more readily from this representation.

As is obvious from the figures thus far, and as has been stressed in the previous reports of this series, the effects of diffraction on a continuous wave iterative reflection scheme are such that the errors in apparent wavelength, if they exist, are usually in the positive direction; that is, if an error exists, the apparent wavelength or sound speed is too large numerically. This is in contrast to the effects of diffraction on time-of-flight or other group or signal velocity techniques where the errors are such as to yield values of sound speed too small. It should not be necessary to repeat that time-of-flight schemes are direct measurements of sound speed while iterative reflection interferometric schemes directly measure wavelength. Figures 17a-f which are the same type plots as Figs. 16 except for the change in boundary conditions to infinite flexibility, show a somewhat different behavior. For this boundary condition the plane wave mode $X_{0m} = 0$ is not one of those permitted, as may be seen by perusal of Tables 2, 3, 4 and 6 of Ref. 2. From those tables we note the interlacing of the individual modes for the respective boundary conditions. That is, the X values increase monotonically for the four boundary conditions and then repeat in the same manner with the exception of the zero mode, which exists only for absolutely rigid boundary conditions. For example, rounding off the numbers in these tables, we find sets of modes, in the order of boundary conditions of liquid, infinitely flexible, elastic, and absolutely rigid, with the following values: for the first mode, 2.27, 2.40, 3.04, 3.83; for the second mode, 5.22, 5.52, 6.53, 7.01; for the third mode, 8.20, 8.65, 9.83, 10.17; etc.

Thus in Figs. 17, for flexible boundary conditions, no peak remains centered about the $n(\lambda/2)$ fiducial point as n increases, as was the case for the absolutely rigid boundary conditions when $b/a = 1$. Indeed the first peak moves beyond the range of the graphs for n slightly greater than 50, as can be seen by comparing Figs. 17d and 17e. In Fig. 17d the usual "peeling off" of "satellites" or subsiduary peaks displaced to the right and of smaller amplitude than the main peak is nicely demonstrated.

Figures 18, for liquid boundary conditions, resemble Figs. 17 except that the shifts of the peaks away from the fiducial points are less than they are for the flexible boundary conditions. This observation holds for both $b/a = 1$ and $b/a = 2$. These figures are drawn from calculations based on an orthogonal assumption of the characteristic functions, but a comparison of them with Figs. 19a-f shows no significant difference from the results for the actual calculations made by not invoking orthogonality. A similar observation of no change in the results obtained by exact calculation rather than by the orthogonal assumption calculation is made in comparing Figs. 20 and 21, which are for the elastic solid boundary condition. This behavior is unlike that found in the previous report of this series (3), which involved guided mode propagation in cylinders with no end termination and thus no iterative reflection, and for which real differences were observed in the end calculations made both ways.

Also from Figs. 20a-f and 21a-f it is noticed that the peaks are displaced greater distances to the right of the fiducial $n(\lambda/2)$ points for this elastic boundary condition than are the peaks for the flexible boundary condition. They are thus also displaced more than for the liquid boundary condition. In fact, as the respective modes X_{0m} themselves indicate, it should be expected that the displacements above the fiducial points would be increased for the various boundary conditions in the following order: liquid, infinitely flexible, elastic, and rigid. The restricted presence of the zero mode to the rigid boundary condition, however, moves this case to the head of the list so the actual observed order of increasing shift is rigid, liquid, infinitely flexible, and elastic.

We now turn our attention to the plots in the impedance plane, referred to as circle diagrams. These plots use 150 points calculated for each loop so that the range of the parameter ℓ is greater than that arbitrarily selected for the peak or reaction curve plots. Specifically, for the $ka = 20\pi$ curves, the range of ℓ for each $n(\lambda/2)$ is $+0.010$ cm and -0.005 cm in steps of 0.0001 cm. Some of the circle diagram plots continue even beyond this range when the subsidiary loops or cardiod-like behavior of the primary loops appeared to warrant further investigation. These diagrams, it should be noted, are used (not in this report) for direct comparison with the experimental plots either photographed from the oscilloscope of an Alford impedance plotter of recorded on an accessory 10-in.-square X-Y recorder.

We will later show tables of apparent sound speed calculated from these circle diagrams and based on the individual imposed characteristics of zero phase, maximum R, and maximum Z. These tables are obtained by direct measurements on the original 30-in.-square plots, with reference as necessary to the actual calculations. In order to permit the reader to satisfy himself as to the imposed characteristic values of ℓ read from the circle diagrams and listed in the tables, the actual plotted points are shown on the circle diagrams where necessary and if possible (remember that the variations with ℓ are compressed for small z). It could bear repeating here that Figs. 22 through 25 are for $k^{\mathrm{I}}a = 20\pi$, Figs. 26 through 29 are for $k^{\mathrm{III}}a = 60\pi$, and $k^{\mathrm{V}}a = 100\pi$ is shown in Figs. 30 through 33. The same values of $\ell = n(\lambda/2)$ were used for all ka, namely $\ell = 0$, 0.075, 0.375, 0.750, 3.750, 7.500, and 11.250 cm, so that the n for λ^{I} are 0, 1, 5, 10, 50, and 150; the n for λ^{III} are 0, 3, 15, 30, 150, 300, and 450; and the n for λ^{V} are 0, 5, 25, 50, 250, and 750. For λ^{I} the ℓ range is $+0.010$ cm and -0.005 cm with point intervals of 0.0001; for λ^{III} the ℓ range and the point intervals are both reduced to one-third that for λ^{I}; for λ^{V} the ℓ range is $+0.002$ cm and -0.001 cm with point intervals of 0.00002 cm. The fiducial $n(\lambda/2)$ points on the circle diagrams are shown as larger point circles with the particular n enclosed. The reader may determine his own ℓ for the selected imposed characteristics by counting the points along the loop from the fiducial $n(\lambda/2)$ to the imposed characteristic, using the appropriate values of ℓ from the above, and interpolating the end point. It is easily shown (4) that the criterion for no error in the wavelength determination is not that the imposed characteristics of maximum R have the same ℓ as the imposed characteristics of zero phase (so that they are common with the points for the imposed characteristic of maximum Z), but rather that the curve joining the various n of a single imposed characteristic describe an orthogonal trajectory to the loops of the circle diagram. Of course, maximum R coinciding with zero phase, and hence also with maximum Z, is simply a limiting case of this orthogonal trajectory.

Figure 22a is just a circle repeating endlessly in ℓ with all $n(\lambda/2)$ points superimposed. Of course, this is the simple result expected for the unrealistic boundary condition of absolute rigidity and $b/a = 1$ where theoretically the plane wave mode is the only one that may be propagated. But, even so small a variation as $b/a = 1.1$ changes the character of the diagram so that the loops are separated through the value $n = 10$. Figures 22b-e show the appearance of satellites or subsidiary loops. The aberrations increase up to about $b/a = 1.75$ and then decrease with larger b/a. It can be noted that the wavelength errors here are much reduced over the nonterminated situation discussed in Ref. 2. There, essentially free-field results were obtained for $b/a > 2$, while here the results approach that of a plane wave as b/a increases. This is a powerful advantage of iterative reflection.

Figures 23a-d indicate that with flexible boundary conditions the maximum abberation occurs at $b/a = 1$ (a consequence of the fact that the plane wave mode is not permitted). Here too it is noticed that the subsidiary loops that occur after the fiducial $n(\lambda/2)$ point are smaller than the main loops, unlike the situation for rigid boundaries where the secondary loops were larger. A comparison of the $b/a = 2$ curves for rigid boundary conditions (Fig. 22c) and flexible boundary conditions (Fig. 23b) shows the marked difference in the nature of the curves for these two boundary conditions. But comparing Figs. 22d and 23c for $b/a = 5$ shows that the

plots are becoming similar, while the $b/a = 10$ plots in Figs. 22e and 23d are virtually indistinguishable.

The liquid boundary condition plots of Figs. 24a-f reiterate the previous observation that the final results of erroneously invoking orthogonality are identical to those obtained by the correct calculations. Here again the maximum aberration occurs for $b/a = 1$, though the effect is smaller than found for flexible boundaries. But the infinitely flexible and liquid boundary condition plots resemble each other closely even for $b/a = 2$ and are nearly indistinguishable for $b/a = 5$. For $b/a = 10$ we find the impedance circle diagrams to be almost identical for rigid, flexible, and liquid boundary conditions.

The elastic boundary condition plots of Figs. 25a-j again show no difference between the final results calculated by the correct procedure and those utilizing the erroneous orthogonal assumption simplification, except for the single case of $b/a = 1$ where the fiducial $n(\lambda/2)$ points for $n = 100$ appear drastically shifted. It will be seen later that the imposed characteristic points lie the same distance ℓ away from the fiducial points in both plots, and so no differences are observed in apparent wavelengths. It is recalled that the elastic boundary condition plots were the only ones that showed a difference between the orthogonal assumption and actual plots in the nonterminated situation of Ref. 2, and then only for $b/a < 1.5$. Like flexible and liquid boundary conditions, the maximum error occurs at $b/a = 1$ for elastic solid boundaries. As was the case for the noniterative reflection or nonterminated situation of Ref. 2, we find that $b/a = 1$ with this realistic elastic solid boundary condition yields the largest aberration of all the conditions considered. These elastic boundary condition plots generally do not resemble those for any of the other boundary conditions, with the exception that the $b/a = 10$ circle diagrams for all four boundary conditions are almost identical. With the single exception of the large error for rigid boundary conditions with $b/a = 2$, the aberration at a given b/a is largest for the elastic solid boundary condition.

As has been generally true, except for the rigid boundary condition for b/a between 1 and 2, the situation improves with increasing b/a. Continuing with the circle diagrams we find that Figs. 26a-d for rigid boundary conditions with $ka = 60\pi$ indicate that the effect of increasing frequency is to decrease the aberration. The subsidiary and major loops for each n found for $ka = 20\pi$ have here merged into one loop, with at most a single cusp. The $n(\lambda/2)$ fiducial points are given for the same ℓ as before so that the respective n are now multiplied by three. Also, the points are separated by one-third the distance between those on the $ka = 20\pi$ plots so that a cursory inspection and comparison of the figures with respect to the number of points between the fiducial points and the imposed characteristic points will immediately indicate the direction of change of the aberration. The flexible boundary condition plots in Figs. 27a-d show the same trend of a decreasing aberration as ka increases. The $b/a = 2$ diagram has somewhat larger satellites than expected, but this has little effect on the apparent wavelength. Again, increasing b/a improves the situation.

Figures 28a-e are similar to Figs. 27a-d except for $b/a = 2$. The respective curves are again similar for both boundary conditions when $b/a = 5$ and when $b/a = 10$. No difference is noted in the orthogonal assumption and actual curves for $b/a = 1$.

The circle diagrams for elastic solid boundary conditions in Figs. 29a-g do not show the small difference between the orthogonal assumption and actual curves for $b/a = 1$ found when $ka = 20\pi$. Again the aberration is significantly larger for this boundary condition than for the others, and again the larger b/a have the smaller aberration.

In general, the $ka = 60\pi$ circles display more of a plane wave nature than do the $ka = 20\pi$ circles. The $ka = 100\pi$ circles of Figs. 30 through 33 carry this trend further. While the $ka = 20\pi$ circle diagrams become nearly identical for the four boundary conditions at $b/a = 10$, the $ka = 60\pi$ circles become similar at $b/a = 5$, and the four boundary conditions plots for $ka = 100\pi$ are nearly alike at $b/a = 2$. Apparently the value of kb, which is the product of ka and b/a, is important here and its significance will be discussed later.

Before indicating and discussing the numerical results of apparent wavelength read from the original large drawings of Figs. 22 through 37, we will indicate the effect of intrinsic absorption of the guide liquid medium. The results shown are for the reference situation of $b/a = 2$ only, with a ka parameter of 20π and α_1 values of 0.001, 0.01, 0.1, and 1 cm^{-1}. A realistic attenuation coefficient of 0.001 cm^{-1} has been attributed to the reflector, although the plane wave results showed no difference between the cases of $\alpha_3 = 0$ and $\alpha_3 = 0.001$ cm^{-1}.

The "a" plots of Figs. 34 through 37, by individual and respective comparison with Figs. 22c, 23b, 24c, and 25e, show that the value 10^{-3} cm^{-1} for the absorption coefficient α_1 has but little effect on the shape of the loops. Since this value is already much higher than that for water at a frequency of 1 MHz it is apparent that absorption, per se, is not significant in the determination of sound speed in water by interferometry at such frequencies. Indeed the absorption coefficient for water is only about twice this value at 3 MHz and about six times this value at 5 MHz so that but little effect from a realistic attenuation coefficient for water is expected at the ka values considered in this report. The higher values of α_1 shown in Figs. 34 through 37 obviously apply to liquids more attenuating than water. Since some experimental values quoted for some liquids are more than 1000 times greater than the absorption coefficient for water, it is apparent that the wide range of α_1 considered here is not excessive. The rapid increase in the rate of shrinkage of the loops with increasing attenuation is evident from these plots.

It should be recalled, however, that the introduction of absorption into the formulation of this report was done in a naive manner, that is, absorption was assumed to affect the propagation of the various modes down the cylinder but not to affect the determination of the modes themselves. This simplification will be removed in a forthcoming report where absorption is introduced by attributing a viscosity to the cylinder liquid. It is anticipated that absorption will be beneficial inasmuch as it should selectively discriminate against the higher order, more complex modes.

APPARENT SOUND SPEEDS

Tables 2 through 78 display the reflector-to-source separations ℓ corresponding to specified orders n of the imposed characteristics of zero phase, maximum resistance R, and maximum impedance Z, respectively. The n are 1, 5, 10, 50, 100, and 150 for $ka = 20\pi$; 3, 15, 30, 150, 300, and 450 for $ka = 60\pi$; and 5, 25, 50, 250, 500, and 750 for $ka = 100\pi$, corresponding in each case to nominal separations of 0.075, 0.375, 0.750, 3.750, 7.500, and 11.250 cm, respectively. The apparent sound speeds calculated from the successive intervals (such as 0 to 0.075 cm, 0.075 to 0.375 cm, etc.) are also tabulated along with the error, in parts per million (ppm), between these tabulated values and the assumed reference value of 1500 m/s.

CONCLUSIONS

The ultrasonic interferometer has decided advantages over pulsing techniques for determinations of absolute sound speed. Although the technique of utilizing acoustic path differences employed in interferometry can be carried over to pulsing methods, the interferometer requires in addition but a simple measurement of frequency as opposed to a more difficult measurement of time interval.

For enhanced specification of pertinent physical parameters, a limited sample in a small enclosure is desirable, and in fact appears mandatory for a large variation in the hydrostatic pressure parameter. For simplicity, a circular-cross-section container is used, and cylindrical guided modes rather than a free-field description is appropriate. Parallel surfaces, concentric with and normal to the cylinder axis, for both the acoustic source and the reflector simplify the determination of acoustic path.

In interferometry, the manifold interference through iterative reflection yields a resultant line sharpening or an effective increased planarity of the wave fronts in comparison to a non-terminated or pulsing situation. The results for increased b/a (the cylinder-to-source radius ratio) approach that of a plane wave in the case of iterative reflection, while in Ref. 2 the approach was to free-field diffraction for $b/a > 2$. However, planarity improves as ka $(=2\pi/\lambda)$ increases for both cases. This is accomplished by an increase in either the source radius, the frequency, or the sound speed in the medium. But measurements are not made routinely at the highest attainable frequency simply because results over a determined frequency range are required in order to investigate intrinsic properties of the medium such as velocity dispersion or relaxation phenomena, in particular the chemical relaxation occuring in natural sea water.

A reflector with infinite or zero impedance would increase the sensitivity of response of the interferometer; the maximum impedance ratio of a metal reflector to the medium is about 30 (28 is used in this report as a standard condition), but an air reflector yields an inverse ratio of 5000. The use of an air reflector, however, is undesirable from the standpoints of non-quiescence and nonplanarity of the boundary, as well as severe complications in realizing an appreciable variation in the hydrostatic pressure parameter.

The aberrations to plane wave results generally increase in the order of rigid, liquid, flexible, and elastic boundary conditions, the plane wave or zero mode existing only for the unattainable situation of absolutely rigid boundary conditions. As was true for the noniterative reflection case, no significant difference was found between the orthogonal assumption simplification and the exact calculations, except for elastic boundary conditions with $b/a = 1$. Maximum aberrations occur at $b/a = 1$ for flexible, liquid, and elastic boundary conditions and at $b/a = 1.75$ for rigid boundaries. The $b/a \geq 2$ plots are indistinguishable for flexible and liquid boundary conditions, and all the $b/a = 10$ plots are remarkably similar, while the rigid and flexible boundary condition plots for $b/a = 2$ could not be more dissimilar.

The effect of absorption on plane wave results is nil except for the large value $\alpha = 1\ \mathrm{cm}^{-1}$, where the zero phase imposed characteristic yields too large an effective wavelength. The opposing absorption-attributable errors in both the maximum R and maximum Z imposed characteristics either cancel or yield too small effective wavelengths for plane waves. Generally, the plane wave absorption results indicate that the maxima, rather than zero phase, are preferred imposed characteristics. All the results further select maximum Z as the most satisfactory imposed characteristic.

The decreasing error with increasing b/a appears to reach a minimum level for the realistic elastic solid boundary conditions. Specifically, the minimum error apparently occurs at kb $(= ka \times b/a) \approx 200\pi$. For $ka = 20\pi$ this indicates that $b/a = 10$, and for $ka = 100\pi$ the minimum error is already attained at the low value of $b/a = 2$. In this latter case, the calculated error in wavelength is 6 ppm, which corresponds to 0.01 m/s for water sound speeds. A thesis to be further tested experimentally, and apparently borne out in Ref. 4, is that a large effective b/a is obtained by deliberately destroying cylindrical symmetry, which minimizes the effect of radial boundaries by increasing the chaotic mutual interference of undesired modes.

In general, the error decreases with increased b/a, increased k, increased a, increased ρ_3/ρ_1, and increased k_1/k_3.

FUTURE WORK

This third theoretical report in this series will be followed by one dealing with noniterative propagation within liquid cylinders contained in shells, both liquid and elastic. Another report, introducing viscosity into the formulation in order to more adequately deal with viscous absorption, is in preparation. Since the experimental work is proceeding apace, it will undoubtedly appear before the final theoretical report.

ACKNOWLEDGMENTS

The author wishes to acknowledge the encouragement of Dr. R. L. Steinberger during the preparation of this report, the excellent work of Mr. R. E. McGill who again programmed the calculations for NAREC, the stimulating discussions with Mr. W. F. Walker and Mr. L. P. LaLumiere, who also did much of the graph reading and calculating, and the assistance of Mrs. Bertha Test for much of the plotting.

REFERENCES

1. Del Grosso, V. A., "Systematic Errors in Ultrasonic Propagation Parameter Measurements, Part 1 – Effect of Free-Field Diffraction," NRL Report 6026, Jan. 1964.
2. Del Grosso, V. A., "Systematic Errors in Ultrasonic Propagation Parameter Measurements, Part 2 – Effects of Guided Cylindrical Modes," NRL Report 6133, Jan. 1965.
3. Del Grosso, V. A., "The Velocity of Sound in Sea Water at Zero Depth," NRL Report 4002, June 1952.
4. Del Grosso, V. A., and Smura, E. J., "Materials Suitable for Sound Applications, Part 1 – Ultrasonic Velocities and Impedances of Selected Liquids," NRL Report 4191, Sept. 1953.

This page intentionally left blank.

FIGURES 16 – 37

Fig. 16 – Real and imaginary parts of impedance $Z = R + iX$ vs source-to-reflector separation $\ell = n(\lambda_1/2) \pm 0.005$ cm for standard reference parameters in Table 1 (except $b/a = 1$ and 2) and absolutely rigid boundary conditions: (a) $n = 1$, (b) $n = 5$, (c) $n = 10$, (d) $n = 50$, (e) $n = 100$, and (f) $n = 150$

Fig. 17 – Real and imaginary parts of impedance $Z = R + iX$ vs source-to-reflector separation $\ell = n(\lambda_1/2) \pm 0.005$ cm for standard reference parameters in Table 1 (except $b/a = 1$ and 2) and infinitely flexible boundary conditions: (a) $n = 1$, (b) $n = 5$, (c) $n = 10$, (d) $n = 50$, (e) $n = 100$, and (f) $n = 150$

Fig. 18 – Real and imaginary parts of impedance $Z = R + iX$ vs source-to-reflector separation $\ell = n(\lambda_1/2) \pm 0.005$ cm for standard reference parameters in Table 1 (except $b/a = 1$ and 2) and liquid boundary conditions with orthogonal functions assumed; (a) $n = 1$, (b) $n = 5$, (c) $n = 10$, (d) $n = 50$, (e) $n = 100$, and (f) $n = 150$

Fig. 19 – Real and imaginary parts of impedance $Z = R + iX$ vs source-to-reflector separation $\ell = n(\lambda_1/2) \pm 0.005$ cm for standard reference parameters in Table 1 (except $b/a = 1$ and 2) and liquid boundary conditions with "actual" functions used; (a) $n = 1$, (b) $n = 5$, (c) $n = 10$, (d) $n = 50$, (e) $n = 100$, and (f) $n = 150$

Fig. 20 – Real and imaginary parts of impedance $Z = R + iX$ vs source-to-reflector separation $\ell = n(\lambda_1/2) \pm 0.005$ cm for standard reference parameters in Table 1 (except $b/a = 1$ and 2) and elastic solid boundary conditions with orthogonal functions assumed; (a) $n = 1$, (b) $n = 5$, (c) $n = 10$, (d) $n = 50$, (e) $n = 100$, and (f) $n = 150$

Fig. 21 – Real and imaginary parts of impedance $Z = R + iX$ vs source-to-reflector separation $\ell = n(\lambda_1/2) \pm 0.005$ cm for standard reference parameters in Table 1 (except $b/a = 1$ and 2) and elastic solid boundary conditions with "actual" functions used; (a) $n = 1$, (b) $n = 5$, (c) $n = 10$, (d) $n = 50$, (e) $n = 100$, and (f) $n = 150$

Fig. 22 – Circle diagrams of real vs imaginary parts of impedance for parameter $\ell = n(\lambda_1^I/2) \pm 0.005$ cm with $n = 0, 1, 5, 10, 50, 100$, and 150 for the standard reference parameters of Table 1 (except the b/a ratios) and absolutely rigid boundary conditions; (a) $b/a = 1$, (b) $b/a = 1.1$, (c) $b/a = 2$, (d) $b/a = 5$, and (e) $b/a = 10$

Fig. 23 – Circle diagrams of real vs imaginary parts of impedance for parameter $\ell = n(\lambda_1^I/2) \pm 0.005$ cm with $n = 0, 1, 5, 10, 50, 100$, and 150 for the standard reference parameters of Table 1 (except the b/a ratios) and infinitely flexible boundary conditions; (a) $b/a = 1$, (b) $b/a = 2$, (c) $b/a = 5$, and (d) $b/a = 10$

Fig. 24 – Circle diagrams of real vs imaginary parts of impedance for parameter $\ell = n(\lambda_1^I/2) \pm 0.005$ cm with $n = 0, 1, 5, 10, 50, 100$, and 150 for the standard reference parameters of Table 1 (except the b/a ratios) and liquid boundary conditions; (a) $b/a = 1$ (orth fns), (b) $b/a = 1$ (actual fns), (c) $b/a = 2$ (orth fns), (d) $b/a = 2$ (actual fns), (e) $b/a = 5$, and (f) $b/a = 10$

Fig. 25 – Circle diagrams of real vs imaginary parts of impedance with parameter $\ell = n(\lambda_1^{I}/2)$ ± 0.005 cm with $n = 0, 1, 5, 10, 50, 100$, and 150 for the standard reference parameters of Table 1 (except the b/a ratios) and elastic solid boundary conditions; (a) $b/a = 1$ (orth fns), (b) $b/a = 1$ (actual fns), (c) $b/a = 1.1$ (orth fns), (d) $b/a = 1.1$ (actual fns), (e) $b/a = 2$ (orth fns), (f) $b/a = 2$ (actual fns), (g) $b/a = 5$, (h) $b/a = 10$, (i) $b/a = 20$, and (j) $b/a = 50$

Fig. 26 – Circle diagrams of real vs imaginary parts of impedance for parameter $\ell = n(\lambda_1^{III}/2)$ $\pm 0.005/3$ cm with $n = 0, 3, 15, 30, 150, 300$, and 450 for the standard reference parameters of Table 1 (except $k_1^{III}a = 60\pi$ and various b/a ratios) and rigid boundary conditions; (a) $b/a = 1$, (b) $b/a = 2$, (c) $b/a = 5$, and (d) $b/a = 10$

Fig. 27 – Circle diagrams of real vs imaginary parts of impedance for parameter $\ell = n(\lambda_1^{III}/2)$ $\pm 0.005/3$ cm with $n = 0, 3, 15, 30, 150, 300$, and 450 for the standard reference parameters of Table 1 (except $k_1^{III}a = 60\pi$ and various b/a ratios) and infinitely flexible boundary conditions; (a) $b/a = 1$, (b) $b/a = 2$, (c) $b/a = 5$, and (d) $b/a = 10$

Fig. 28 – Circle diagrams of real vs imaginary parts of impedance for parameter $\ell = n(\lambda_1^{III}/2)$ $\pm 0.005/3$ cm with $n = 0, 3, 15, 30, 150, 300$, and 450 for the standard reference parameters of Table 1 (except $k_1^{III}a = 60\pi$ and various b/a ratios) and liquid boundary conditions; (a) $b/a = 1$ (orth fns), (b) $b/a = 1$ (actual fns), (c) $b/a = 2$, (d) $b/a = 5$, and (e) $b/a = 10$

Fig. 29 – Circle diagrams of real vs imaginary parts of impedance for parameter $\ell = n(\lambda_1^{III}/2)$ $\pm 0.005/3$ cm with $n = 0, 3, 15, 30, 150, 300$, and 450 for the standard reference parameters of Table 1 (except $k_1^{III}a = 60\pi$ and various b/a ratios) and elastic solid boundary conditions; (a) $b/a = 1$ (orth fns), (b) $b/a = 1$ (actual fns), (c) $b/a = 1.1$ (orth fns), (d) $b/a = 1.1$ (actual fns), (e) $b/a = 2$, (f) $b/a = 5$, and (g) $b/a = 10$

Fig. 30 – Circle diagrams of real vs imaginary parts of impedance for parameter $\ell = n(\lambda_1^{V}/2)$ ± 0.001 cm with $n = 0, 5, 25, 50, 250, 500$, and 750 for the standard reference parameters in Table 1 (except $k_1^{V}a = 100\pi$ and various b/a ratios) and absolutely rigid boundary conditions; (a) $b/a = 1.1$, (b) $b/a = 2$, (c) $b/a = 5$, and (d) $b/a = 10$

Fig. 31 – Circle diagrams of real vs imaginary parts of impedance for parameter $\ell = n(\lambda_1^{V}/2)$ ± 0.001 cm with $n = 0, 5, 25, 50, 250, 500$, and 750 for the standard reference parameters in Table 1 (except $k_1^{V}a = 100\pi$ and various b/a ratios) and infinitely flexible boundary conditions; (a) $b/a = 1$, (b) $b/a = 2$, (c) $b/a = 5$, and (d) $b/a = 10$

Fig. 32 – Circle diagrams of real vs imaginary parts of impedance for parameter $\ell = n(\lambda_1^{V}/2)$ ± 0.001 cm with $n = 0, 5, 25, 50, 250, 500$, and 750 for the standard reference parameters in Table 1 (except $k_1^{V}a = 100\pi$ and various b/a ratios) and liquid boundary conditions (a) $b/a = 1$, (b) $b/a = 2$, (c) $b/a = 5$, and (d) $b/a = 10$

Fig. 33 – Circle diagrams of real vs imaginary parts of impedance for parameter $\ell = n(\lambda_1^{V}/2)$ ± 0.001 cm with $n = 0, 5, 25, 50, 250, 500$, and 750 for the standard reference parameters in Table 1 (except $k_1^{V}a = 100\pi$ and various b/a ratios) and elastic solid boundary conditions; (a) $b/a = 1$, (b) $b/a = 1.1$, (c) $b/a = 2$, (d) $b/a = 5$, and (e) $b/a = 10$

Fig. 34 – Circle diagrams of real vs imaginary parts of impedance for parameter $\ell = n(\lambda_1^{I}/2)$ ± 0.005 cm with $n = 0, 1, 5, 10, 50, 100$, and 150 for the standard reference parameters of Table 1 (except $\alpha_3 = 10^{-3}$ cm^{-1} and various values of α_1) and absolutely rigid boundary conditions; (a) $\alpha_1 = 10^{-3}$ cm^{-1}, (b) $\alpha_1 = 10^{-2}$ cm^{-1}, (c) $\alpha_1 = 10^{-1}$ cm^{-1}, and (d) $\alpha_1 = 1$ cm^{-1}

Fig. 35 – Circle diagrams of real vs imaginary parts of impedance for parameter $\ell = n(\lambda_1^I/2) \pm 0.005$ cm with $n = 0, 1, 5, 10, 50, 100$, and 150 for the standard reference parameters of Table 1 (except $\alpha_3 = 10^{-3}$ cm^{-1} and various values of α_1) and infinitely flexible boundary conditions; (a) $\alpha_1 = 10^{-3}$ cm^{-1}, (b) $\alpha_1 = 10^{-2}$ cm^{-1}, (c) $\alpha_1 = 10^{-1}$ cm^{-1}, and (d) $\alpha_1 = 1$ cm^{-1}

Fig. 36 – Circle diagrams of real vs imaginary parts of impedance for parameter $\ell = n(\lambda_1^I/2) \pm 0.005$ cm with $n = 0, 1, 5, 10, 50, 100$, and 150 for the standard reference parameters of Table 1 (except $\alpha_3 = 10^{-3}$ cm^{-1} and various values of α_1) and liquid boundary conditions; (a) $\alpha_1 = 10^{-3}$ cm^{-1}, (b) $\alpha_1 = 10^{-2}$ cm^{-1}, (c) $\alpha_1 = 10^{-1}$ cm^{-1}, and (d) $\alpha_1 = 1$ cm^{-1}

Fig. 37 – Circle diagrams of real vs imaginary parts of impedance for parameter $\ell = n(\lambda_1^I/2) \pm 0.005$ cm with $n = 0, 1, 5, 10, 50, 100$, and 150 for the standard reference parameters of Table 1 (except $\alpha_3 = 10^{-3}$ cm^{-1} and various values of α_1) and elastic solid boundary conditions; (a) $\alpha_1 = 10^{-3}$ cm^{-1}, (b) $\alpha_1 = 10^{-2}$ cm^{-1}, (c) $\alpha_1 = 10^{-1}$cm^{-1}, and (d) $\alpha_1 = 1$ cm^{-1}

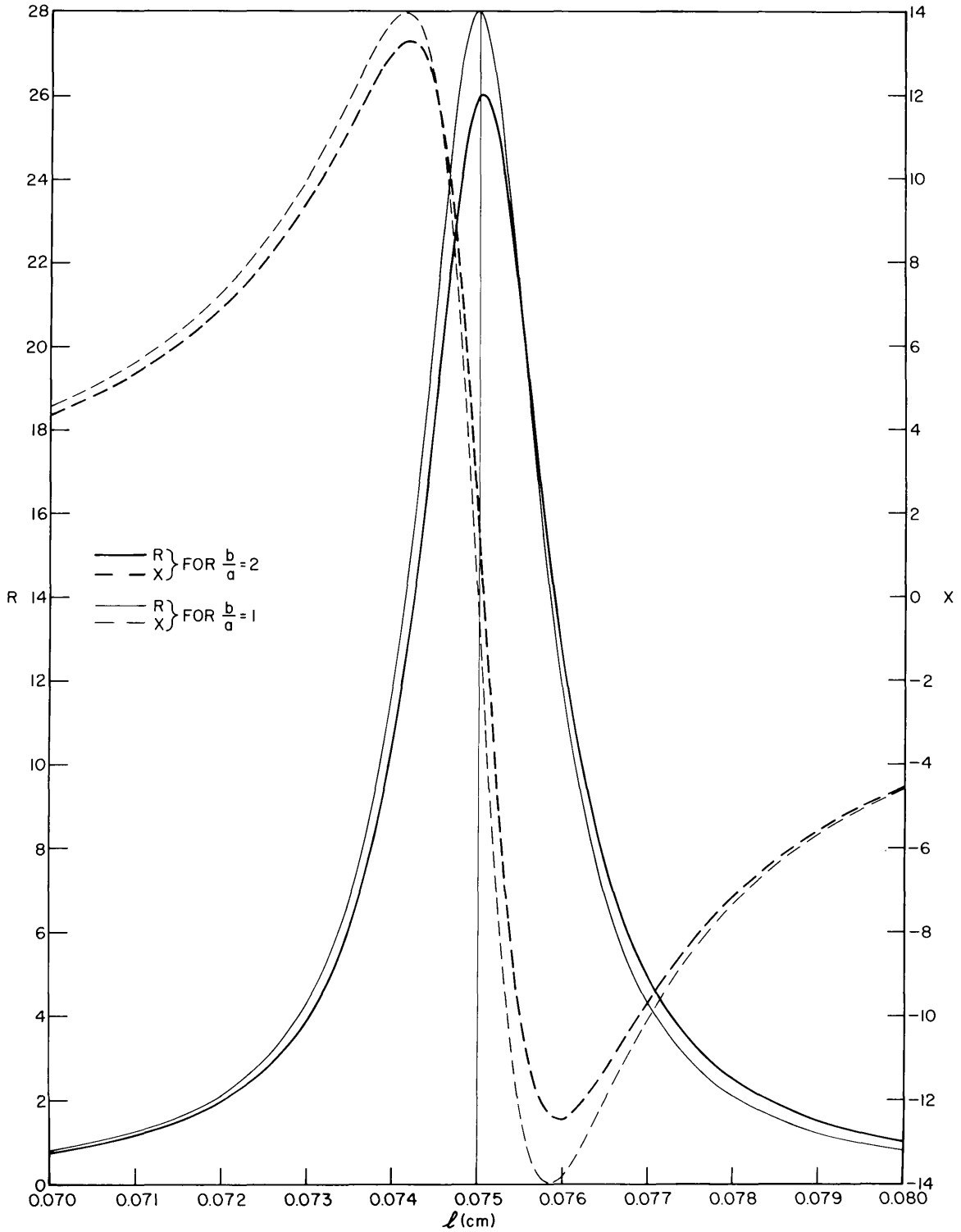

Fig. 16a—R and X vs ℓ for absolutely rigid boundary conditions and $n = 1$

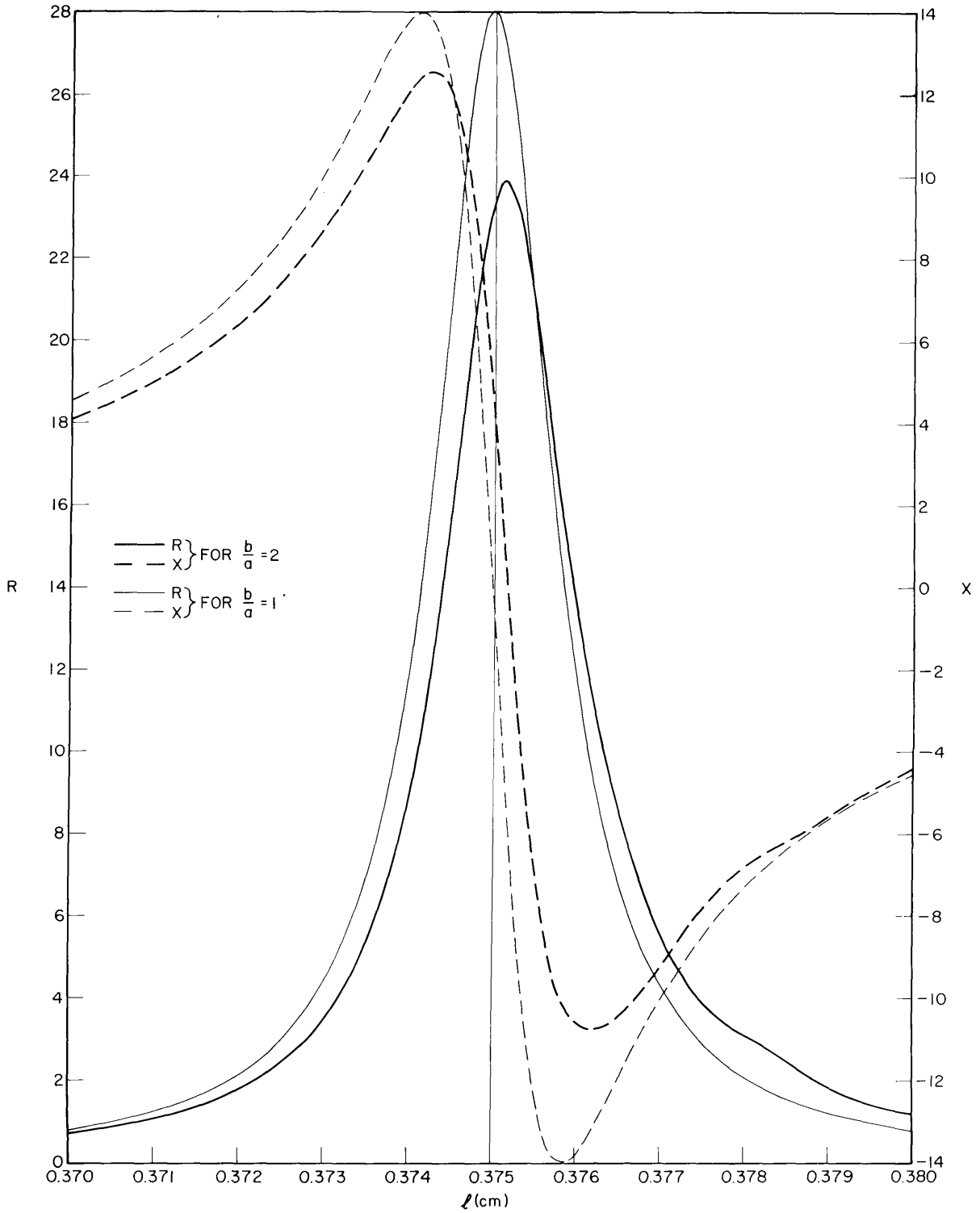

Fig. 16b—R and X vs ℓ for absolutely rigid boundary conditions and $n = 5$

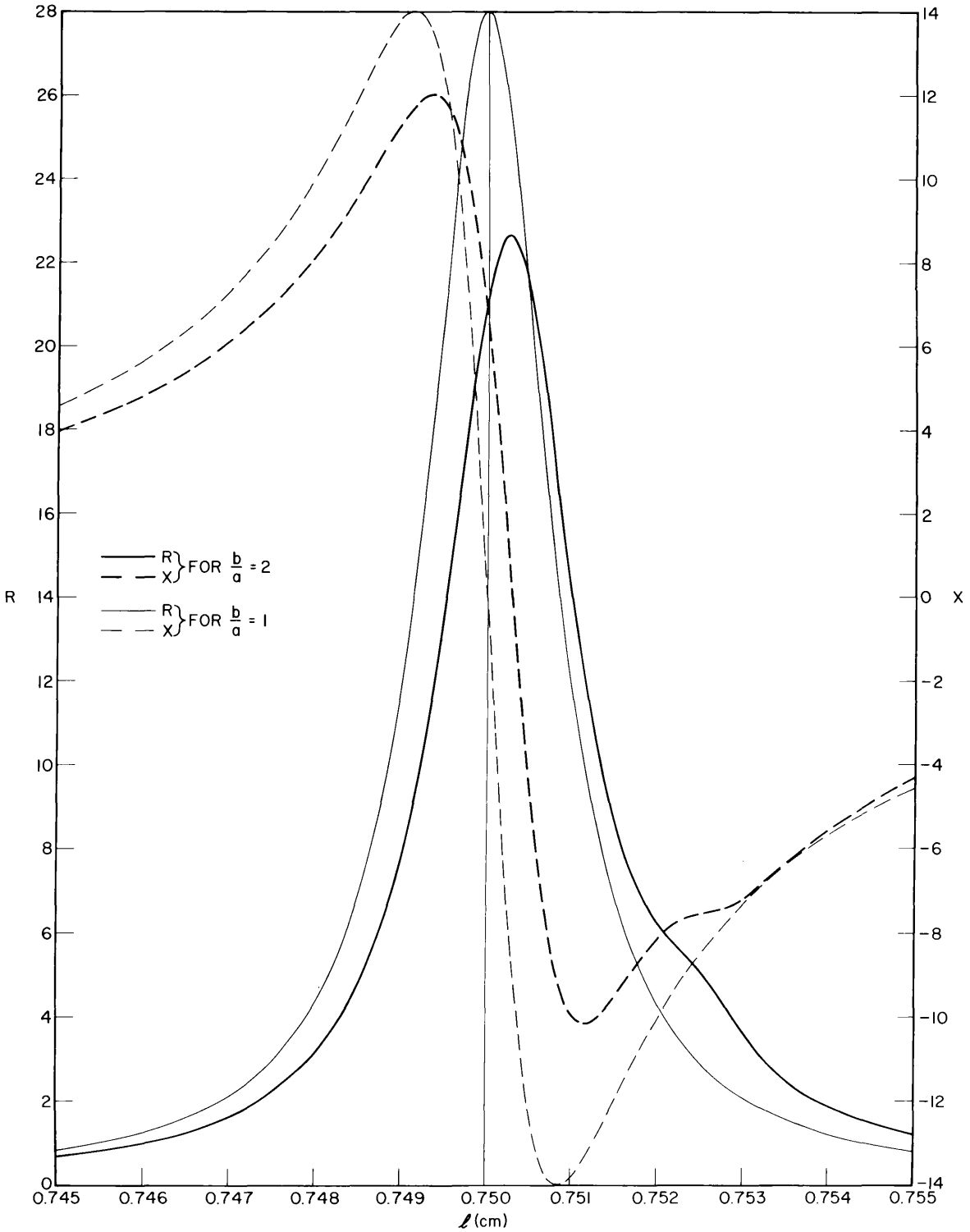

Fig. 16c—R and X vs ℓ for absolutely rigid boundary conditions and $n = 10$

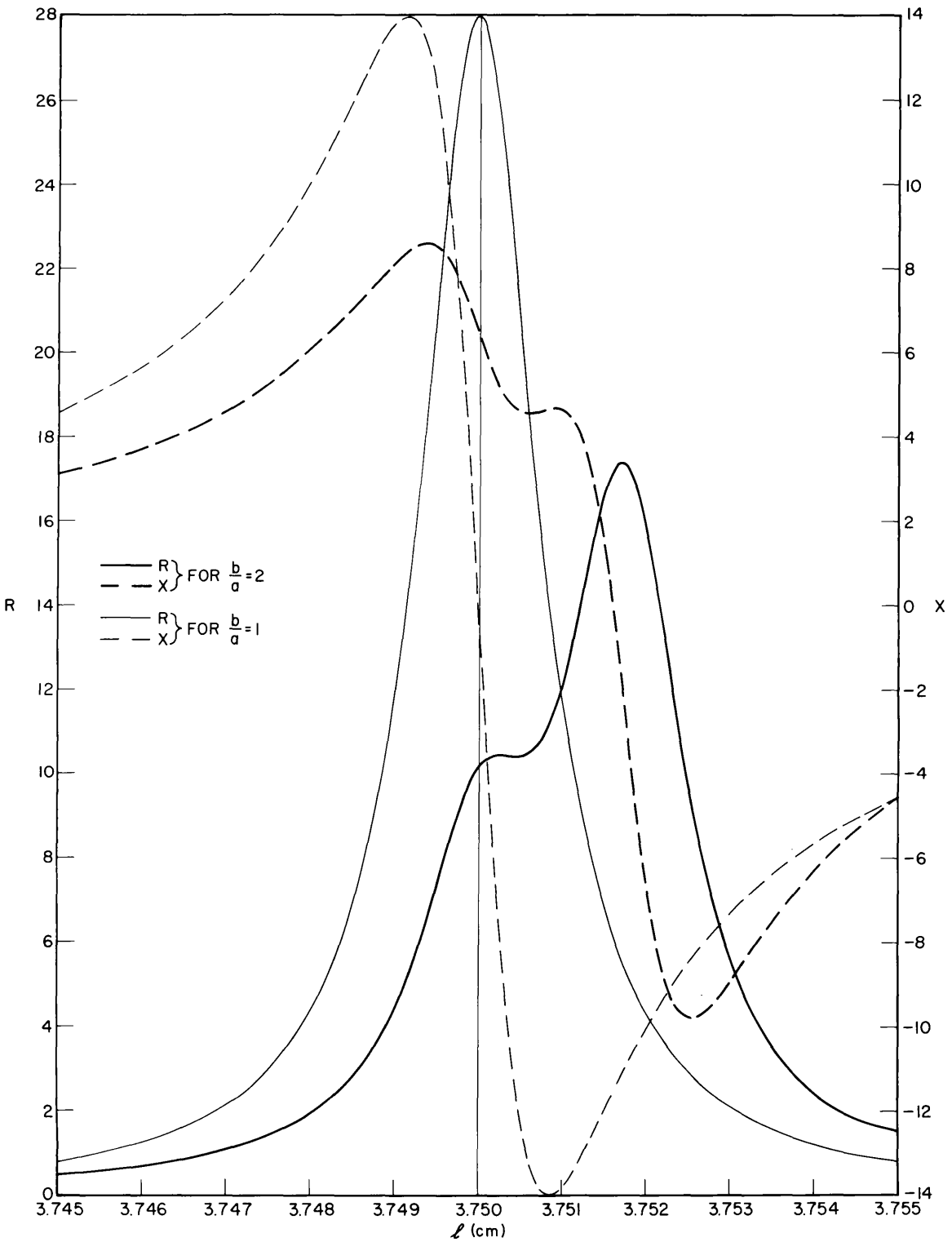

Fig. 16d—R and X vs ℓ for absolutely rigid boundary conditions and $n = 50$

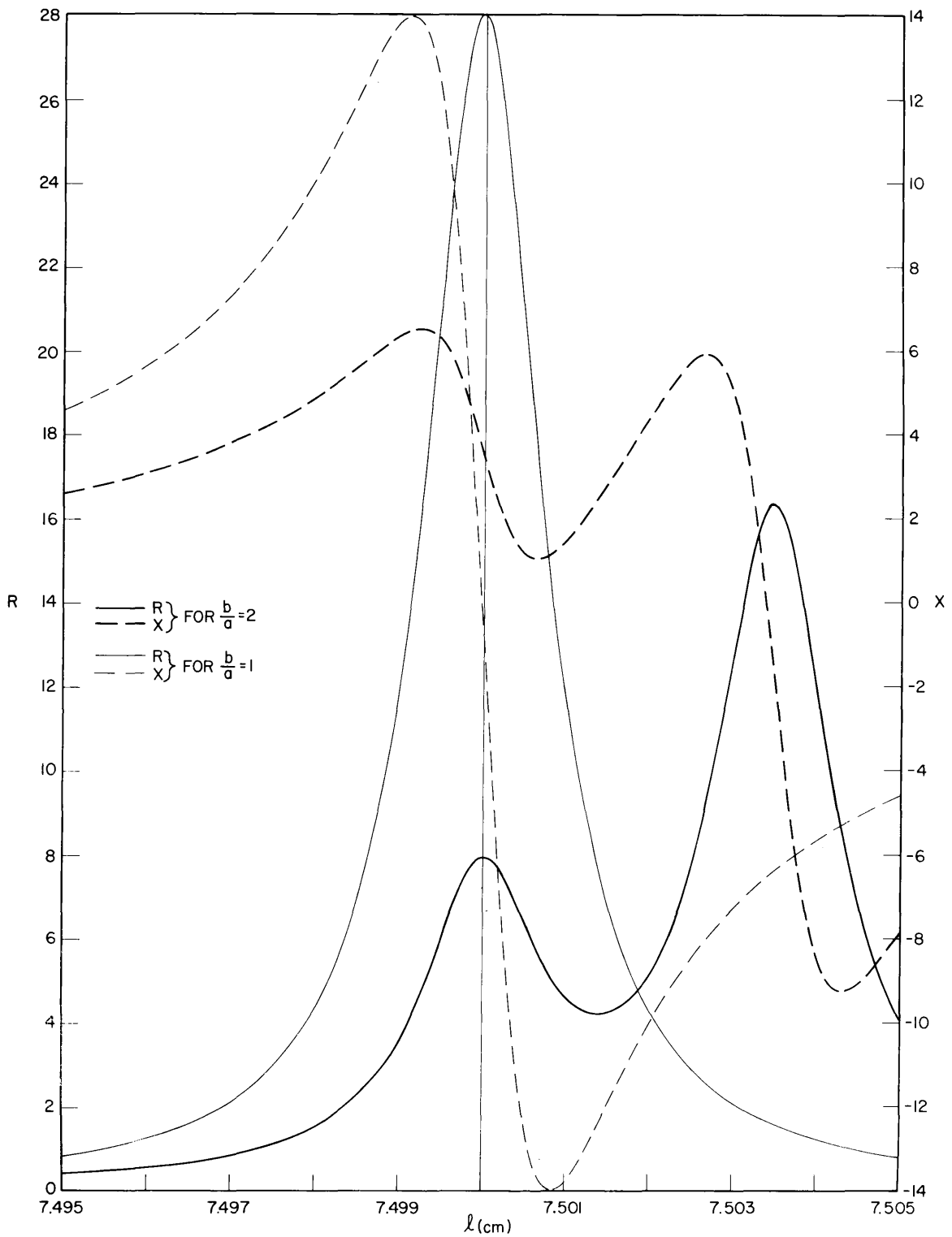

Fig. 16e—R and X vs ℓ for absolutely rigid boundary conditions and $n = 100$

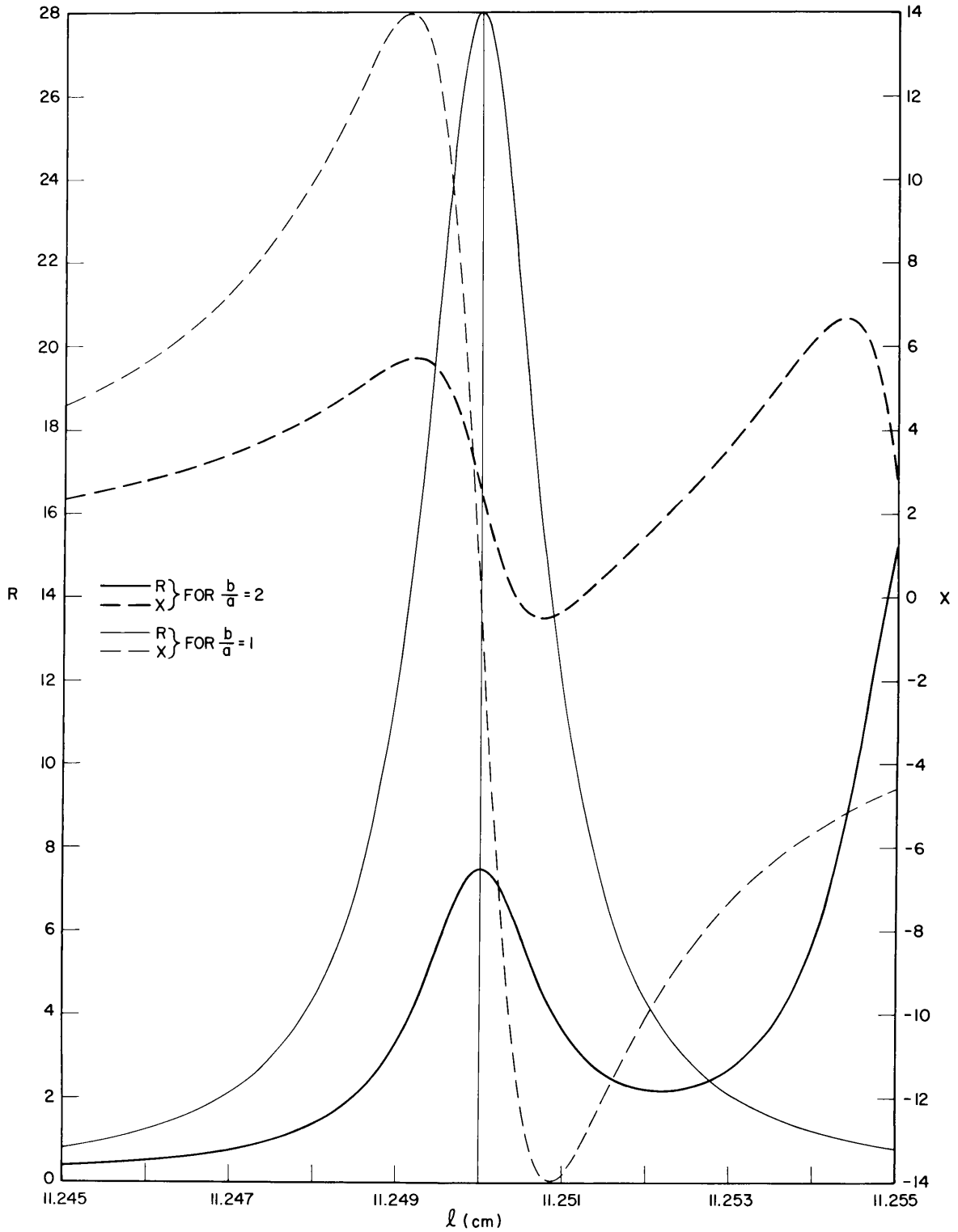

Fig. 16f—R and X vs ℓ for absolutely rigid boundary conditions and n = 150

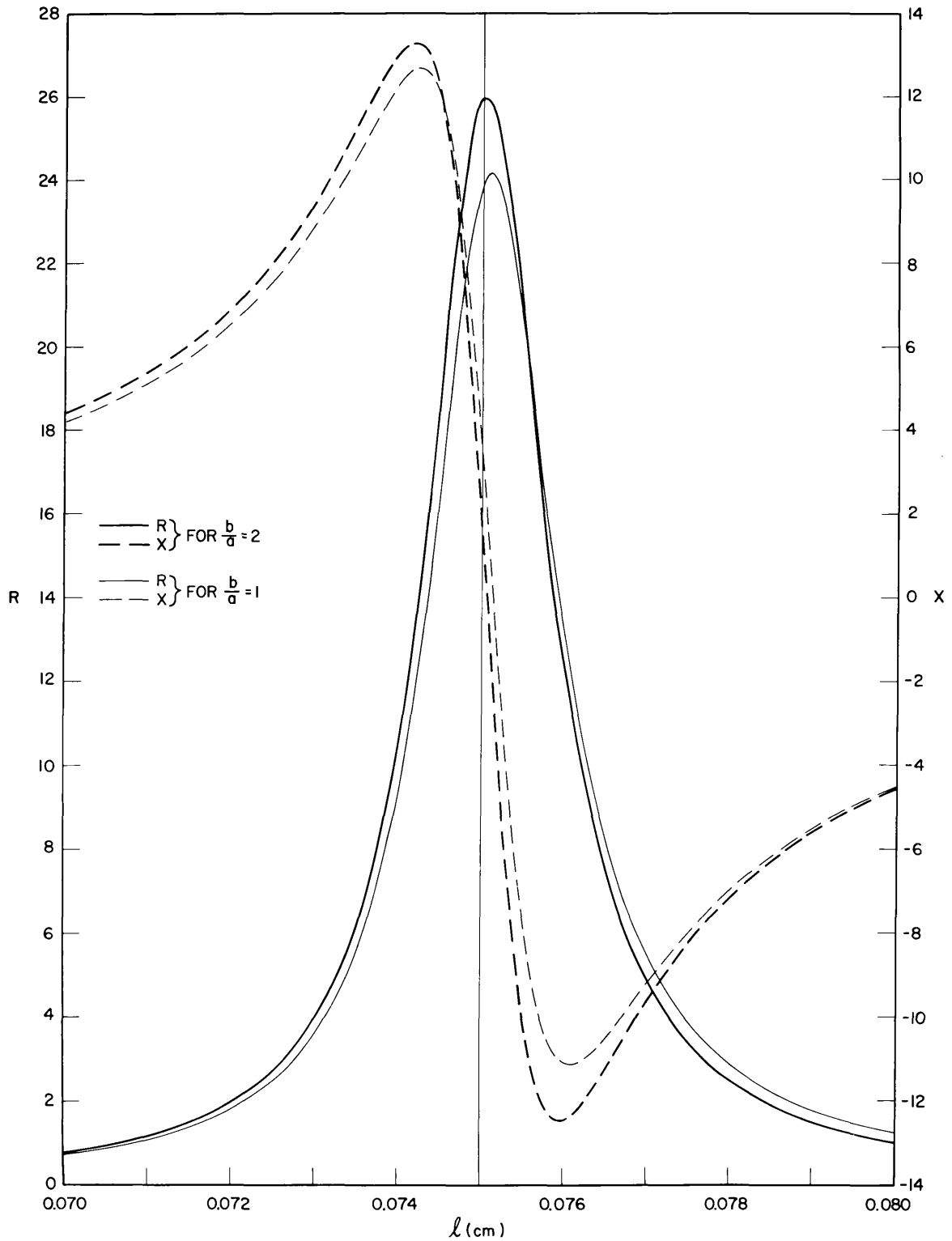

Fig. 17a—R and X vs ℓ for infinitely flexible boundary conditions and $n = 1$

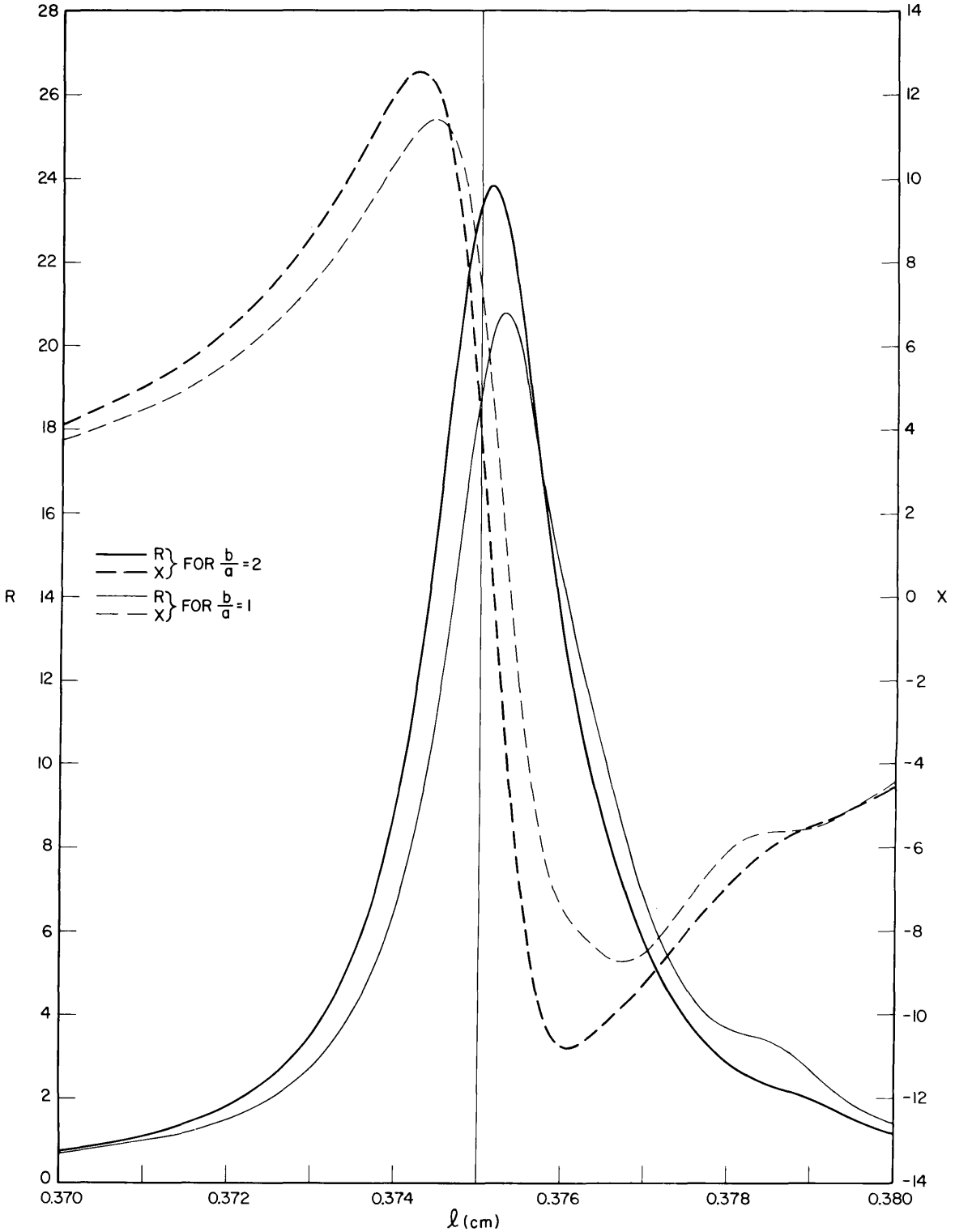

Fig. 17b—R and X vs ℓ for infinitely flexible boundary conditions and $n = 5$

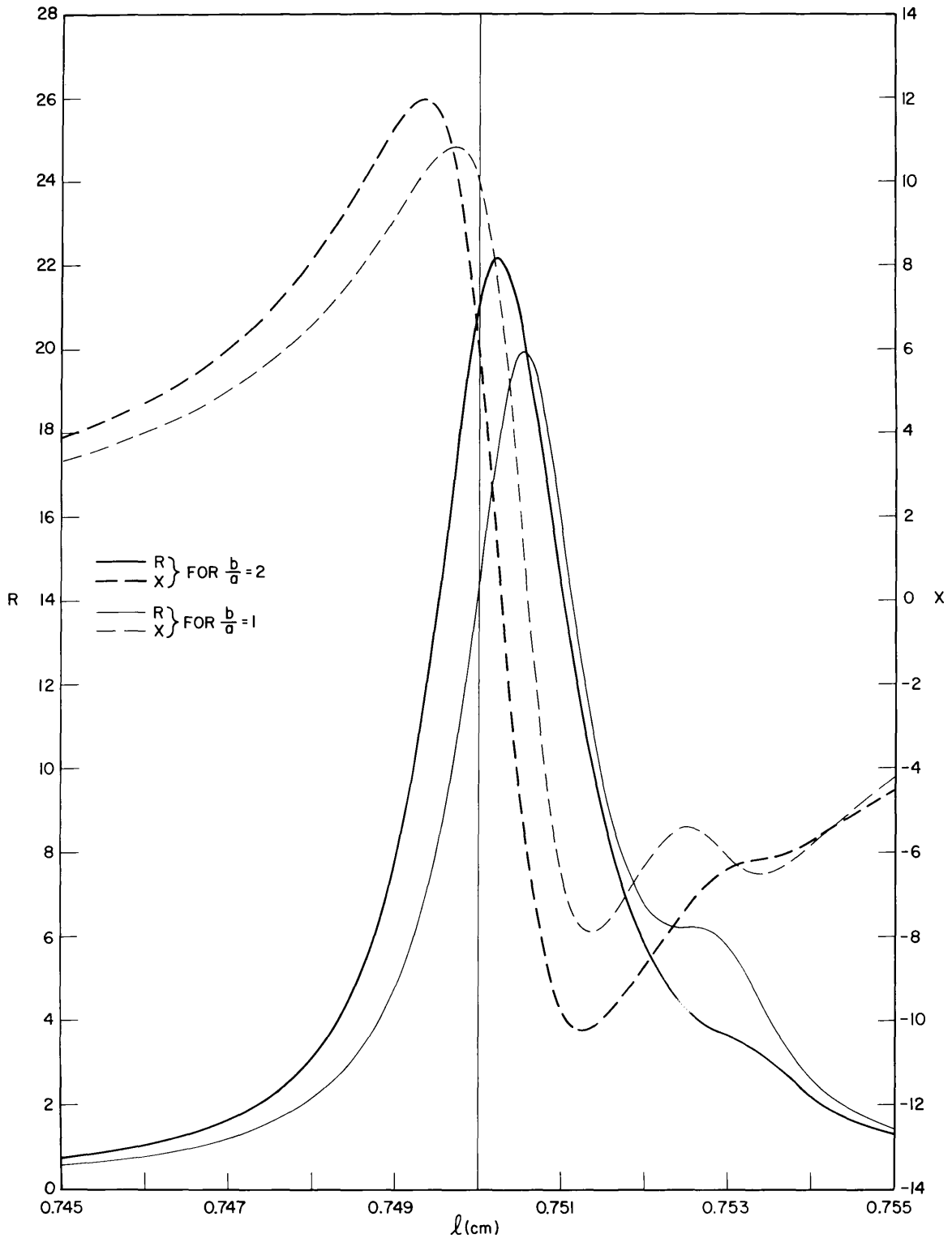

Fig. 17c—R and X vs ℓ for infinitely flexible boundary conditions and $n = 10$

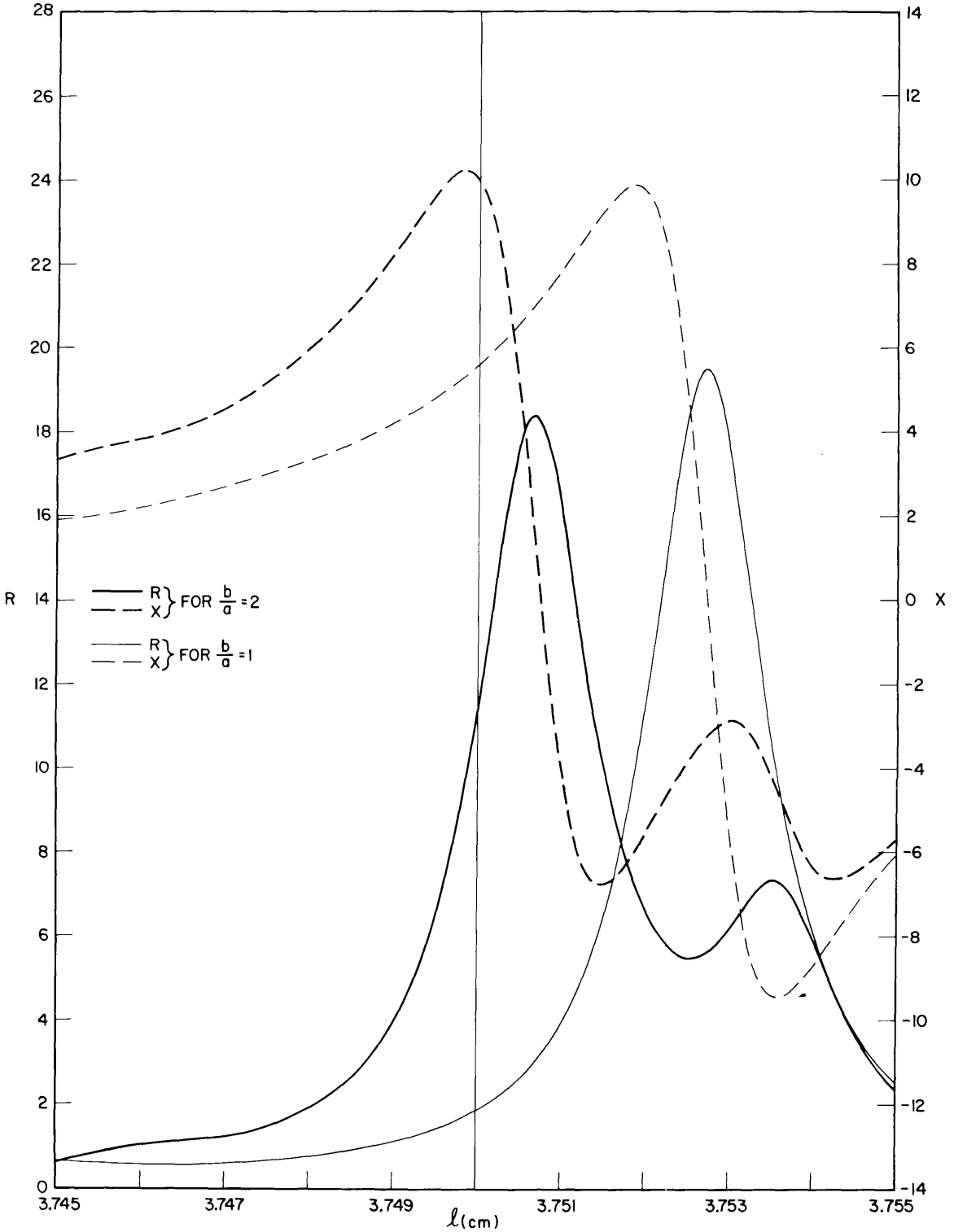

Fig. 17d—R and X vs ℓ for infinitely flexible boundary conditions and $n = 50$

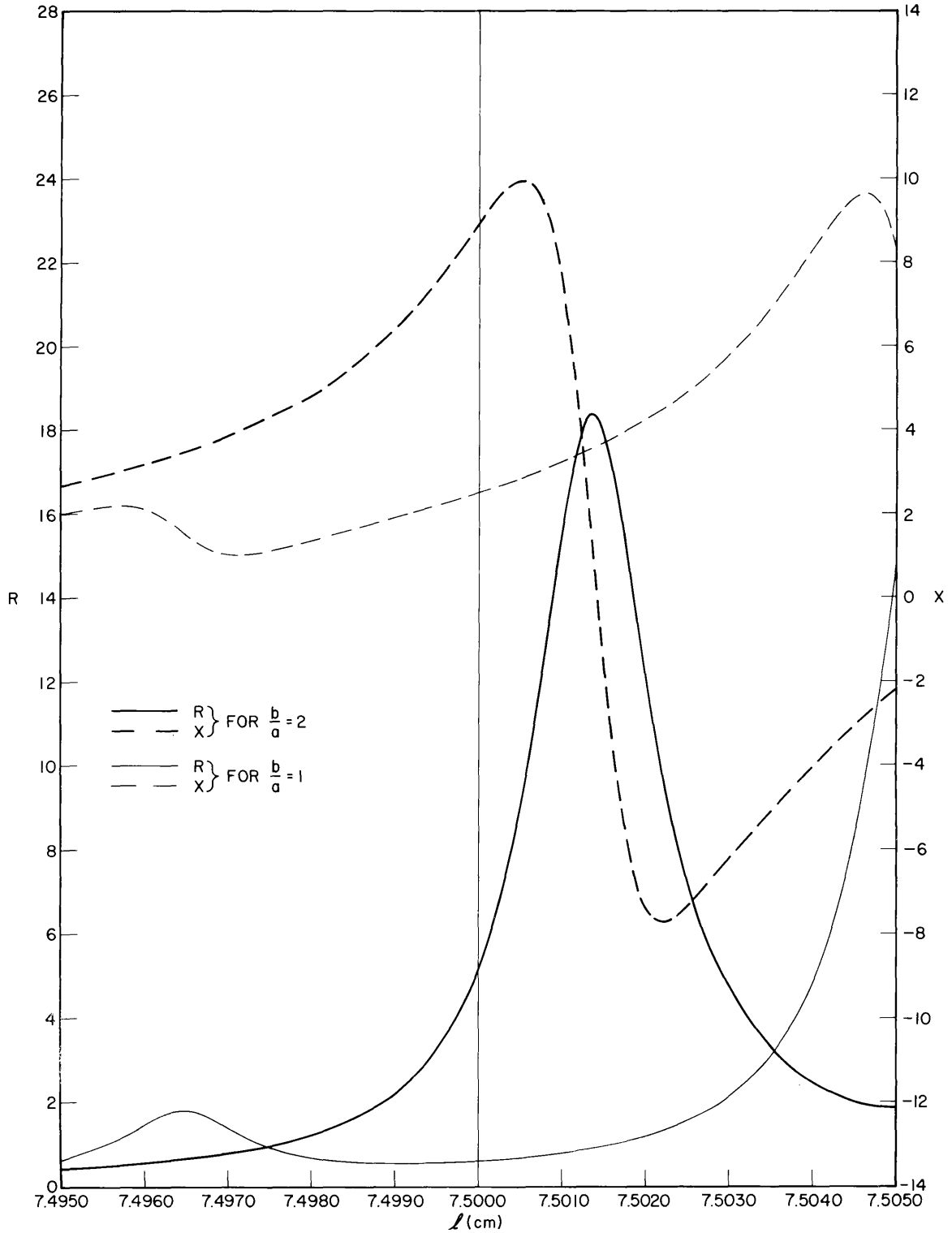

Fig. 17e—R and X vs ℓ for infinitely flexible boundary conditions and $n = 100$

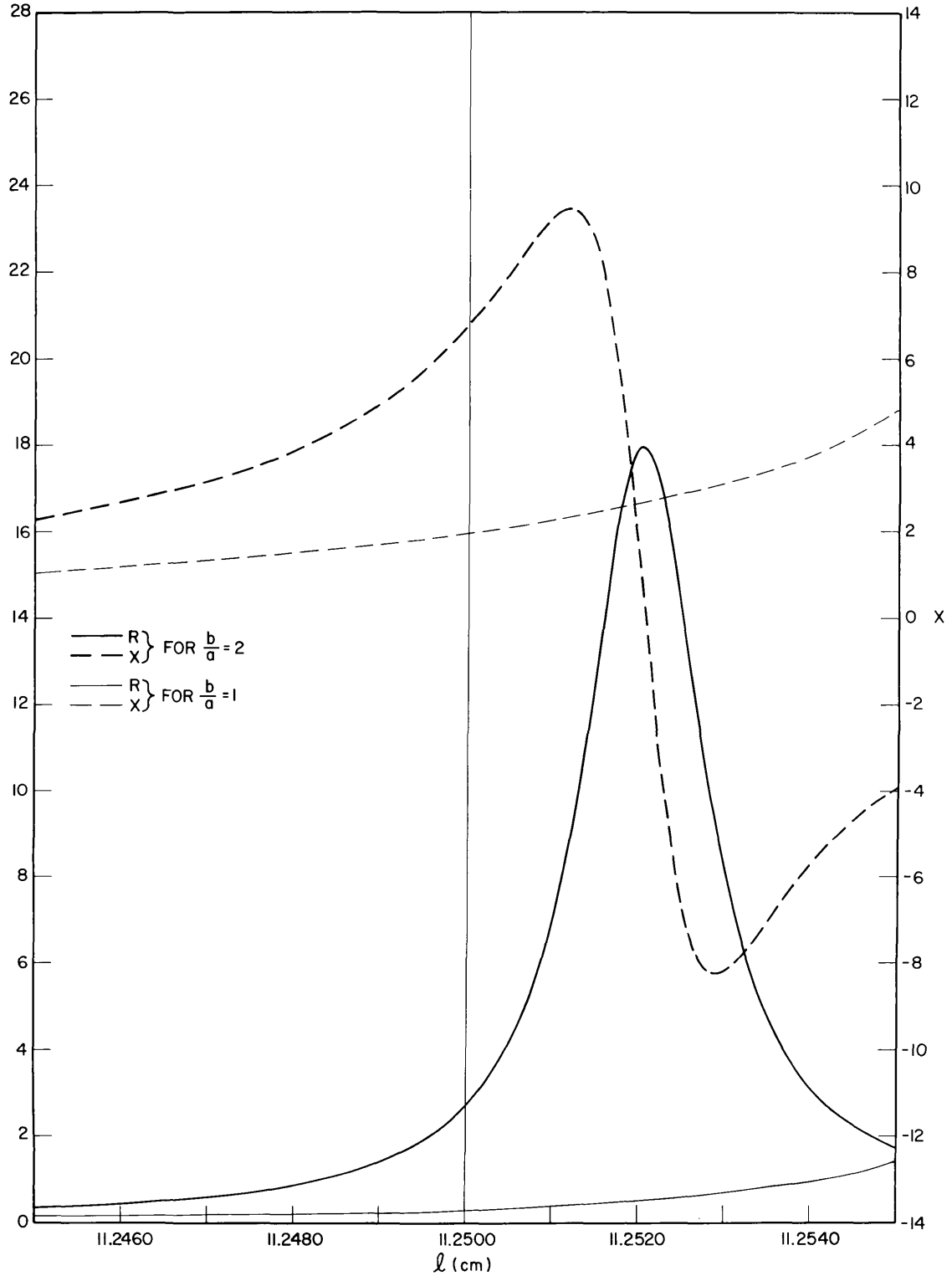

Fig. 17f—R and X vs ℓ for infinitely flexible boundary conditions and n = 150

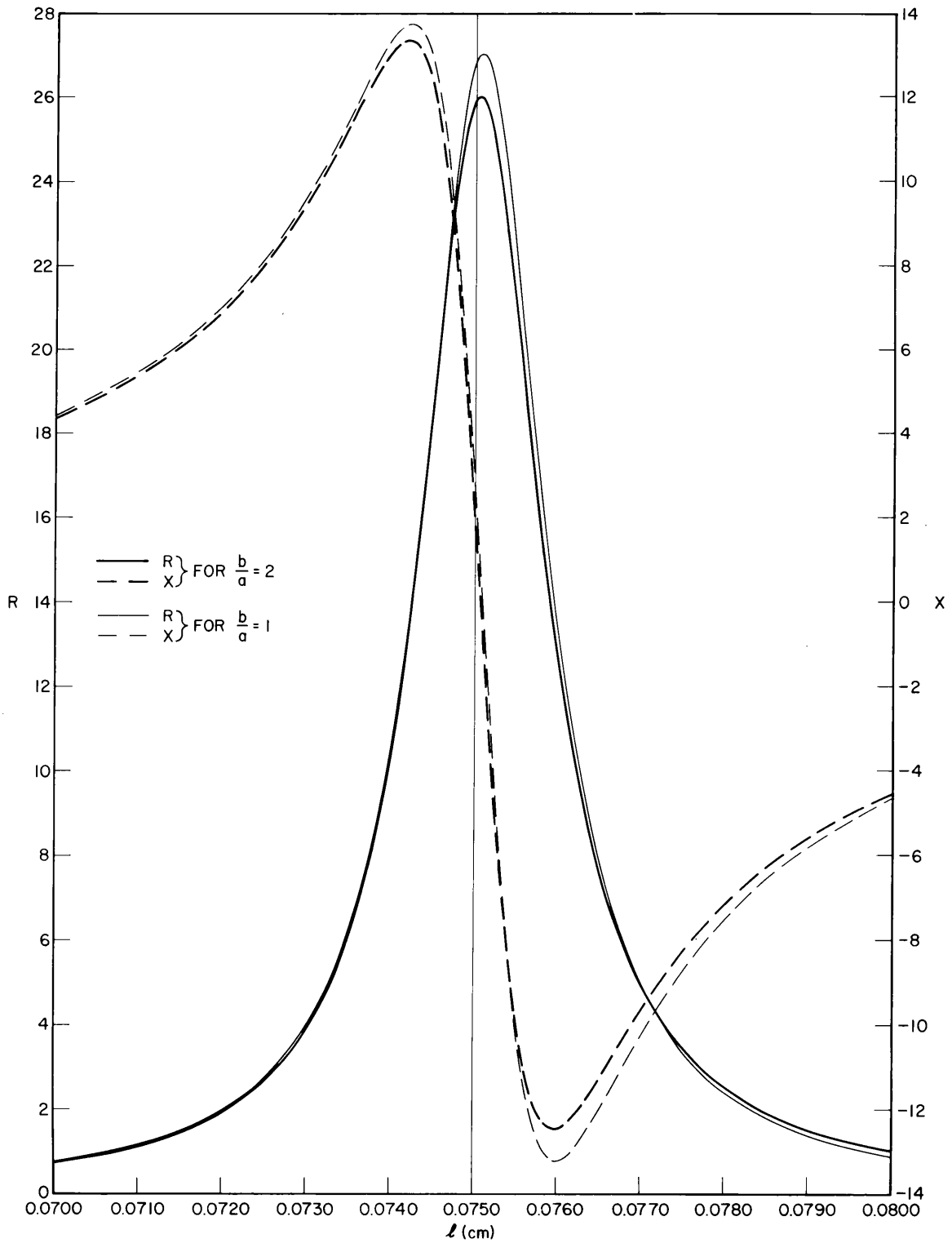

Fig. 18a—R and X vs ℓ for liquid boundary conditions (assuming orthogonal functions) and $n = 1$

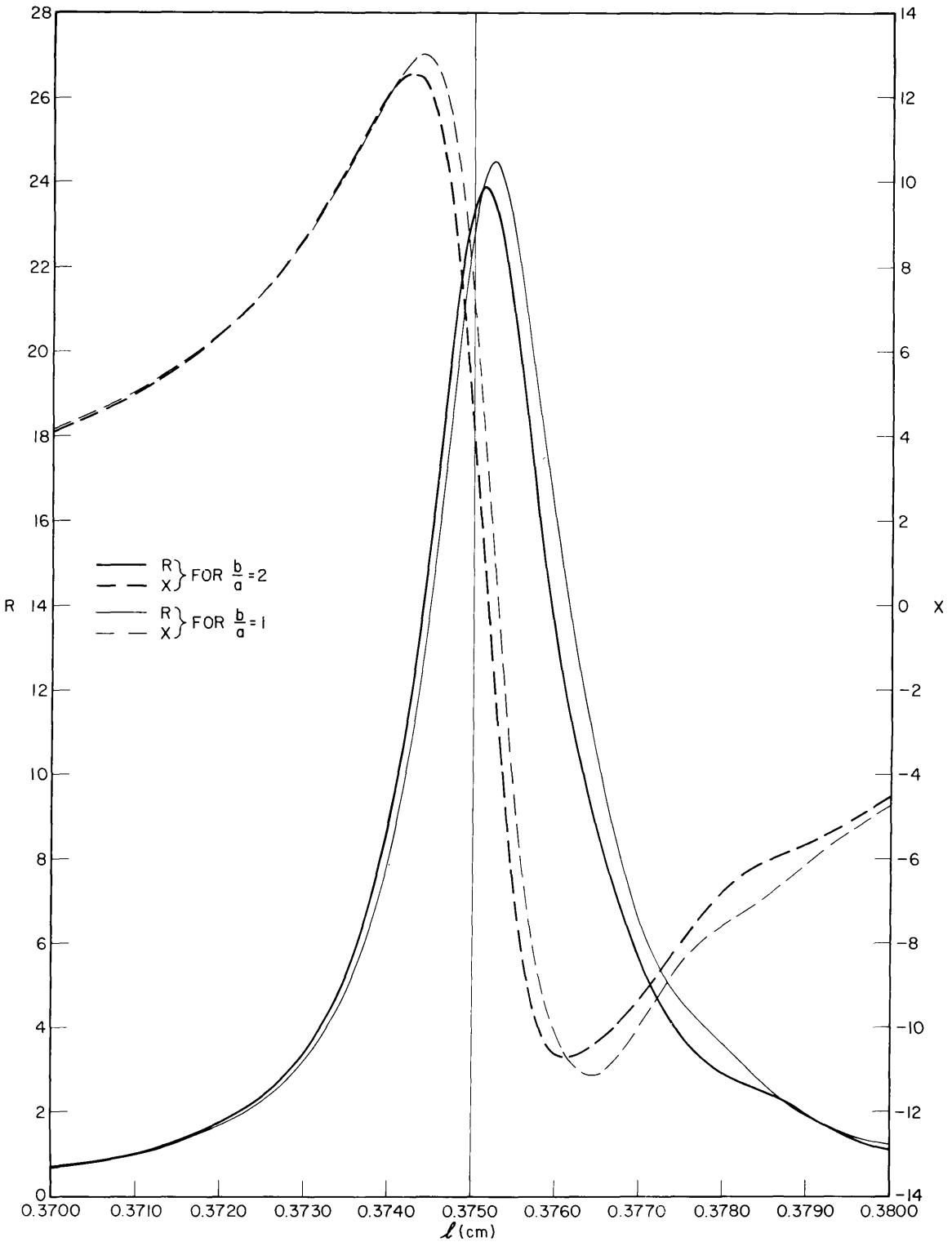

Fig. 18b—R and X vs ℓ for liquid boundary conditions (assuming orthogonal functions) and $n = 5$

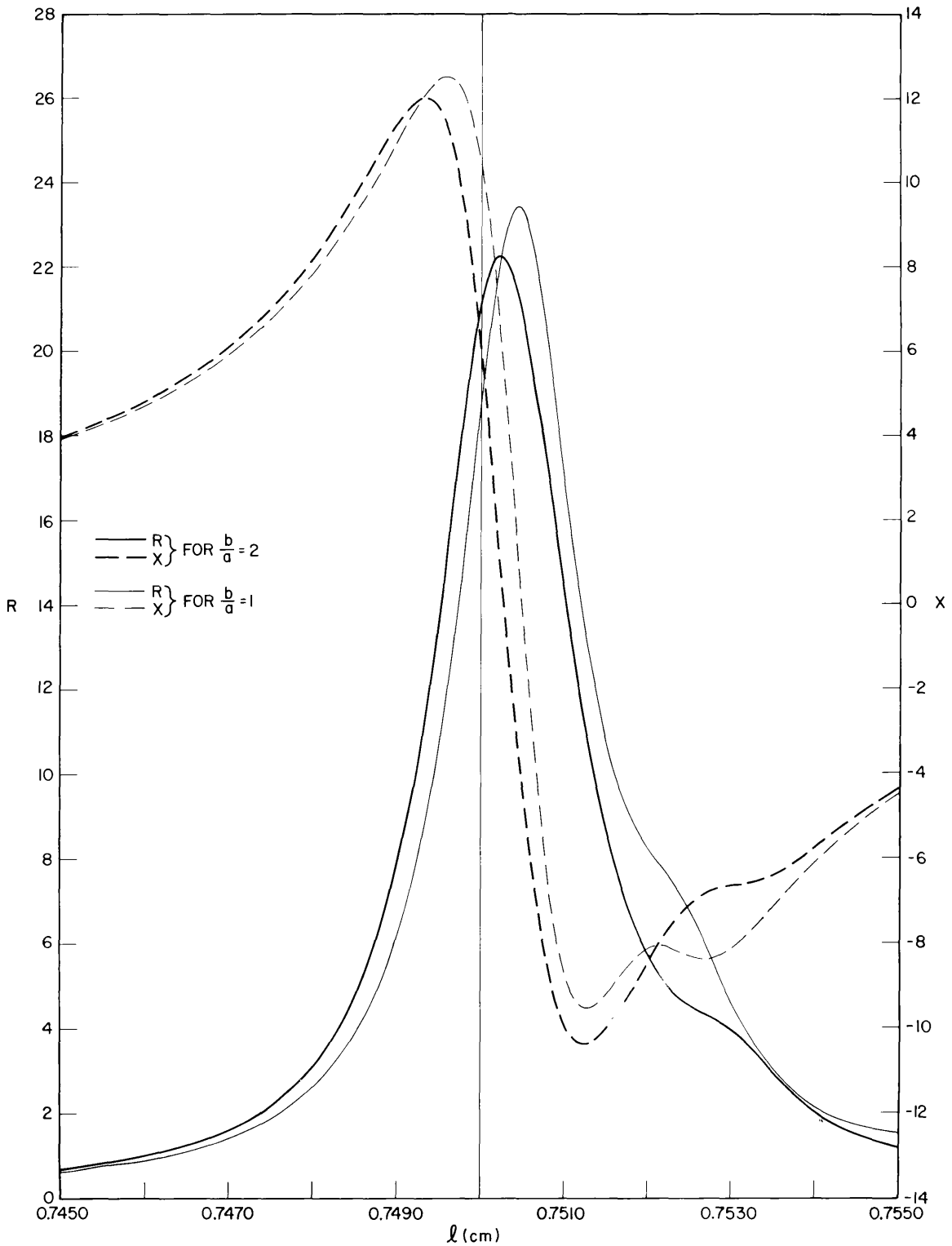

Fig. 18c – R and X vs ℓ for liquid boundary conditions (assuming orthogonal functions) and $n = 10$

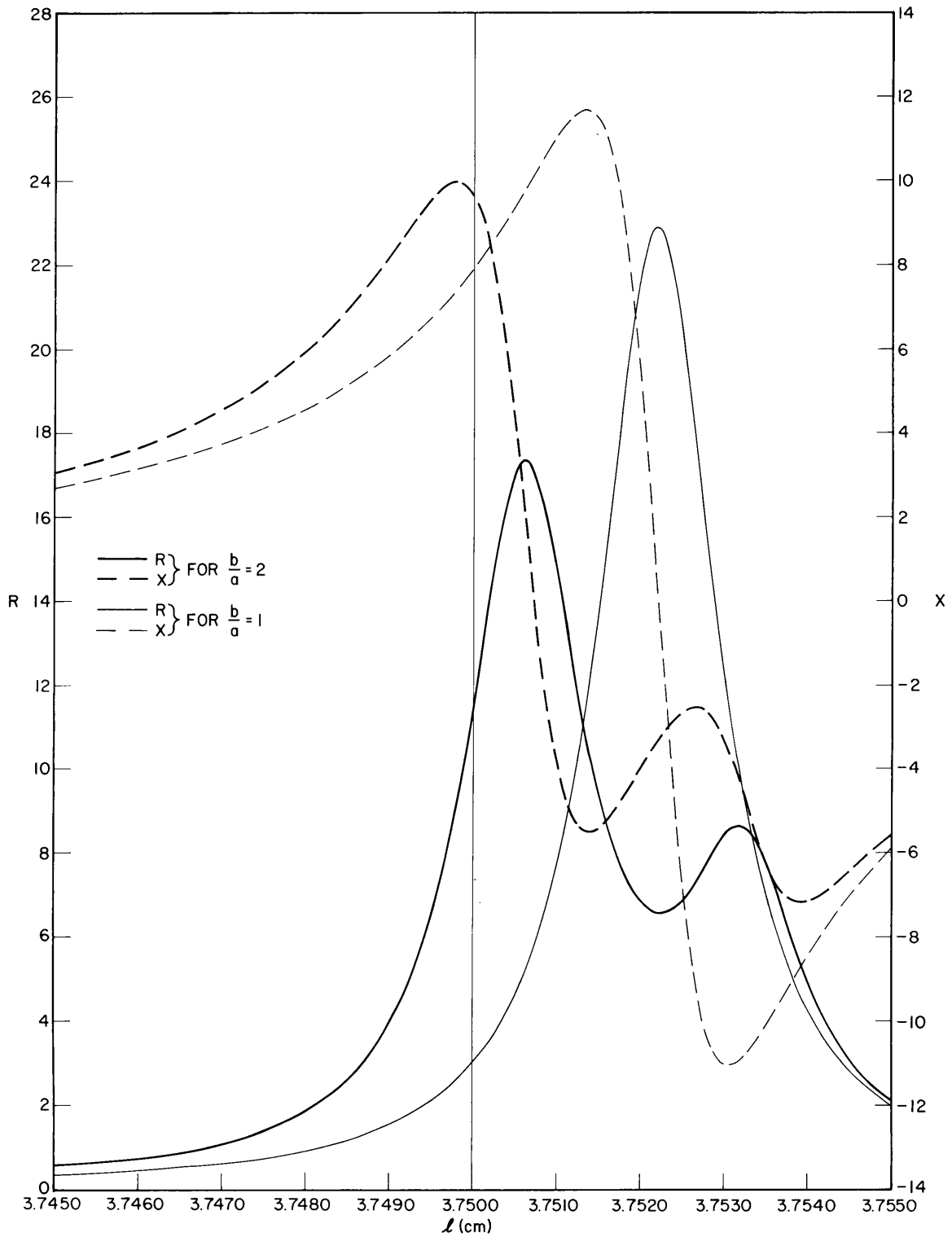

Fig. 18d—R and X vs ℓ for liquid boundary conditions (assuming orthogonal functions) and n = 50

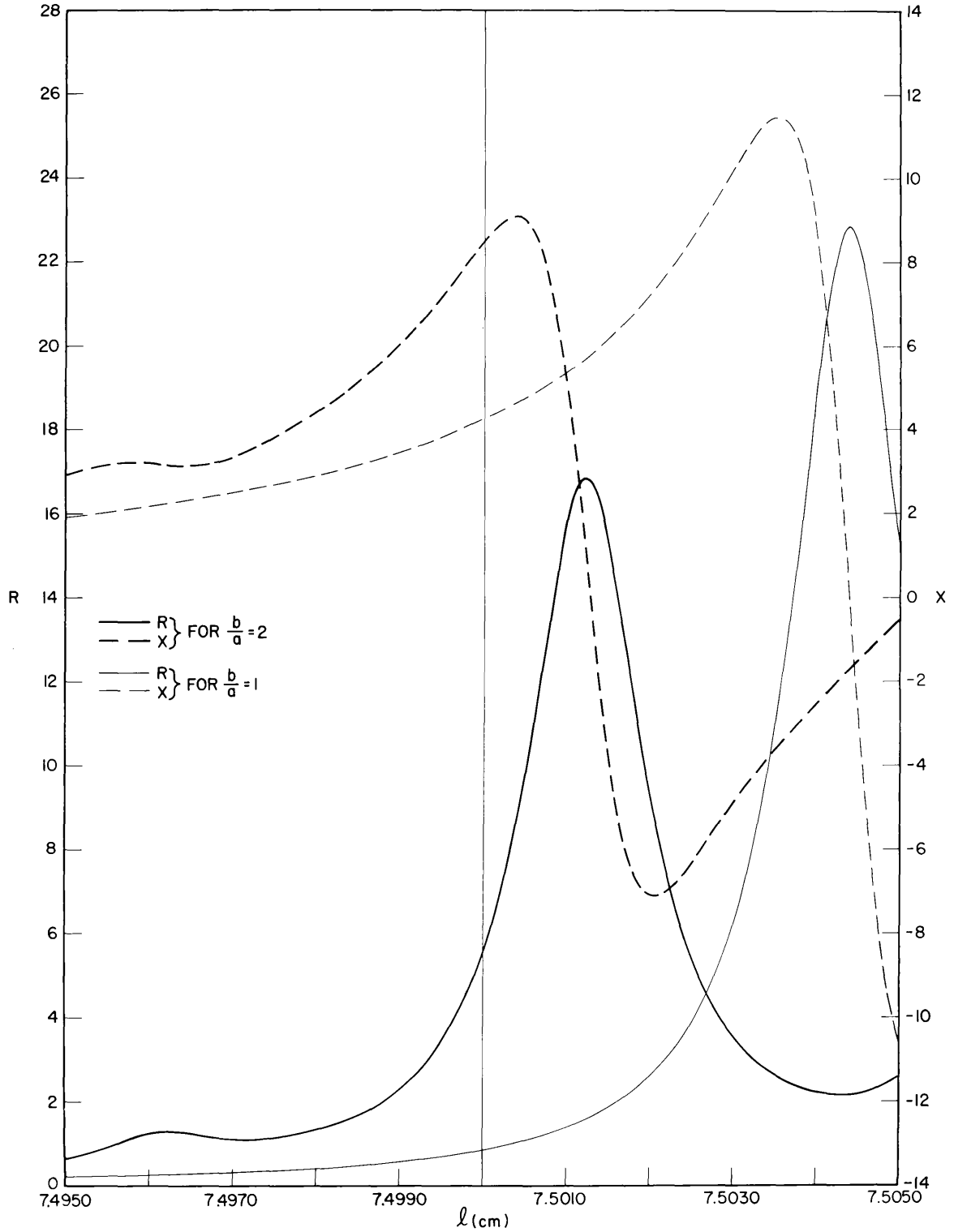

Fig. 18e—R and X vs ℓ for liquid boundary conditions (assuming orthogonal functions) and $n = 100$

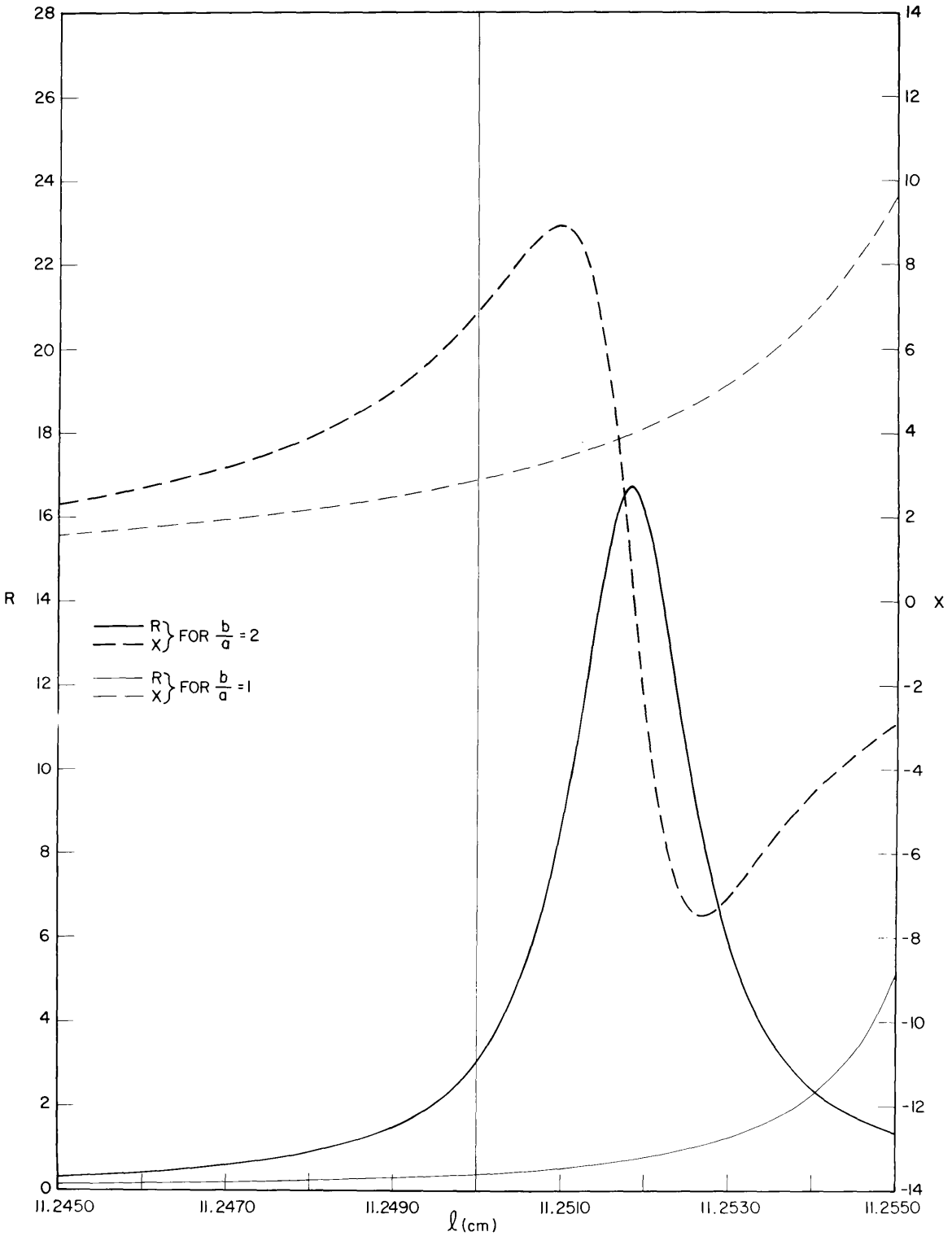

Fig. 18f—R and X vs ℓ for liquid boundary conditions (assuming orthogonal functions) and n = 150

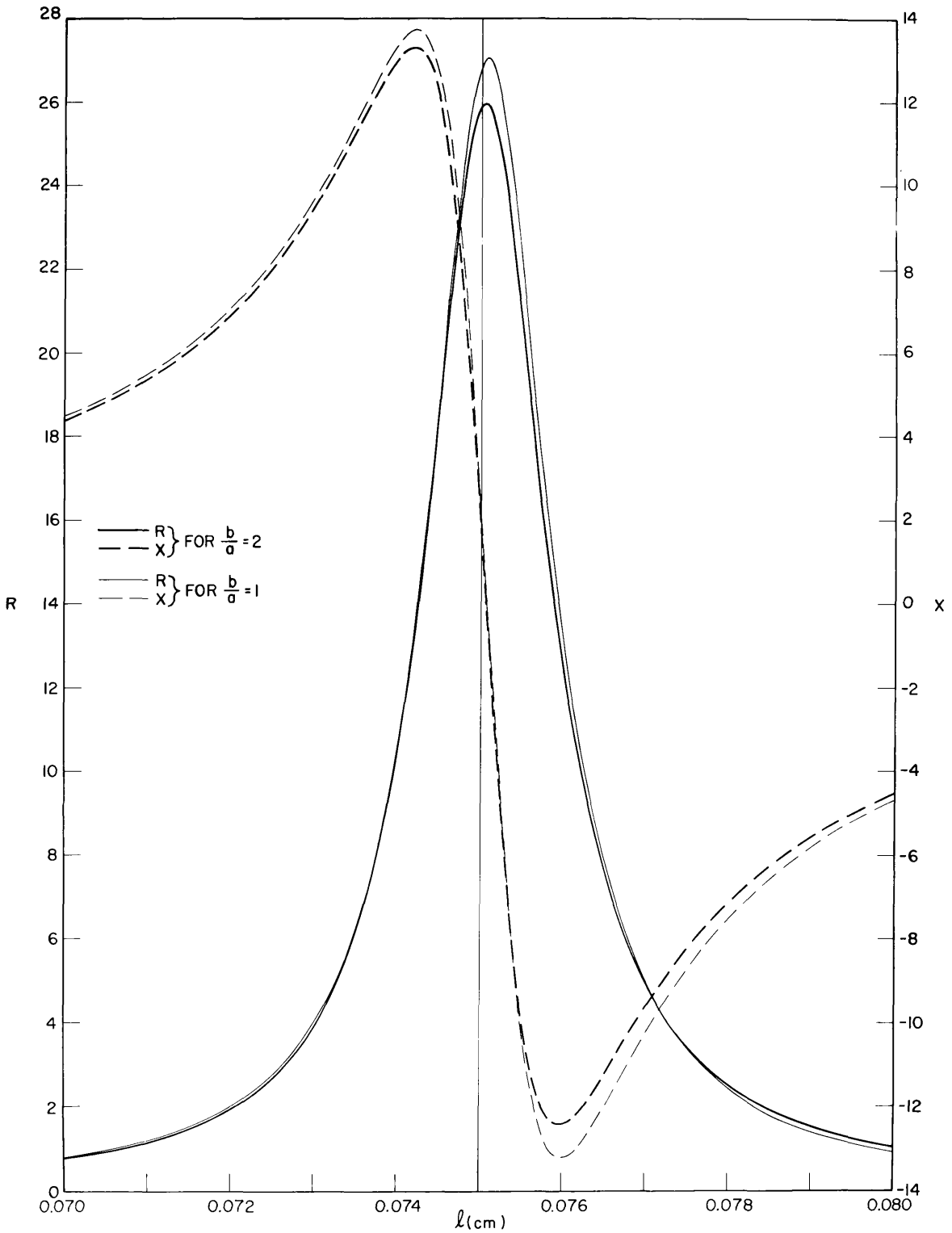

Fig. 19a—R and X vs ℓ for liquid boundary conditions (using actual functions) and $n = 1$

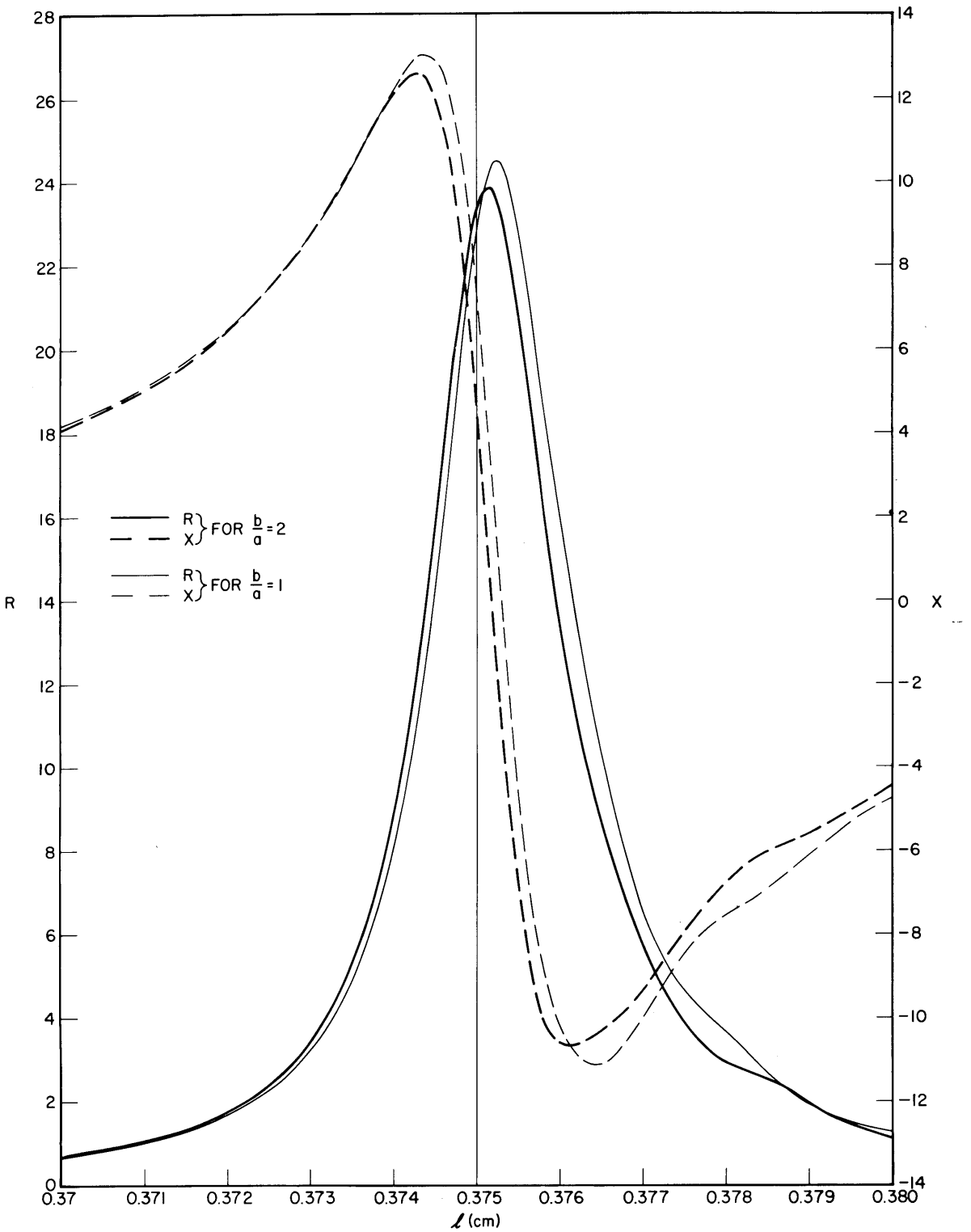

Fig. 19b—R and X vs ℓ for liquid boundary conditions (using actual functions) and $n = 5$

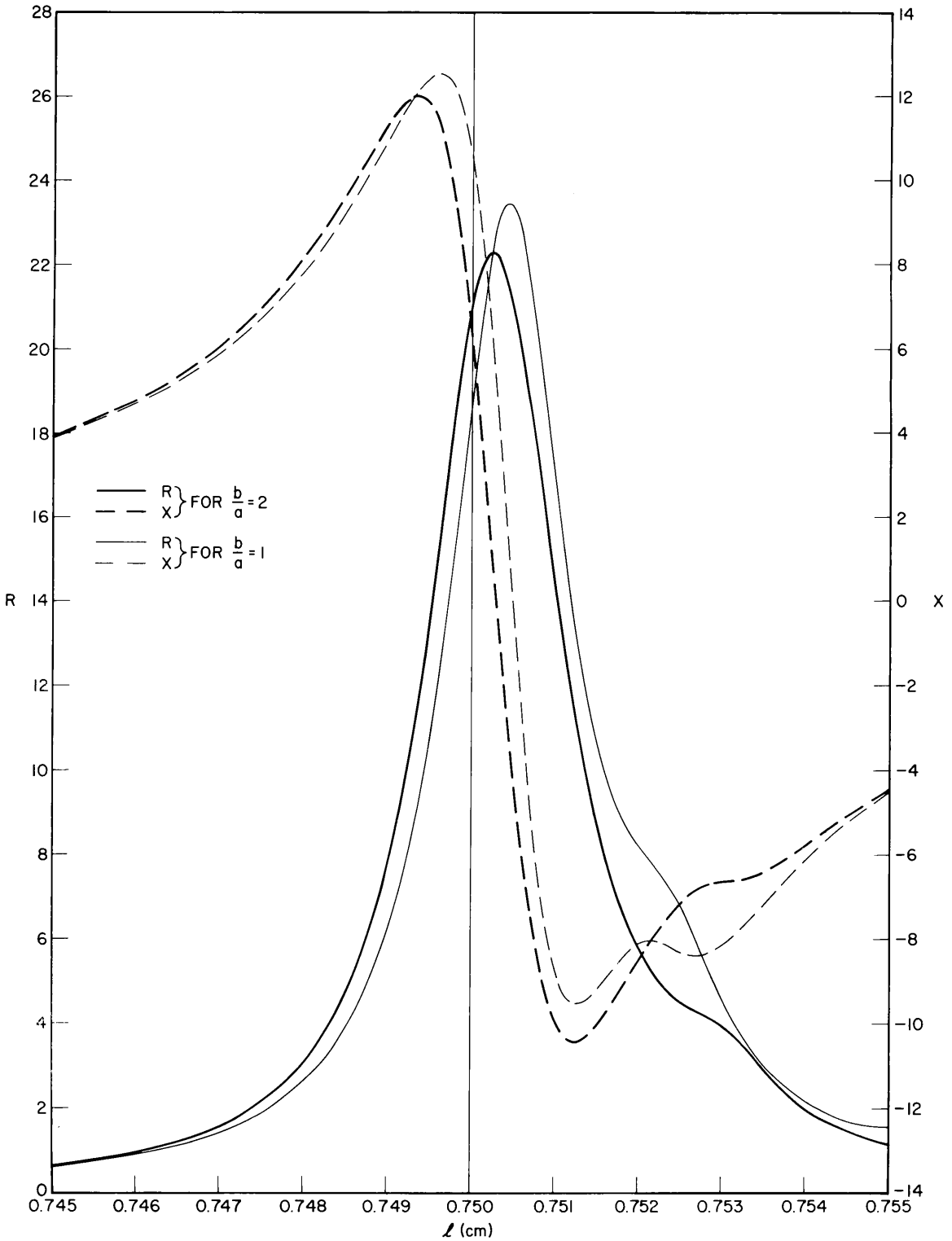

Fig. 19c—R and X vs ℓ for liquid boundary conditions (using actual functions) and $n = 10$

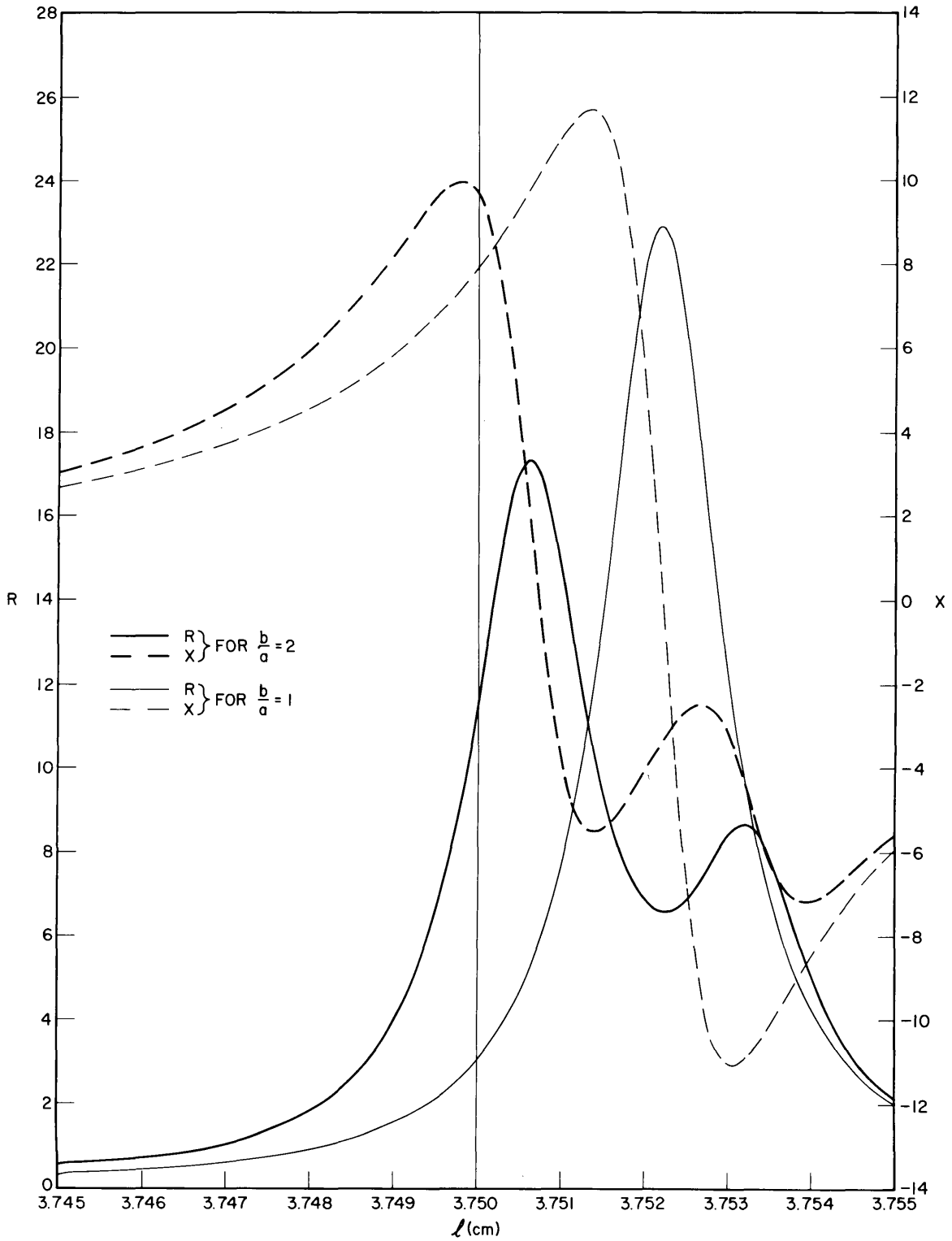

Fig. 19d—R and X vs ℓ for liquid boundary conditions (using actual functions) and $n = 50$

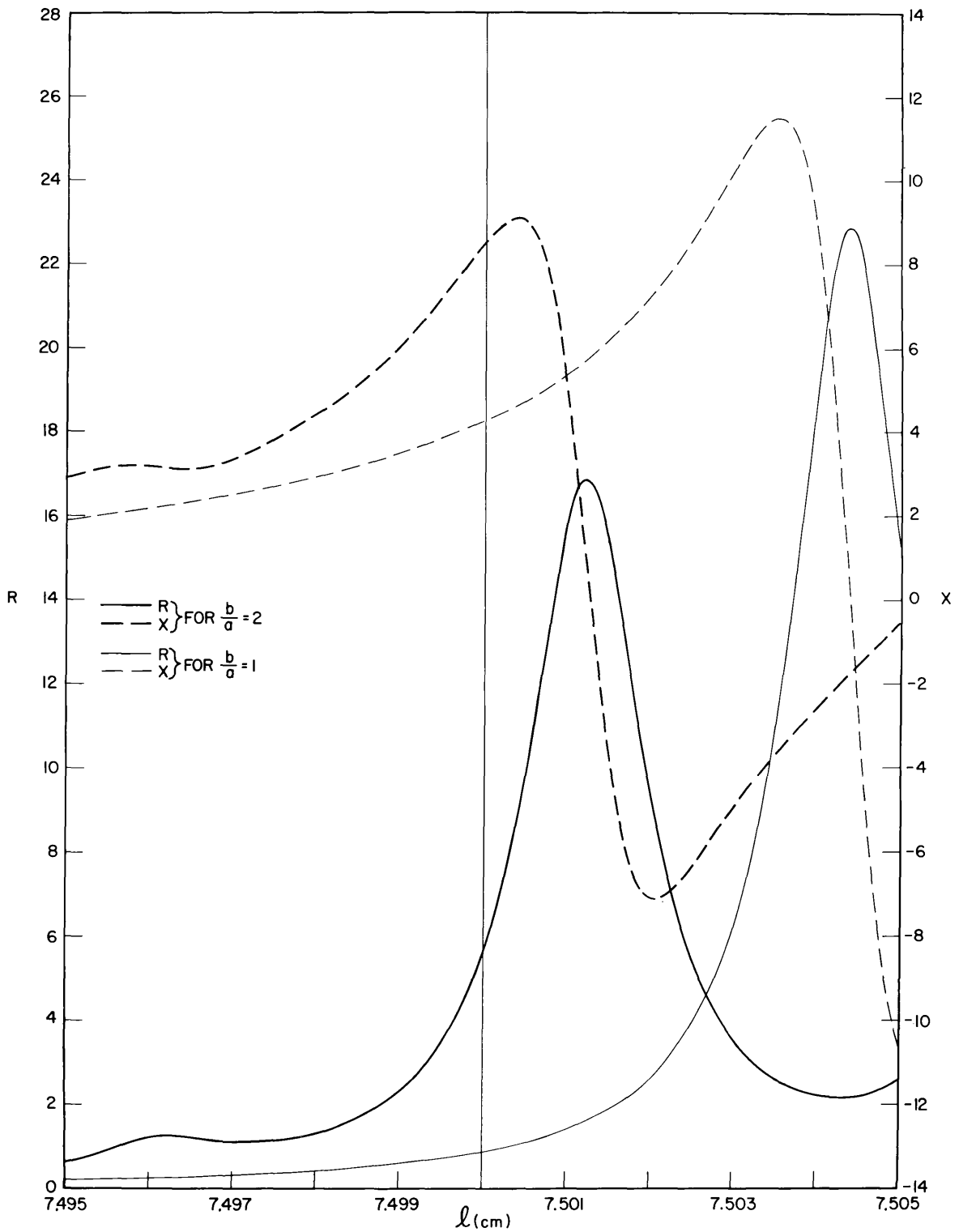

Fig. 19e—R and X vs ℓ for liquid boundary conditions (using actual functions) and $n = 100$

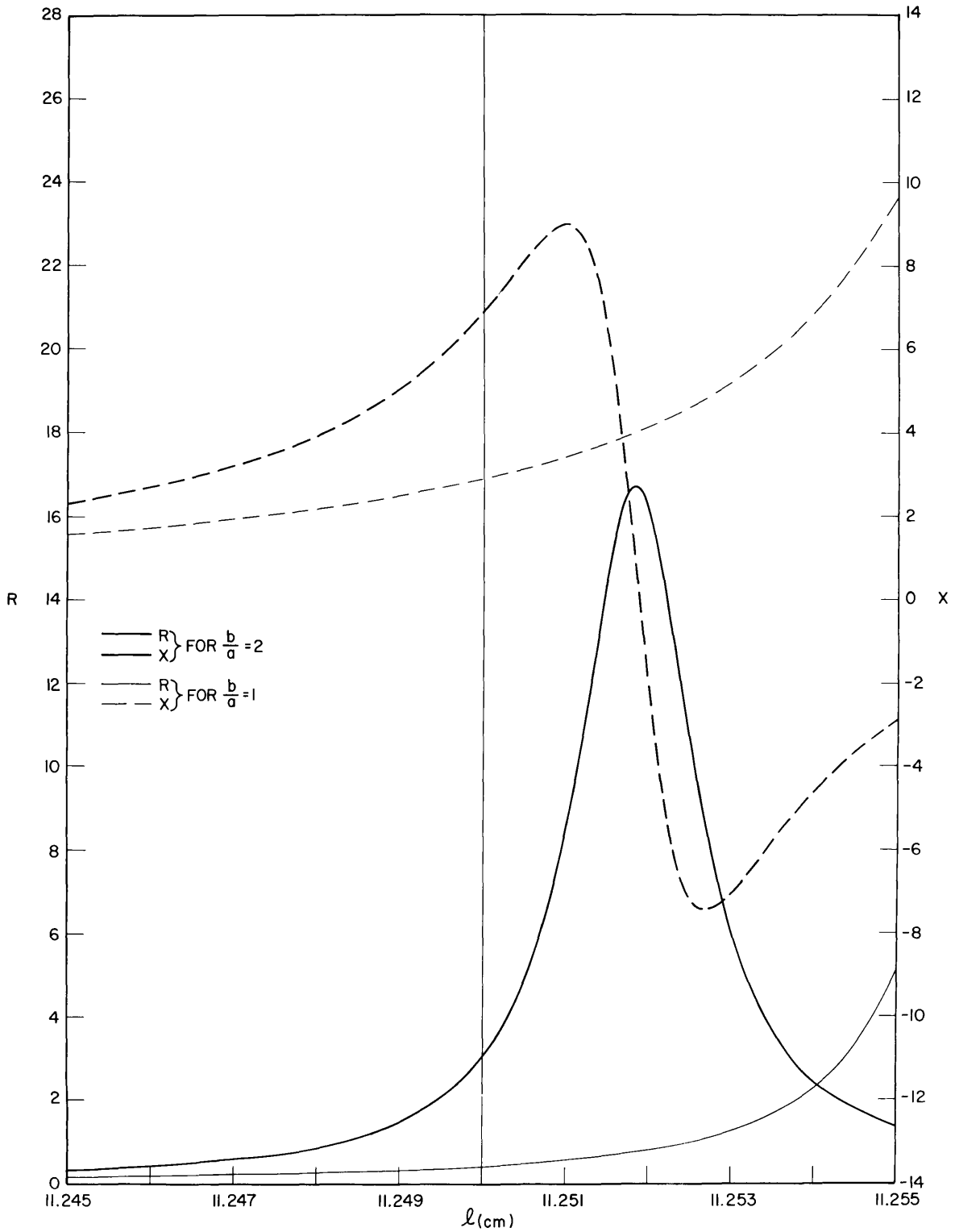

Fig. 19f—R and X vs ℓ for liquid boundary conditions (using actual functions) and $n = 150$

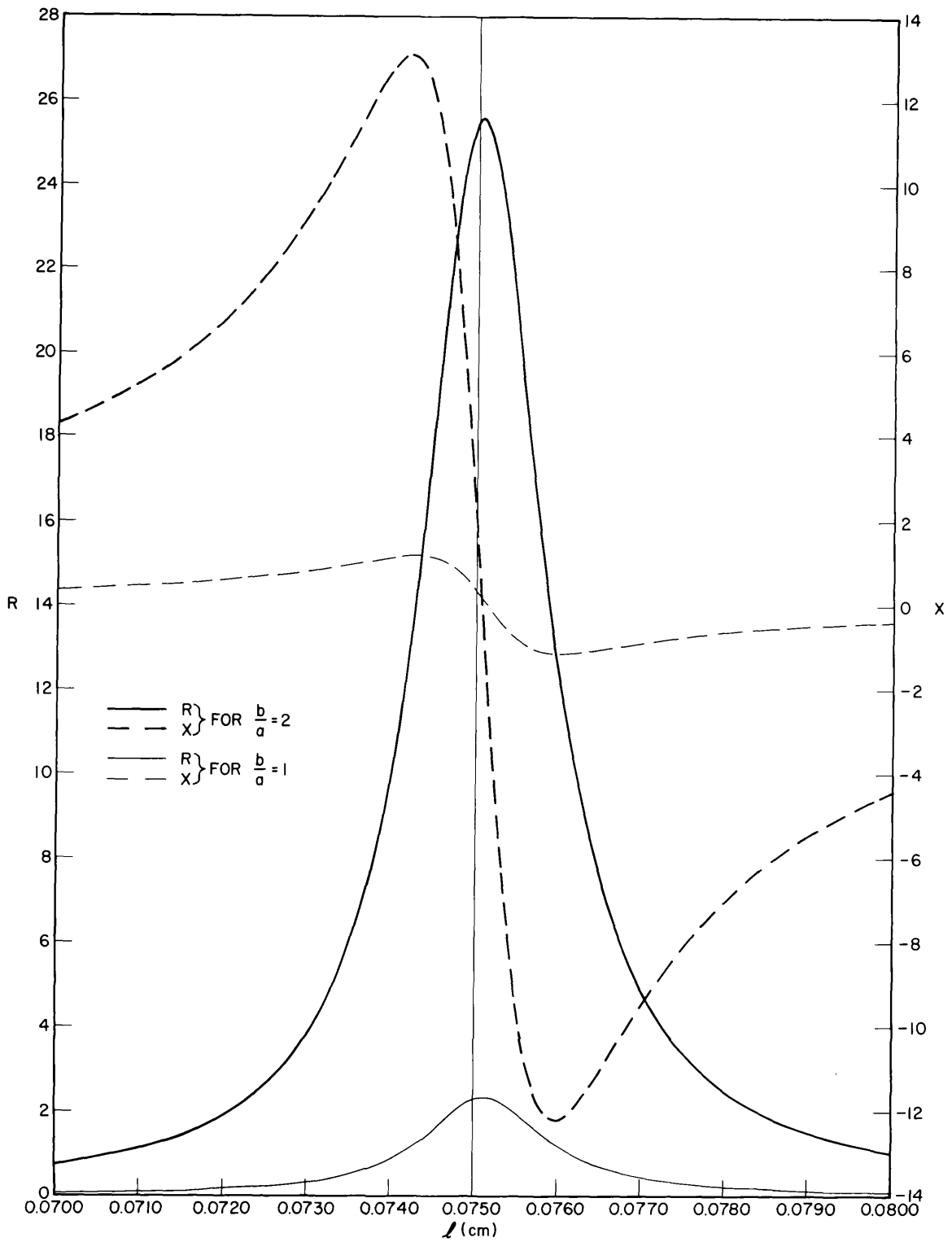

Fig. 20a—R and X vs ℓ for elastic solid boundary conditions (assuming orthogonal functions) and $n = 1$

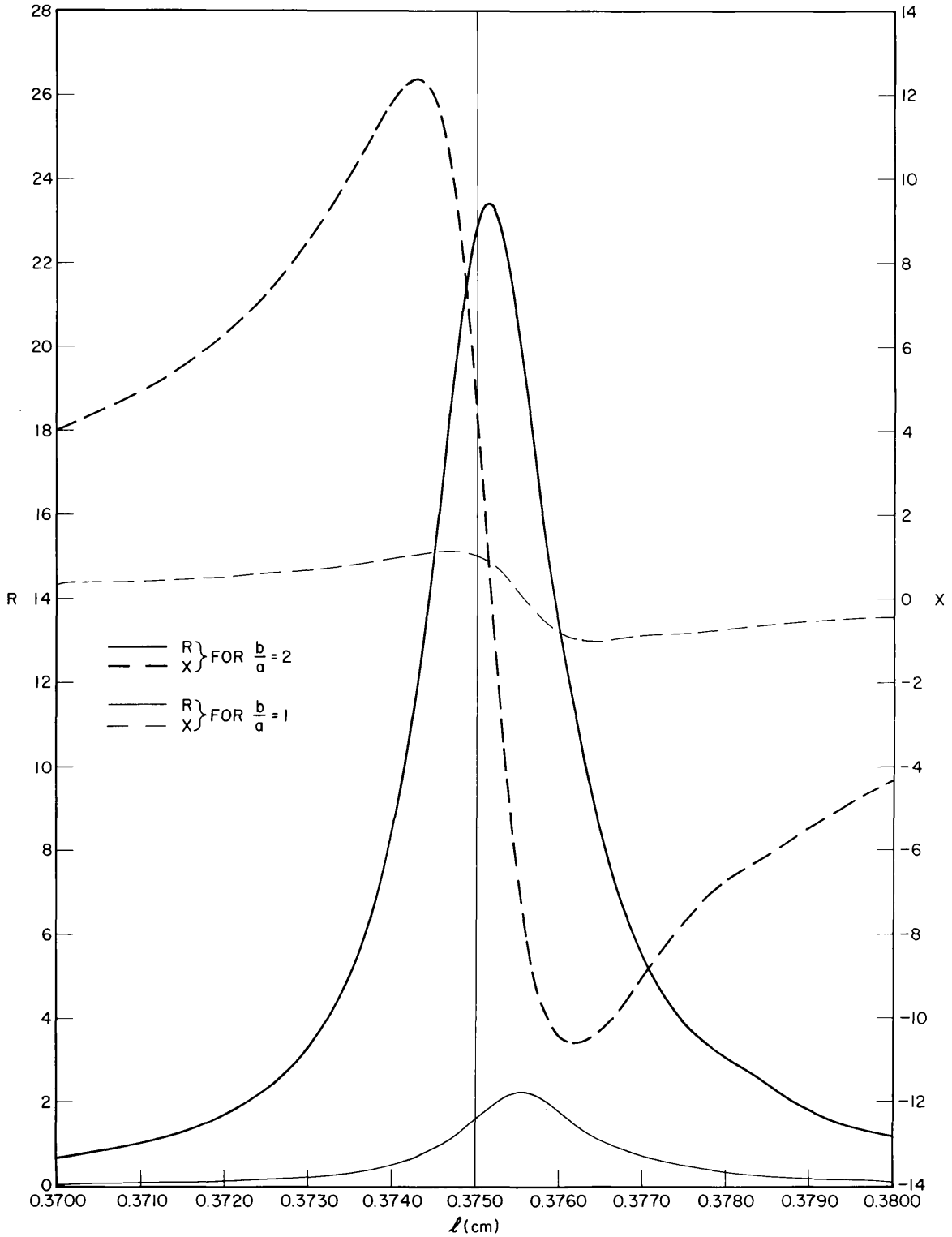

Fig. 20b—R and X vs ℓ for elastic solid boundary conditions (assuming orthogonal functions) and $n = 5$

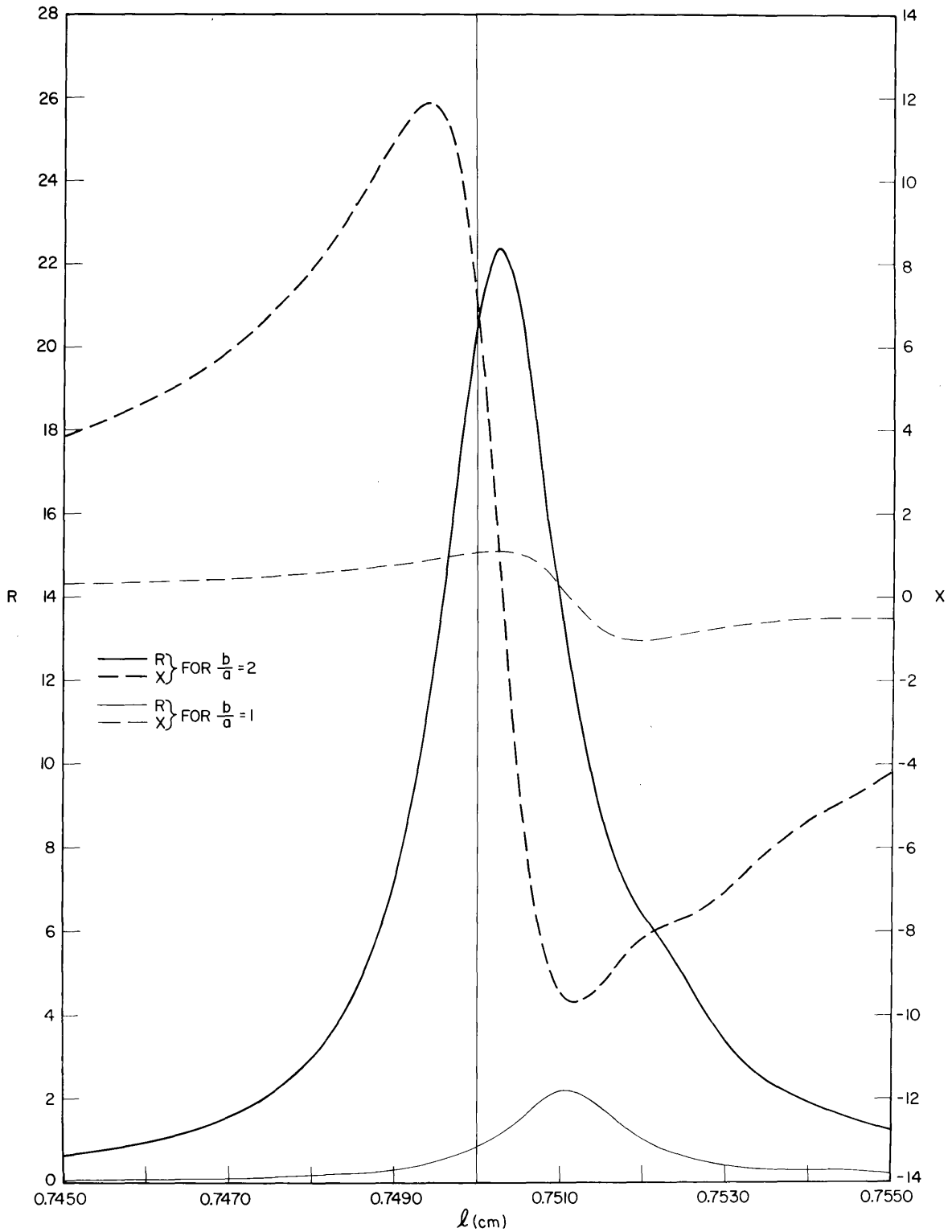

Fig. 20c—R and X vs ℓ for elastic solid boundary conditions (assuming orthogonal functions) and $n = 10$

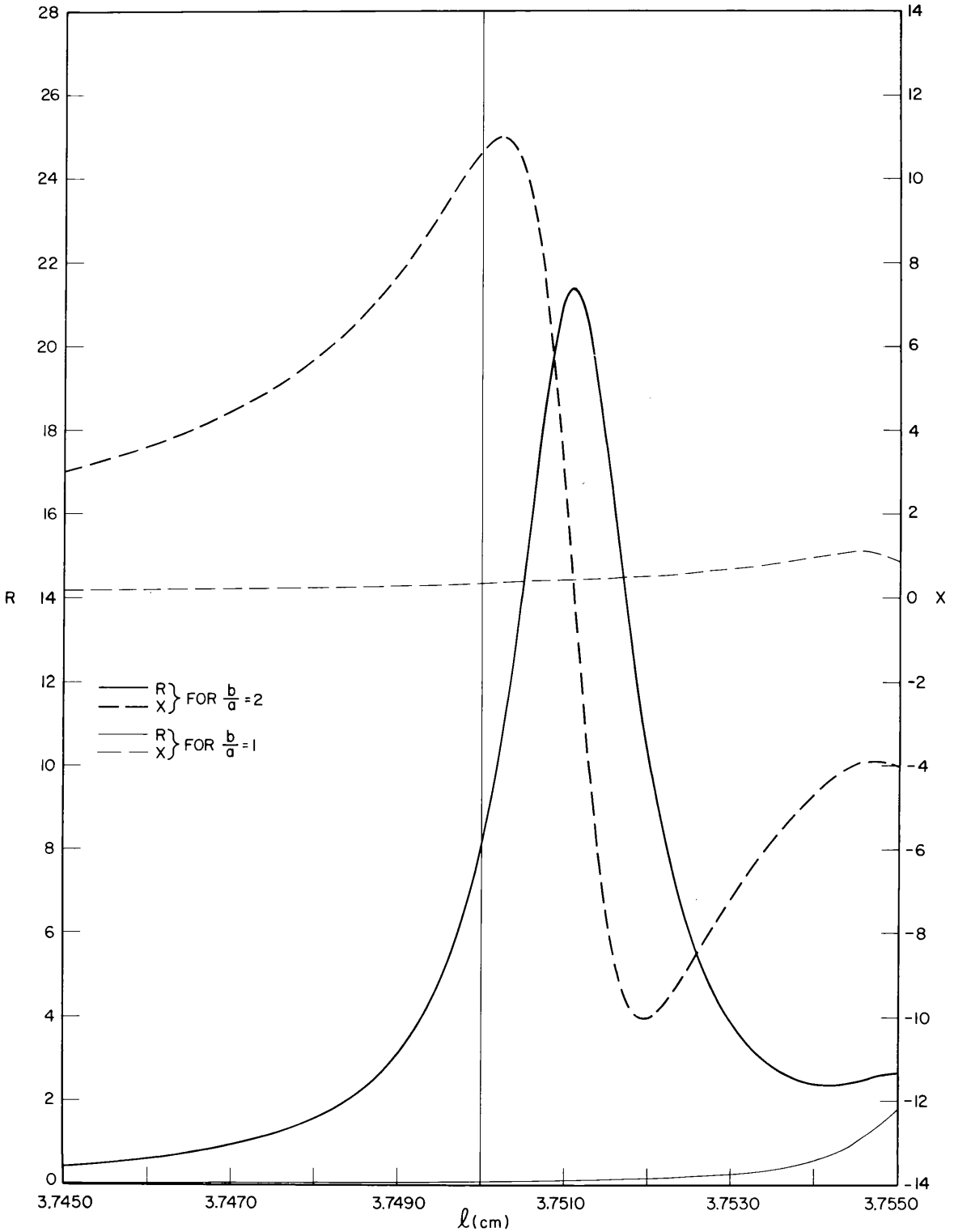

Fig. 20d—R and X vs ℓ for elastic solid boundary conditions (assuming orthogonal functions) and $n = 50$

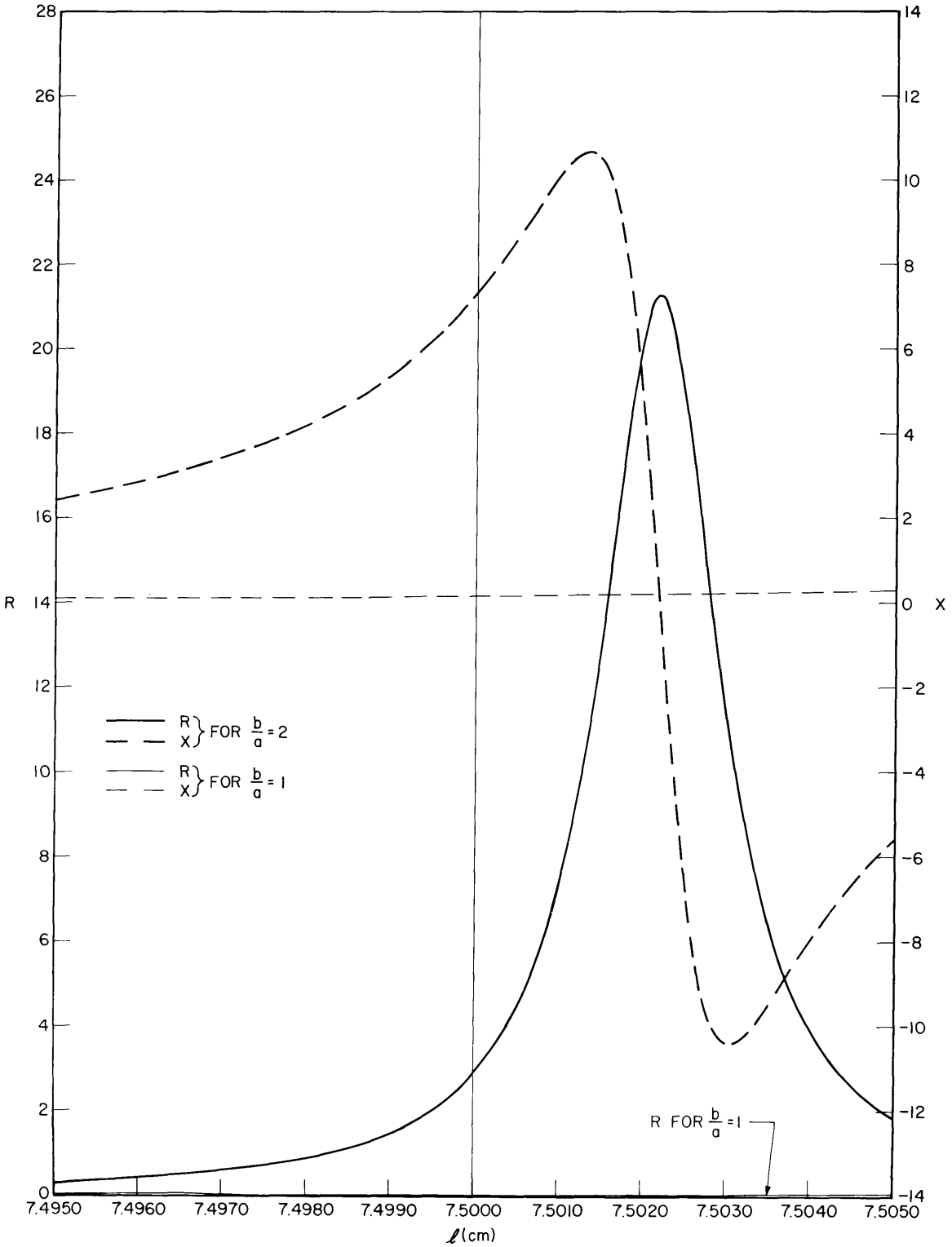

Fig. 20e—R and X vs ℓ for the elastic solid boundary conditions (assuming orthogonal functions) and $n = 100$

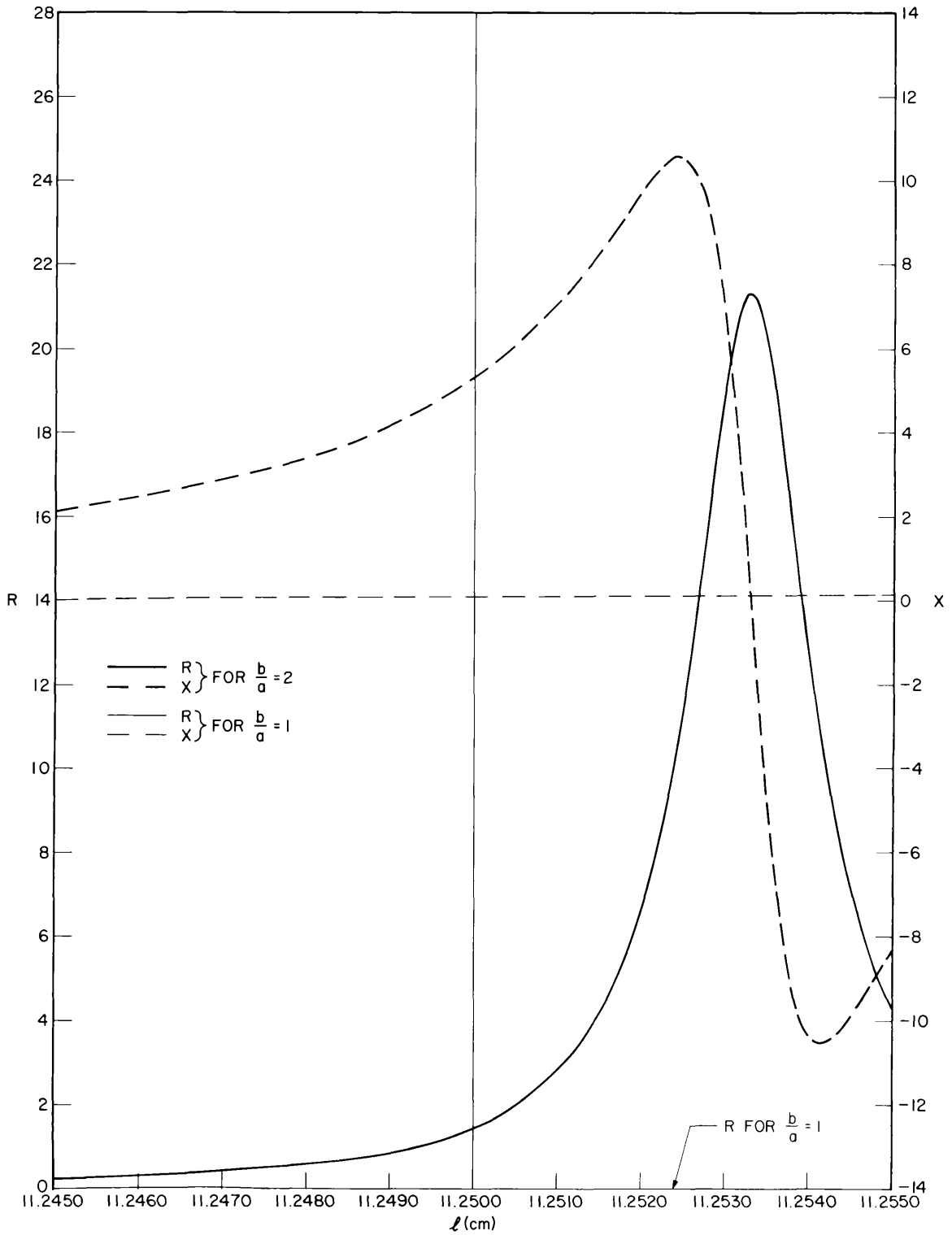

Fig. 20f—R and X vs ℓ for elastic solid boundary conditions (assuming orthogonal functions) and $n = 150$

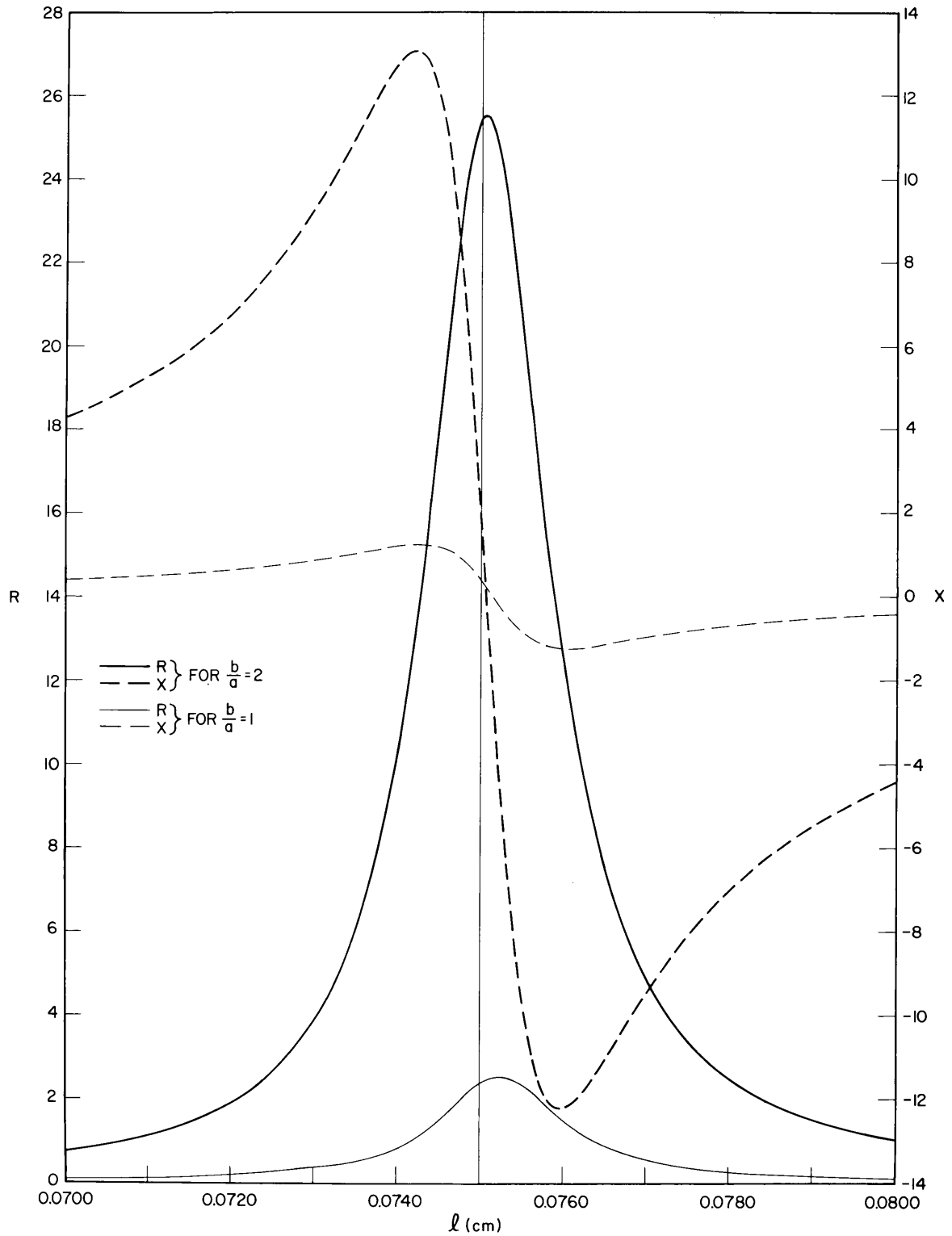

Fig. 21a—R and X vs ℓ for elastic solid boundary conditions (using actual functions) and $n = 1$

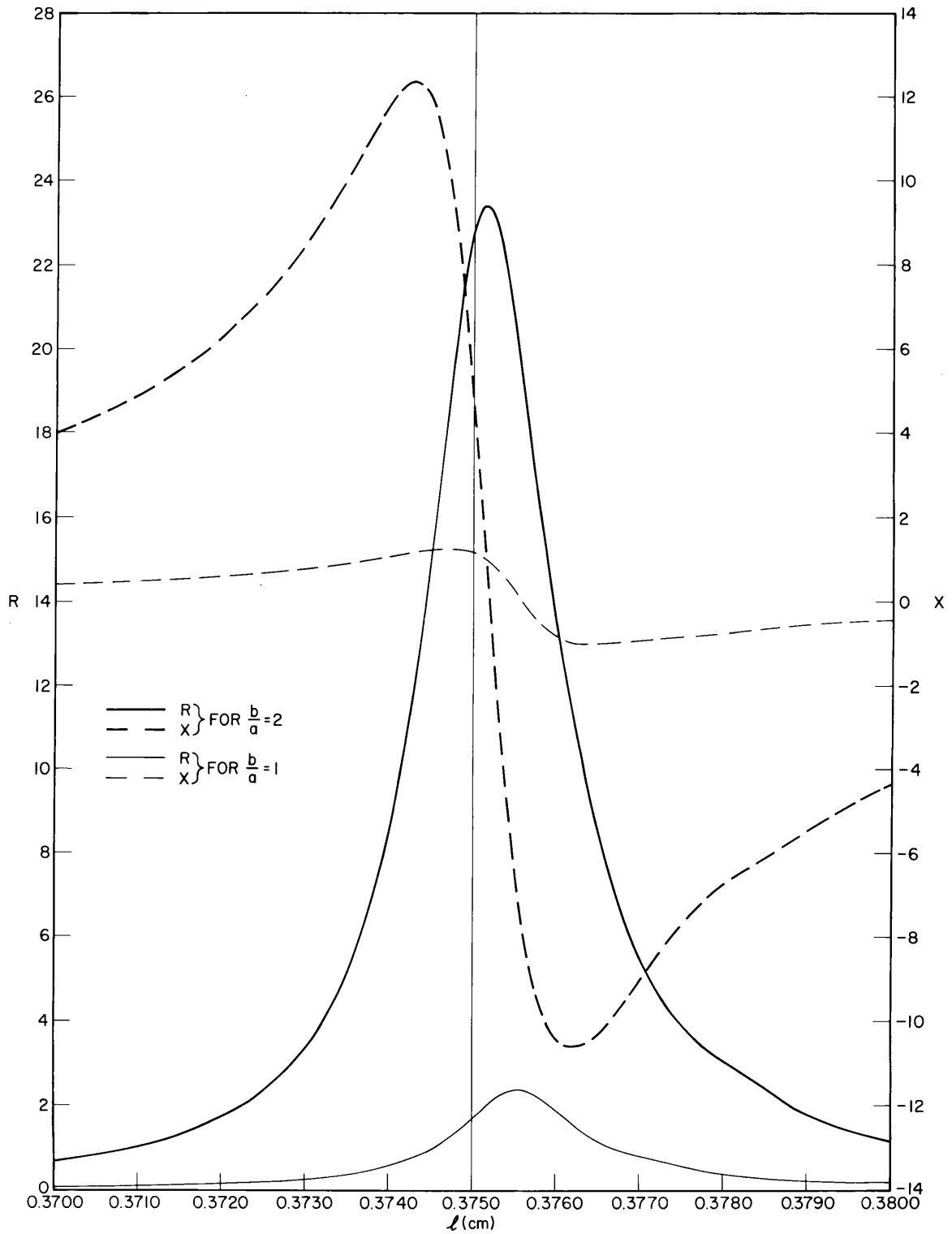

Fig. 21b—R and X vs ℓ for elastic solid boundary conditions (using actual functions) and $n = 5$

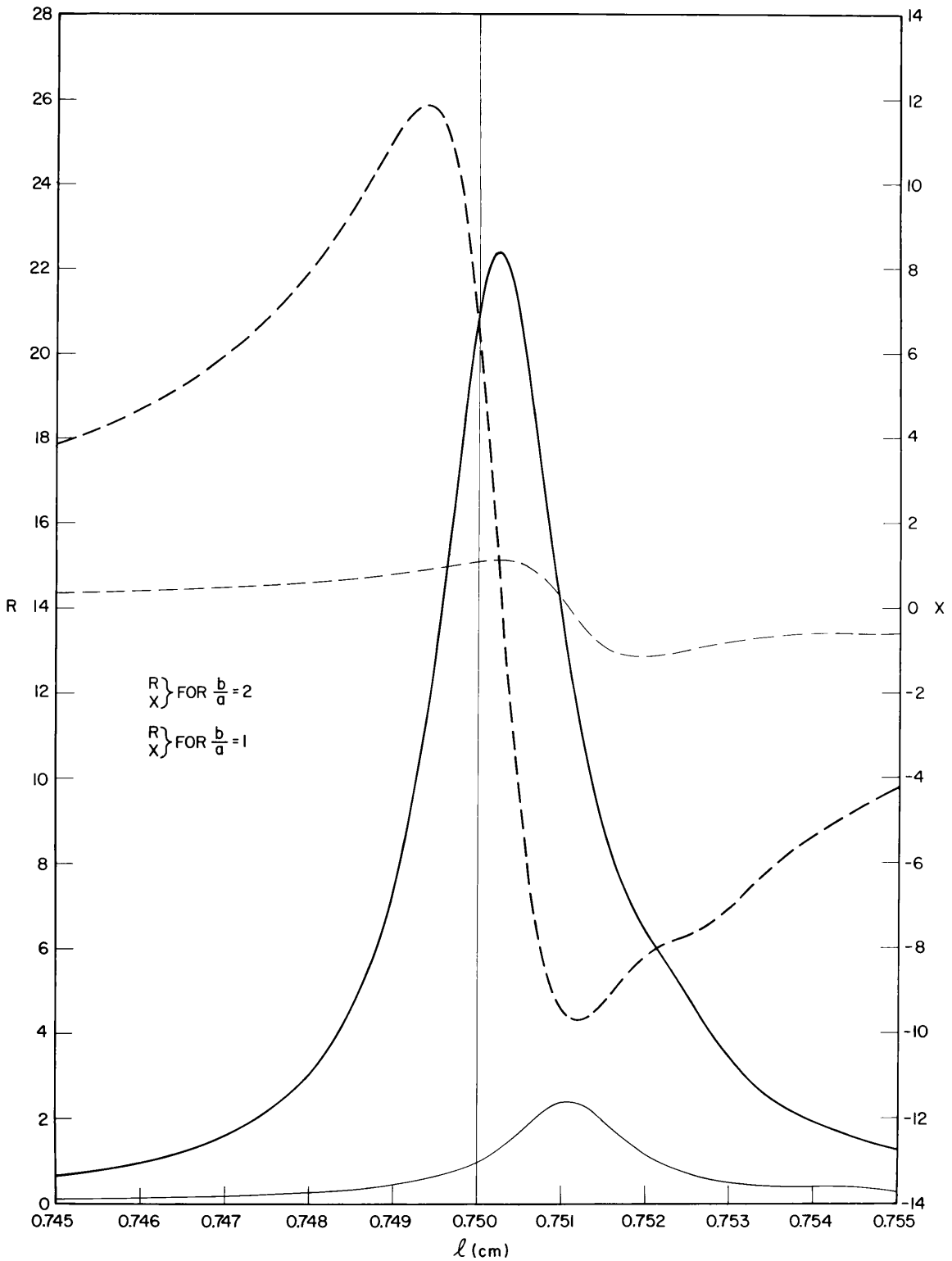

Fig. 21c—R and X vs ℓ for elastic solid boundary conditions (using actual functions) and $n = 10$

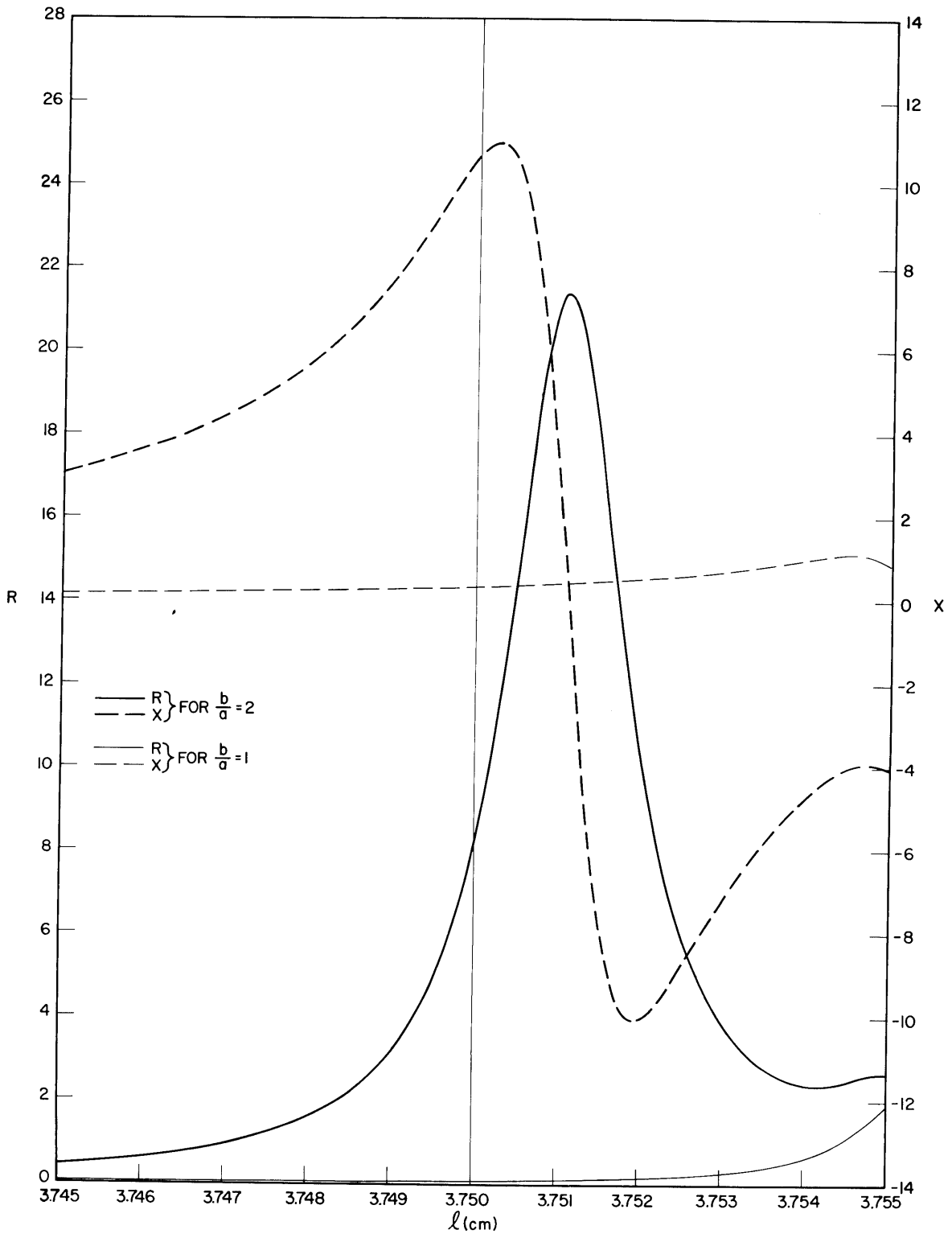

Fig. 21d – R and X vs ℓ for elastic solid boundary conditions (using actual functions) and $n = 50$

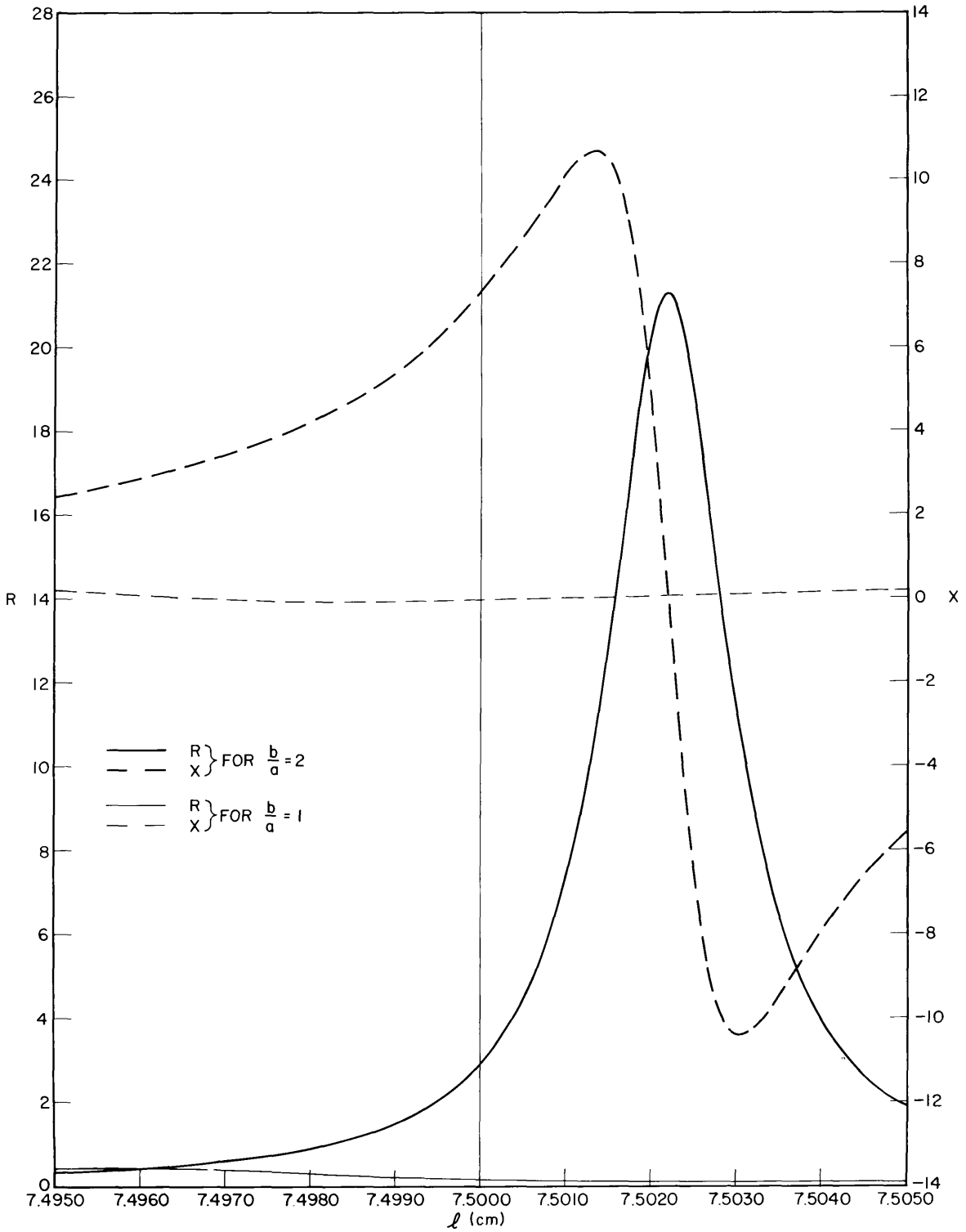

Fig. 21e—R and X vs ℓ for elastic solid boundary conditions (using actual functions) and n = 100

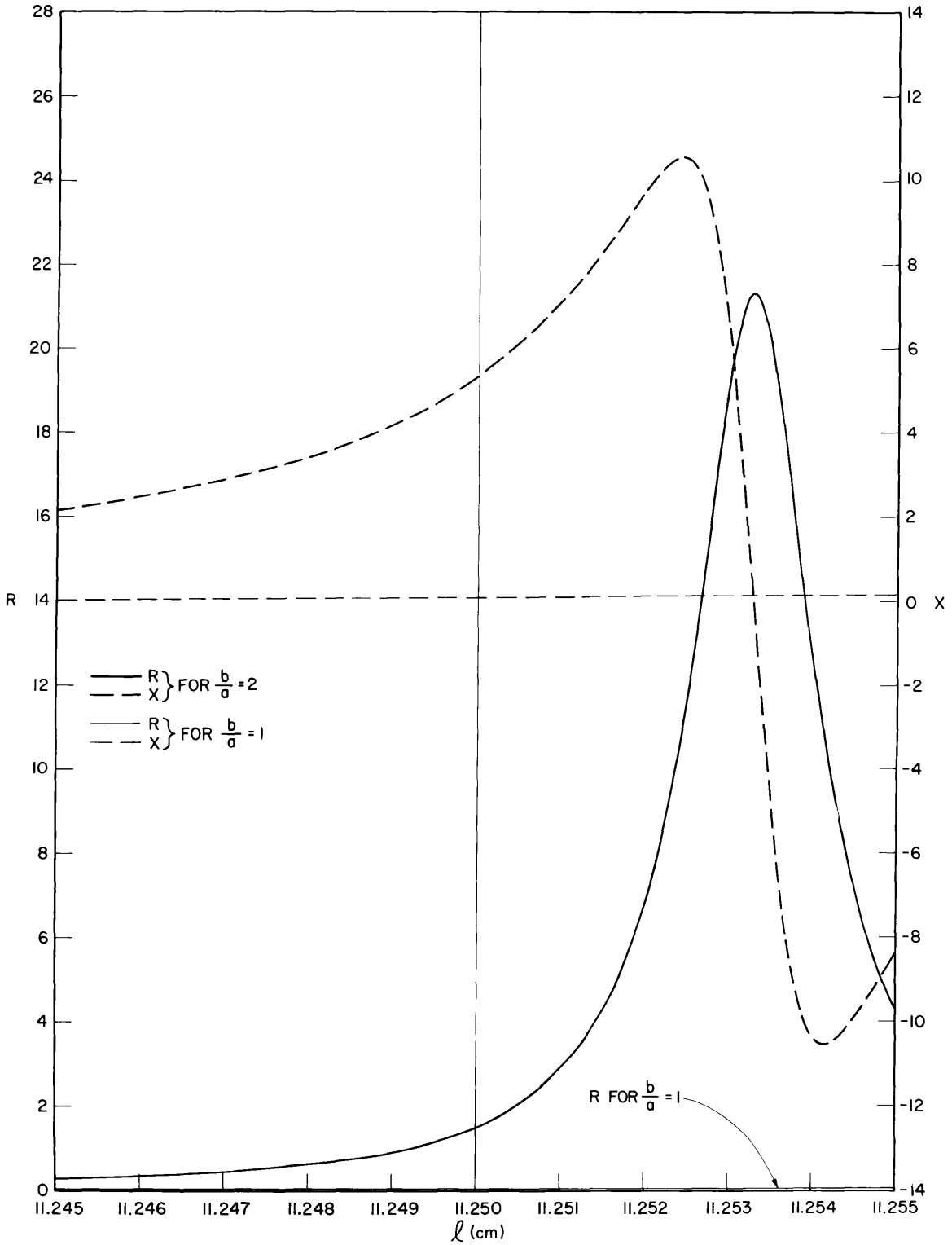

Fig. 21f—R and X vs ℓ for elastic solid boundary conditions (using actual functions) and n = 150

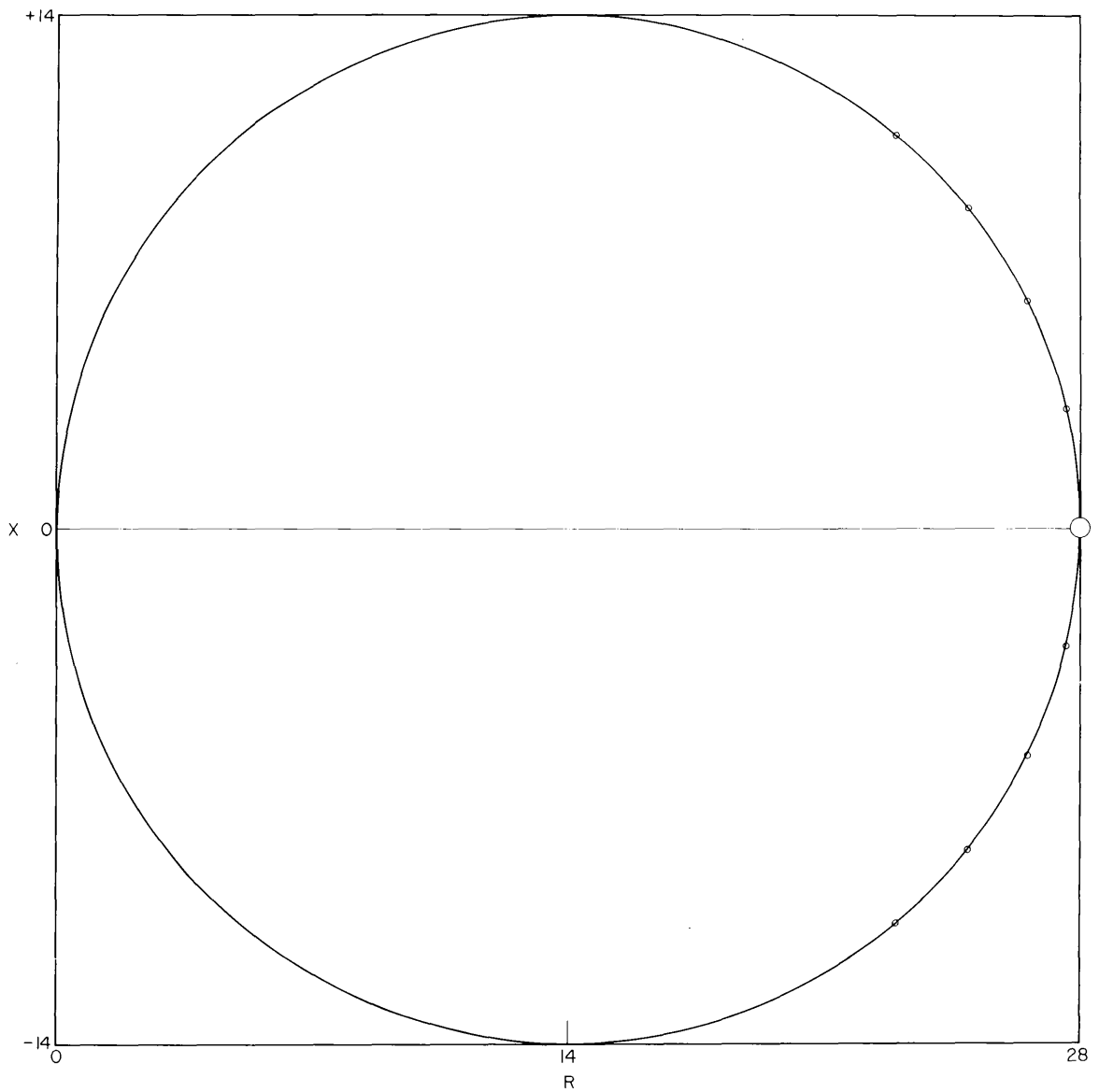

Fig. 22a—R vs X for absolutely rigid boundary conditions and $b/a = 1$

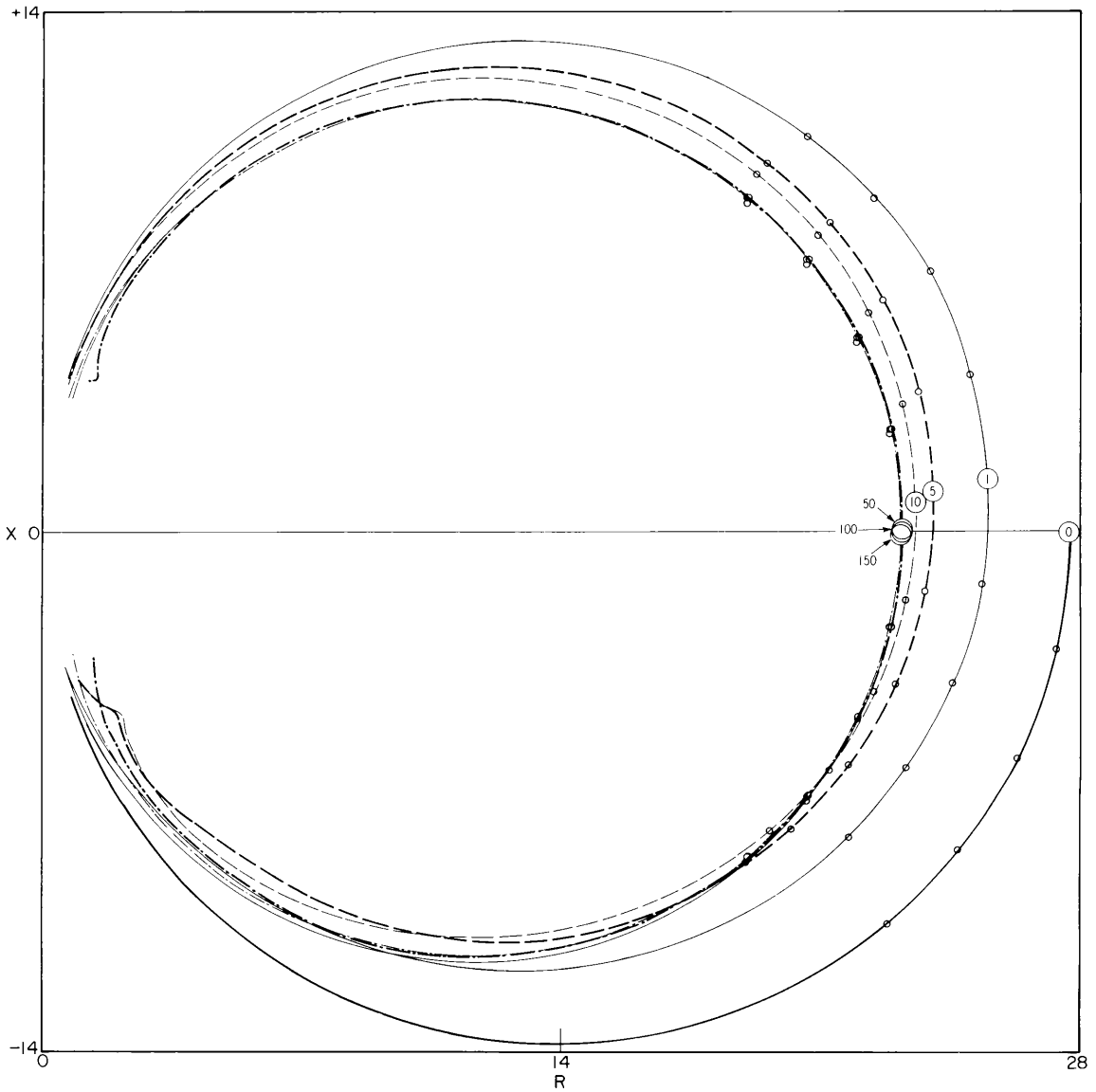

Fig. 22b—R vs X for absolutely rigid boundary conditions and b/a = 1.1 (see Table 2)

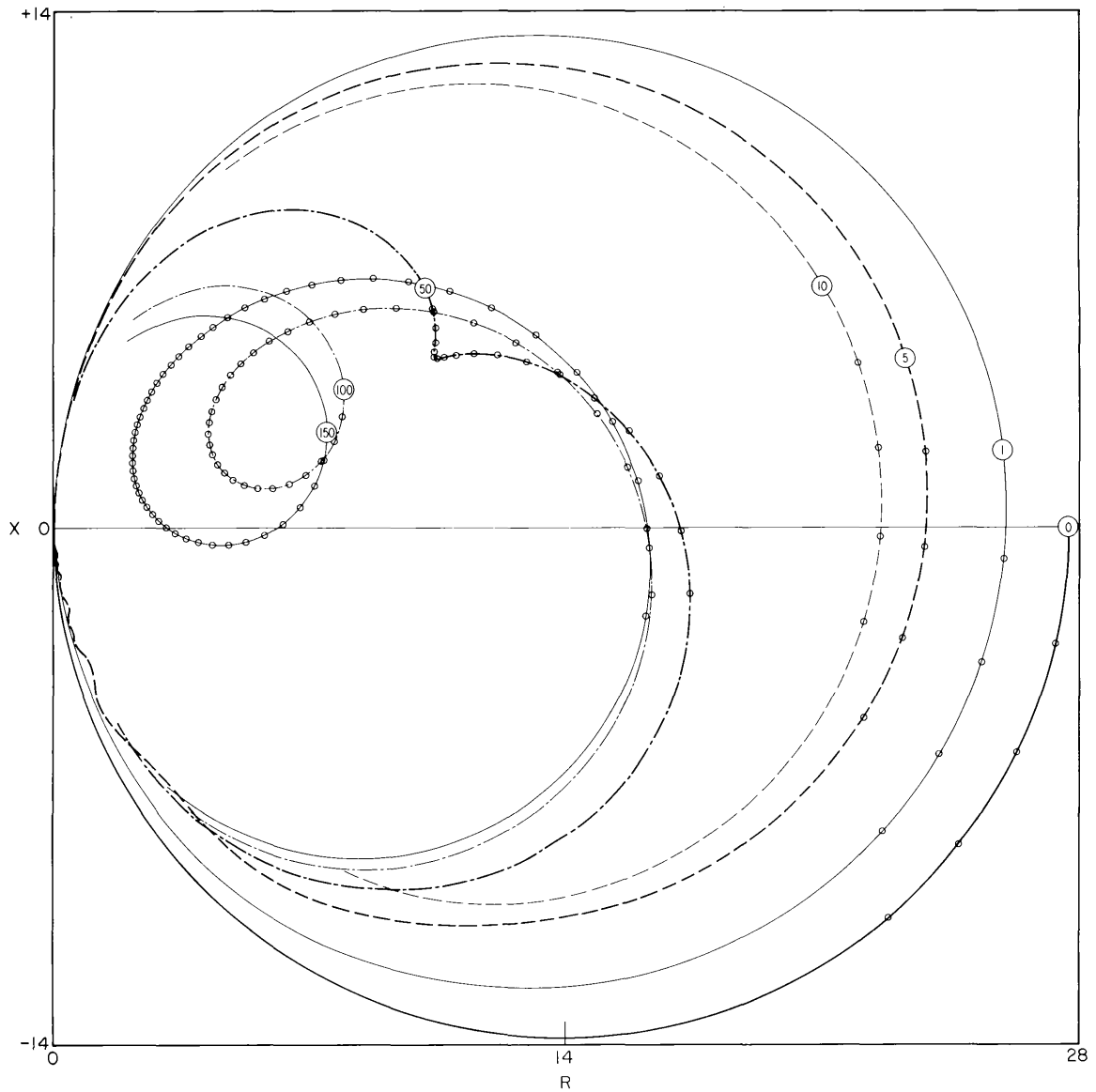

Fig. 22c—R vs X for absolutely rigid boundary conditions and $b/a = 2$ (see Table 3)

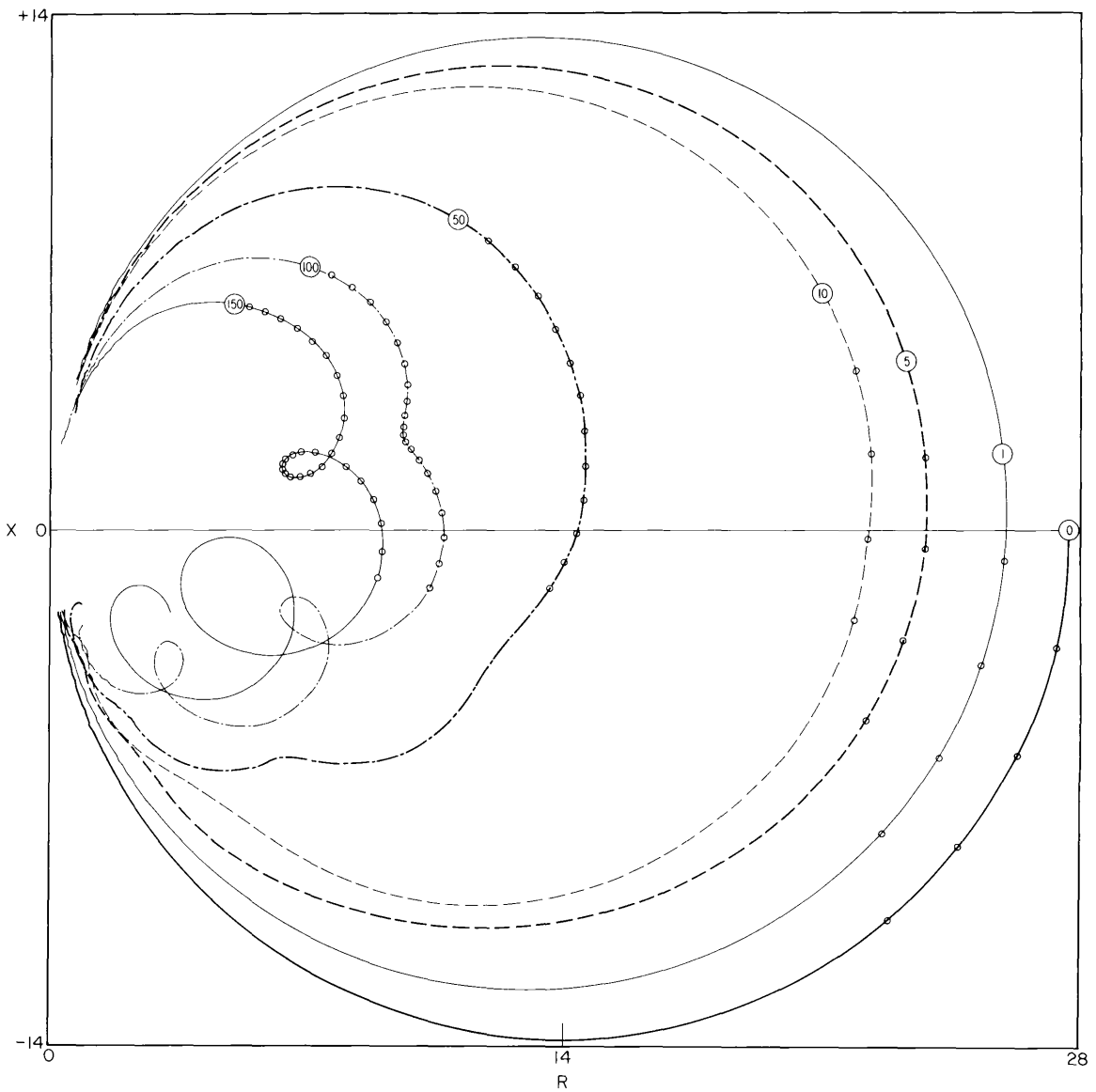

Fig. 22d—R vs X for absolutely rigid boundary conditions and $b/a = 5$ (see Table 4)

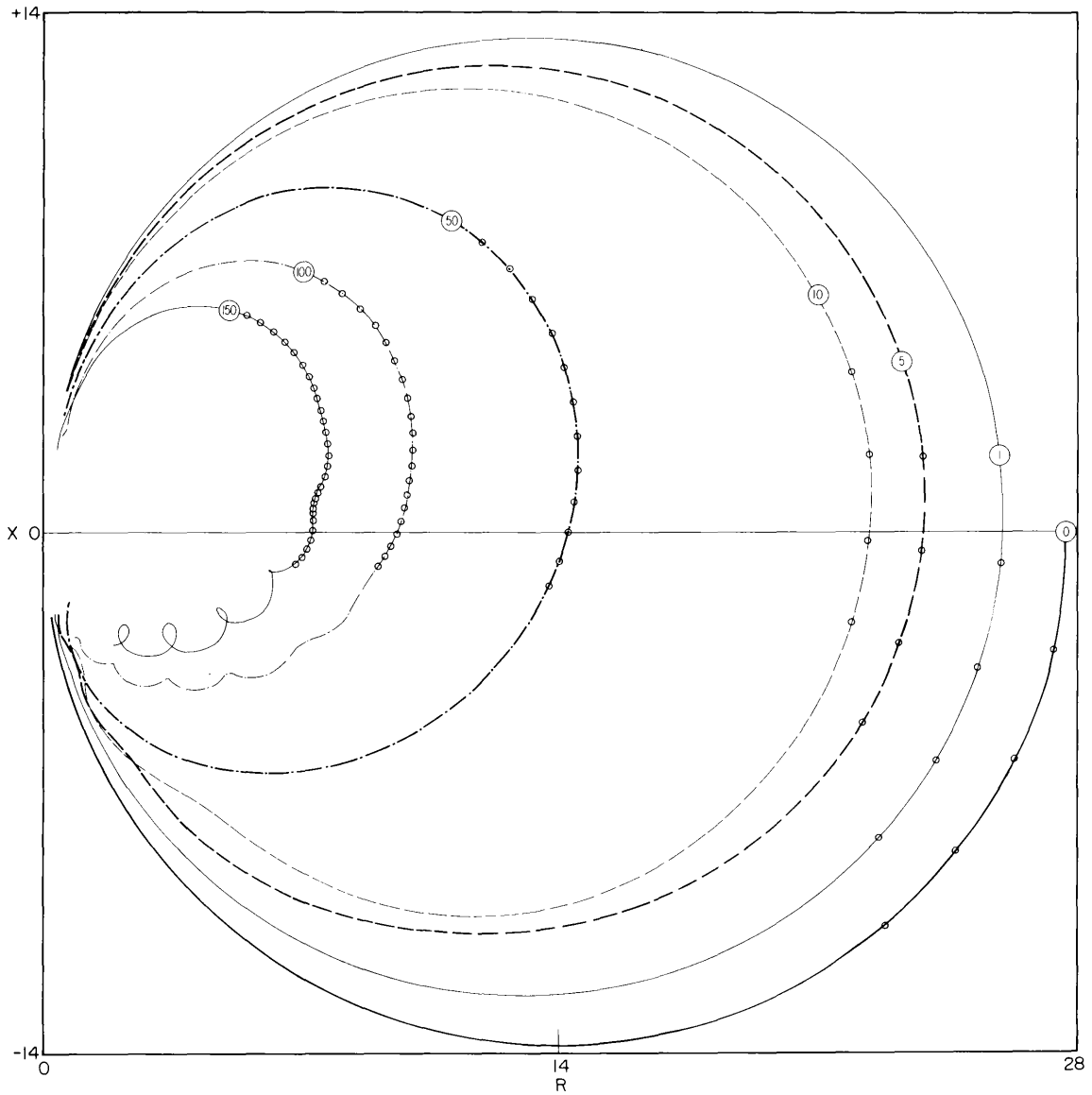

Fig. 22e—R vs X for absolutely rigid boundary conditions and $b/a = 10$ (see Table 5)

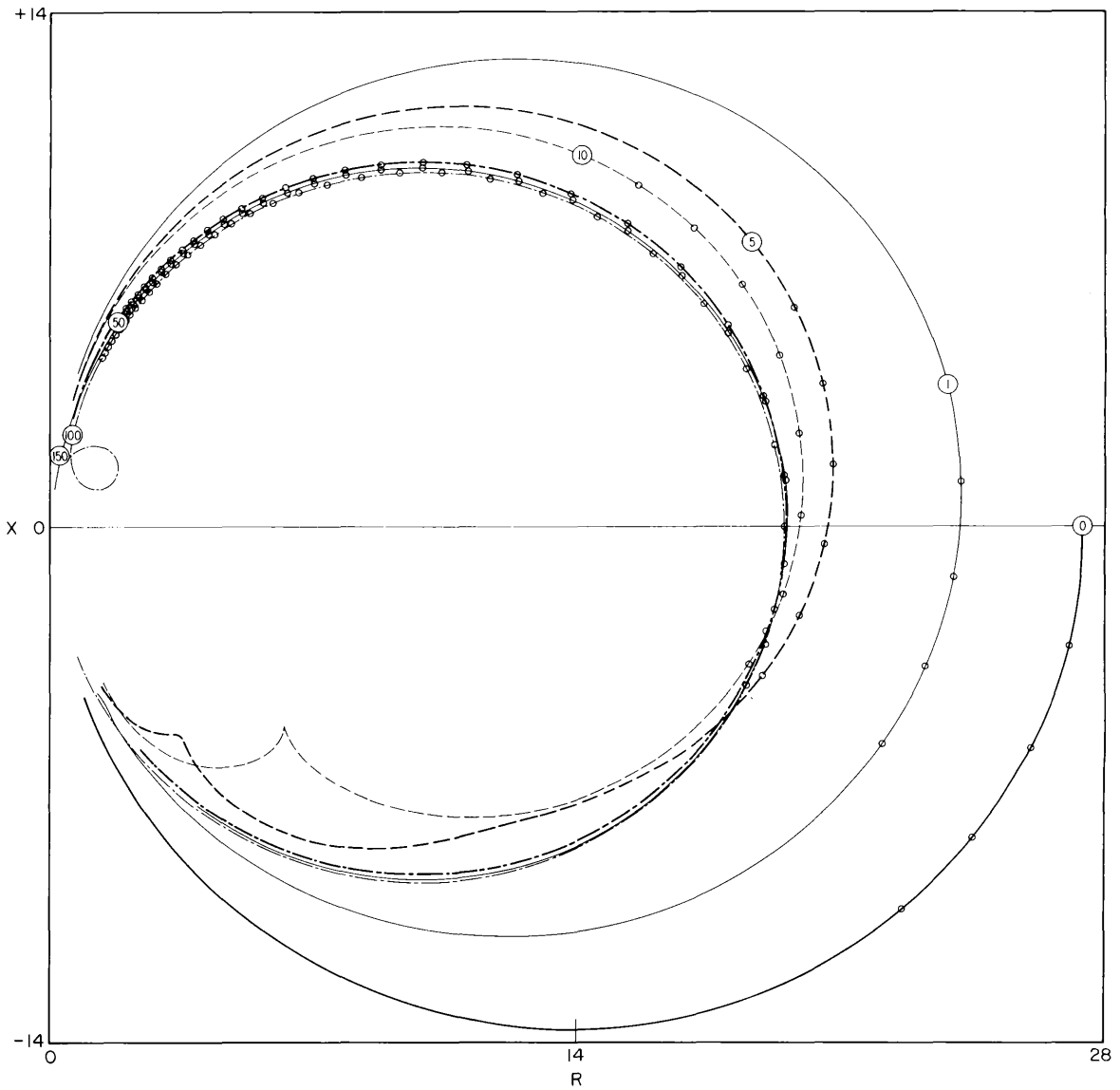

Fig. 23a—R vs X for infinitely flexible boundary conditions and $b/a = 1$ (see Table 6)

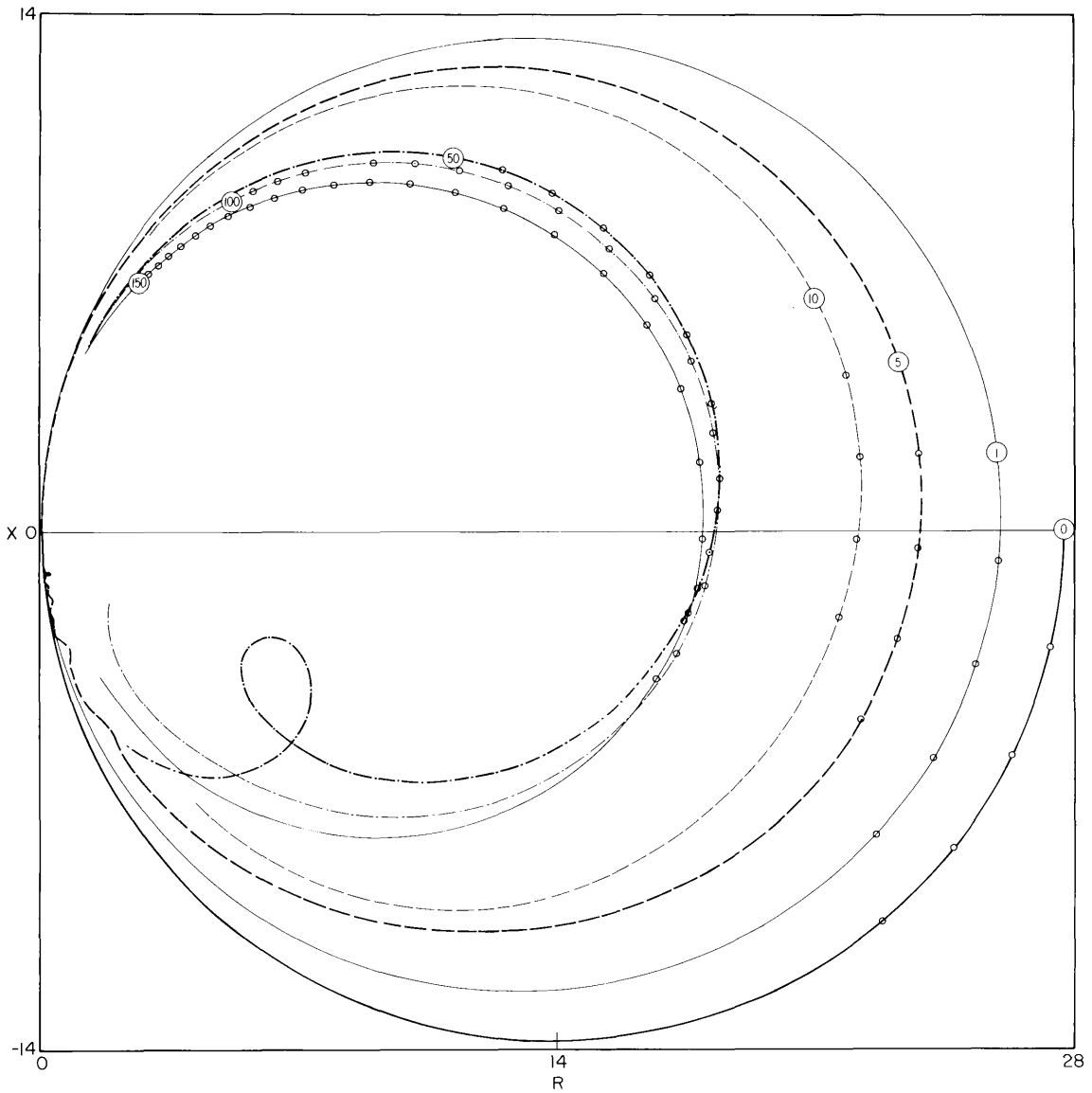

Fig. 23b—R vs X for infinitely flexible boundary conditions and $b/a = 2$ (see Table 7)

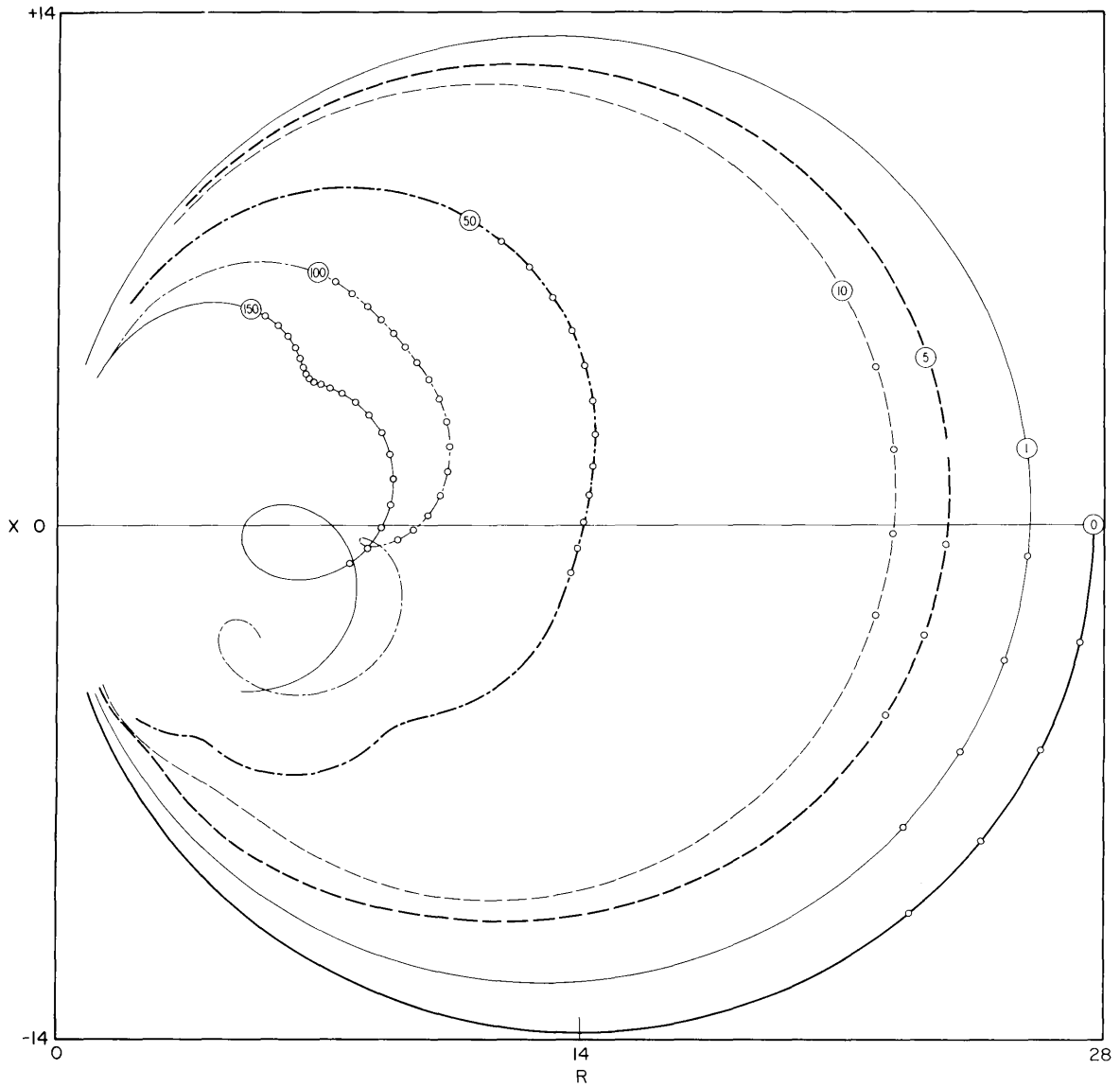

Fig. 23c – R vs X for infinitely flexible boundary conditions and $b/a = 5$ (see Table 8)

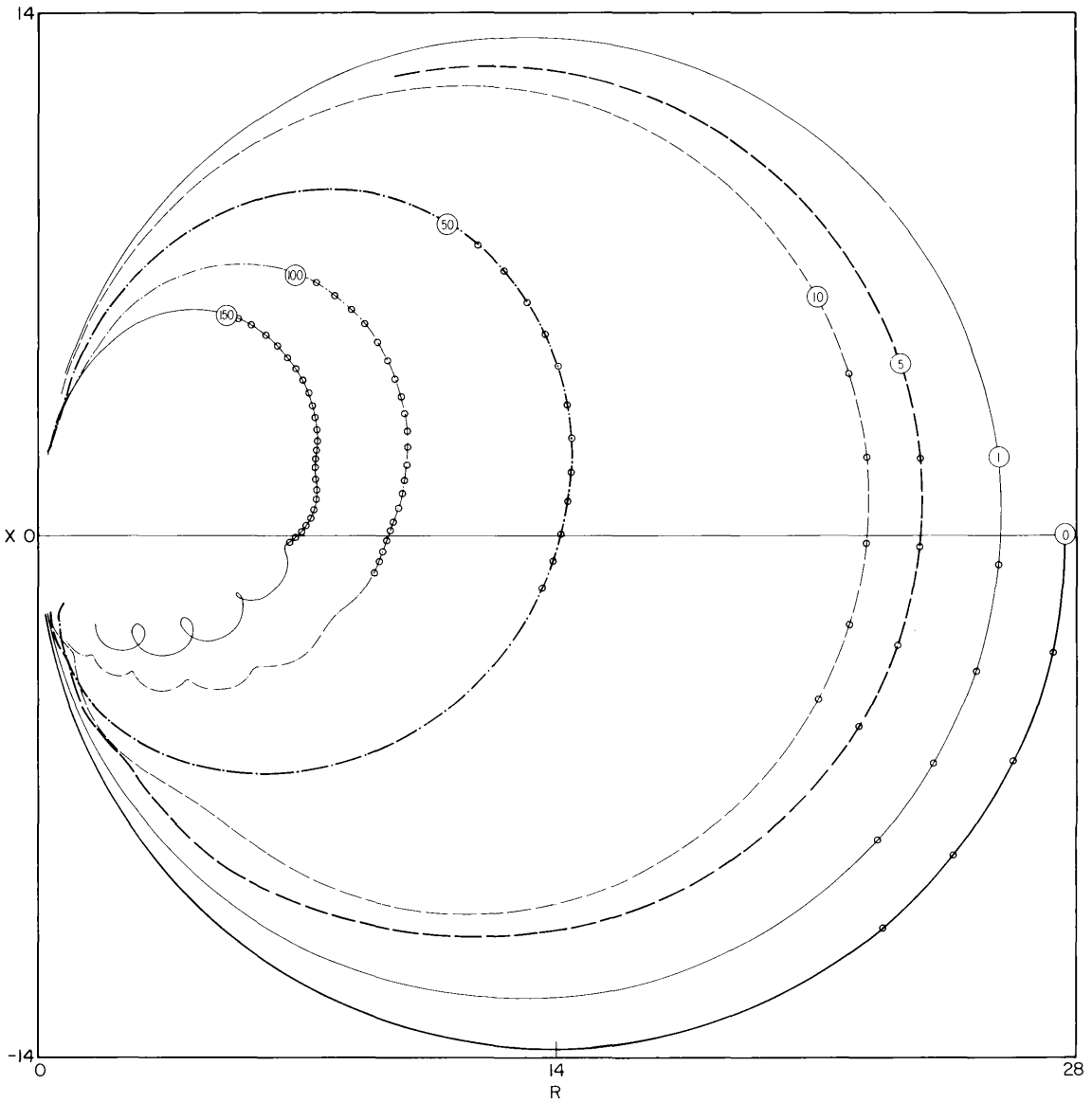

Fig. 23d—R vs X for infinitely flexible boundary conditions and $b/a = 10$ (see Table 9)

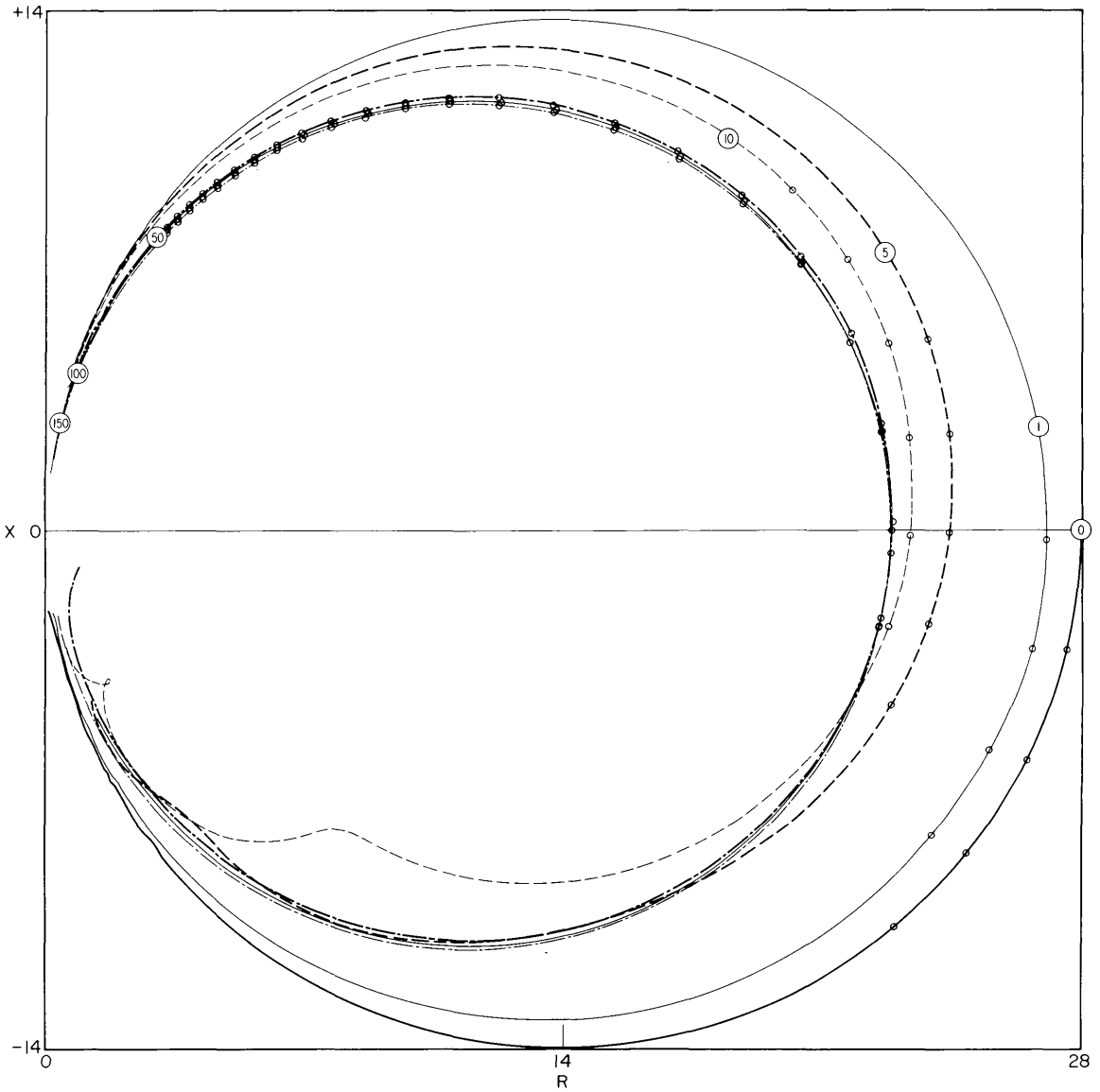

Fig. 24a—R vs X for liquid boundary conditions (assuming orthogonal functions) and $b/a = 1$ (see Table 10)

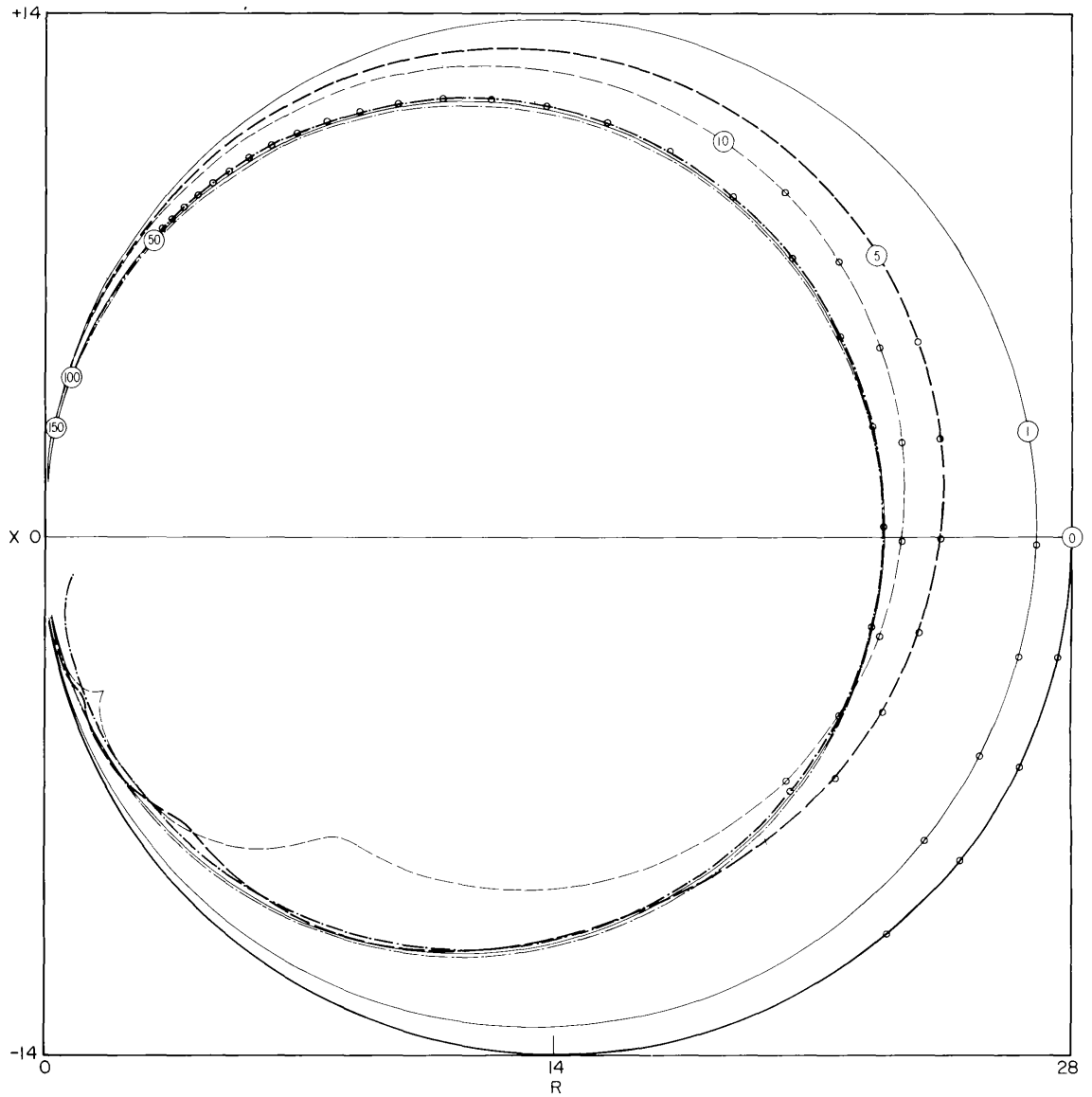

Fig. 24b—R vs X for liquid boundary conditions (using actual functions) and $b/a = 1$ (see Table 11)

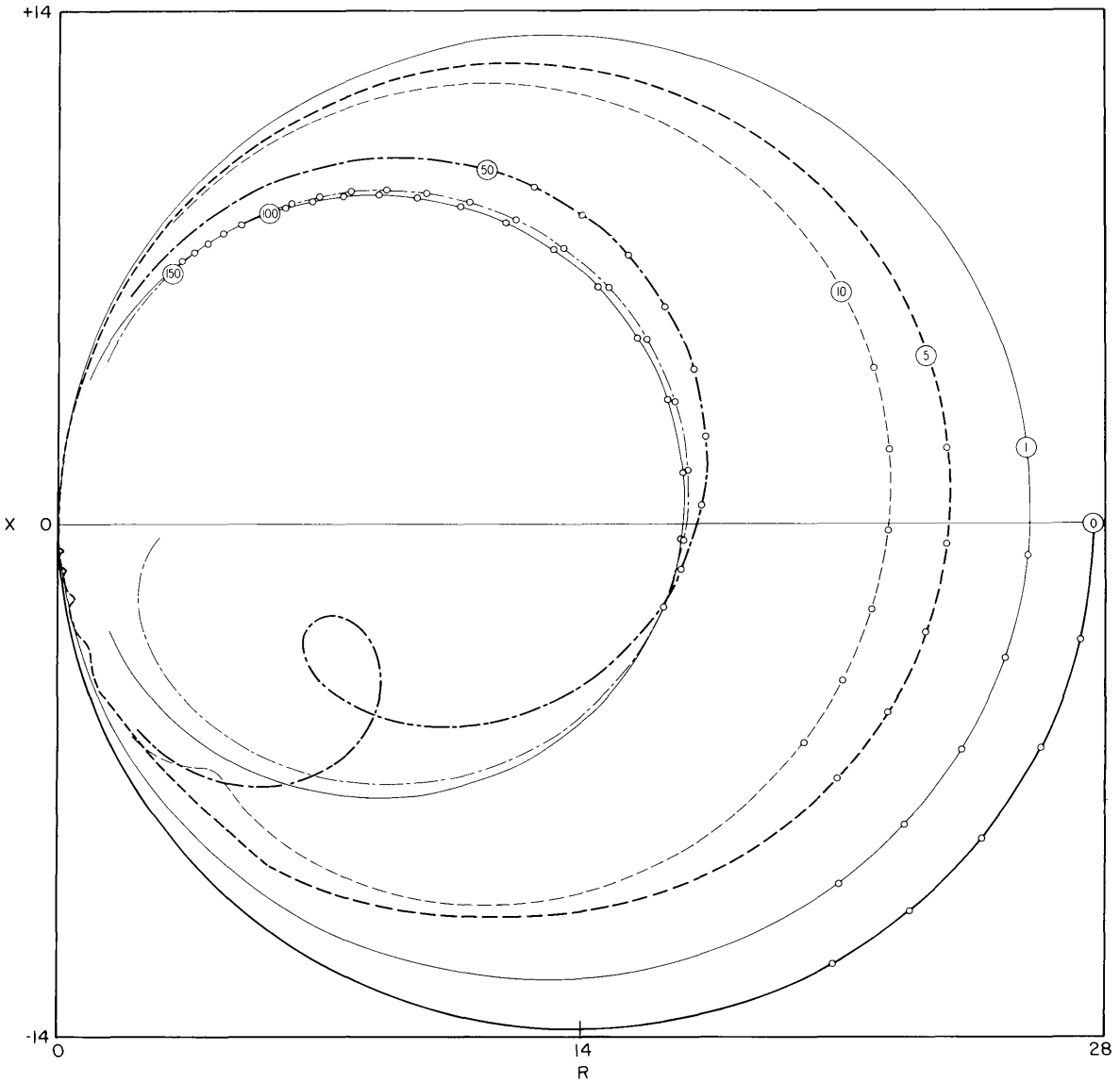

Fig. 24c—R vs X for liquid boundary conditions (assuming orthogonal functions) and $b/a = 2$ (see Table 12)

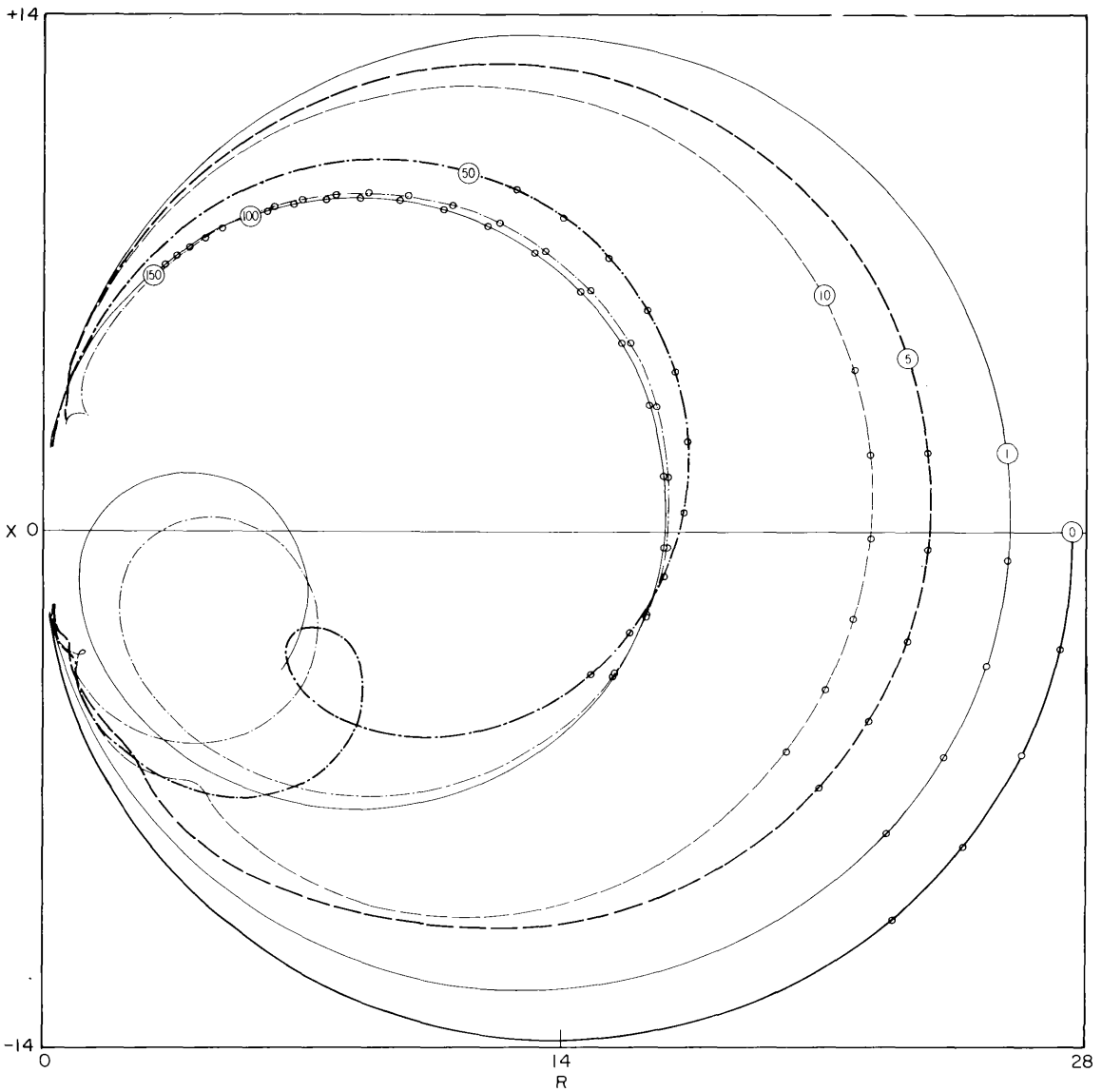

Fig. 24d—R vs X for liquid boundary conditions (using actual functions) and $b/a = 2$ (see Table 13)

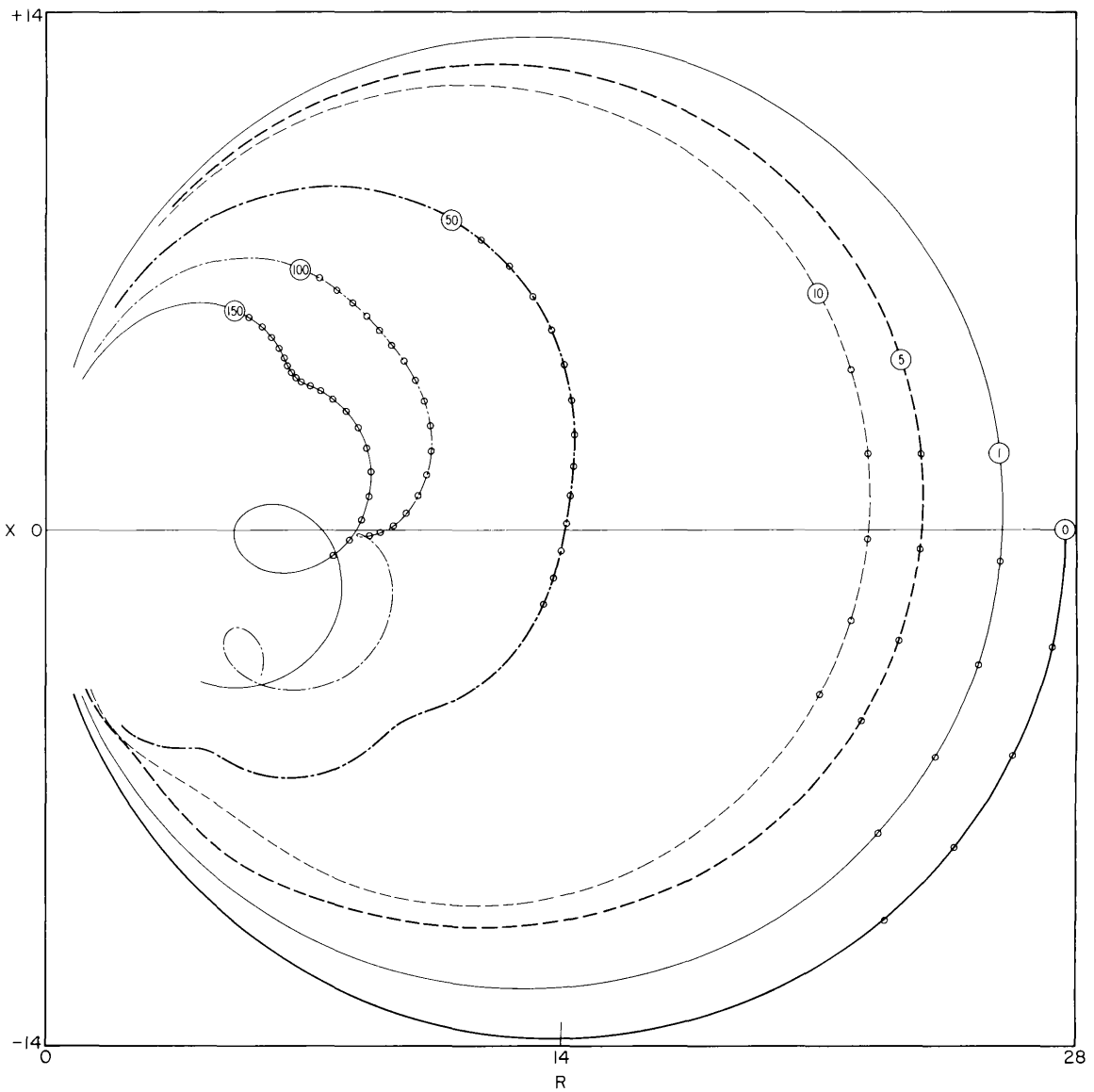

Fig. 24e – R vs X for liquid boundary conditions and $b/a = 5$ (see Table 14)

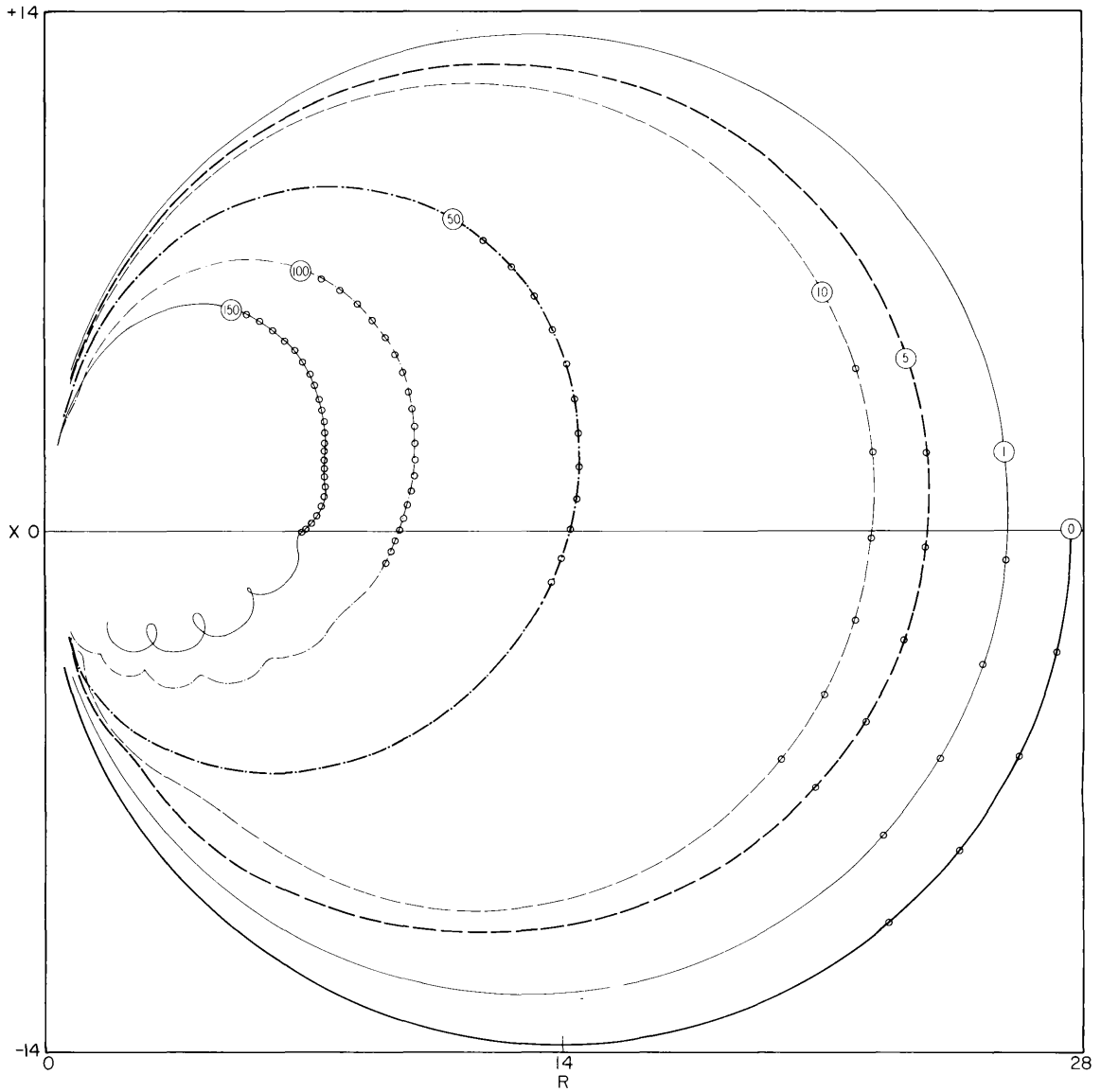

Fig. 24f—R vs X for liquid boundary conditions and $b/a = 10$ (see Table 15)

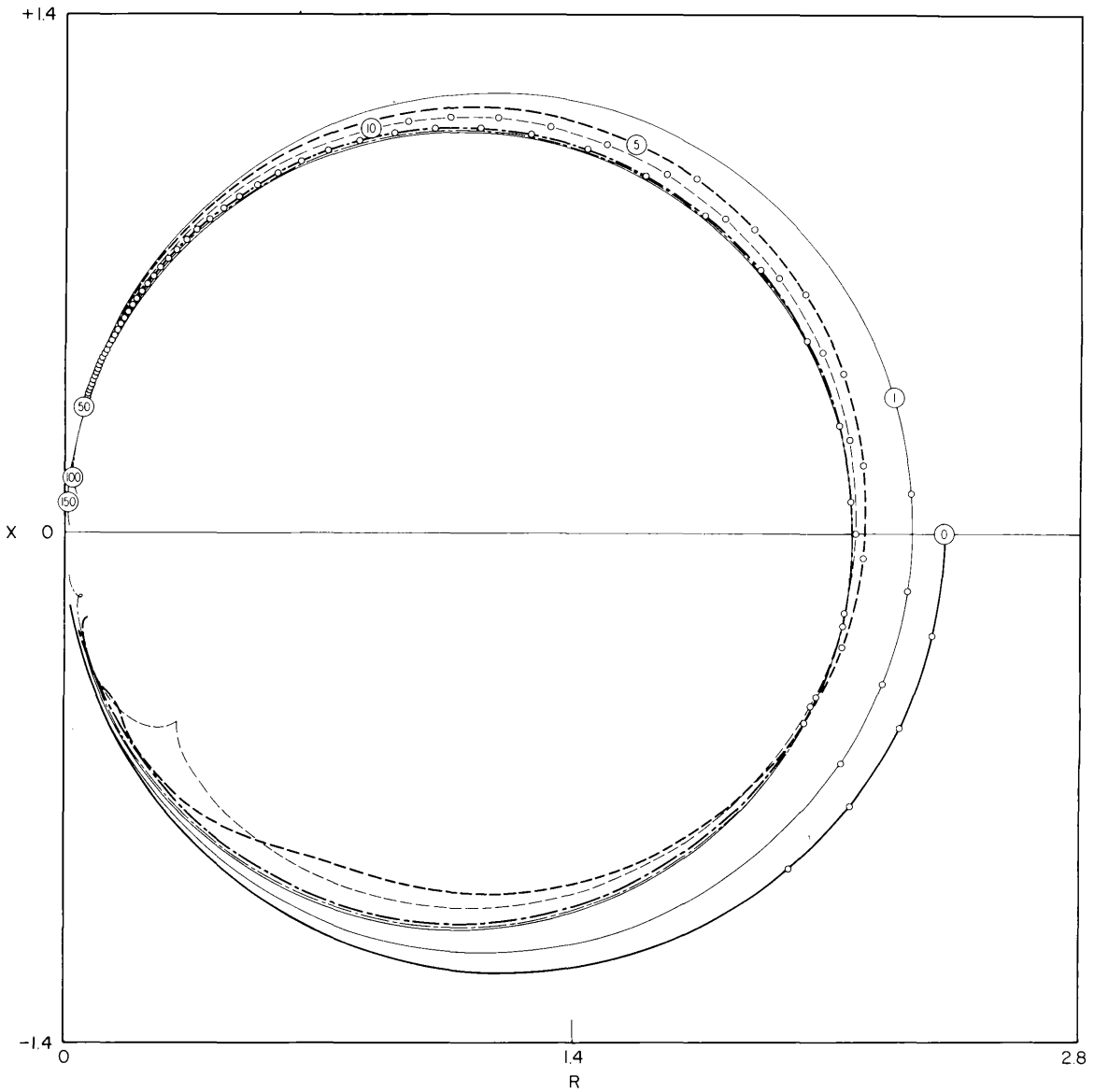

Fig. 25a—R vs X for elastic solid boundary conditions (assuming orthogonal functions) and $b/a = 1$ (see Table 16)

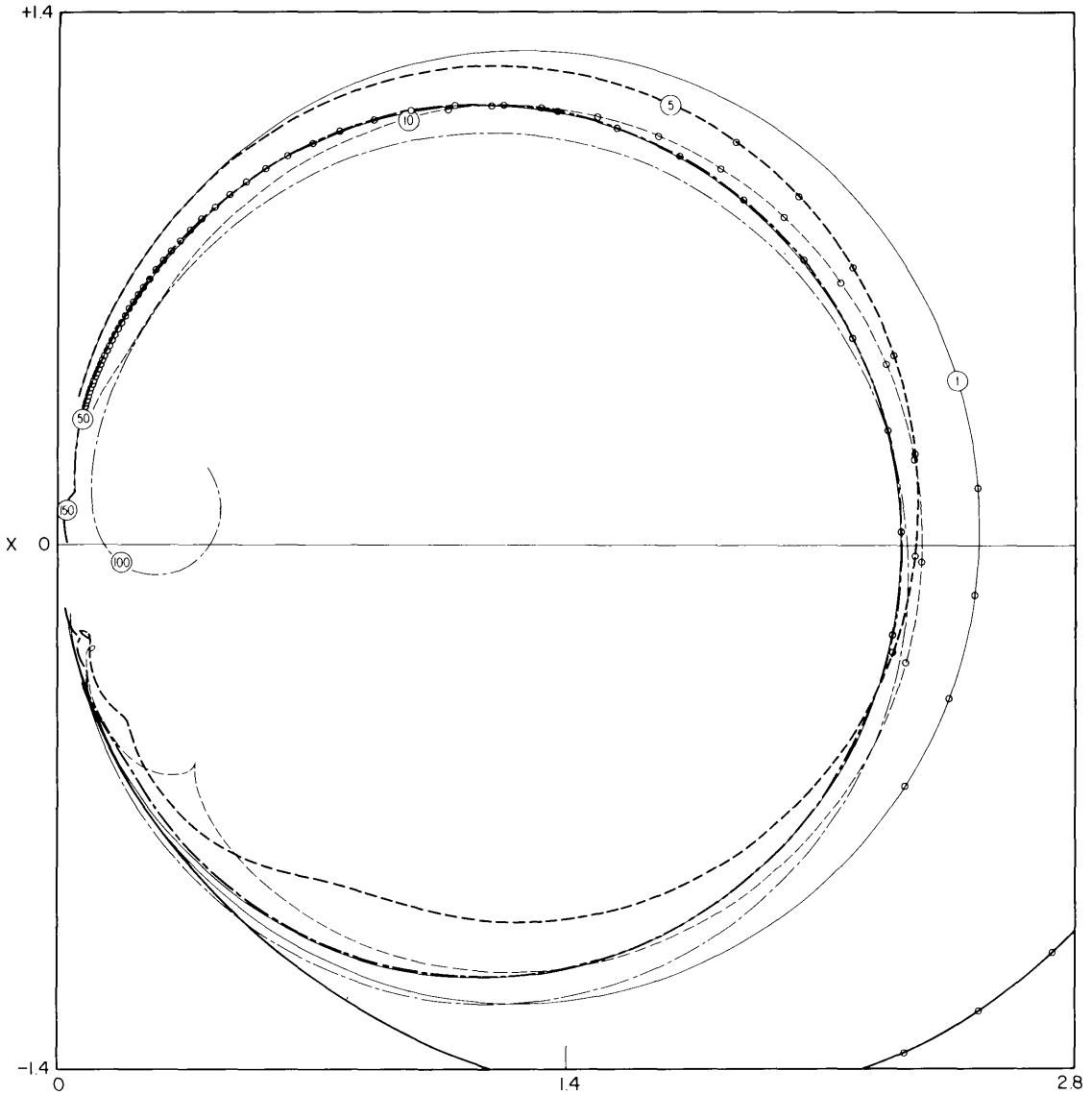

Fig. 25b—R vs X for elastic solid boundary conditions (using actual functions) and $b/a = 1$ (see Table 17)

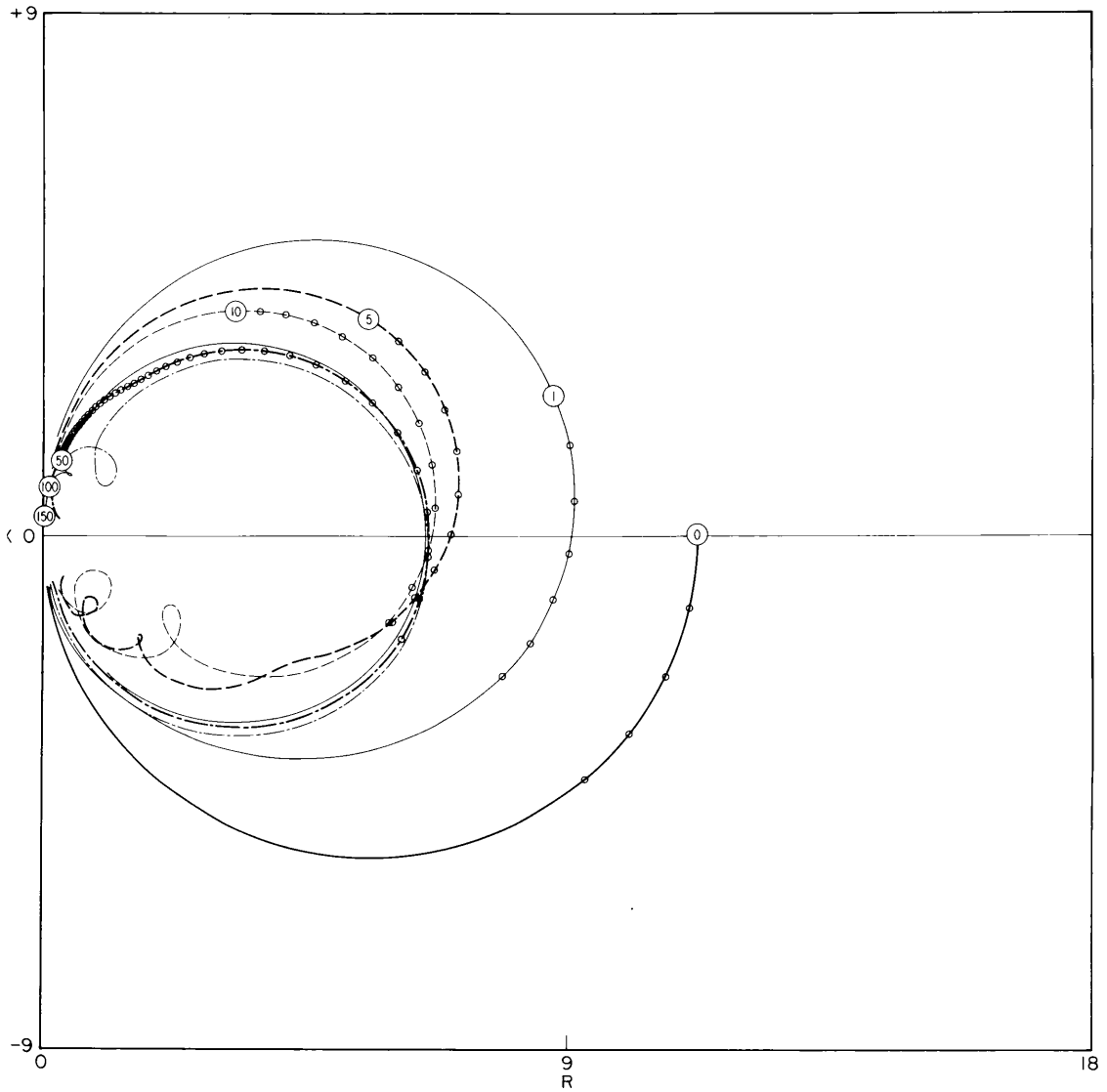

Fig. 25c—R vs X for elastic solid boundary conditions (assuming orthogonal functions) and $b/a = 1.1$ (see Table 18)

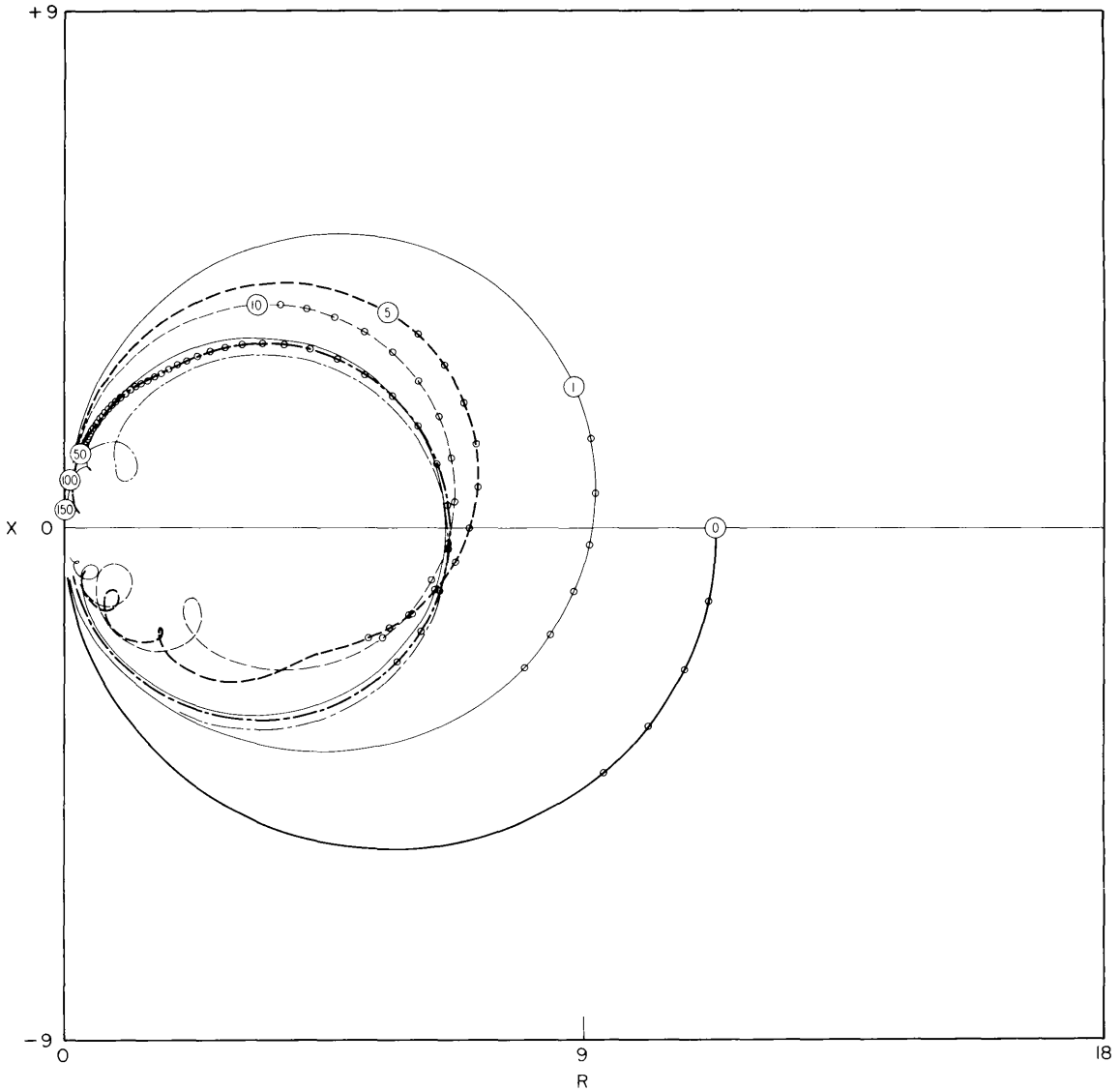

Fig. 25d—R vs X for elastic solid boundary conditions (using actual functions) and $b/a = 1.1$ (see Table 19)

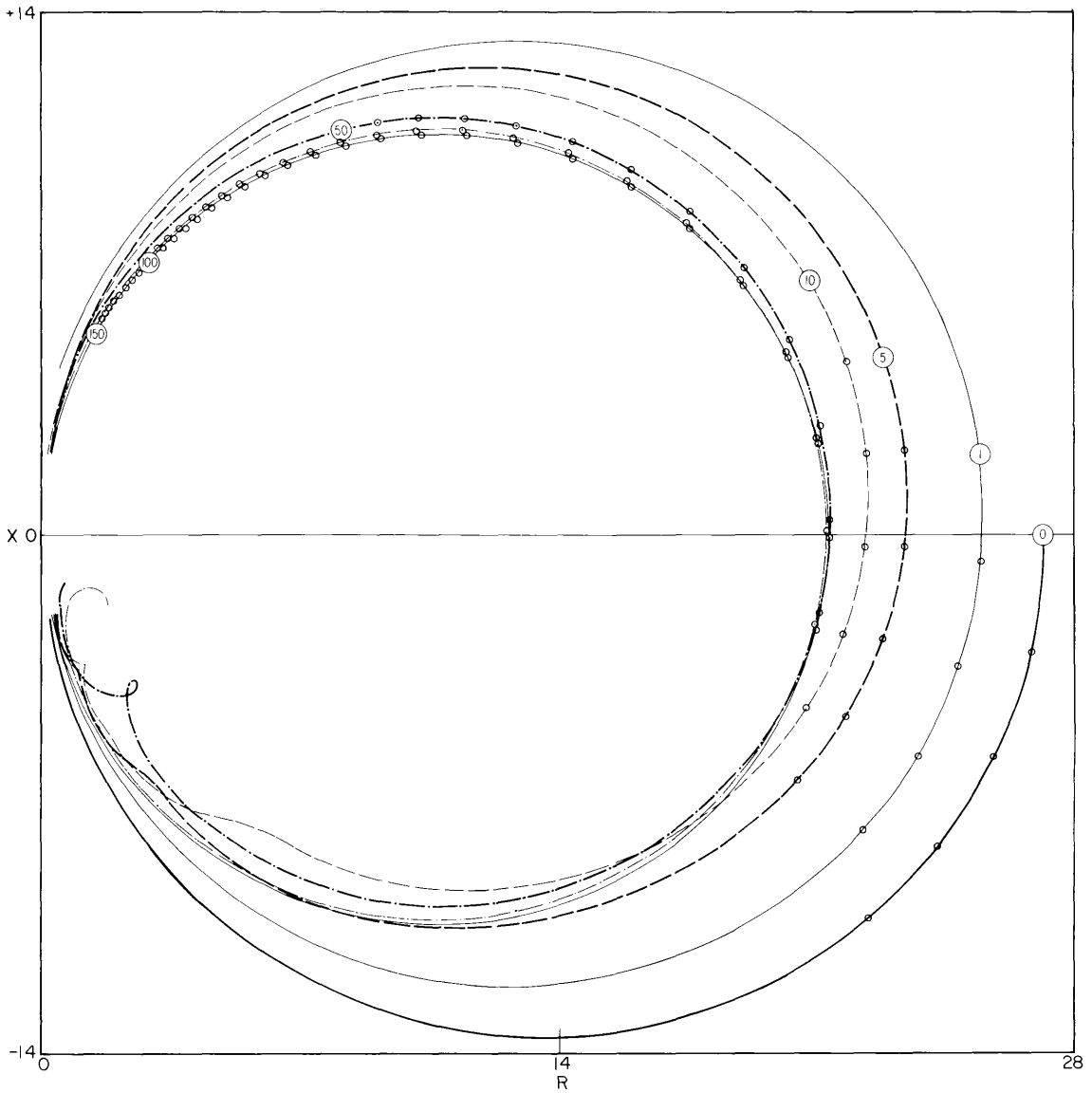

Fig. 25e—R vs X for elastic solid boundary conditions (assuming orthogonal functions) and $b/a = 2$ (see Table 20)

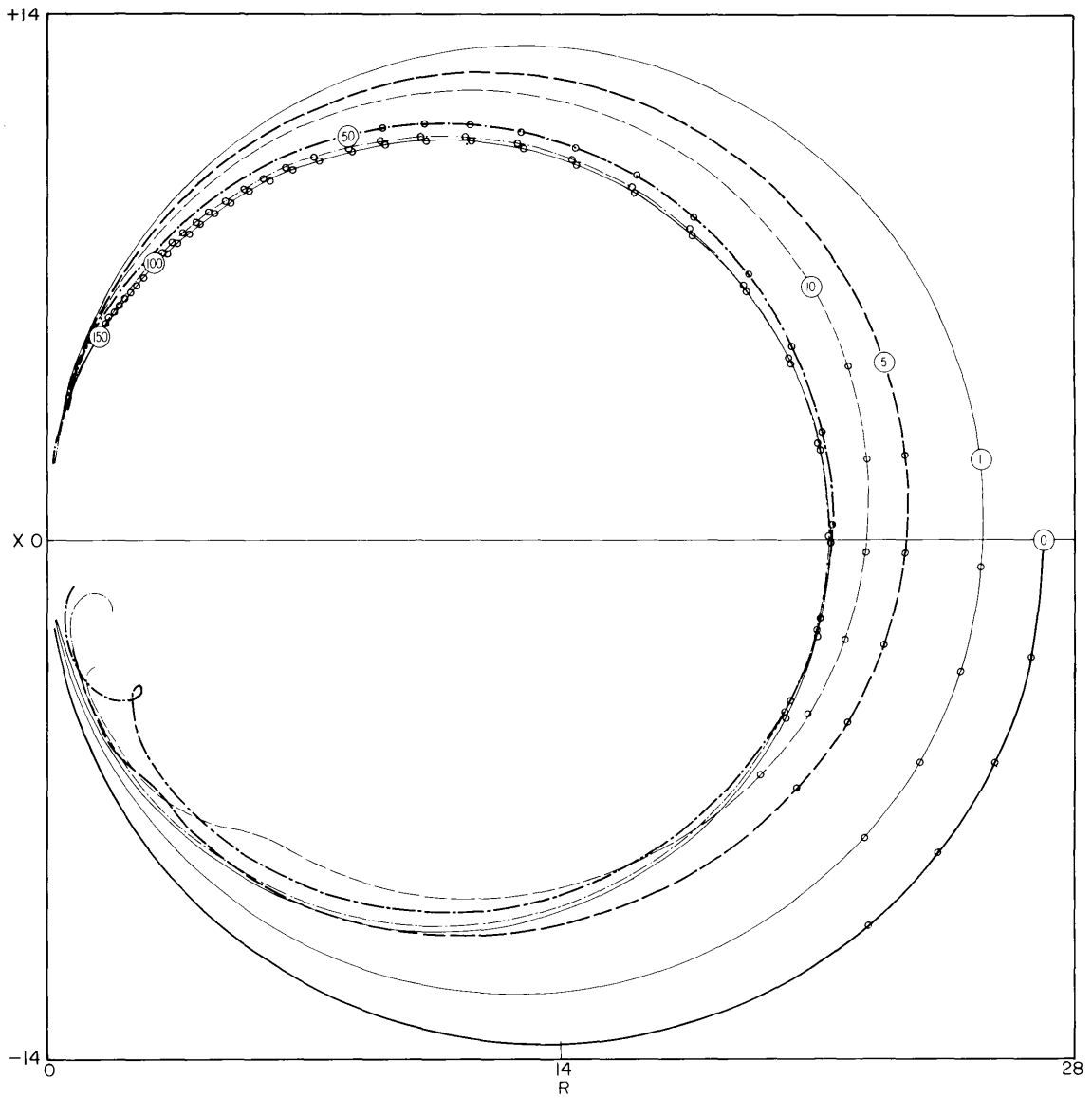

Fig. 25f—R vs X for elastic solid boundary conditions (using actual functions) and $b/a = 2$ (see Table 21)

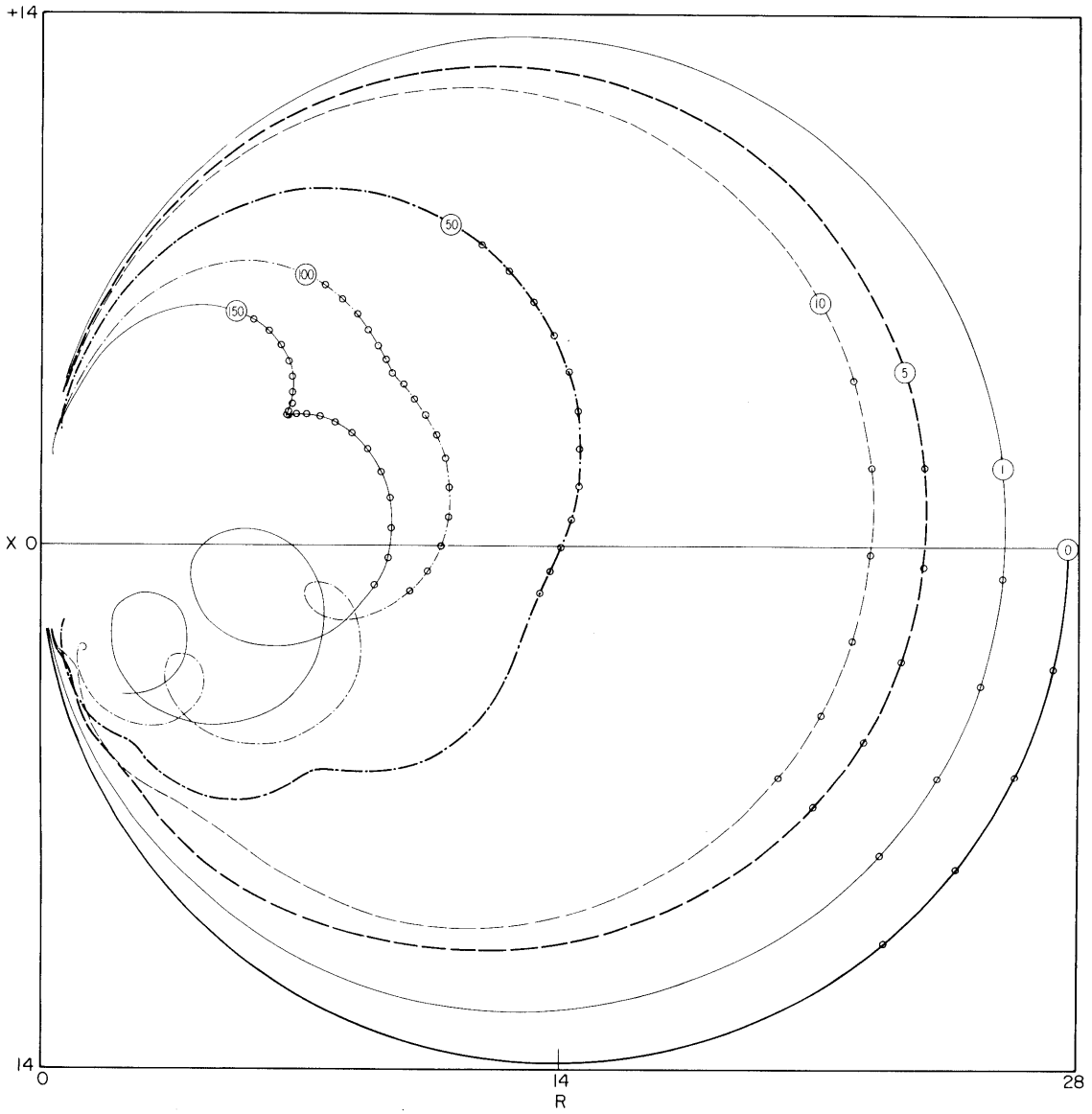

Fig. 25g—R vs X for elastic solid boundary conditions and $b/a = 5$ (see Table 22)

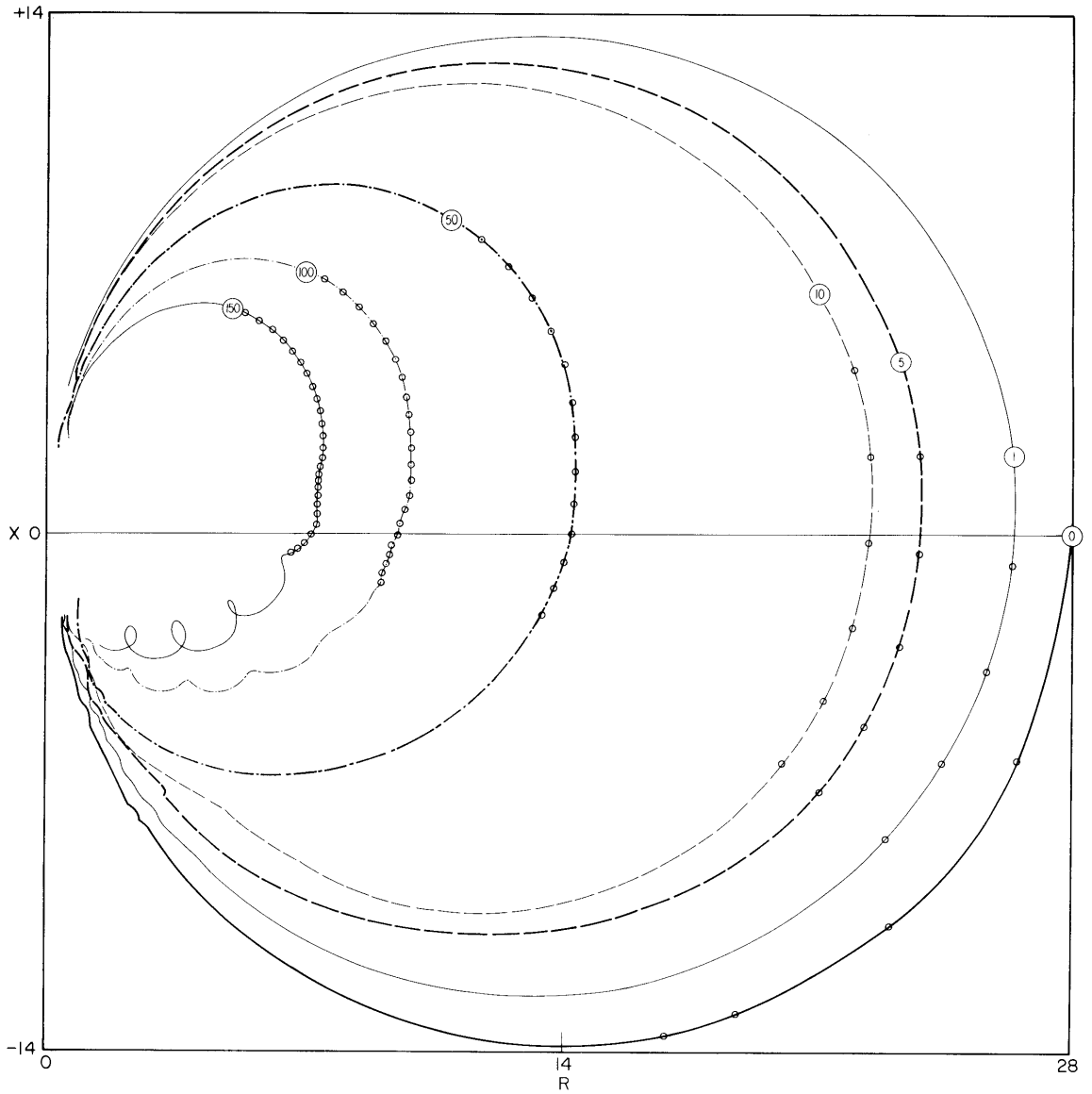

Fig. 25h—R vs X for elastic solid boundary conditions and $b/a = 10$ (see Table 23)

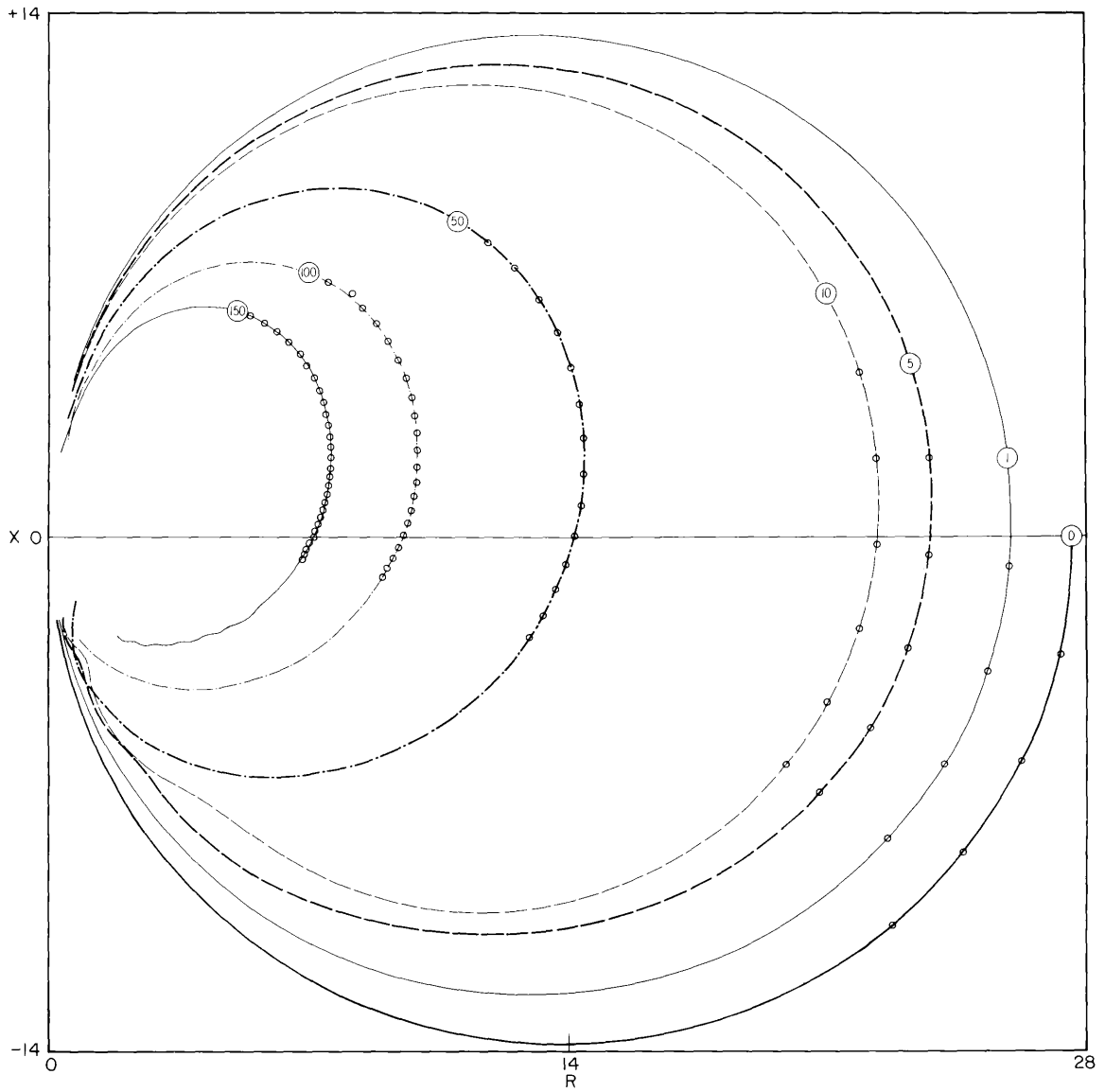

Fig. 25i—R vs X for elastic solid boundary conditions and b/a = 20 (see Table 24)

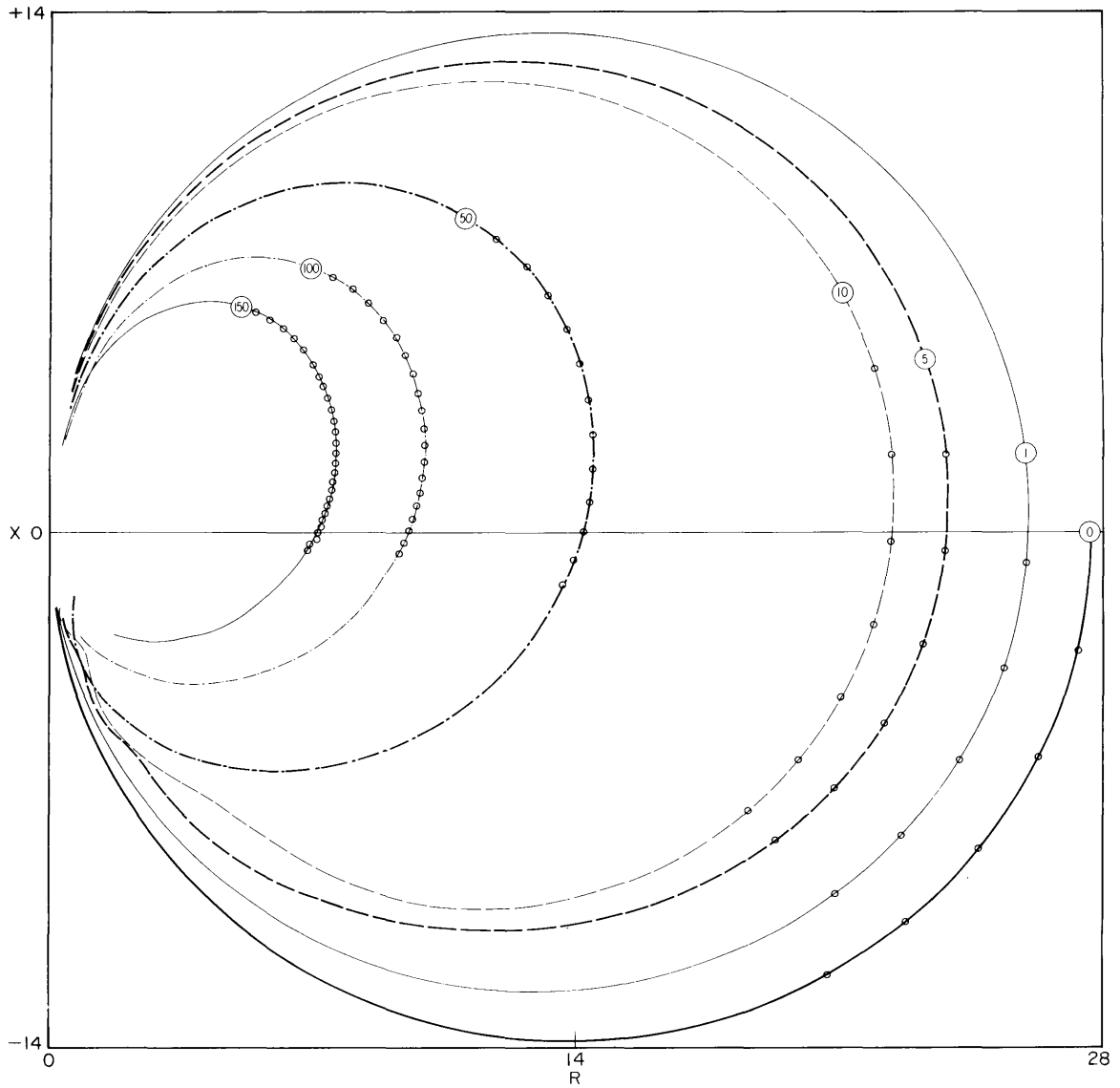

Fig. 25j—R vs X for elastic solid boundary conditions and $b/a = 50$ (see Table 25)

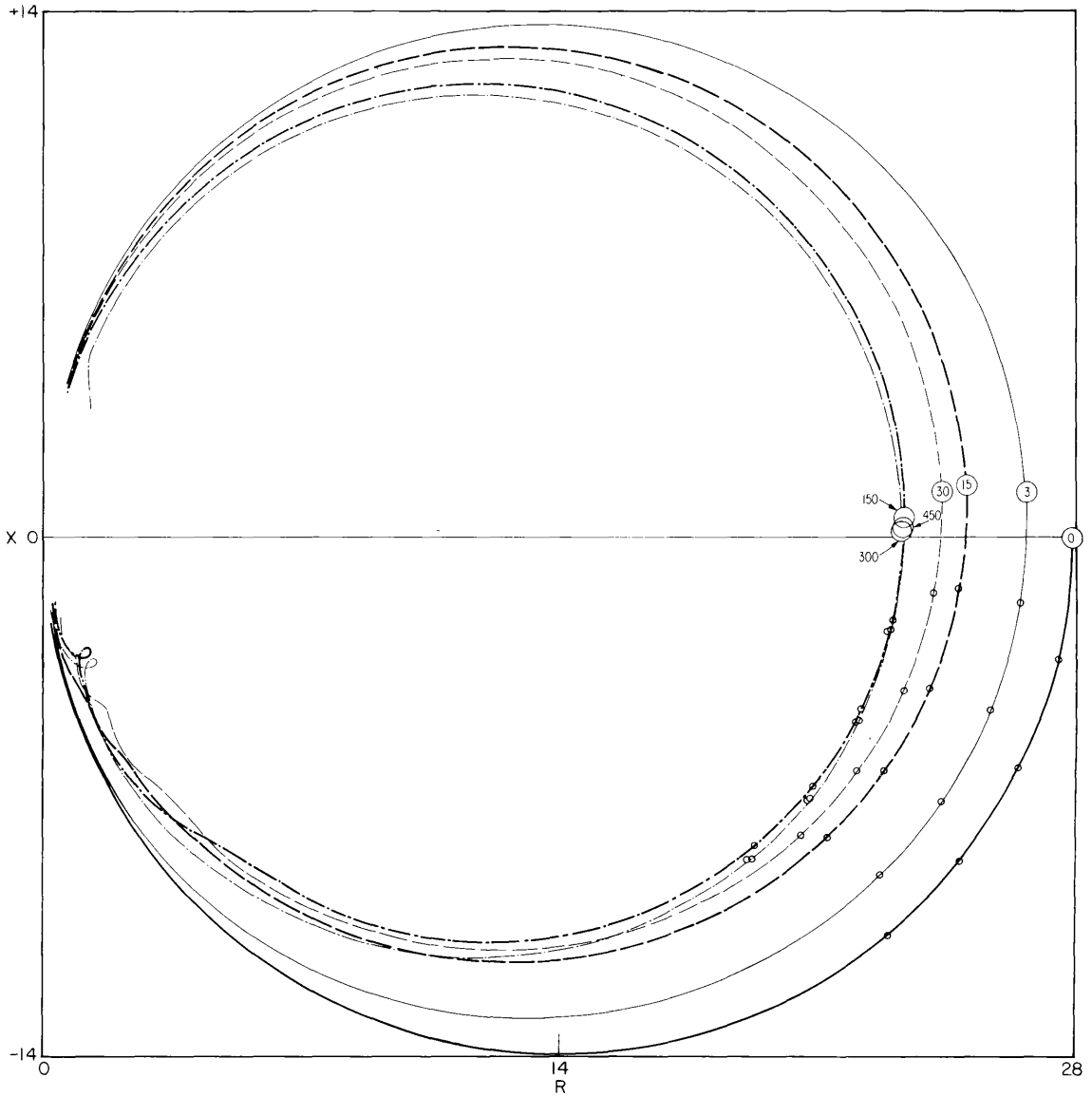

Fig. 26a—R vs X for absolutely rigid boundary conditions with $k_1^{III}a = 60\pi$ and $b/a = 1$ (see Table 26)

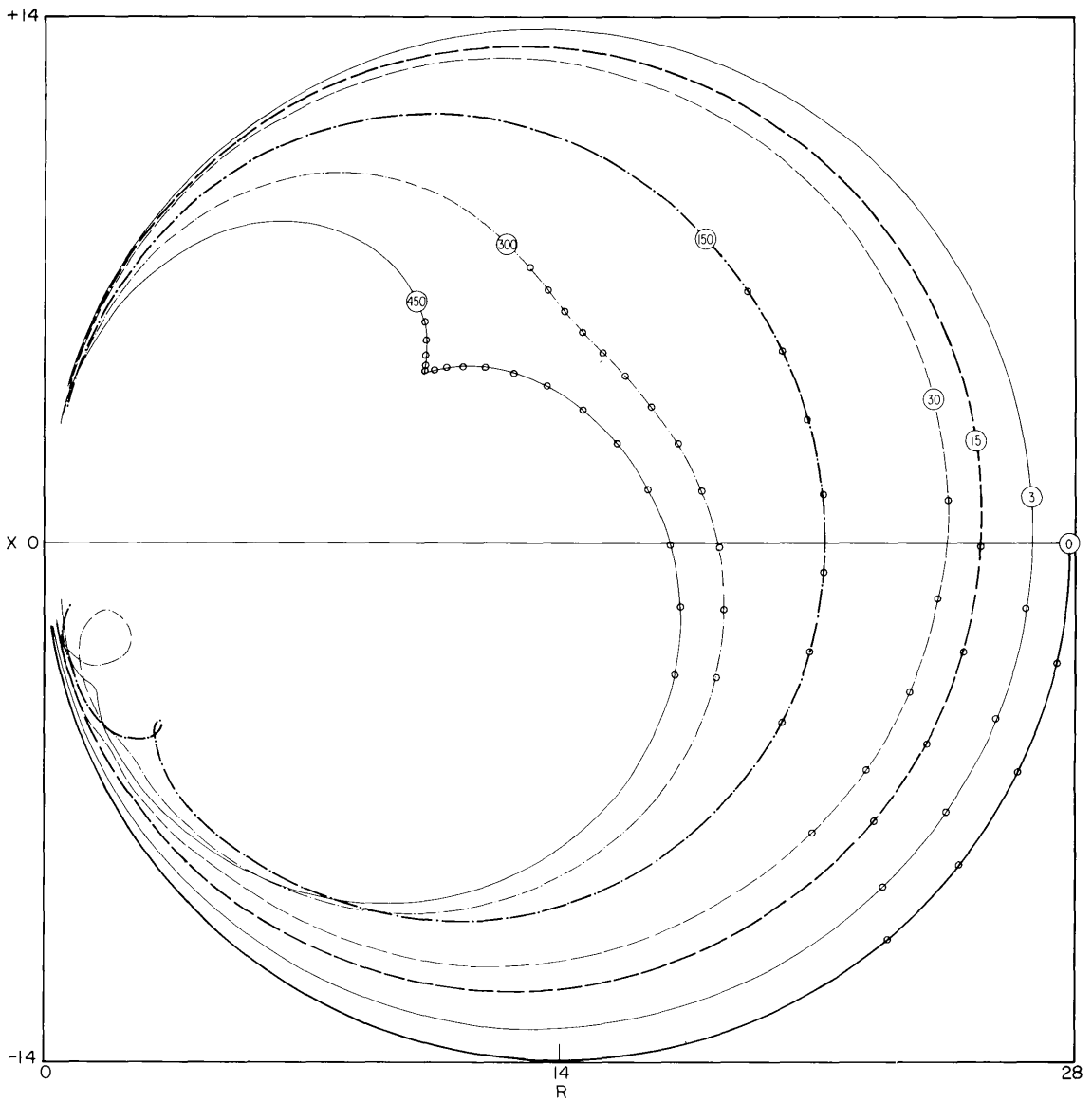

Fig. 26b—R vs X for absolutely rigid boundary conditions with $k_1^{\mathrm{III}} a = 60\pi$ and $b/a = 2$ (see Table 27)

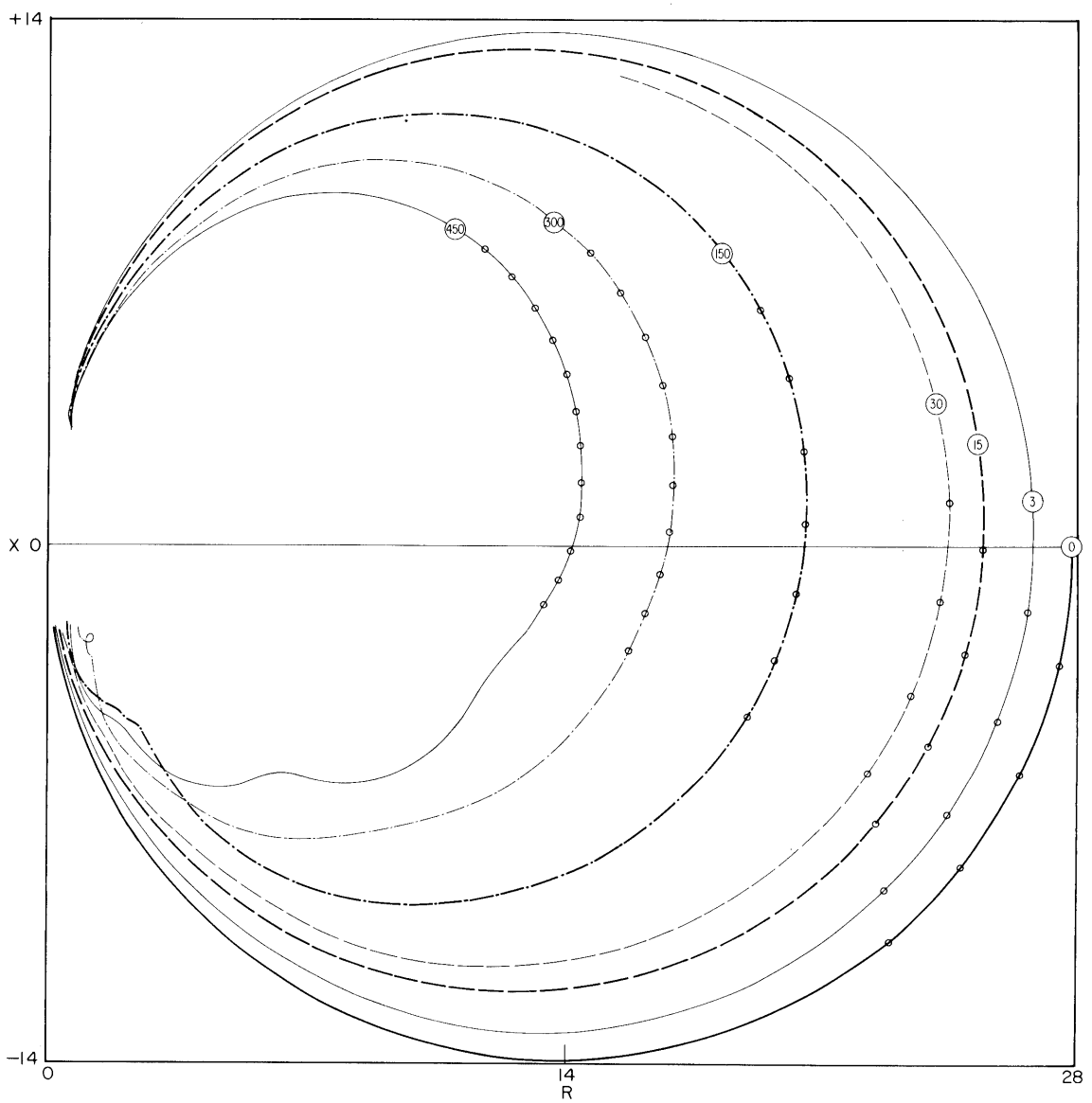

Fig. 26c—R vs X for absolutely rigid boundary conditions with $k_1^{\mathrm{III}} a = 60\pi$ and $b/a = 5$ (see Table 28)

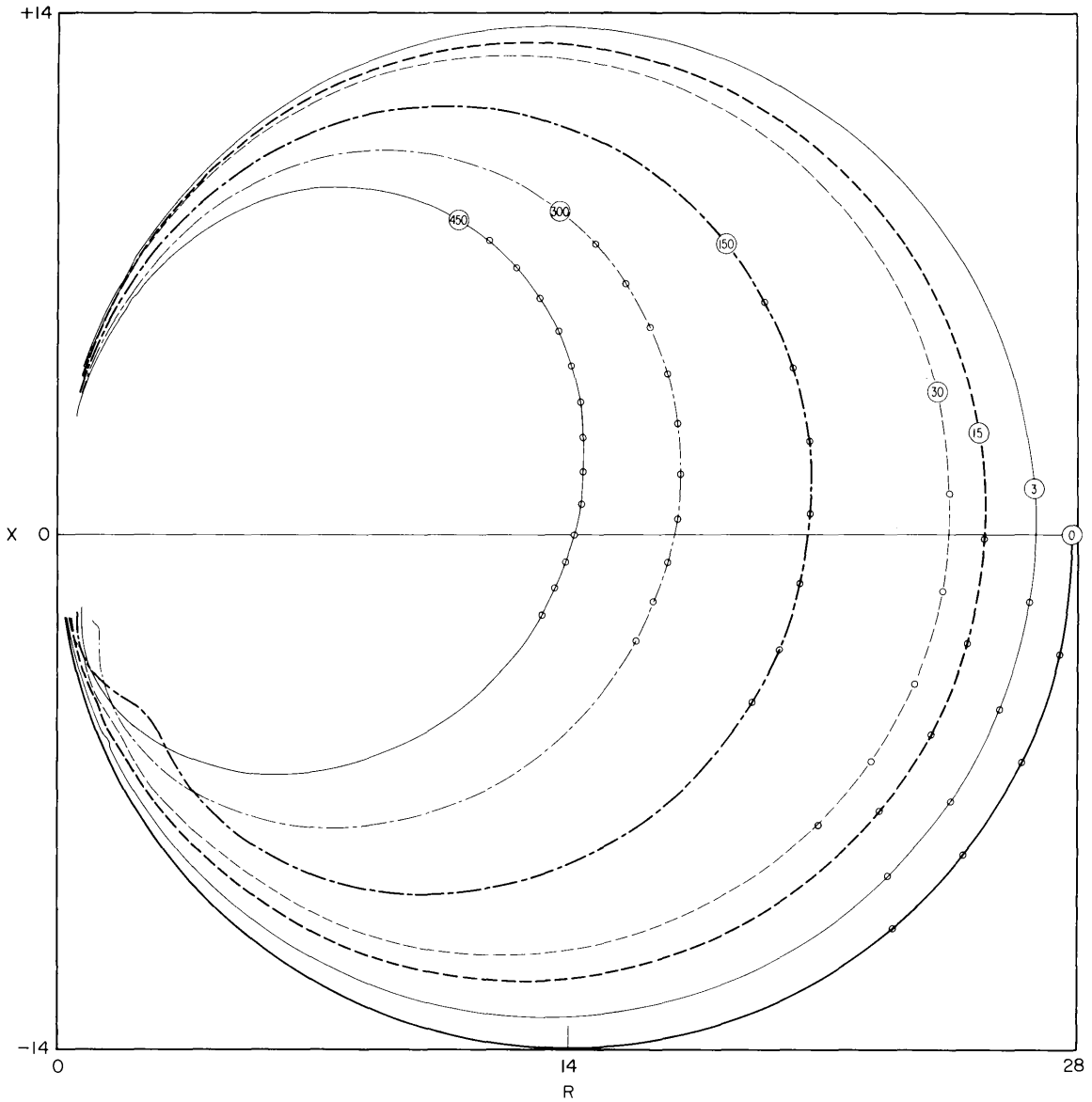

Fig. 26d—R vs X for absolutely rigid boundary conditions with $k_1^{\mathrm{III}}a = 60\pi$ and $b/a = 10$ (see Table 29)

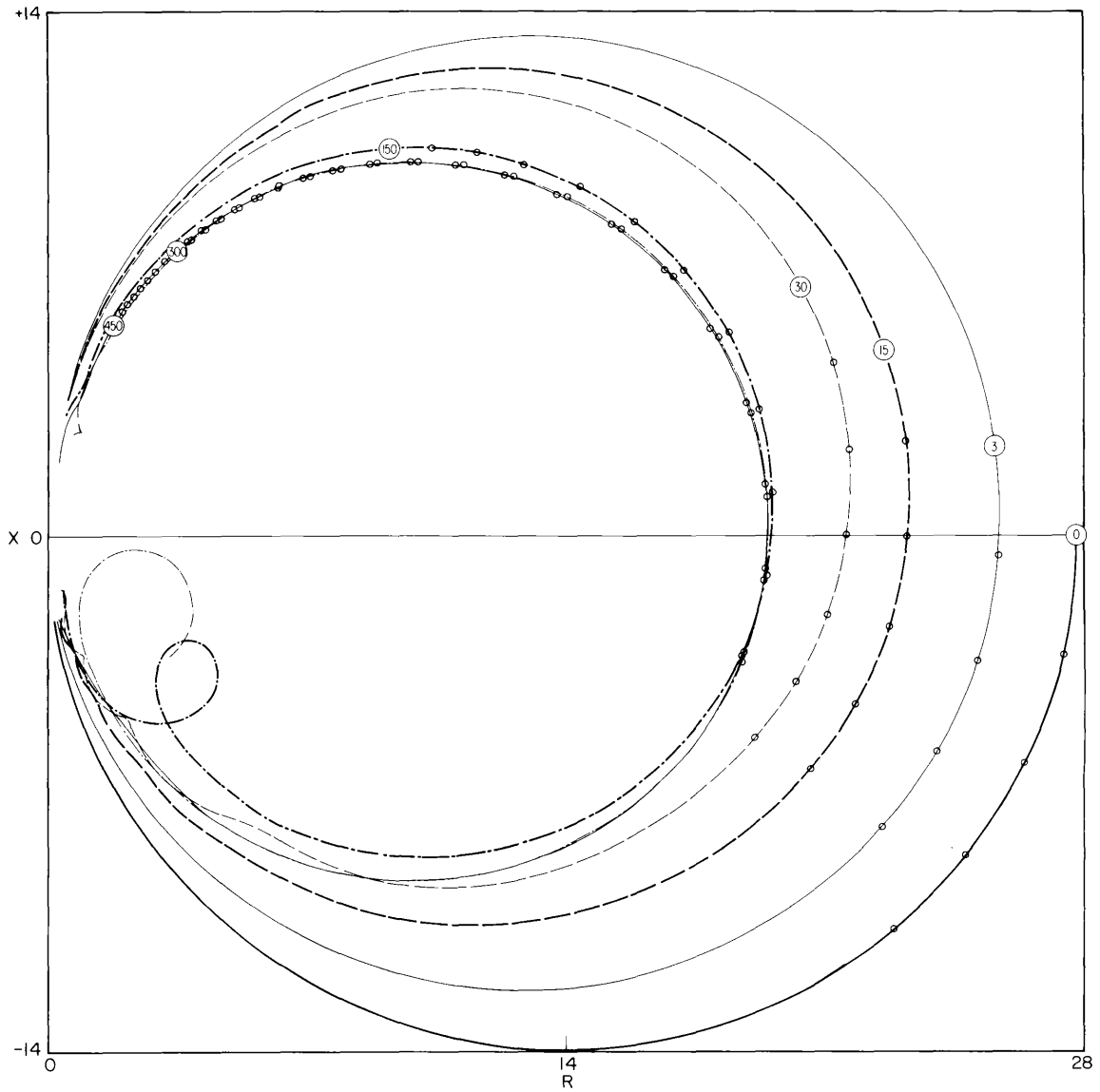

Fig. 27a – R vs X for infinitely flexible boundary conditions with $k_1^{III}a = 60\pi$ and $b/a = 1$ (see Table 30)

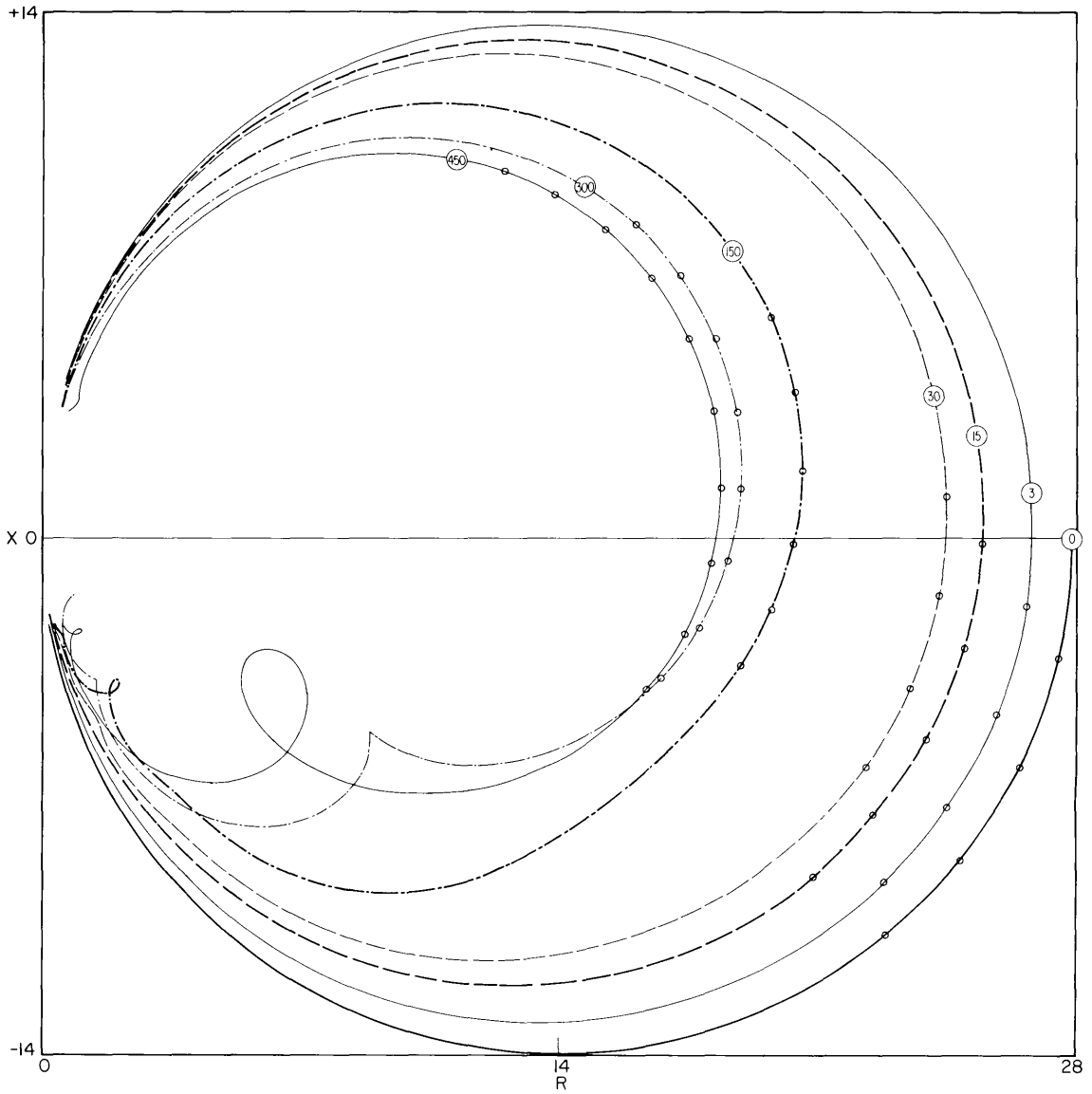

Fig. 27b – R vs X for infinitely flexible boundary conditions with $k_1^{\mathrm{III}}a = 60\pi$ and $b/a = 2$ (see Table 31)

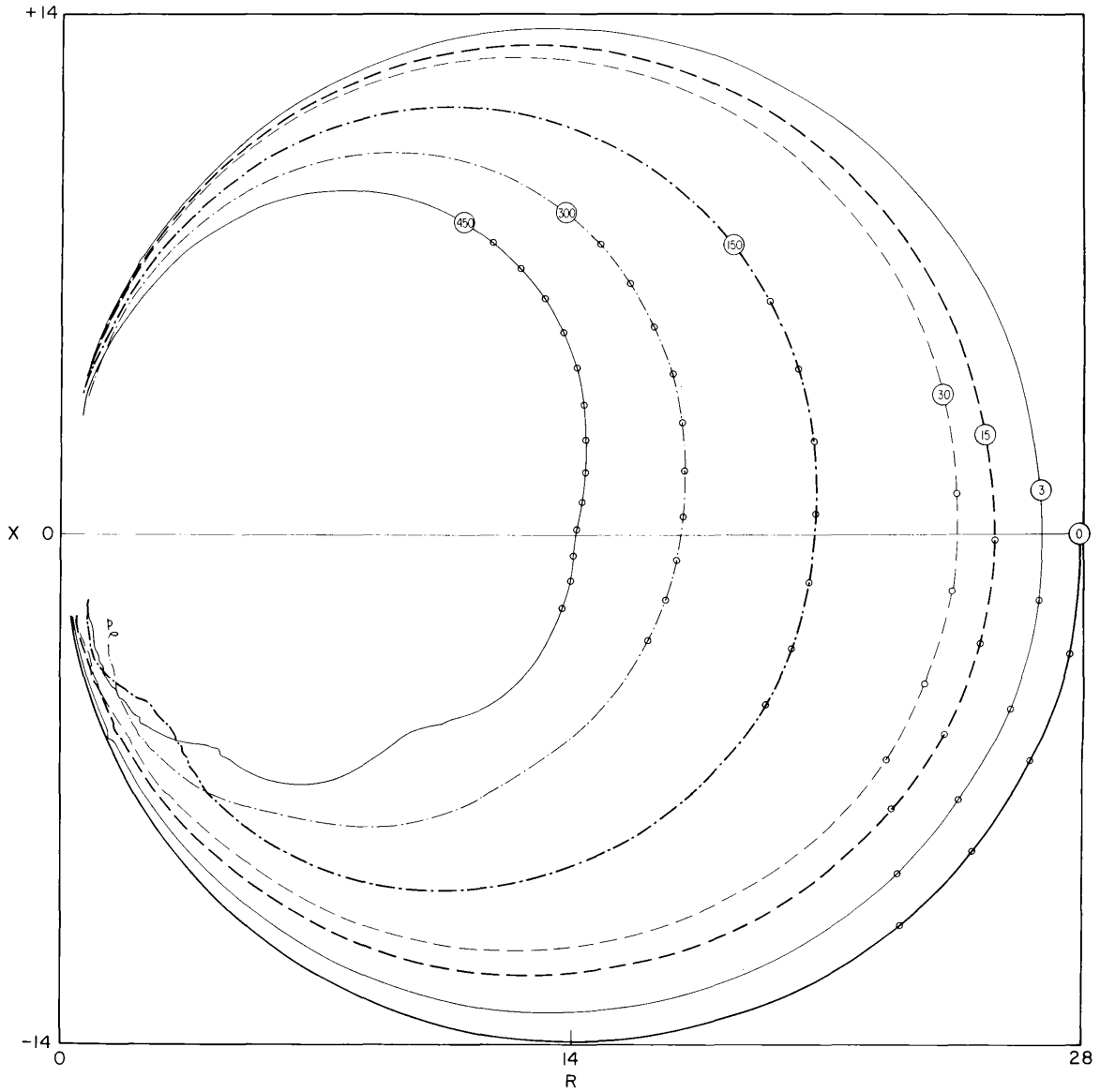

Fig. 27c—R vs X for infinitely flexible boundary conditions with $k_1^{III}a = 60\pi$ and $b/a = 5$ (see Table 32)

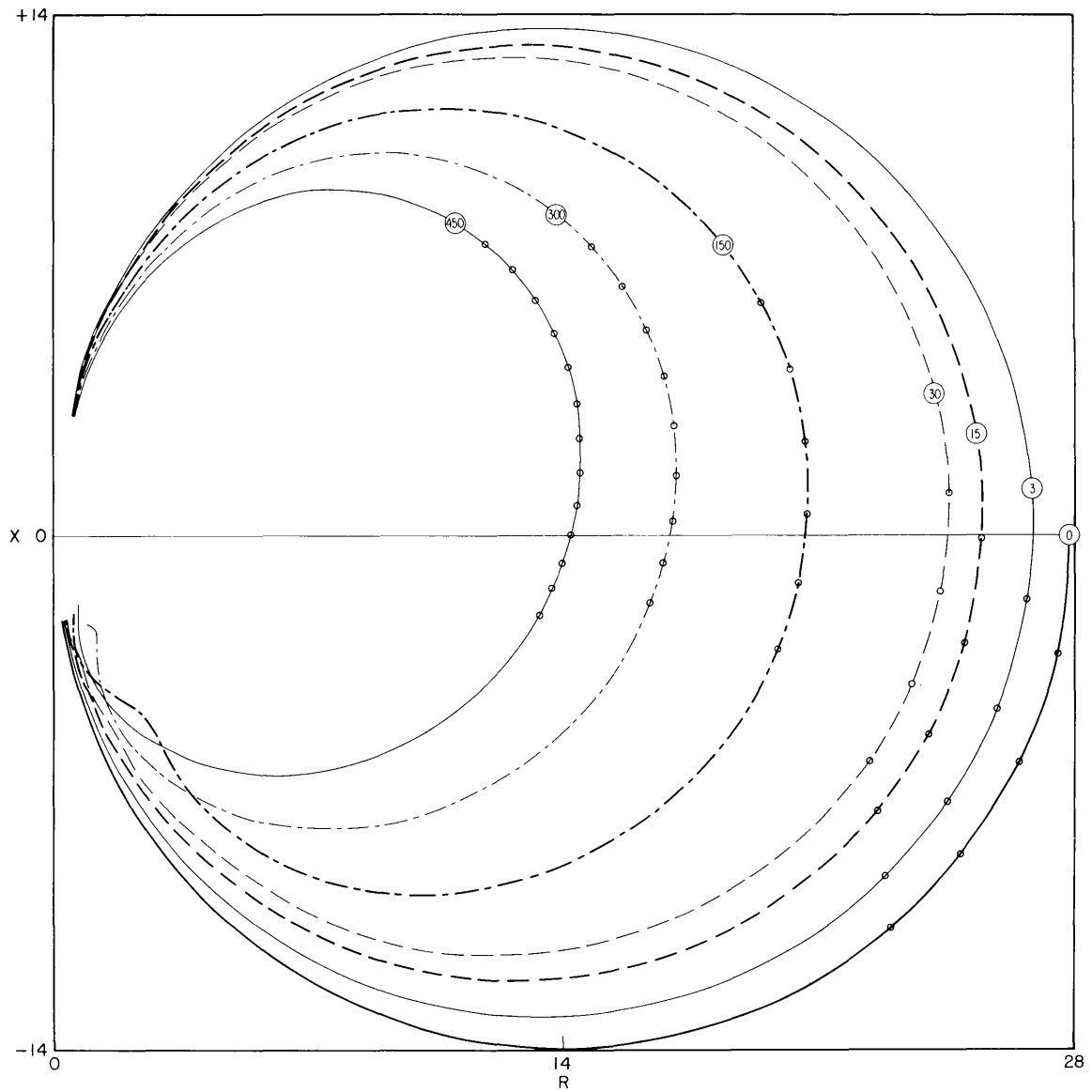

Fig. 27d – R vs X for infinitely flexible boundary conditions with $k_1^{\mathrm{III}}a = 60\pi$ and $b/a = 10$ (see Table 33)

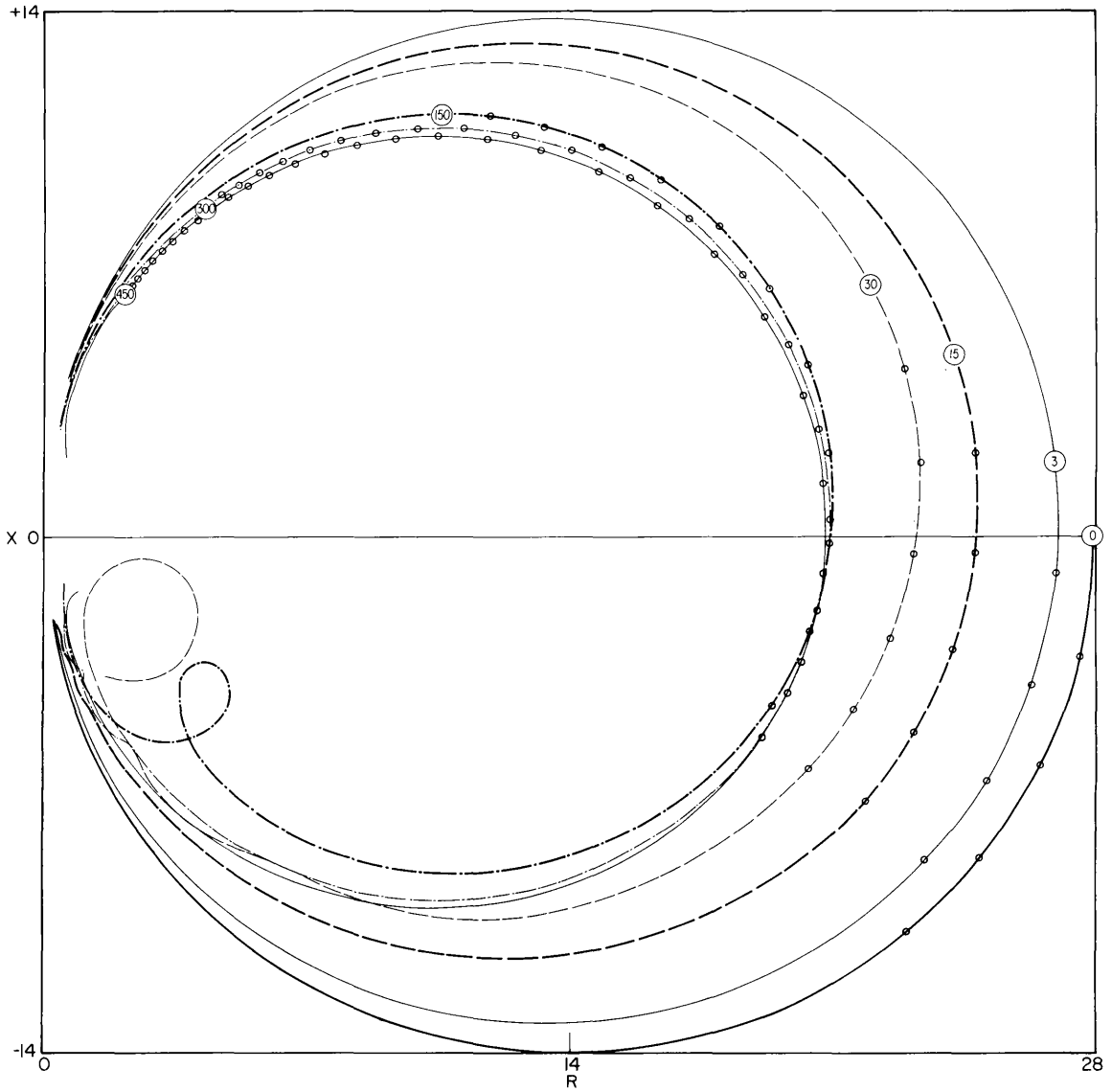

Fig. 28a – R vs X for liquid boundary conditions (assuming orthogonal functions) with $k_1^{III}a = 60\pi$ and $b/a = 1$ (see Table 34)

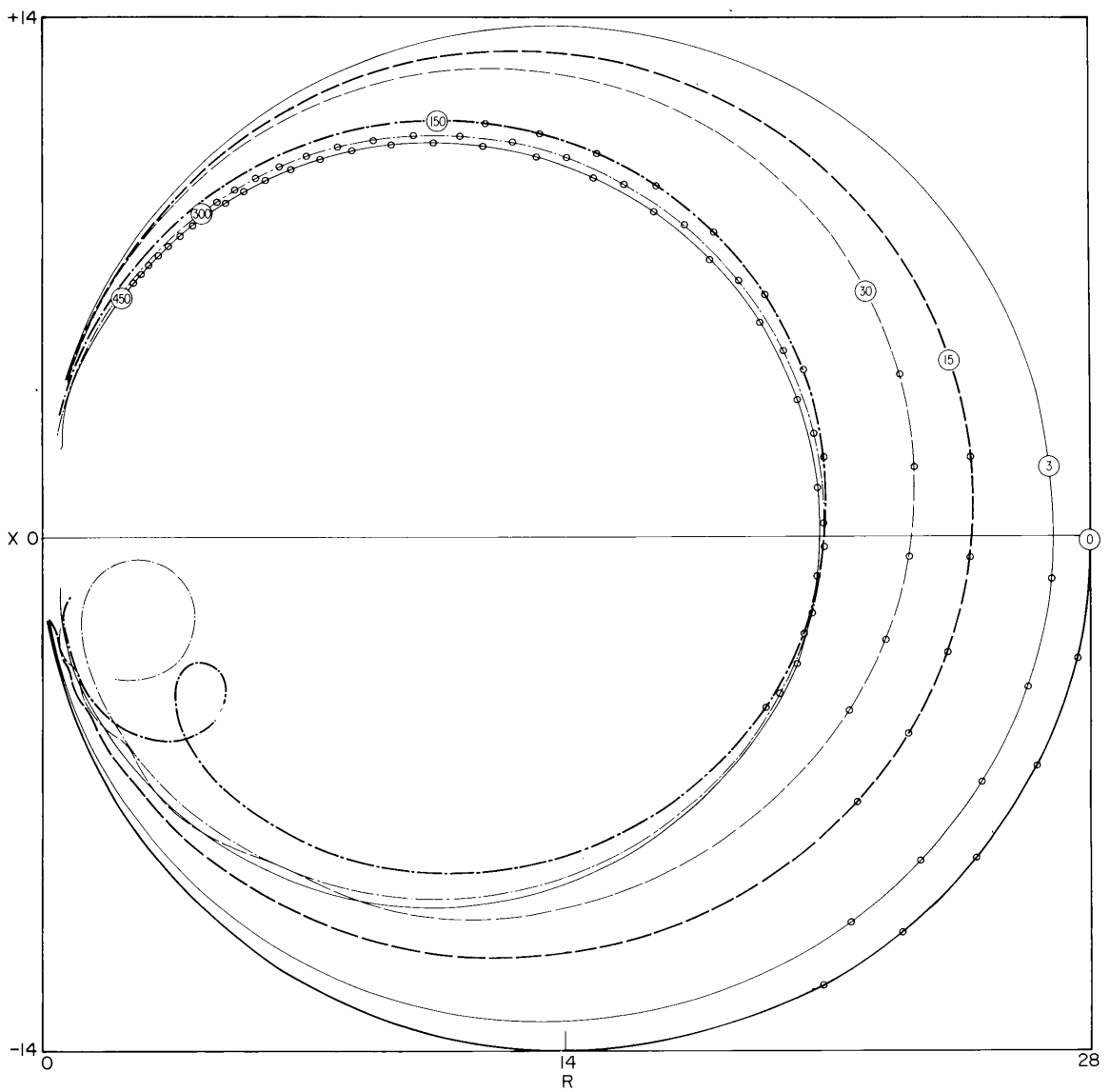

Fig. 28b—R vs X for liquid boundary conditions (using actual functions) with $k_1^{\mathrm{III}}a = 60\pi$ and $b/a = 1$ (see Table 35)

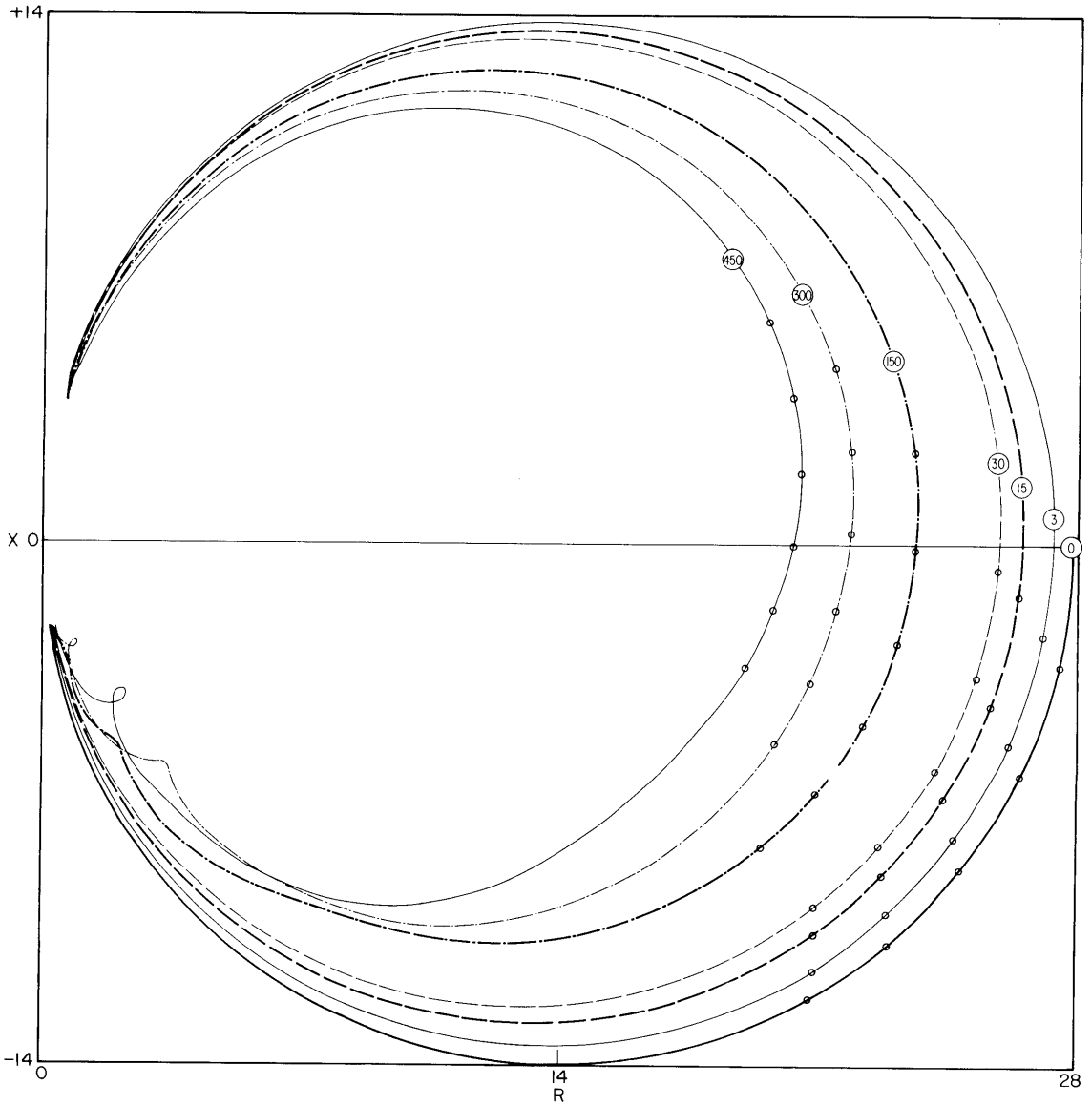

Fig. 28c—R vs X for liquid boundary conditions with $k_1^{III}a = 60\pi$ and $b/a = 2$ (see Table 36)

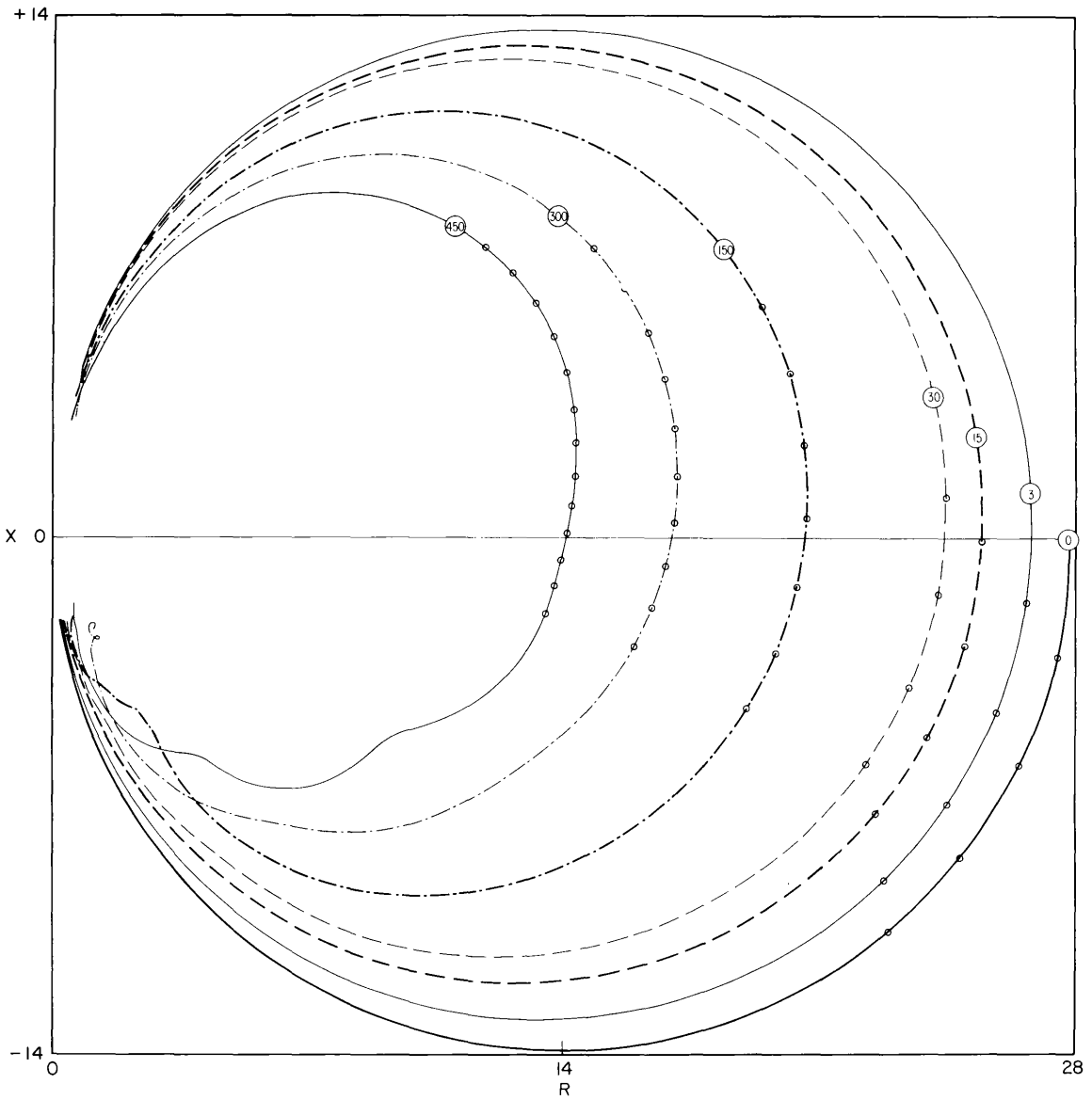

Fig. 28d—R vs X for liquid boundary conditions with $k_1^{\mathrm{III}}a = 60\pi$ and $b/a = 5$ (see Table 37)

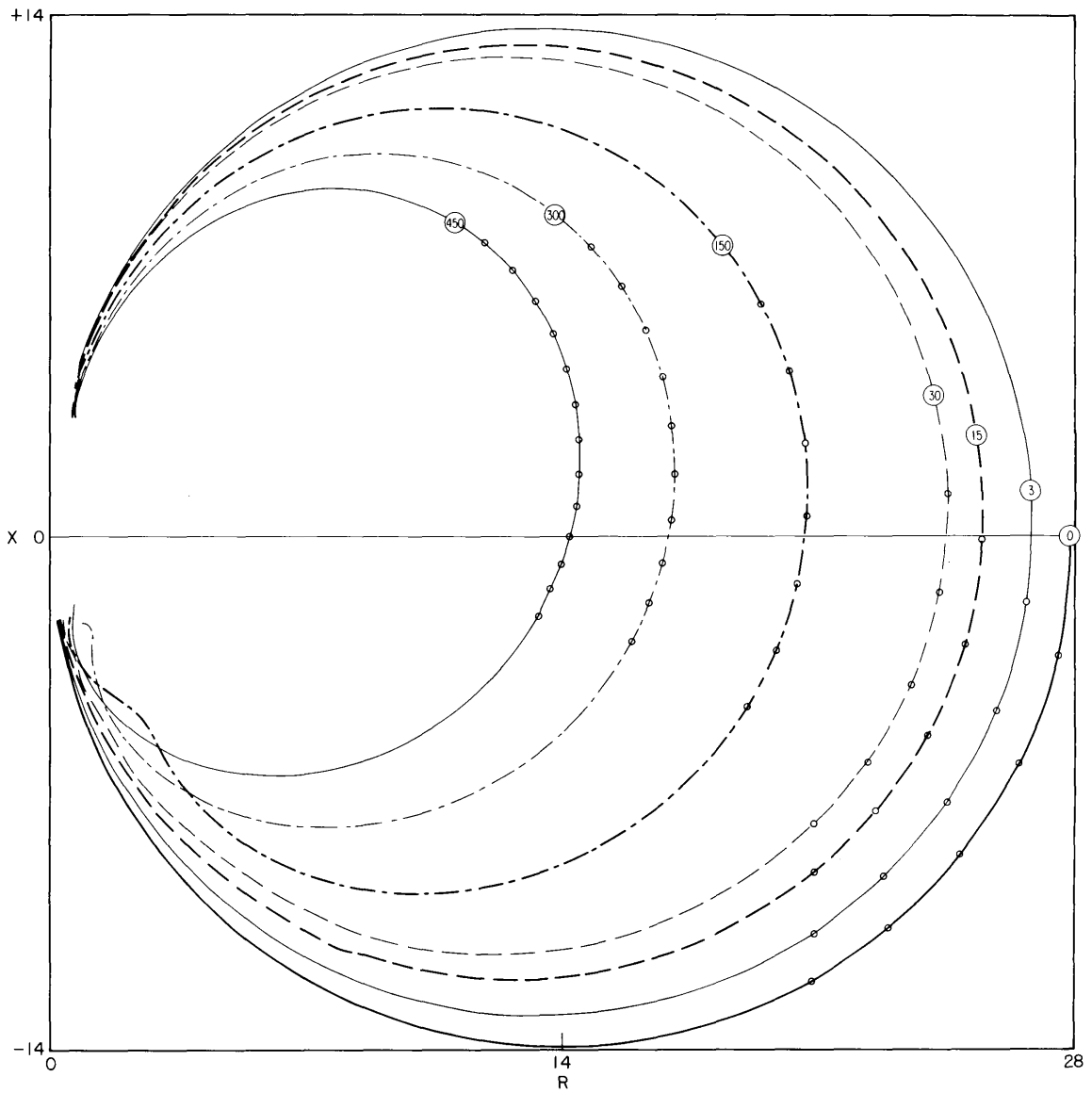

Fig. 28e – R vs X for liquid boundary conditions with $k_1^{III}a = 60\pi$ and $b/a = 10$ (see Table 38)

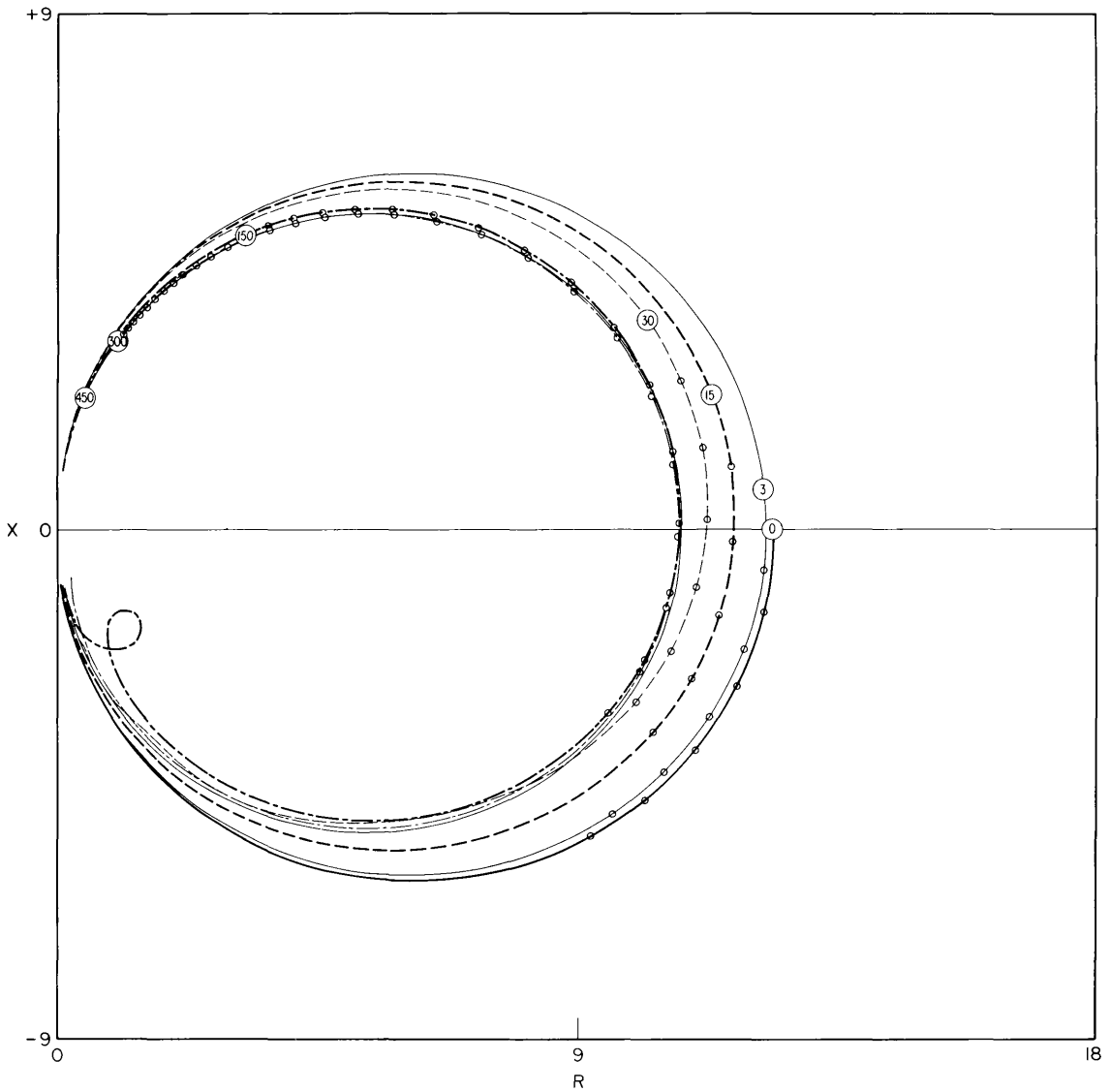

Fig. 29a—R vs X for elastic solid boundary conditions (assuming orthogonal functions) with $k_1^{\mathrm{III}}a = 60\pi$ and $b/a = 1$ (see Table 39)

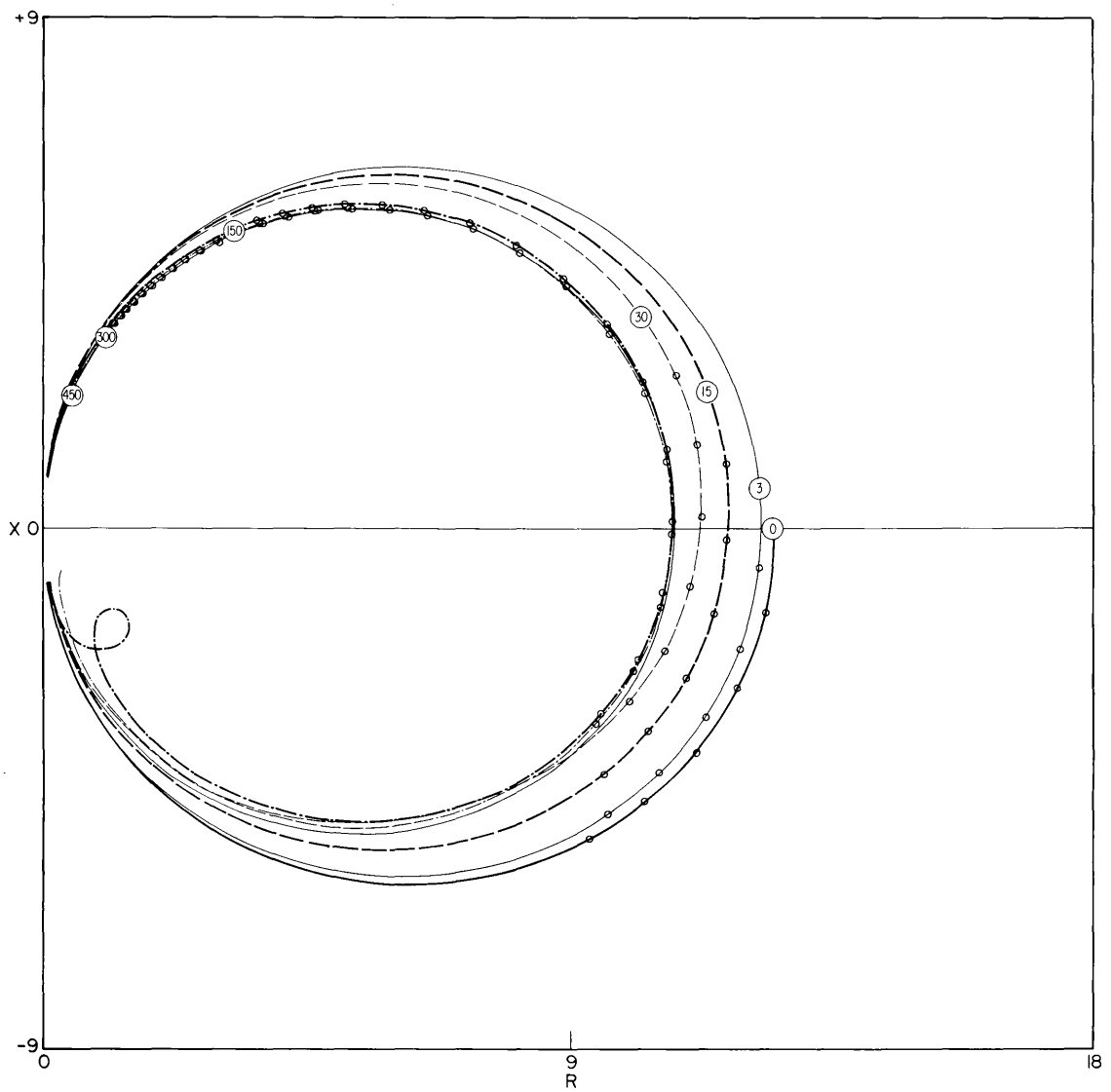

Fig. 29b – R vs X for elastic solid boundary conditions (using actual functions) with $k_1^{III}a = 60\pi$ and $b/a = 1$ (see Table 40)

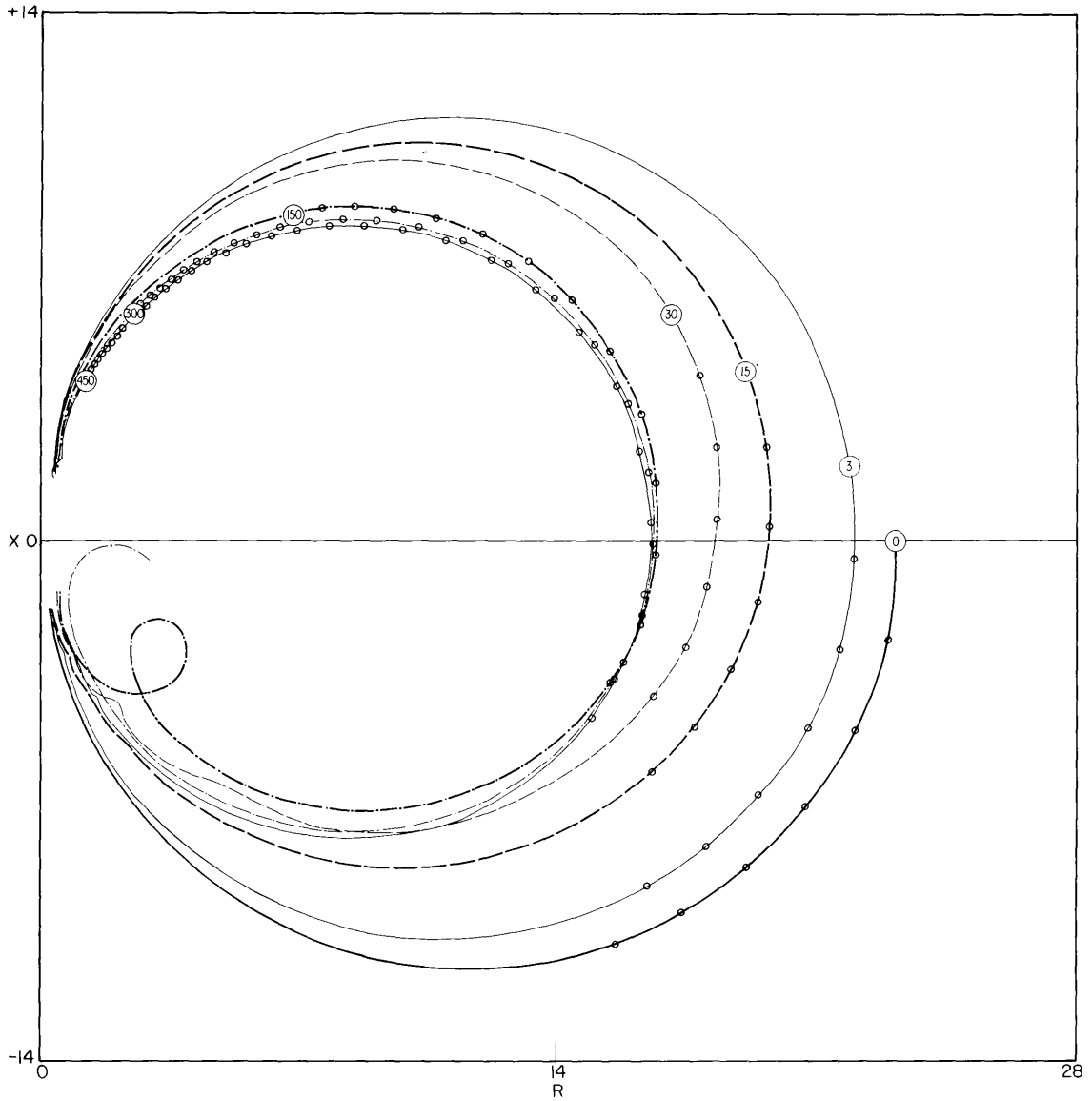

Fig. 29c—R vs X for elastic solid boundary conditions (assuming orthogonal functions) with $k_1^{\mathrm{III}}a = 60\pi$ and $b/a = 1.1$ (see Table 41)

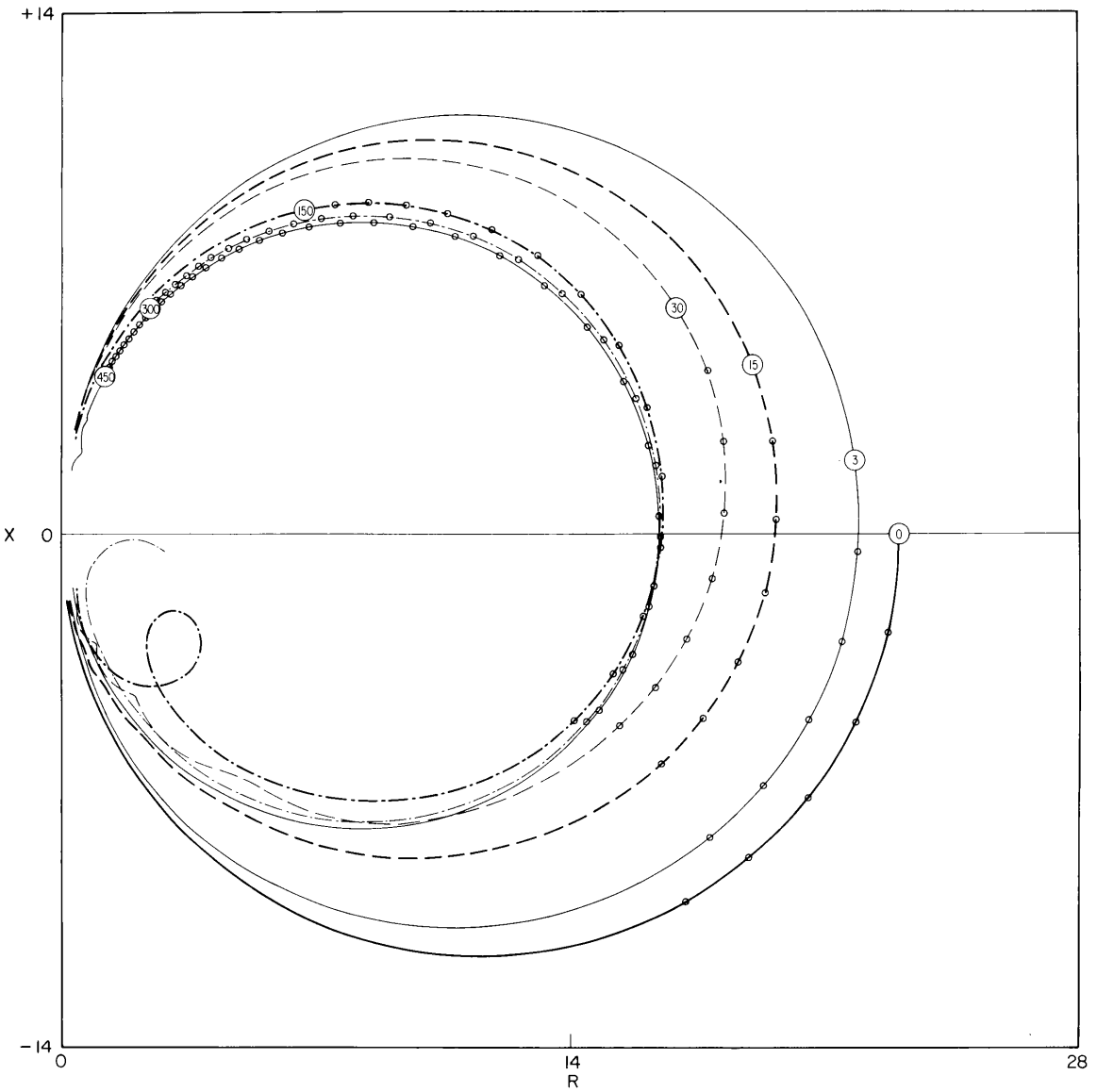

Fig. 29d—R vs X for elastic solid boundary conditions (using actual functions) with $k_1^{III}a = 60\pi$ and $b/a = 1.1$ (see Table 42)

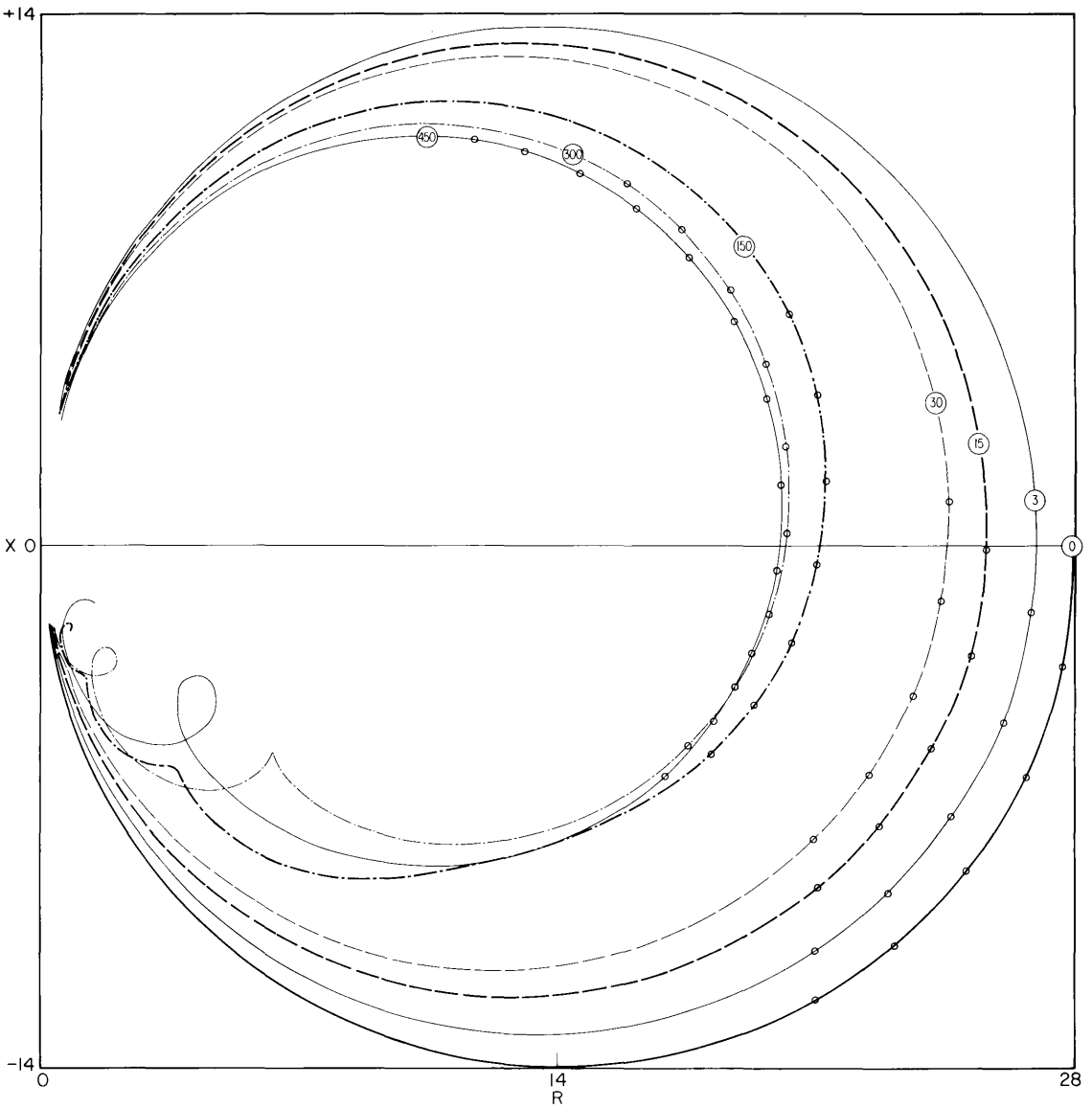

Fig. 29e—R vs X for elastic solid boundary conditions with $k_1^{\mathrm{III}}a = 60\pi$ and $b/a = 2$ (see Table 43)

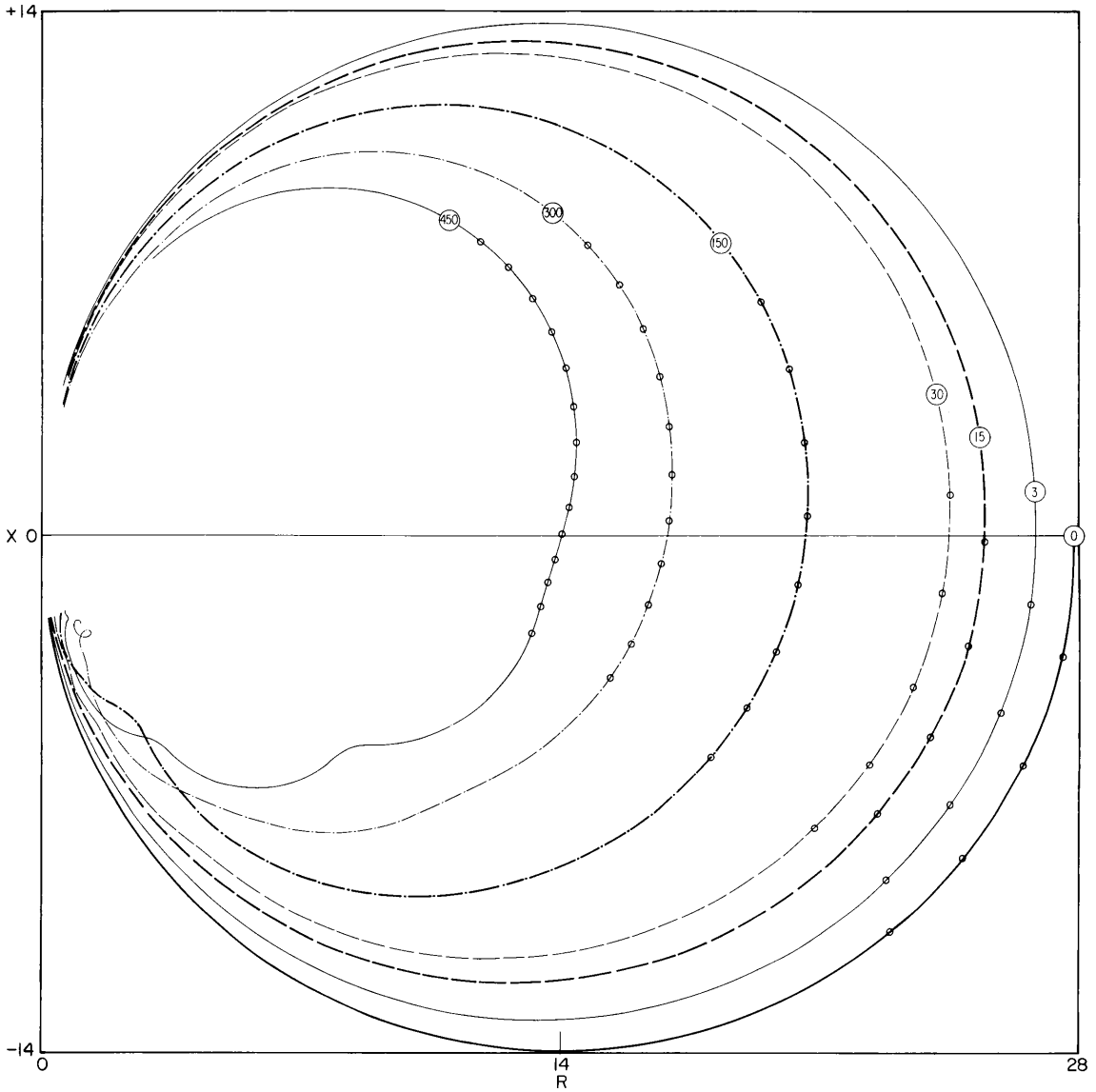

Fig. 29f—R vs X for elastic solid boundary conditions with $k_1^{\mathrm{III}}a = 60\pi$ and $b/a = 5$ (see Table 44)

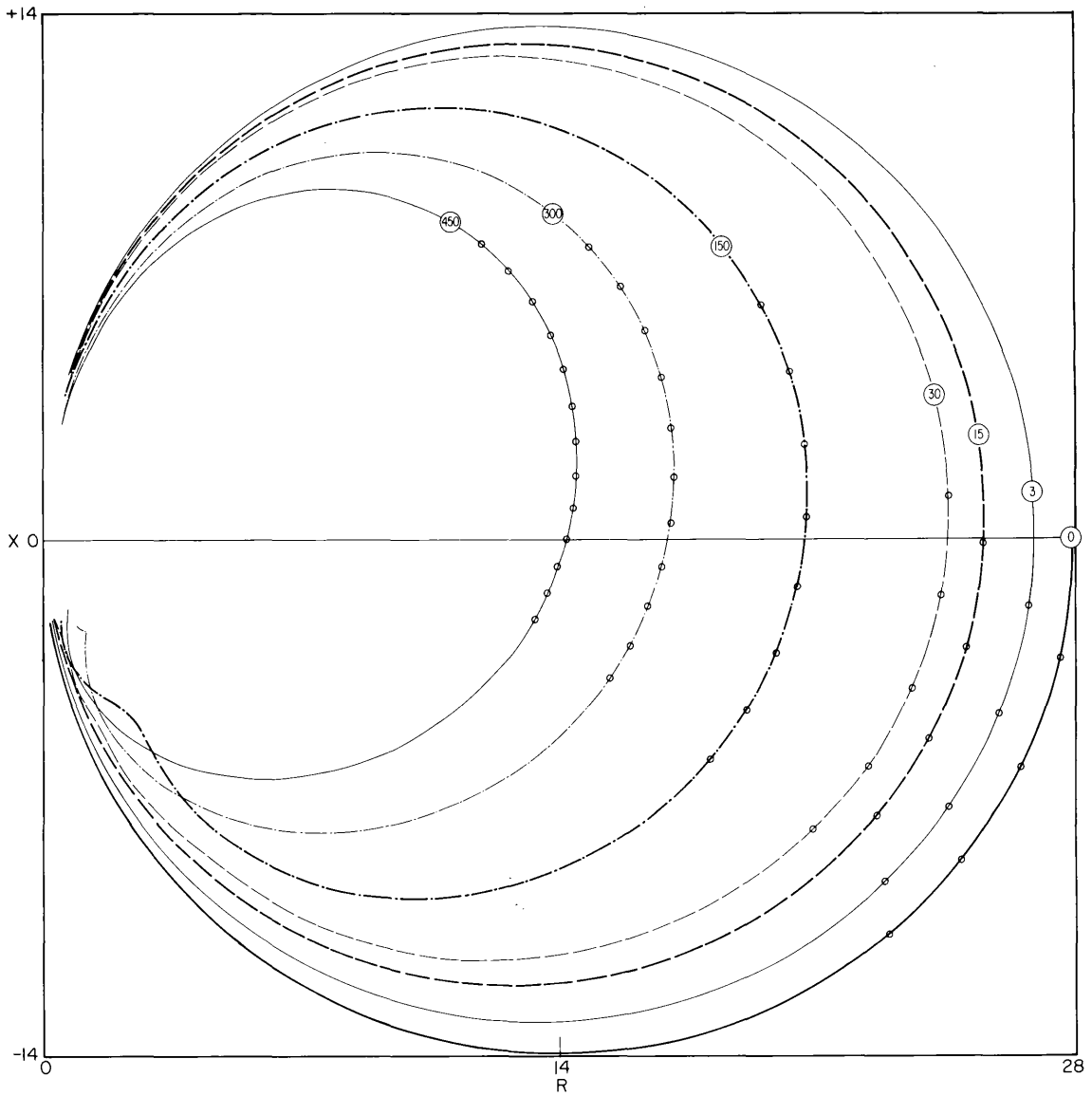

Fig. 29g—R vs X for elastic solid boundary conditions with $k_1^{\mathrm{III}}a = 60\pi$ and $b/a = 10$ (see Table 45)

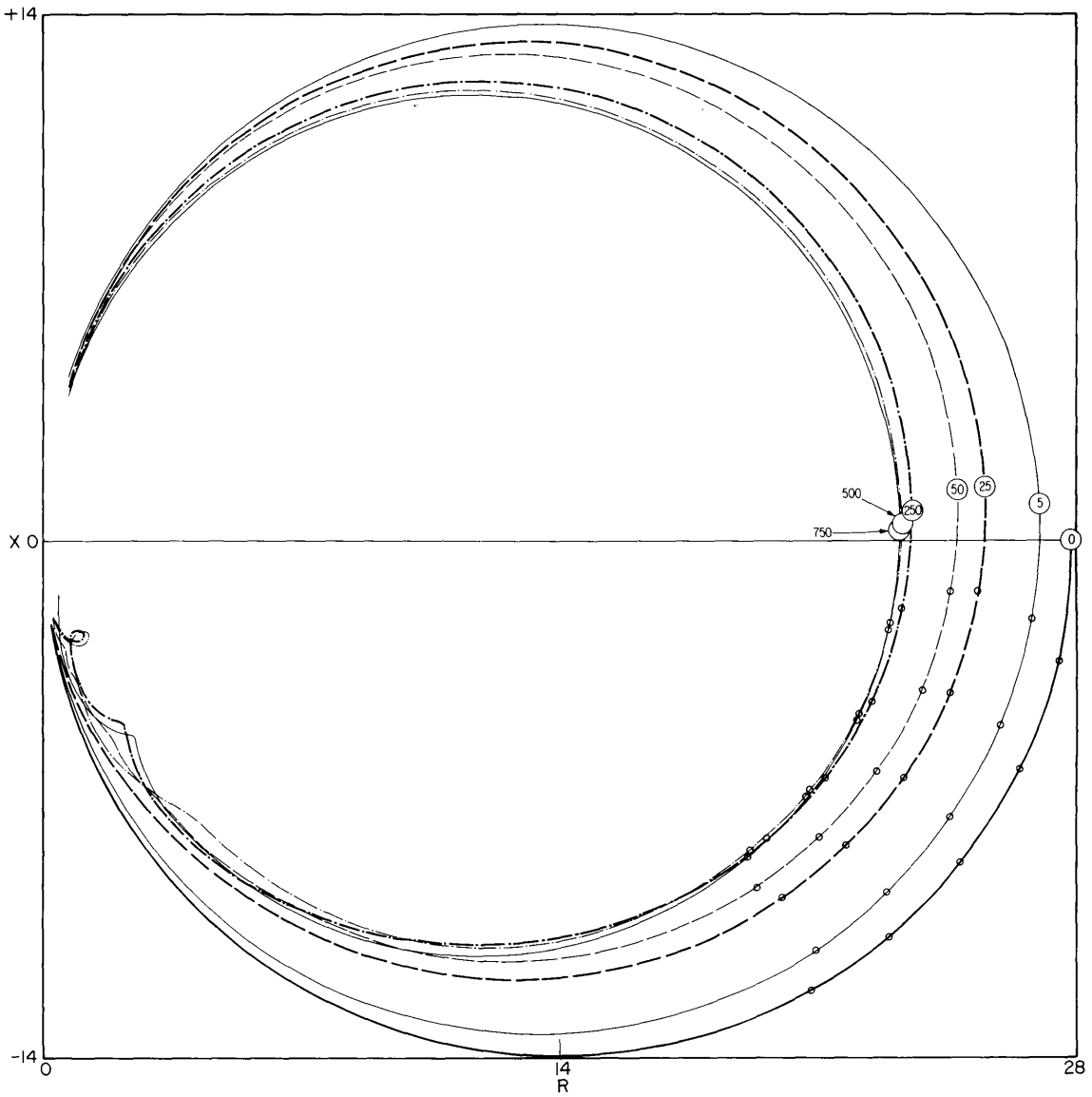

Fig. 30a—R vs X for absolutely rigid boundary conditions with $k_1^V a = 100\pi$ and $b/a = 1.1$ (see Table 46)

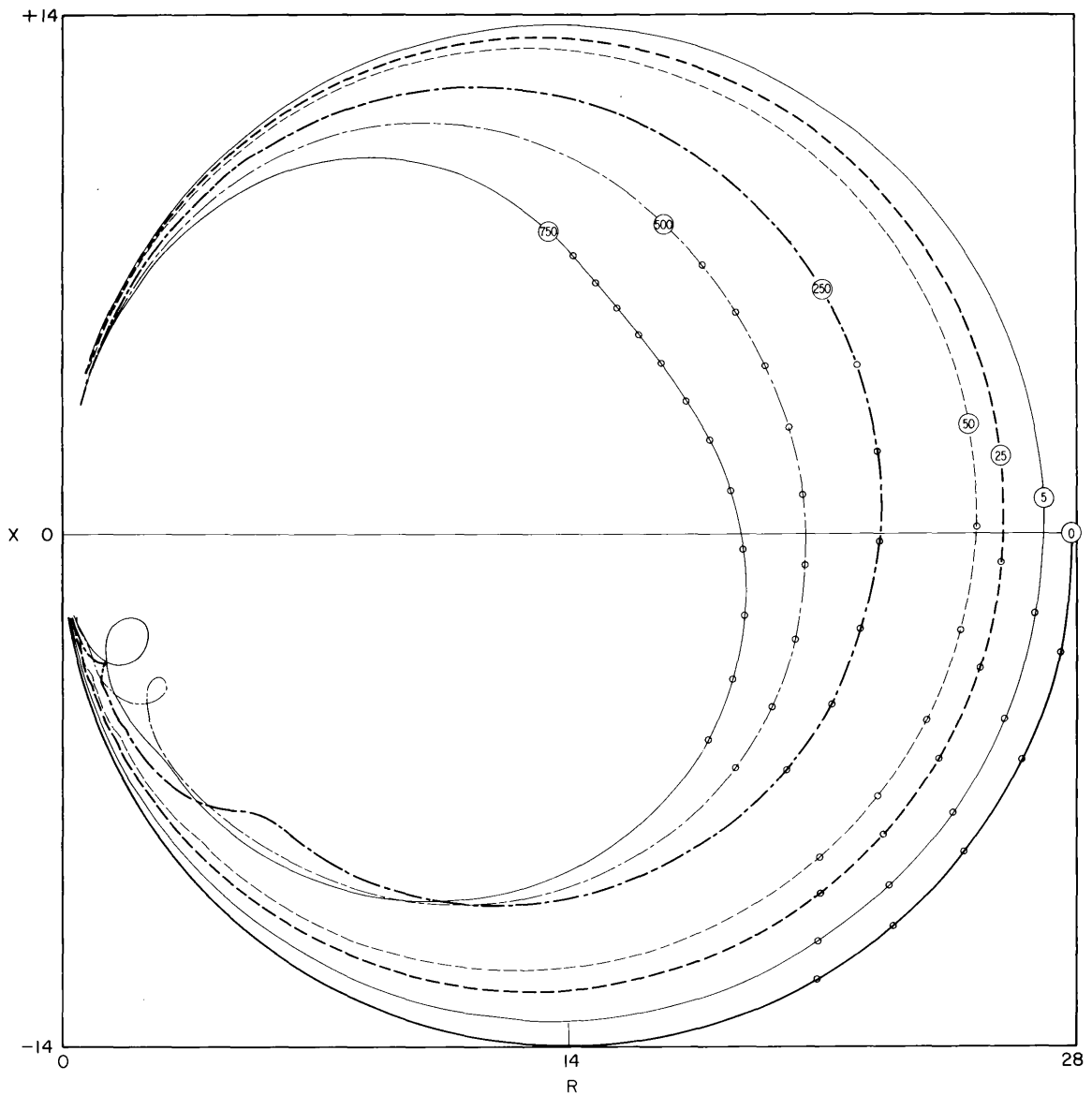

Fig. 30b—R vs X for absolutely rigid boundary conditions with $k_1^V a = 100\pi$ and $b/a = 2$ (see Table 47)

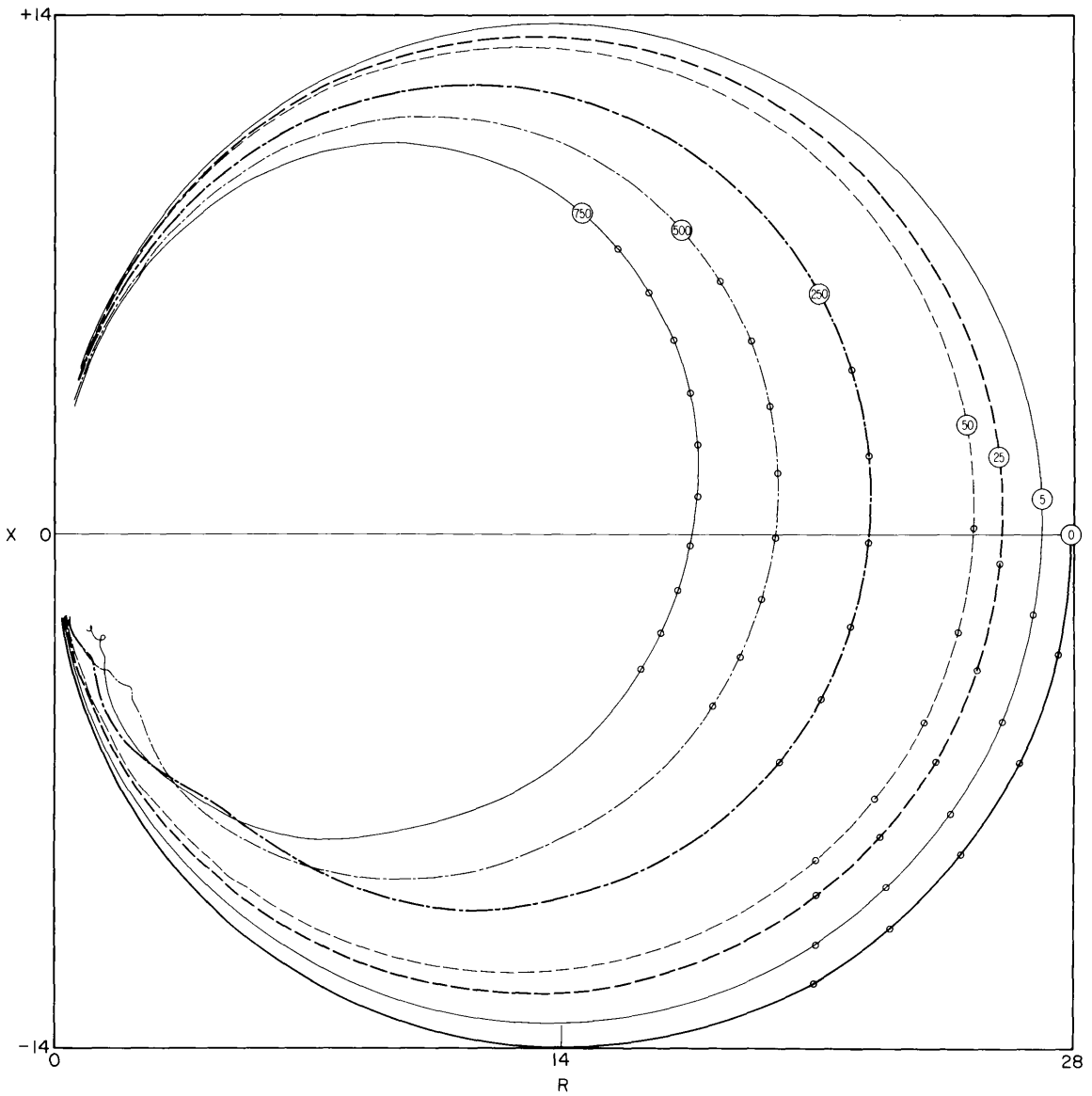

Fig. 30c—R vs X for absolutely rigid boundary conditions with $k_1^V a = 100\pi$ and $b/a = 5$ (see Table 48)

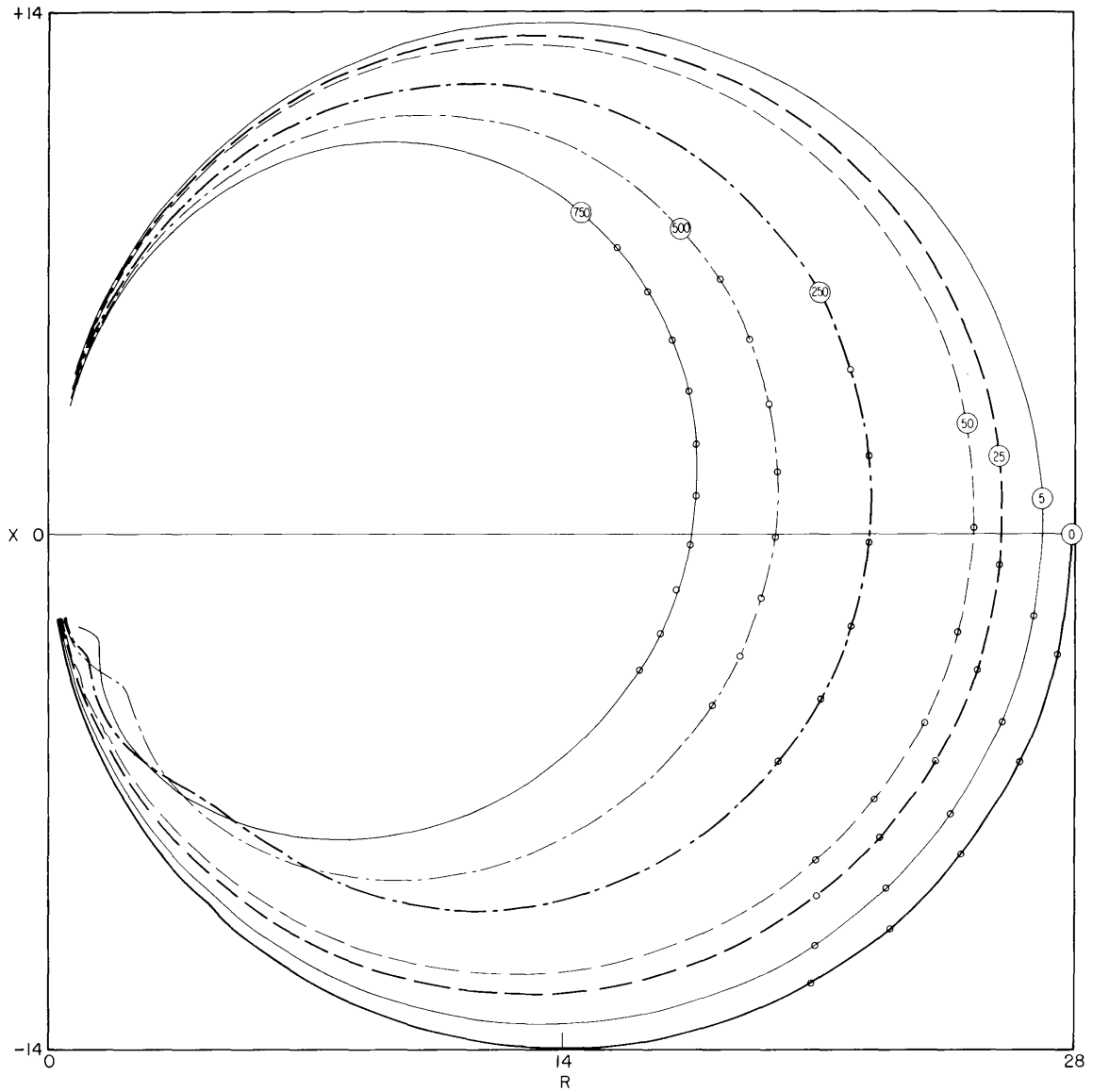

Fig. 30d – R vs X for absolutely rigid boundary conditions with $k_1^V a = 100\pi$ and $b/a = 10$ (see Table 49)

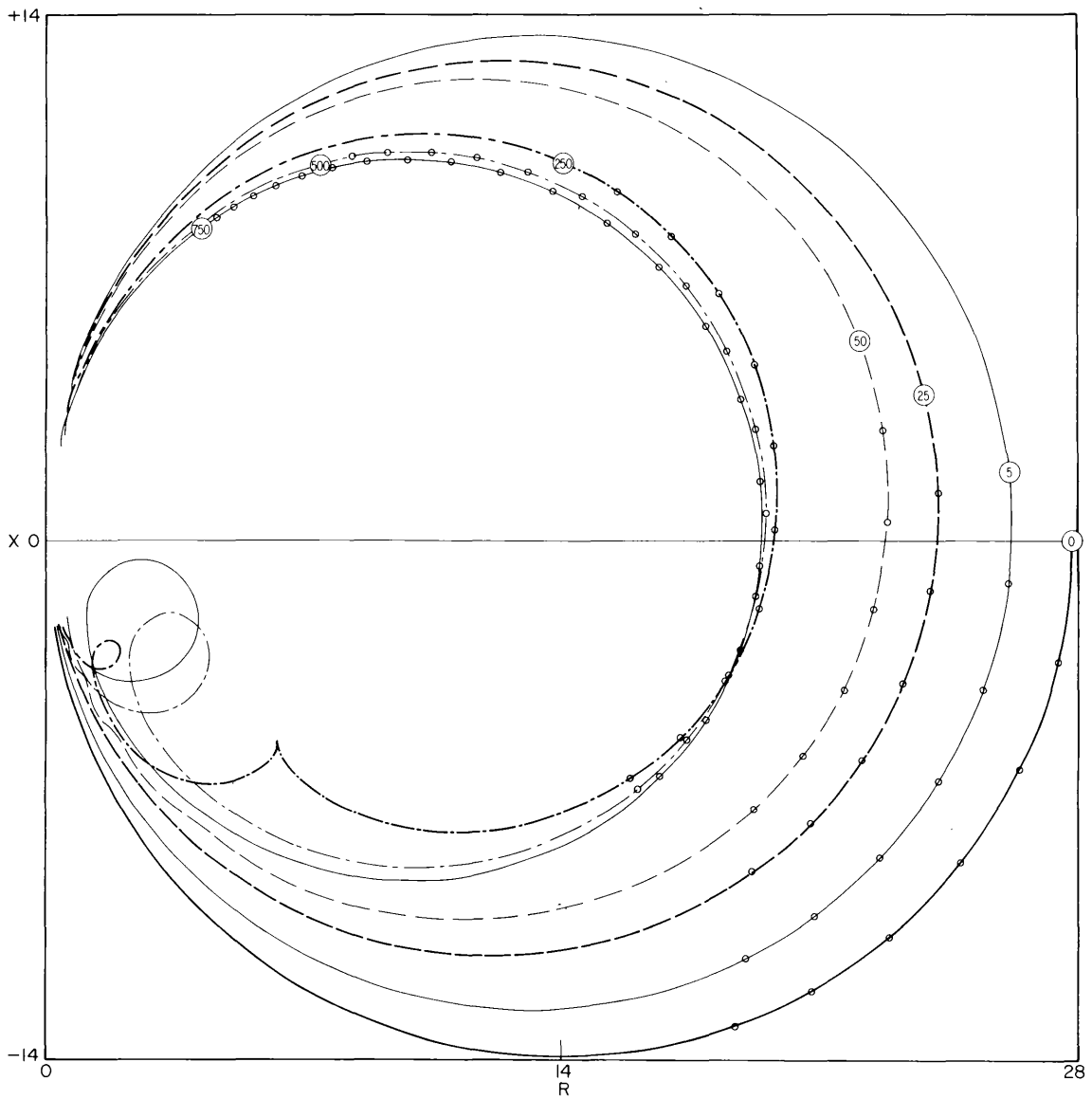

Fig. 31a—R vs X for infinitely flexible boundary conditions with $k_1^V a = 100\pi$ and $b/a = 1$ (see Table 50)

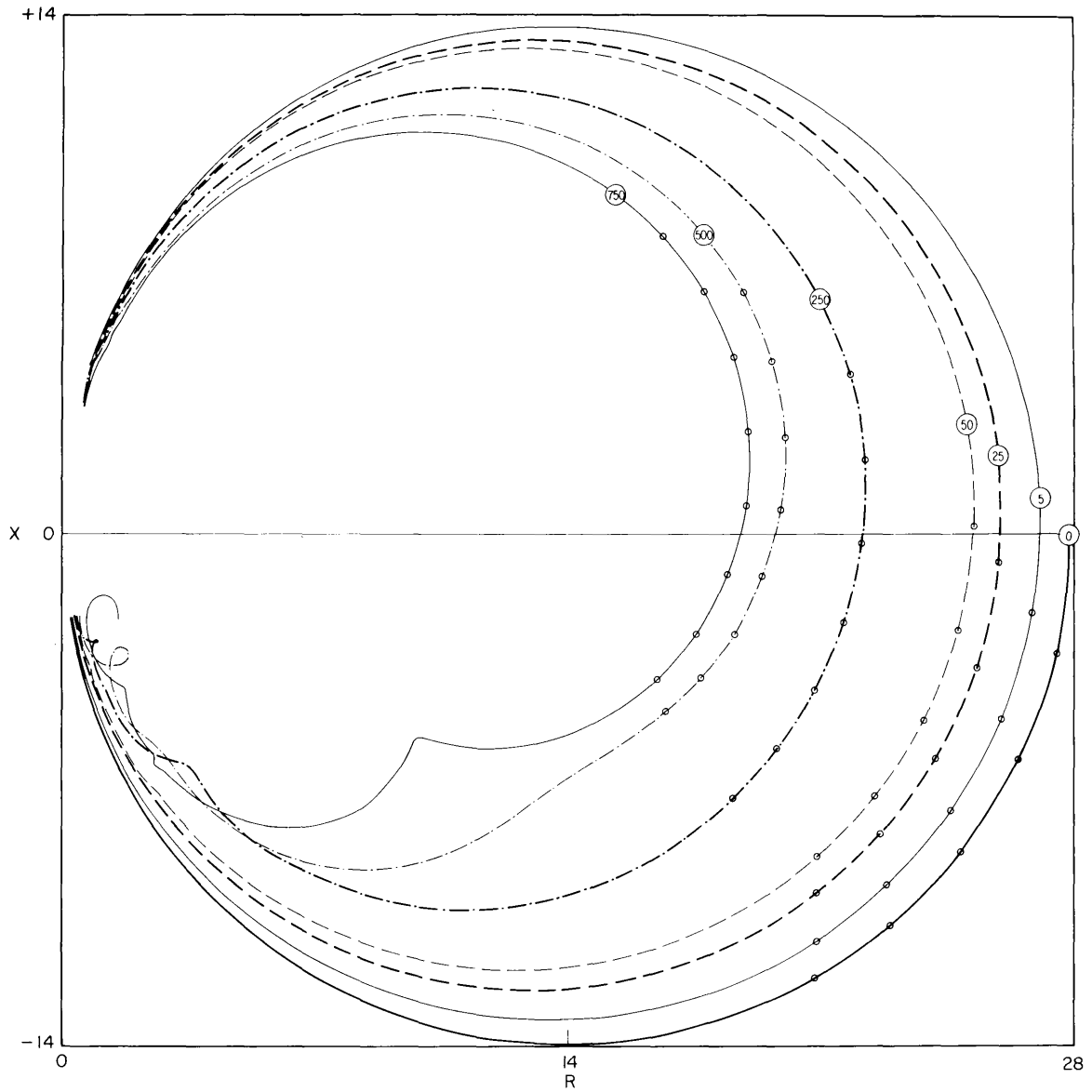

Fig. 31b—R vs X for infinitely flexible boundary conditions with $k_1^V a = 100\pi$ and $b/a = 2$ (see Table 51)

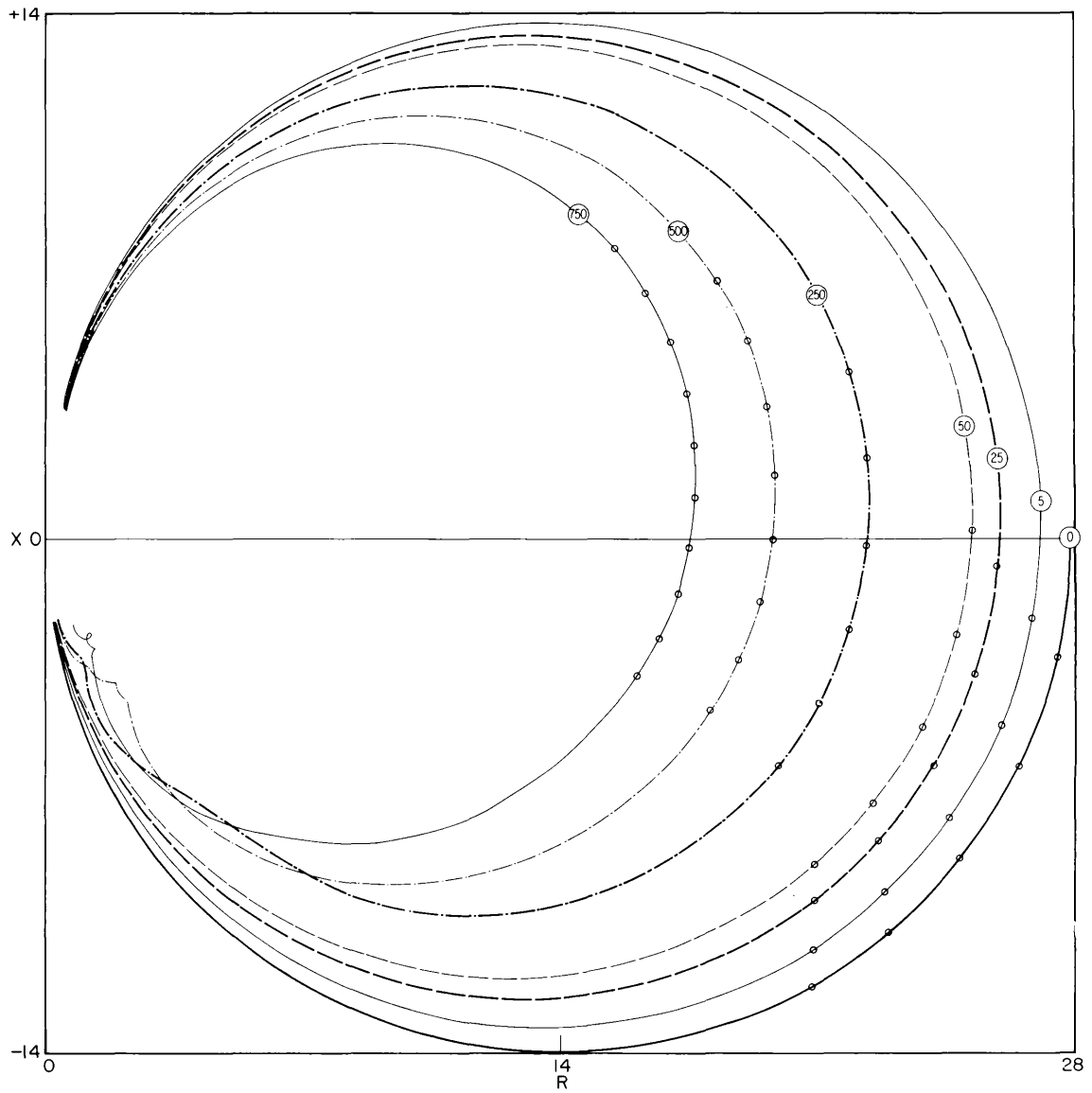

Fig. 31c—R vs X for infinitely flexible boundary conditions with $k_1^V a = 100\pi$ and $b/a = 5$ (see Table 52)

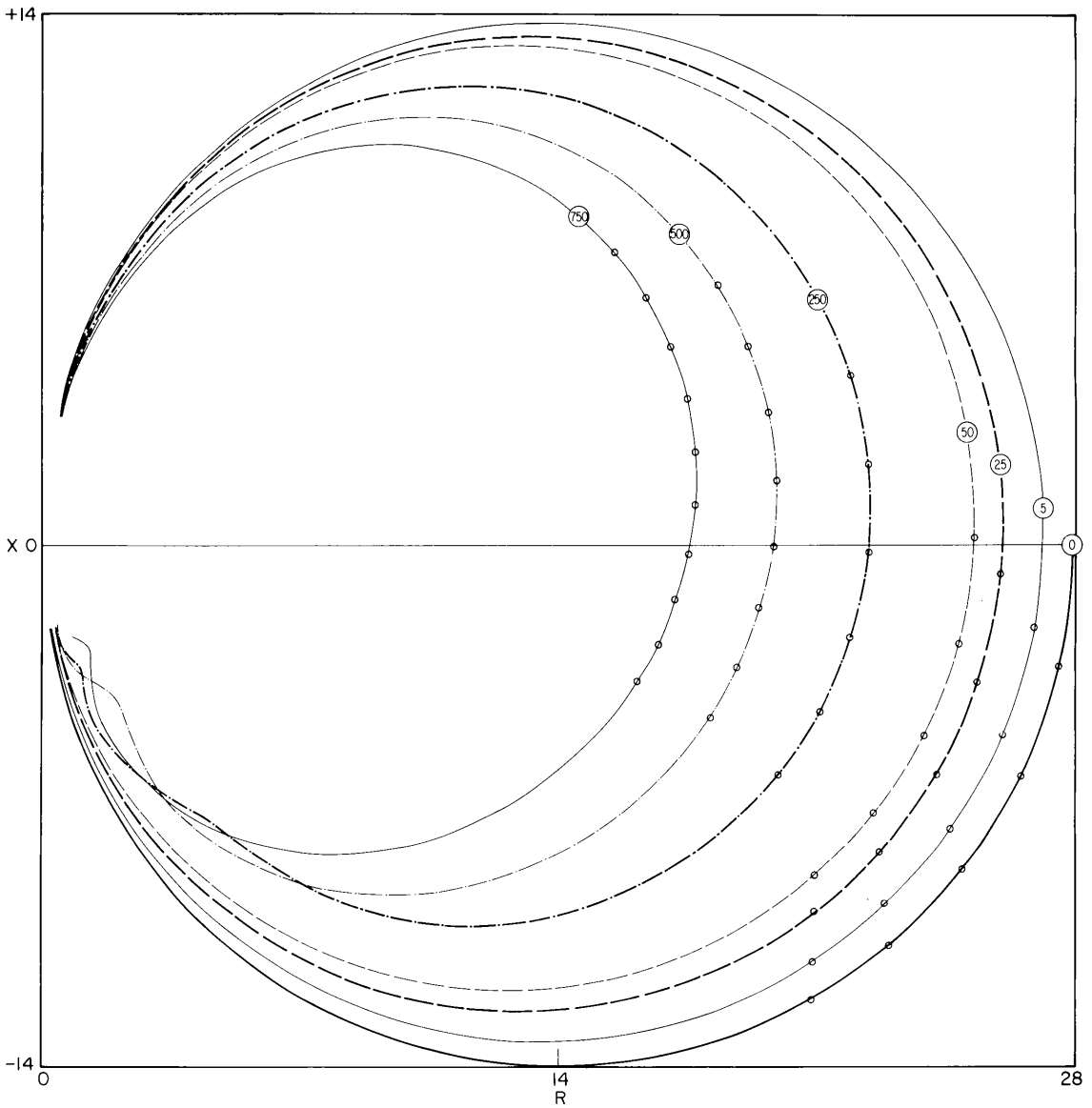

Fig. 31d—R vs X for infinitely flexible boundary conditions with $k_1^V a = 100\pi$ and $b/a = 10$ (see Table 53)

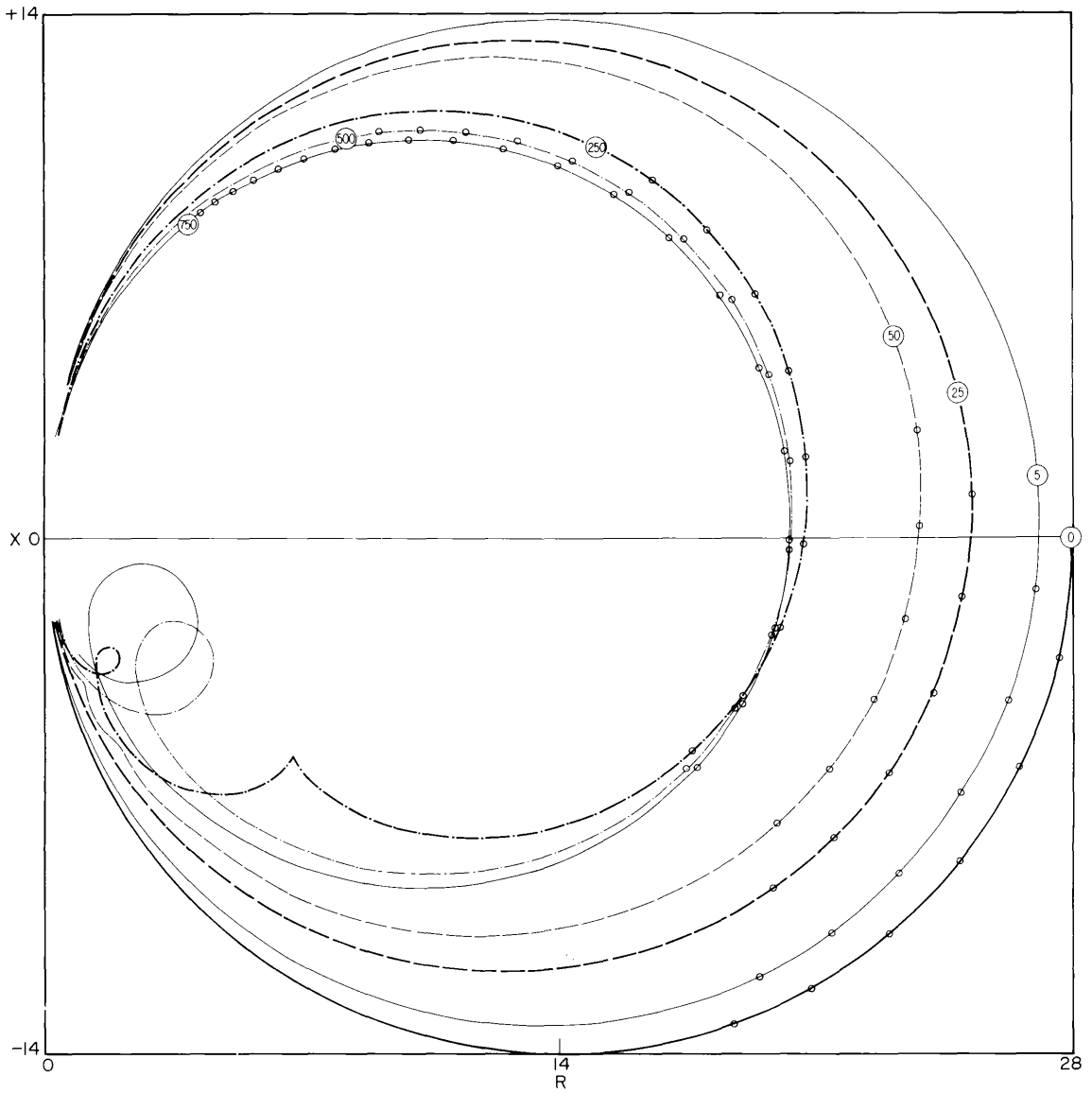

Fig. 32a—R vs X for liquid boundary conditions with $k_1^V a = 100\pi$ and $b/a = 1$ (see Table 54)

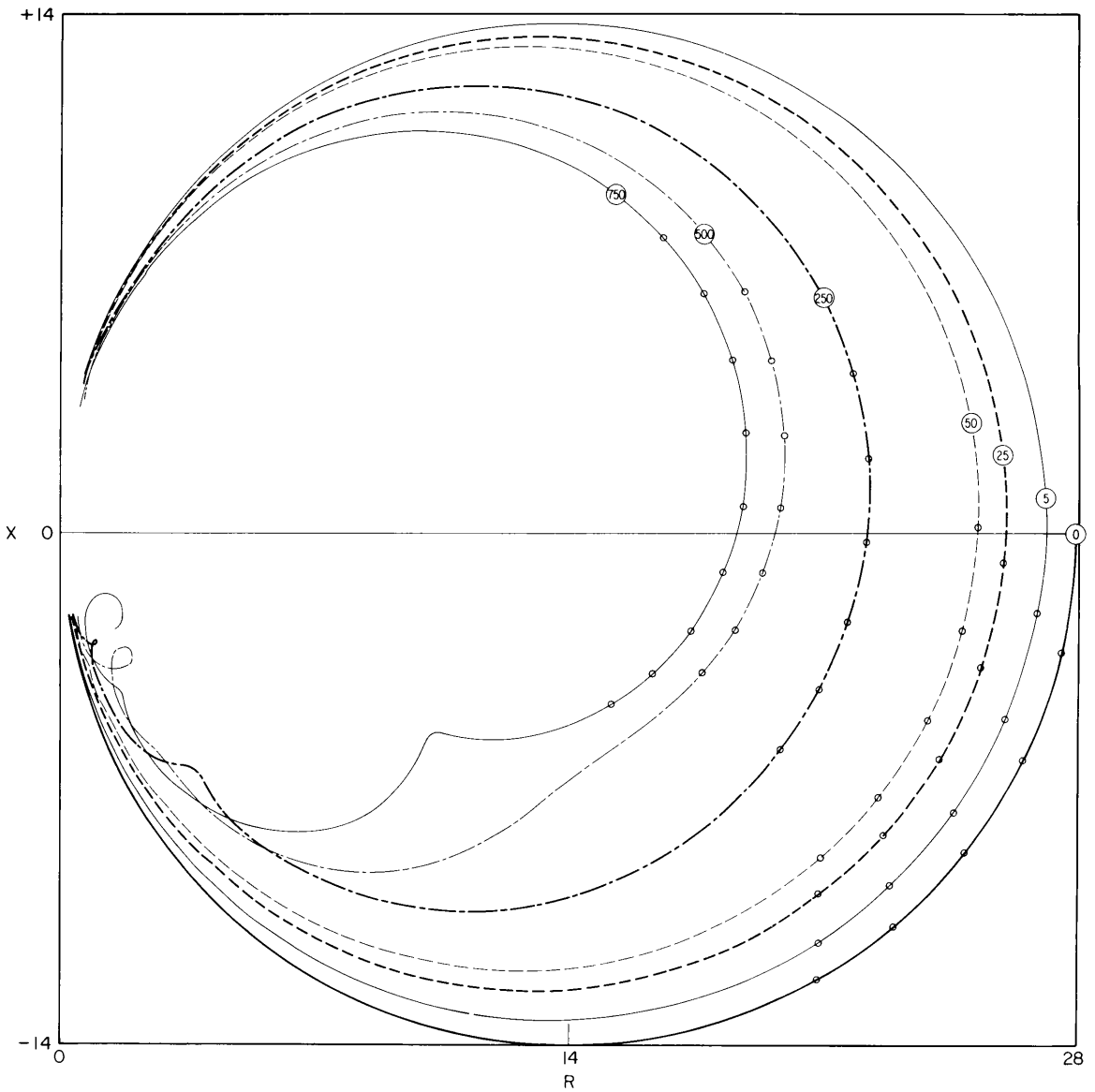

Fig. 32b—R vs X for liquid boundary conditions with $k_1^V a = 100\pi$ and $b/a = 2$ (see Table 55)

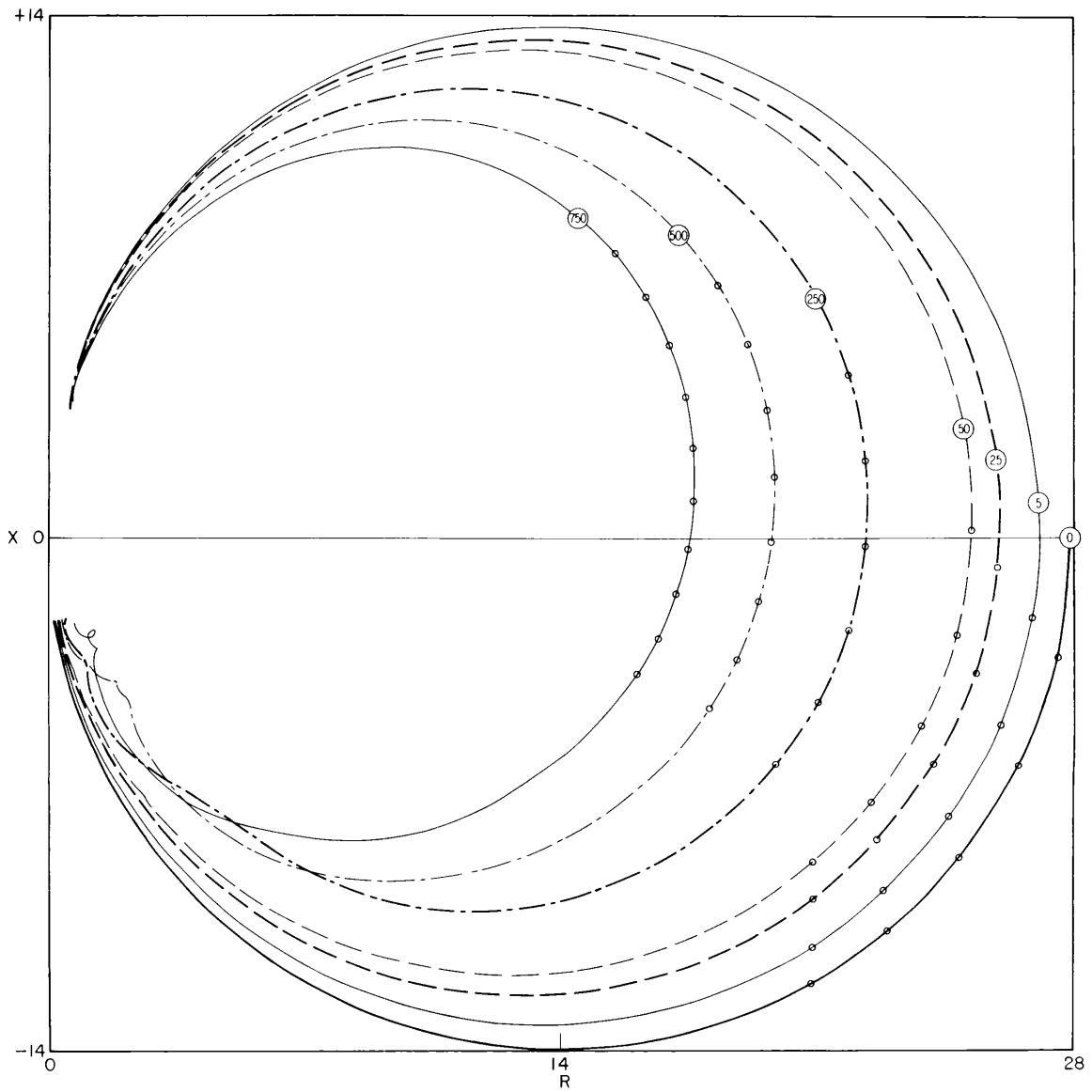

Fig. 32c—R vs X for liquid boundary conditions with $k_1^V a = 100\pi$ and $b/a = 5$ (see Table 56)

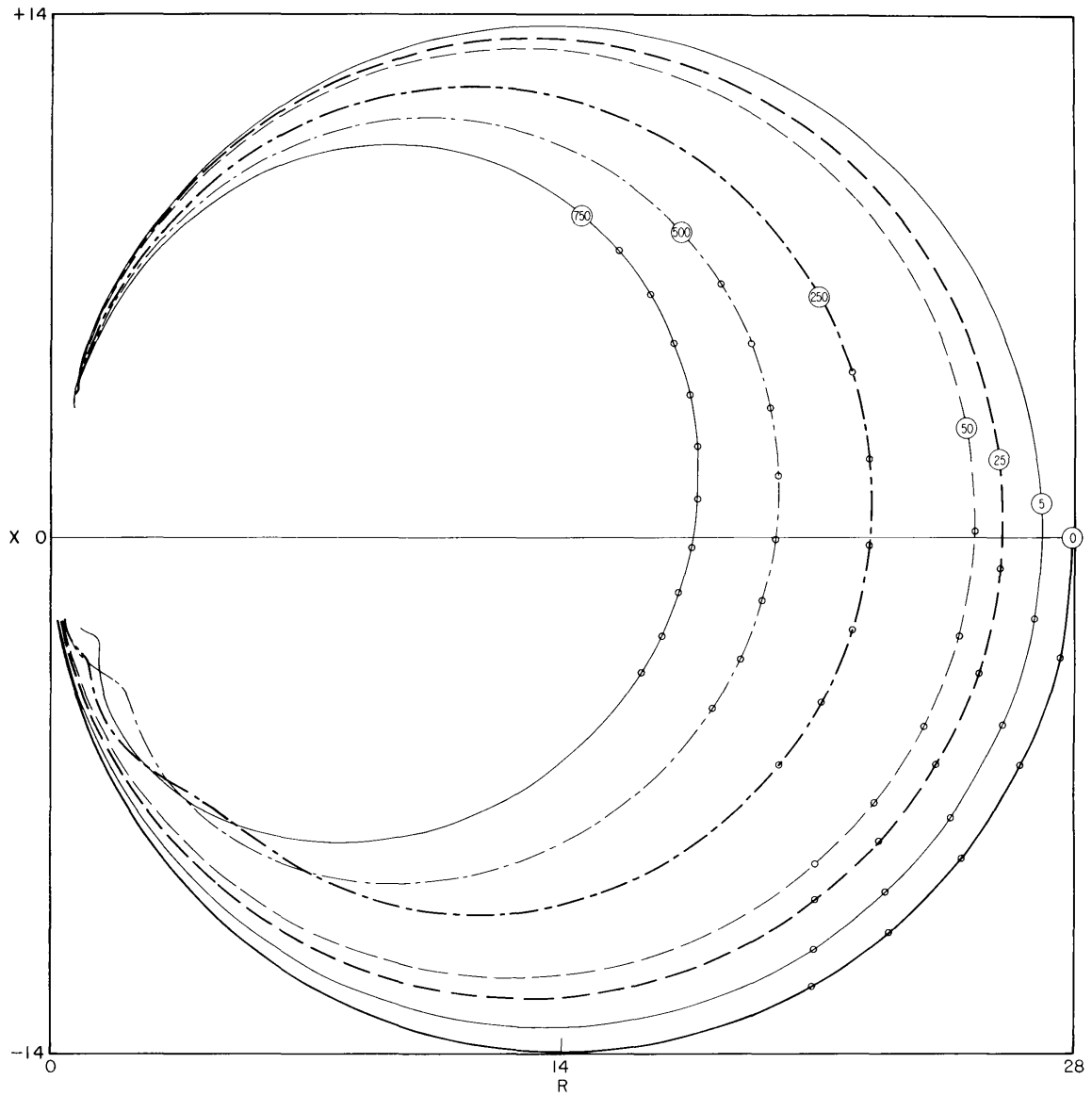

Fig. 32d—R vs X for liquid boundary conditions with $k_1^V a = 100\pi$ and $b/a = 10$ (see Table 57)

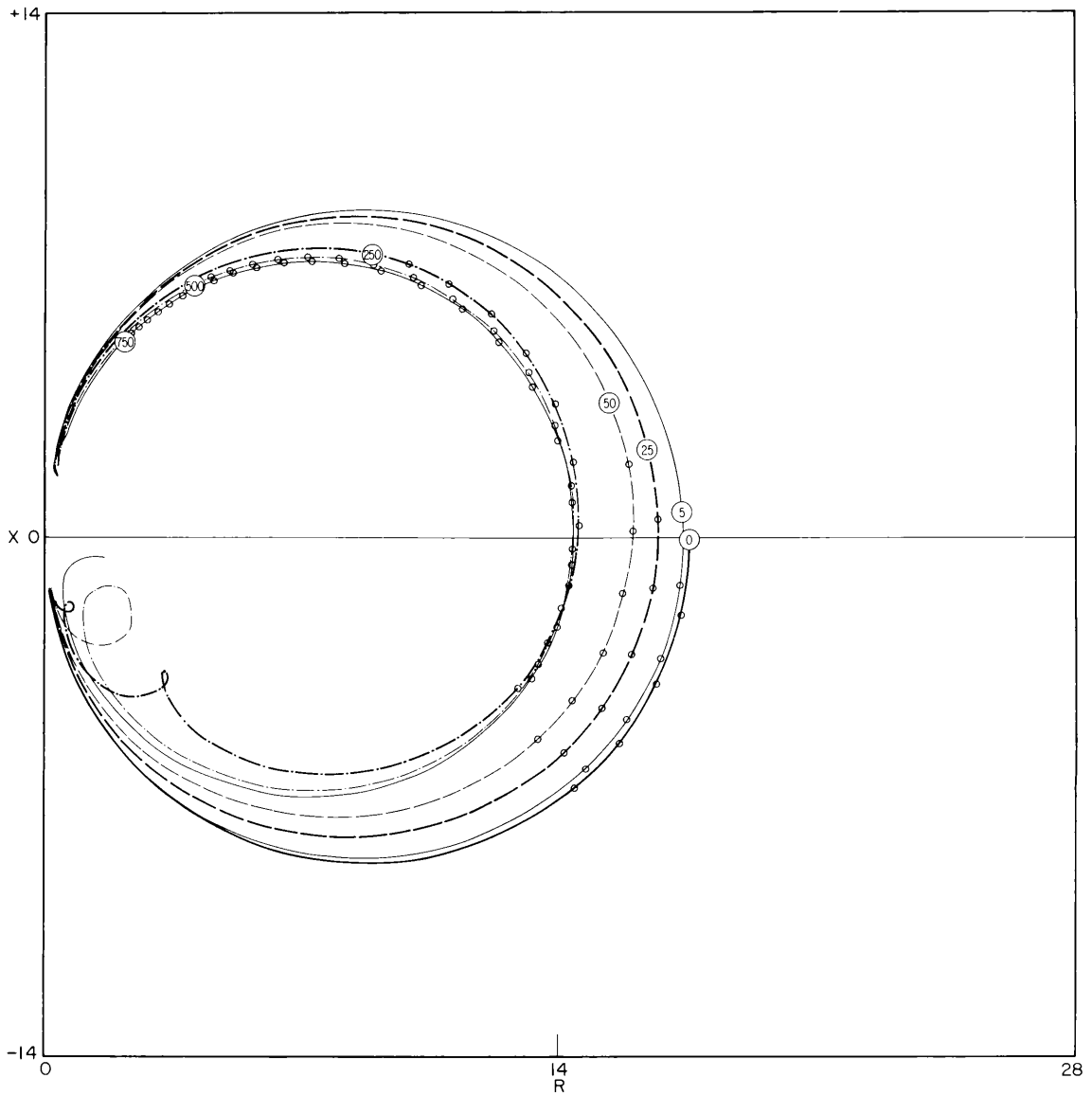

Fig. 33a—R vs X for elastic solid boundary conditions with $k_1^V a = 100\pi$ and $b/a = 1$ (see Table 58)

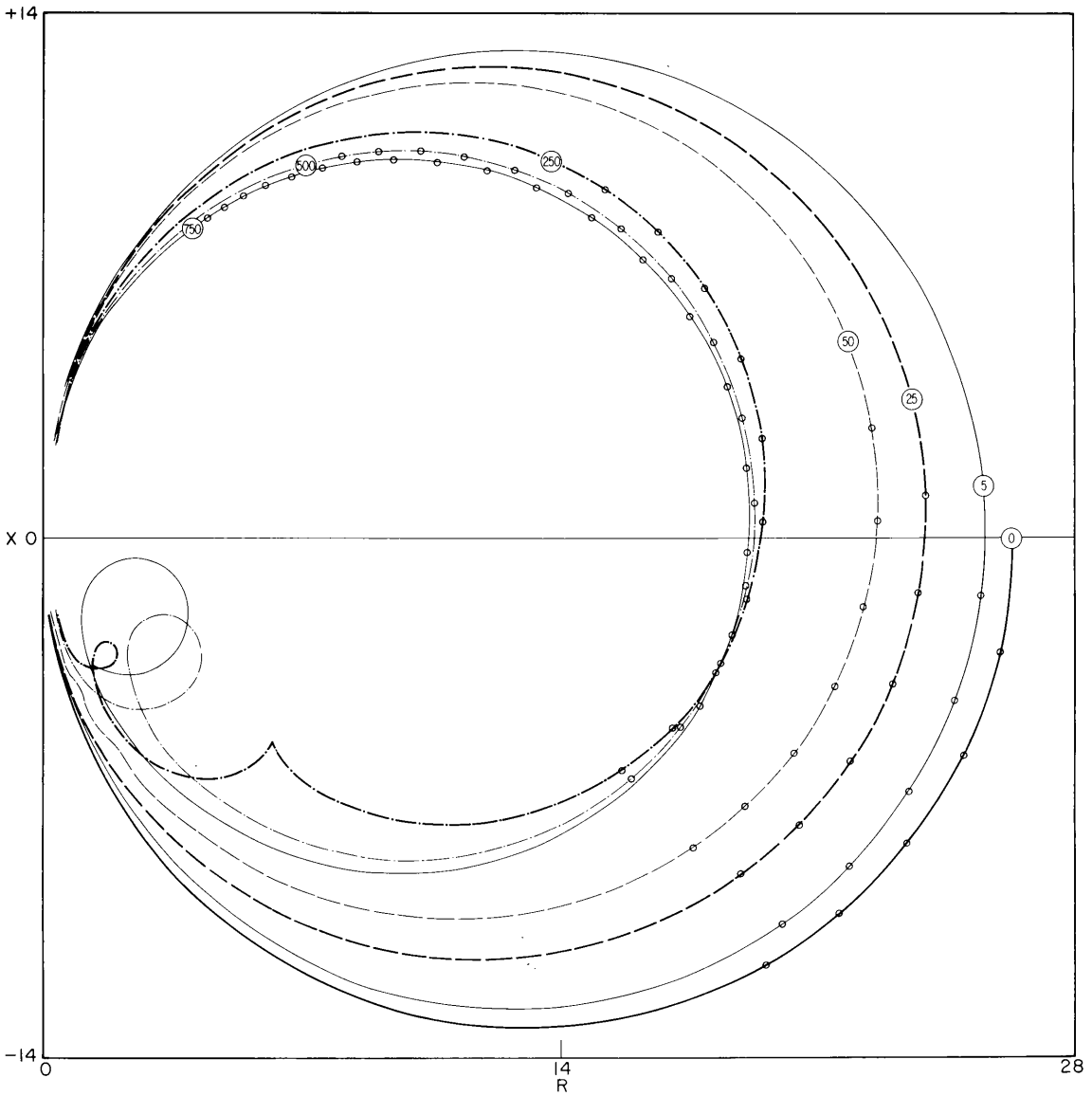

Fig. 33b—R vs X for elastic solid boundary conditions with $k_1^V a = 100\pi$ and $b/a = 1.1$ (see Table 59)

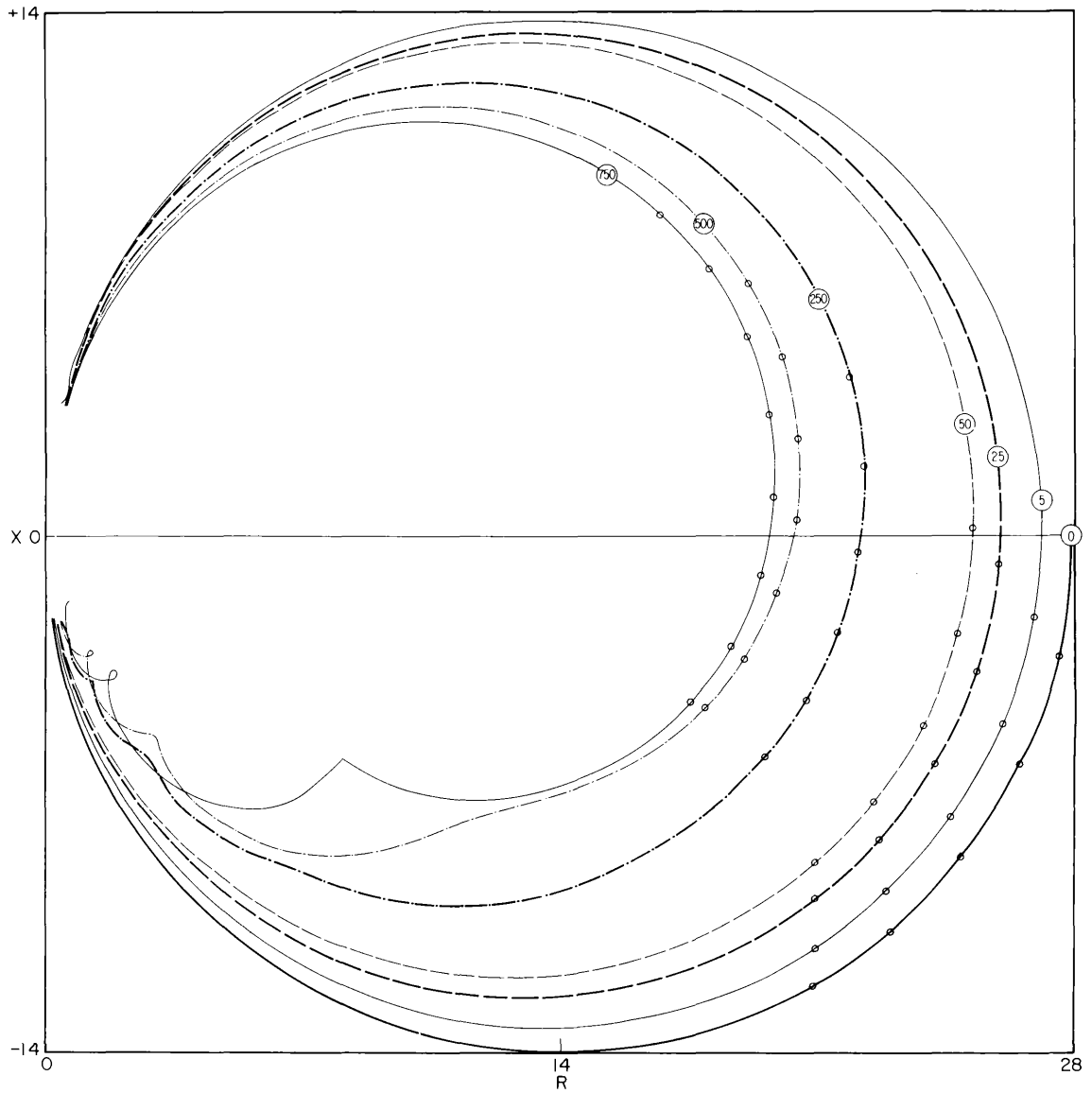

Fig. 33c—R vs X for elastic solid boundary conditions with $k_1^V a = 100\pi$ and $b/a = 2$ (see Table 60)

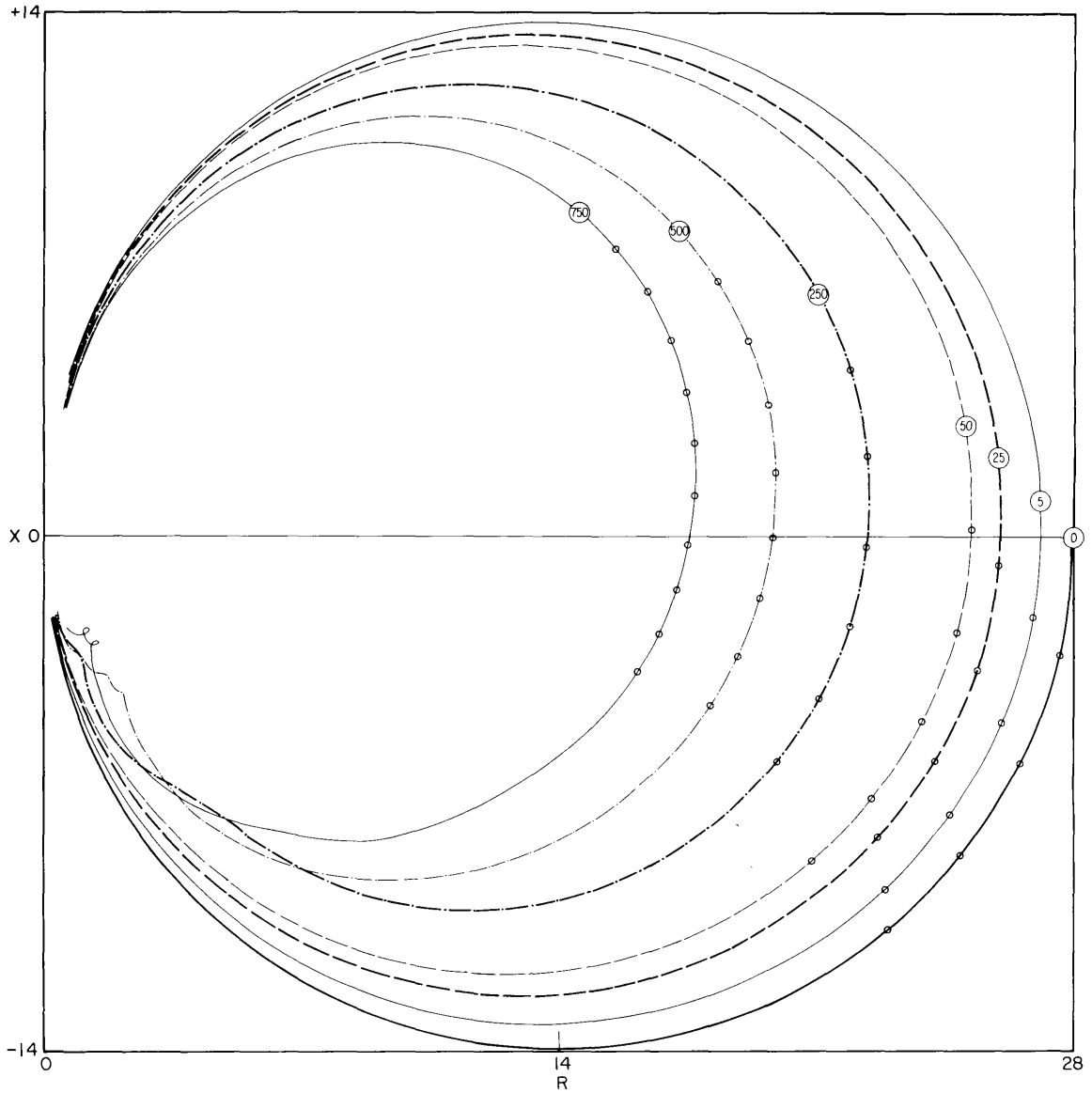

Fig. 33d—R vs X for elastic solid boundary conditions with $k_1^V a = 100\pi$ and $b/a = 5$ (see Table 61)

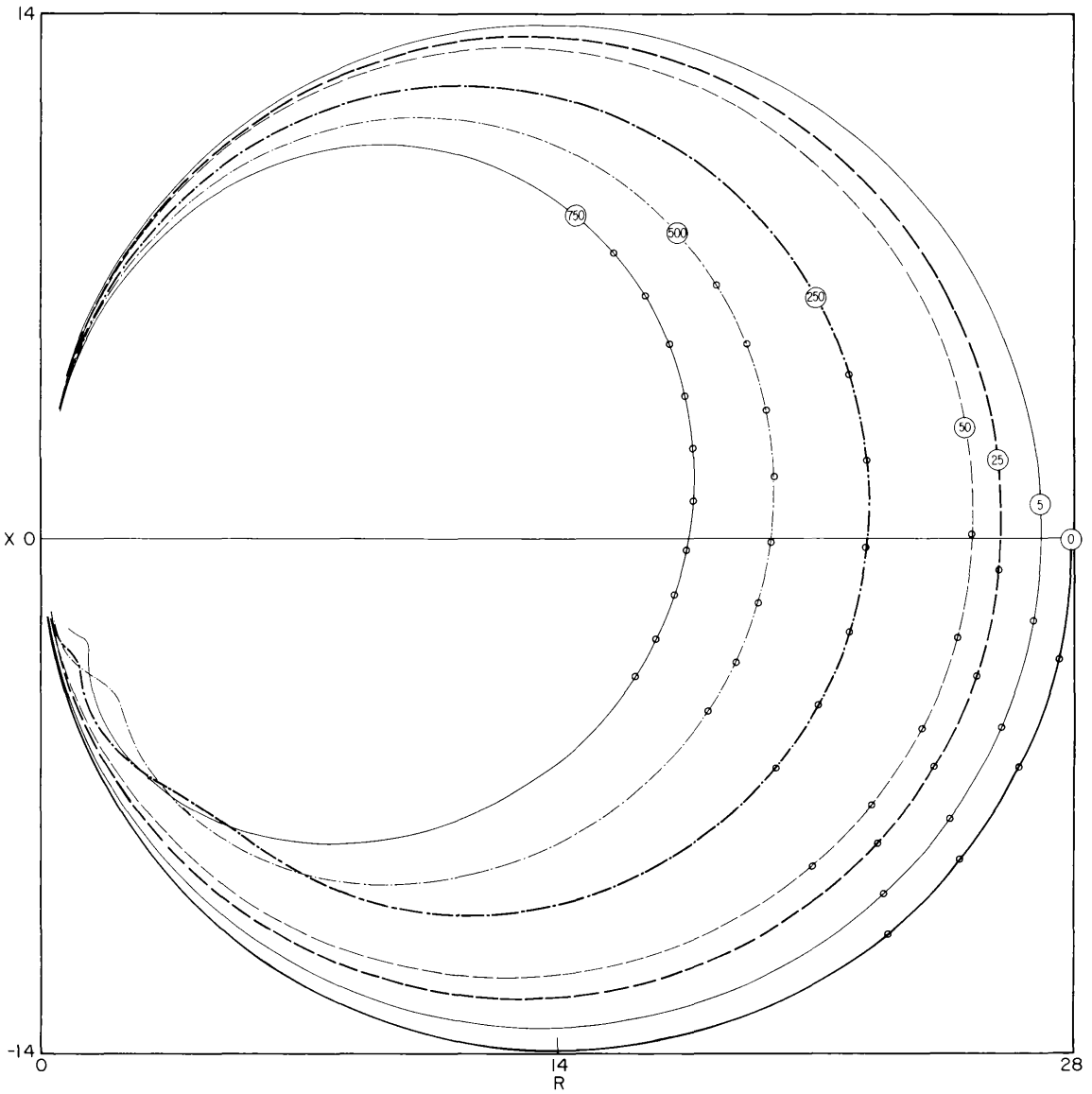

Fig. 33e—R vs X for elastic solid boundary conditions with $k_1^V a = 100\pi$ and $b/a = 10$ (see Table 62)

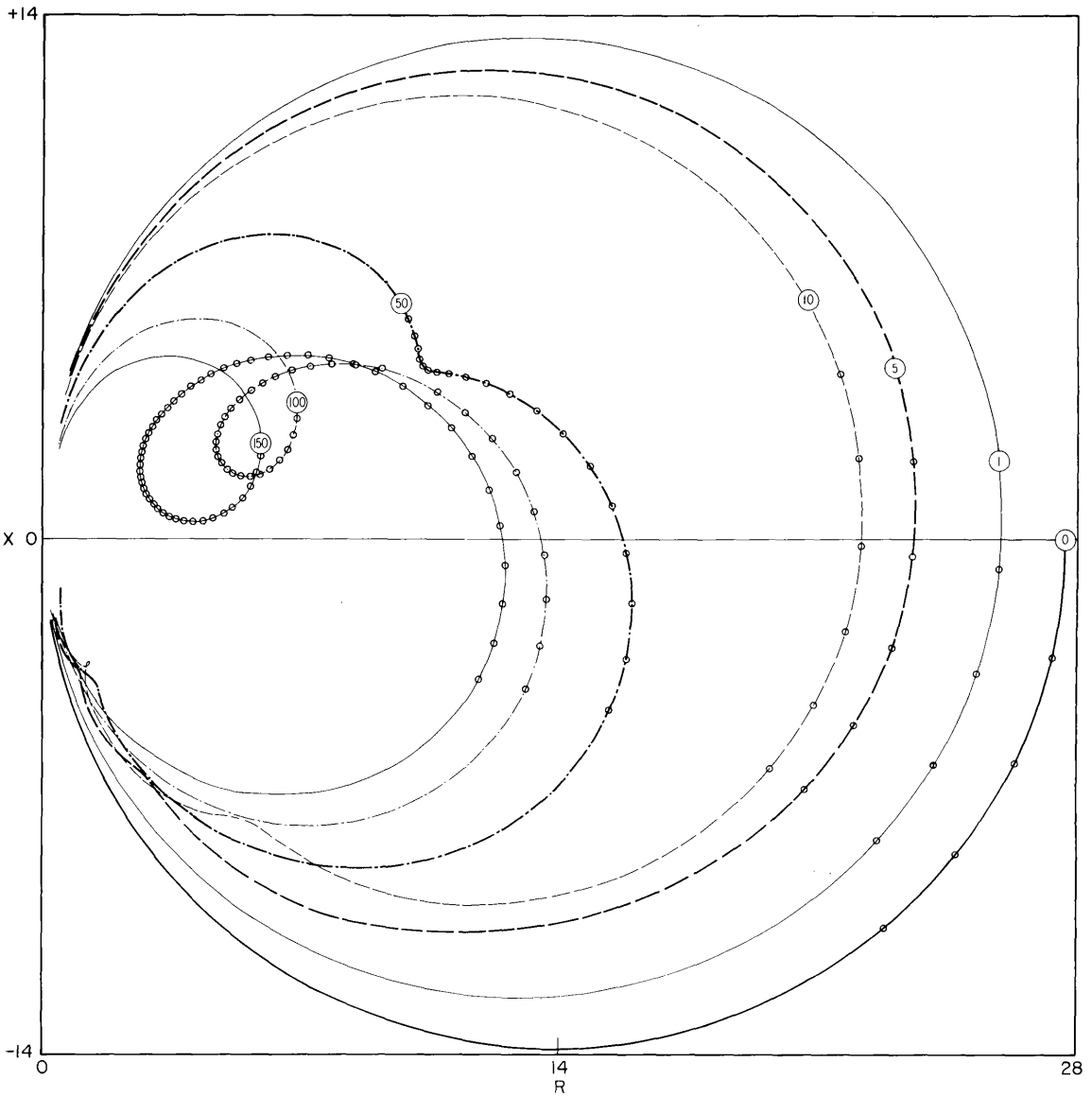

Fig. 34a—R vs X for absolutely rigid boundary conditions with $\alpha_1 = 10^{-3}$ cm^{-1} and $\alpha_3 = 10^{-3}$ cm^{-1} (see Table 63)

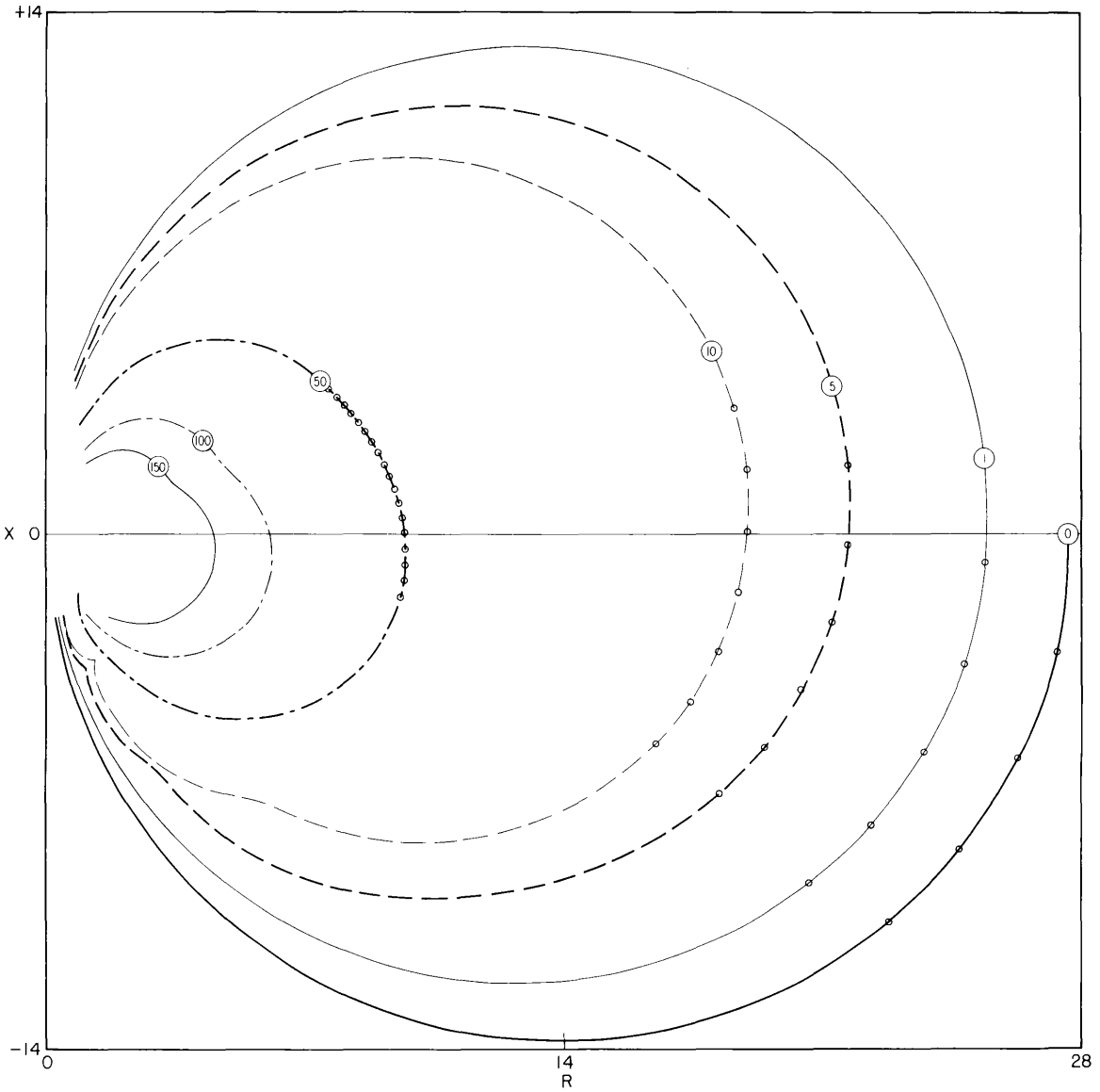

Fig. 34b—R vs X for absolutely rigid boundary conditions with $\alpha_1 = 10^{-2}$ cm^{-1} and $\alpha_3 = 10^{-3}$ cm^{-1} (see Table 64)

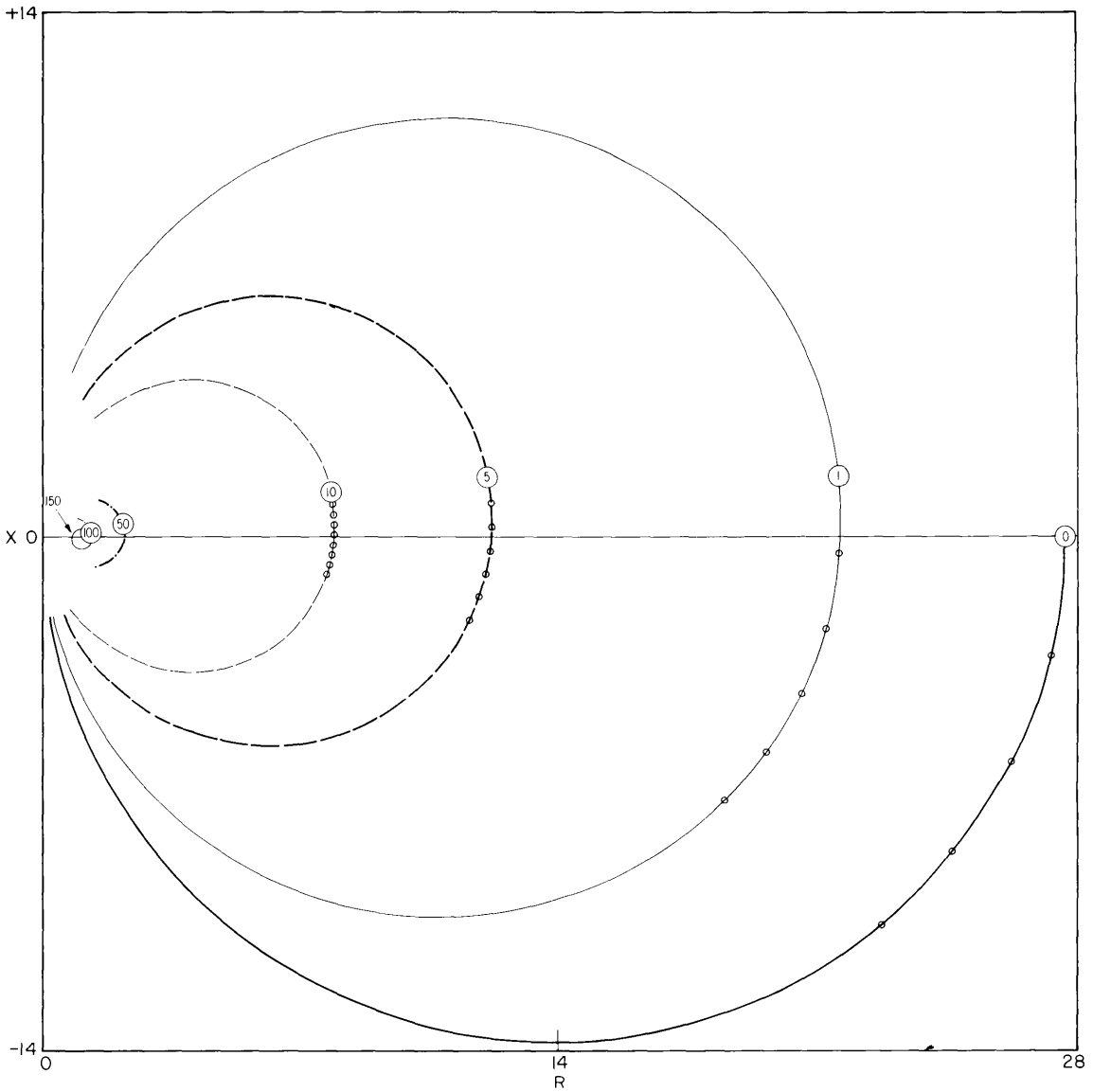

Fig. 34c—R vs X for absolutely rigid boundary conditions with $\alpha_1 = 10^{-1}$ cm^{-1} and $\alpha_3 = 10^{-3}$ cm^{-1} (see Table 65)

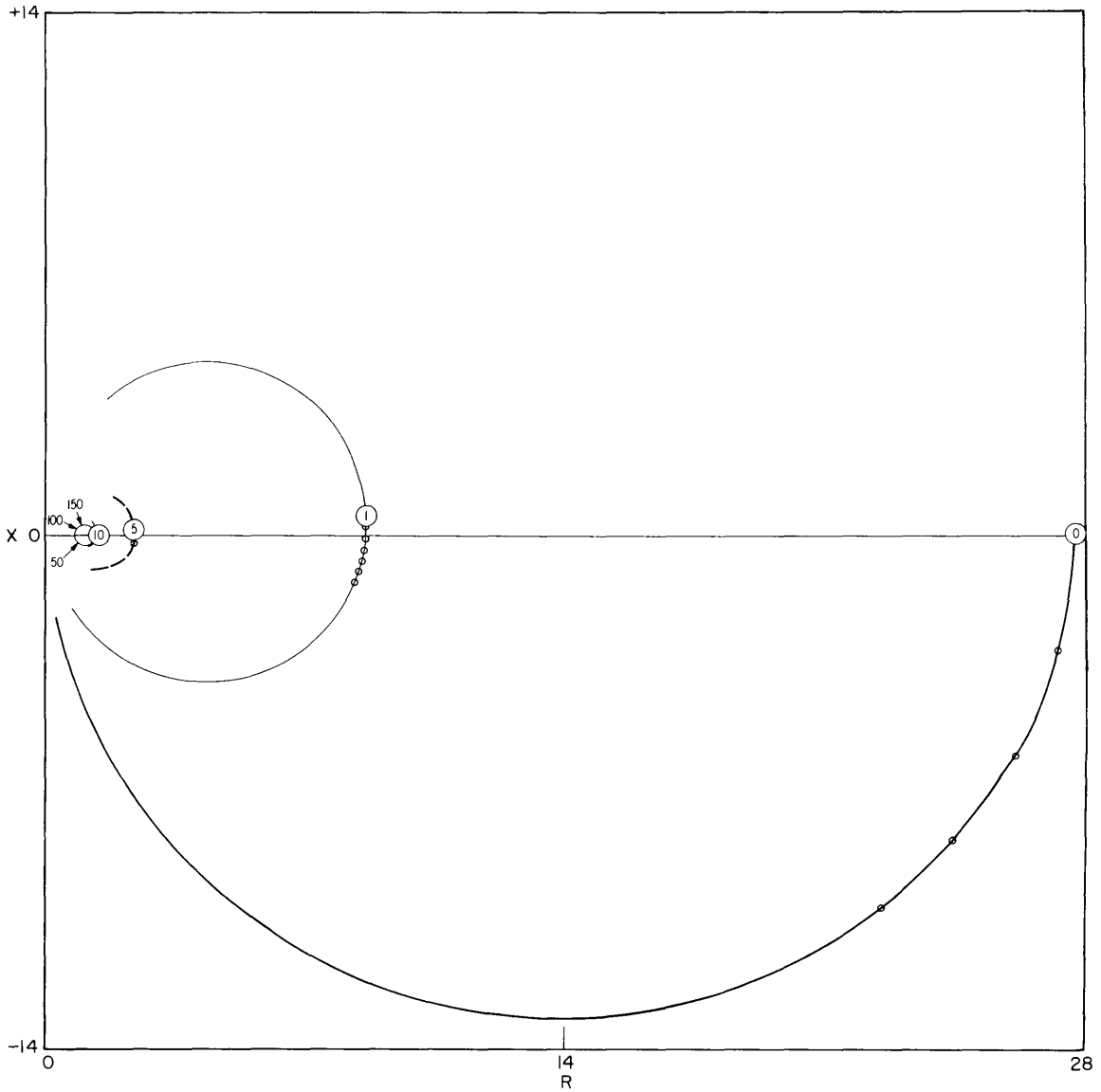

Fig. 34d—R vs X for absolutely rigid boundary conditions with $\alpha_1 = 1$ cm^{-1} and $\alpha_3 = 10^{-3}$ cm^{-1} (see Table 66)

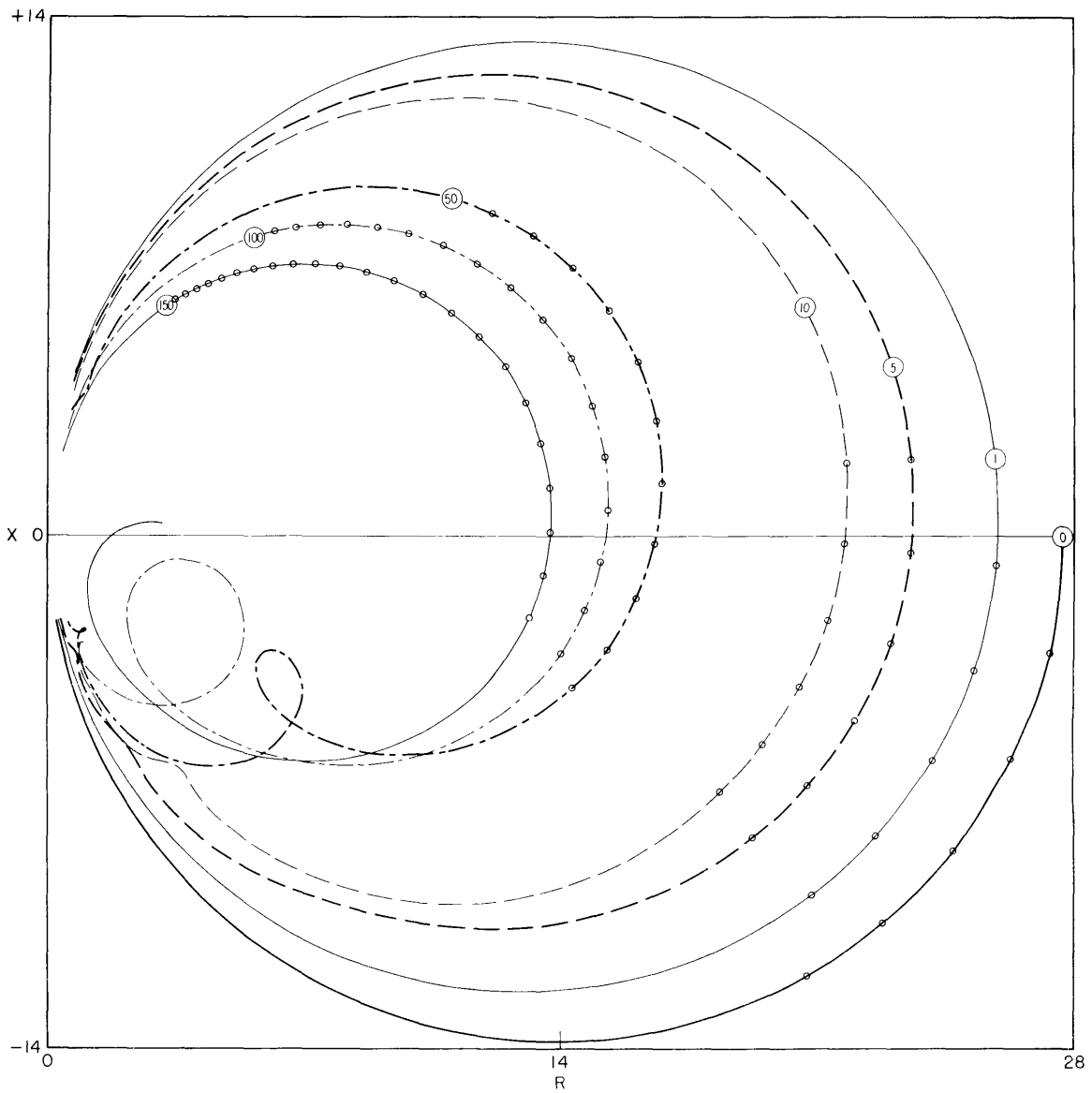

Fig. 35a – R vs X for infinitely flexible boundary conditions with $\alpha_1 = 10^{-3}$ cm^{-1} and $\alpha_3 = 10^{-3}$ cm^{-1} (see Table 67)

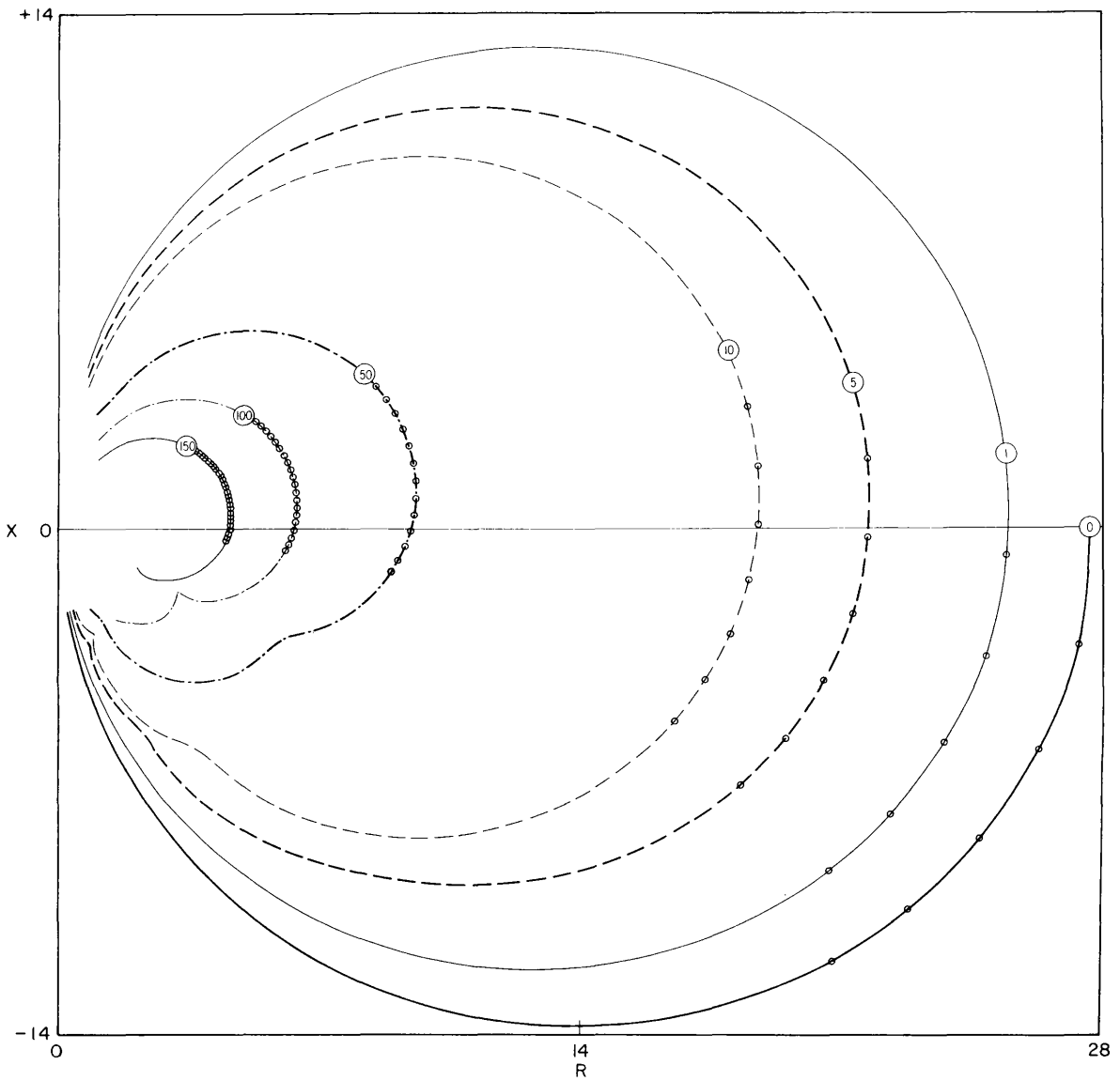

Fig. 35b—R vs X for infinitely flexible boundary conditions with $\alpha_1 = 10^{-2}$ cm^{-1} and $\alpha_3 = 10^{-3}$ cm^{-1} (see Table 68)

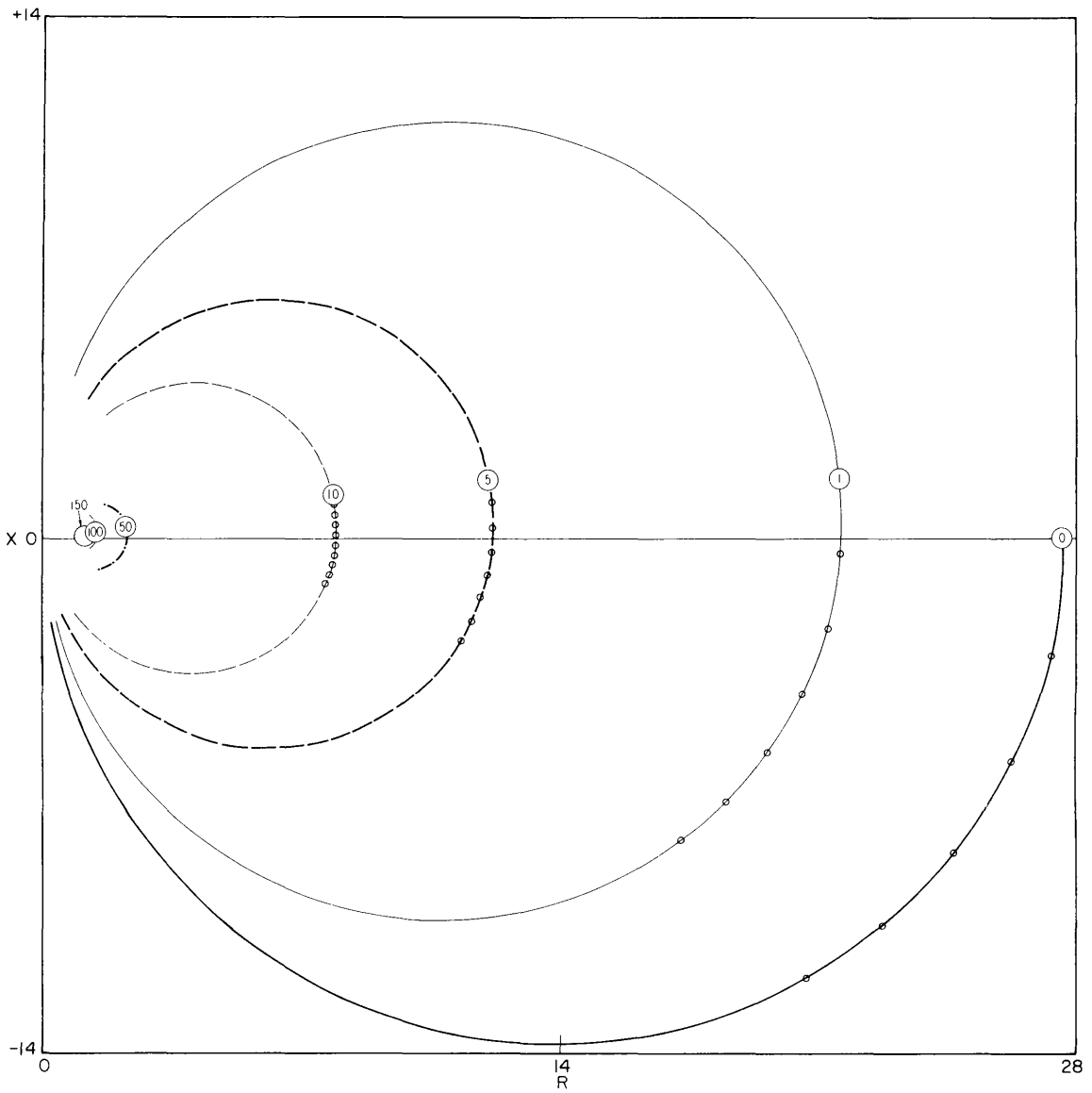

Fig. 35c—R vs X for infinitely flexible boundary conditions with $\alpha_1 = 10^{-1}$ cm^{-1} and $\alpha_3 = 10^{-3}$ cm^{-1} (see Table 69)

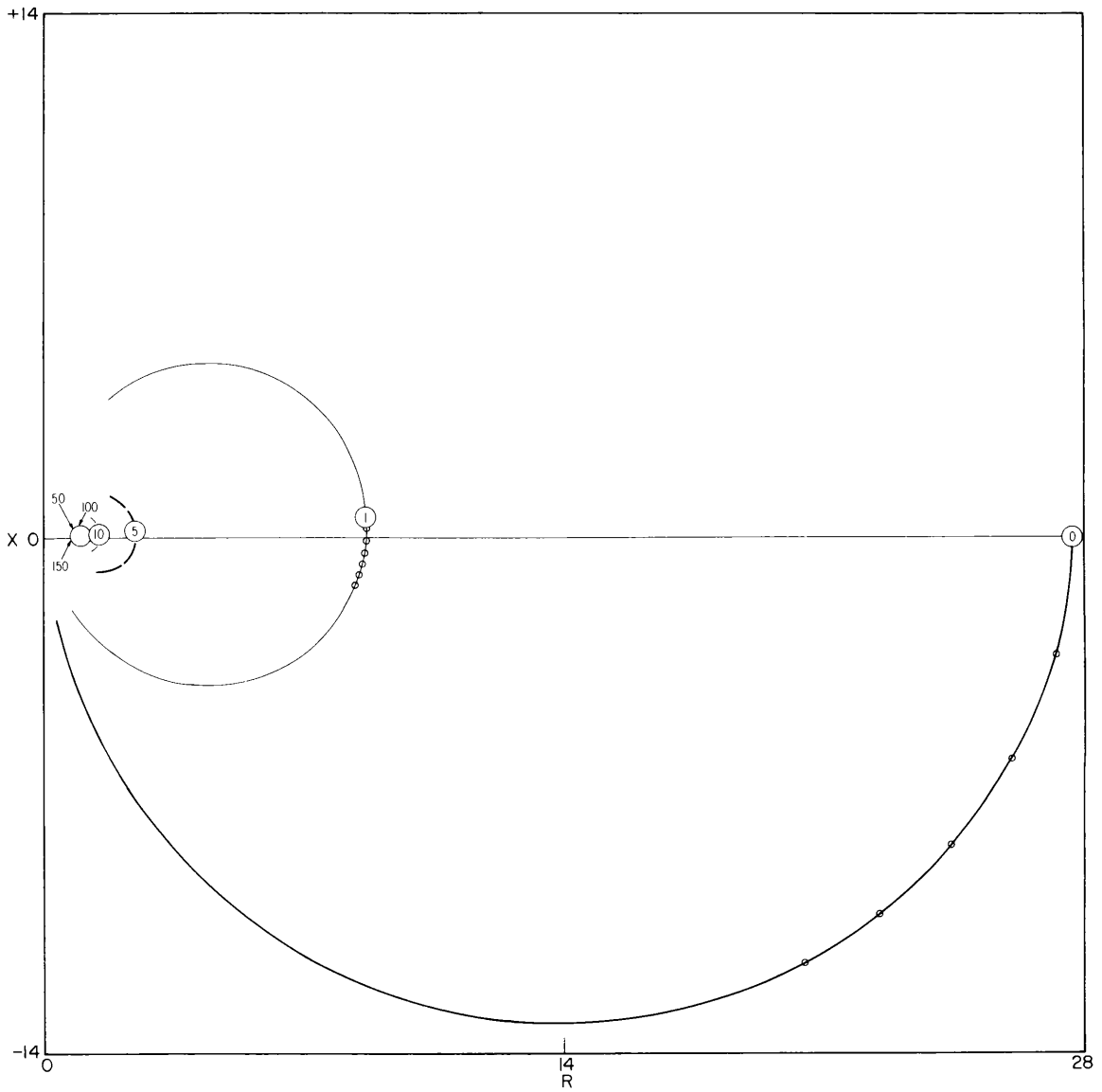

Fig. 35d—R vs X for infinitely flexible boundary conditions with $\alpha_1 = 1$ cm^{-1} and $\alpha_3 = 10^{-3}$ cm^{-1} (see Table 70)

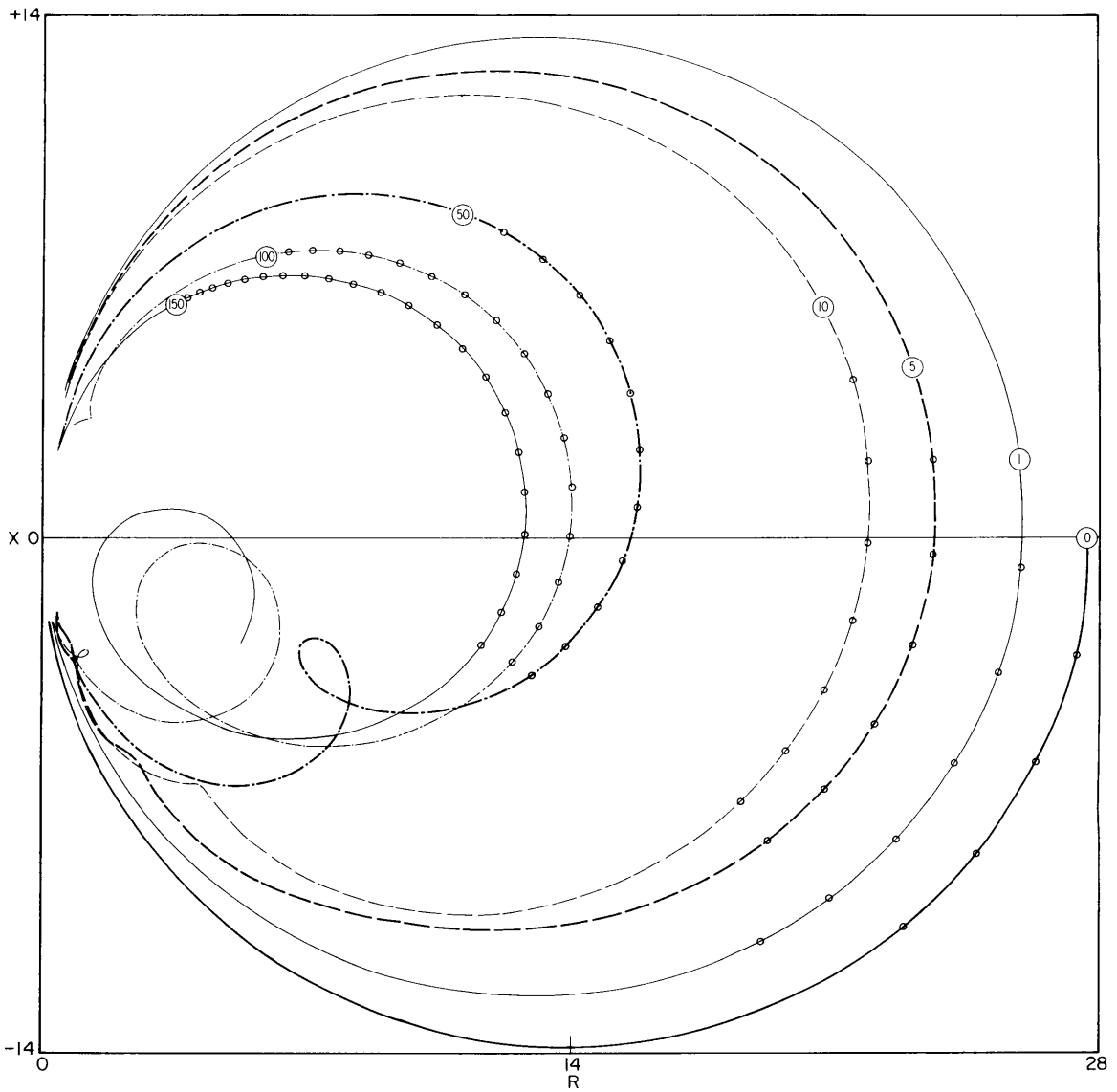

Fig. 36a—R vs X for liquid boundary conditions with $\alpha_1 = 10^{-3}$ cm^{-1} and $\alpha_3 = 10^{-3}$ cm^{-1} (see Table 71)

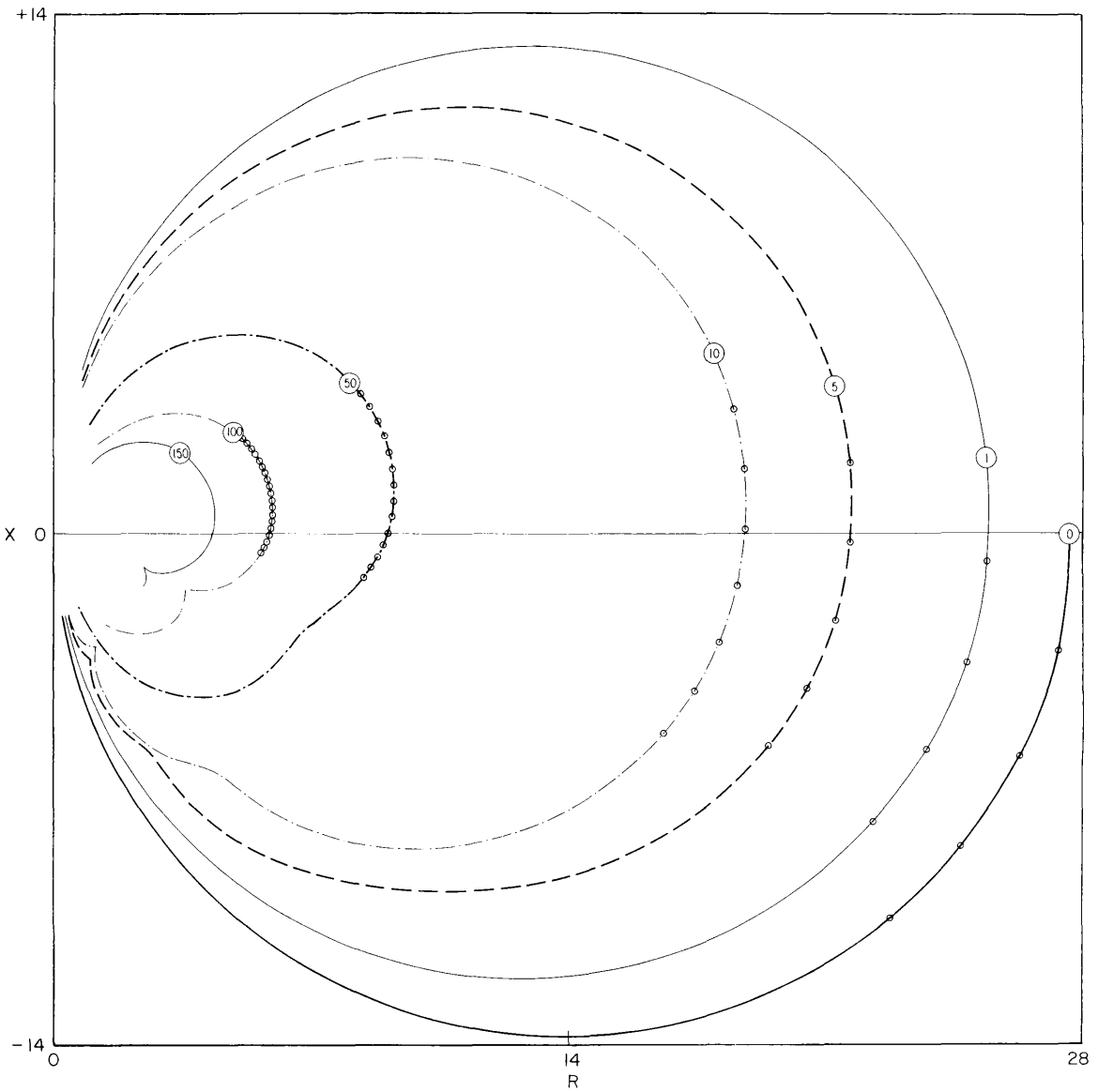

Fig. 36b – R vs X for liquid boundary conditions with $\alpha_1 = 10^{-2}$ cm^{-1} and $\alpha_3 = 10^{-3}$ cm^{-1} (see Table 72)

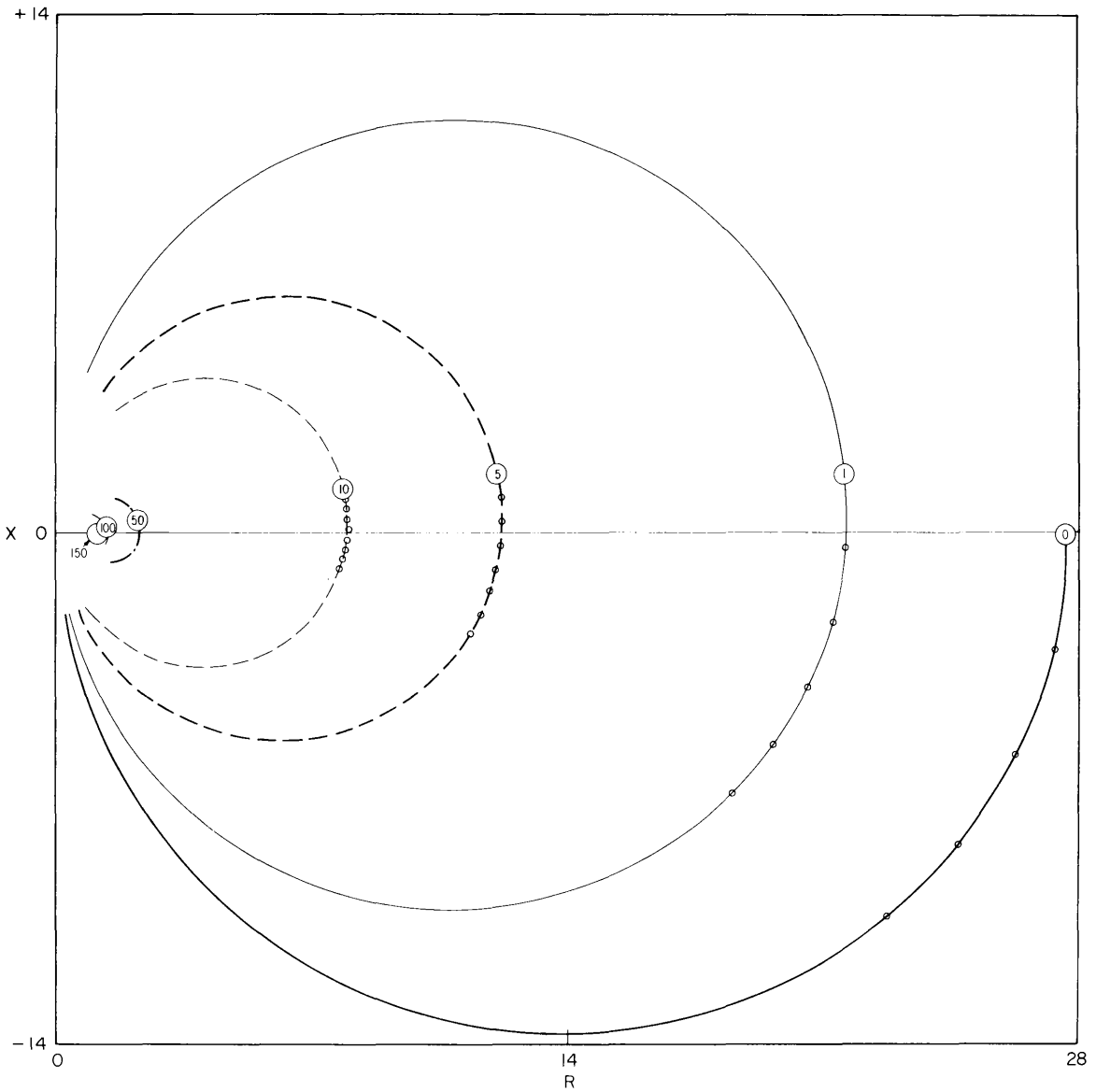

Fig. 36c—R vs X for liquid boundary conditions with $\alpha_1 = 10^{-1}$ cm^{-1} and $\alpha_3 = 10^{-3}$ cm^{-1} (see Table 73)

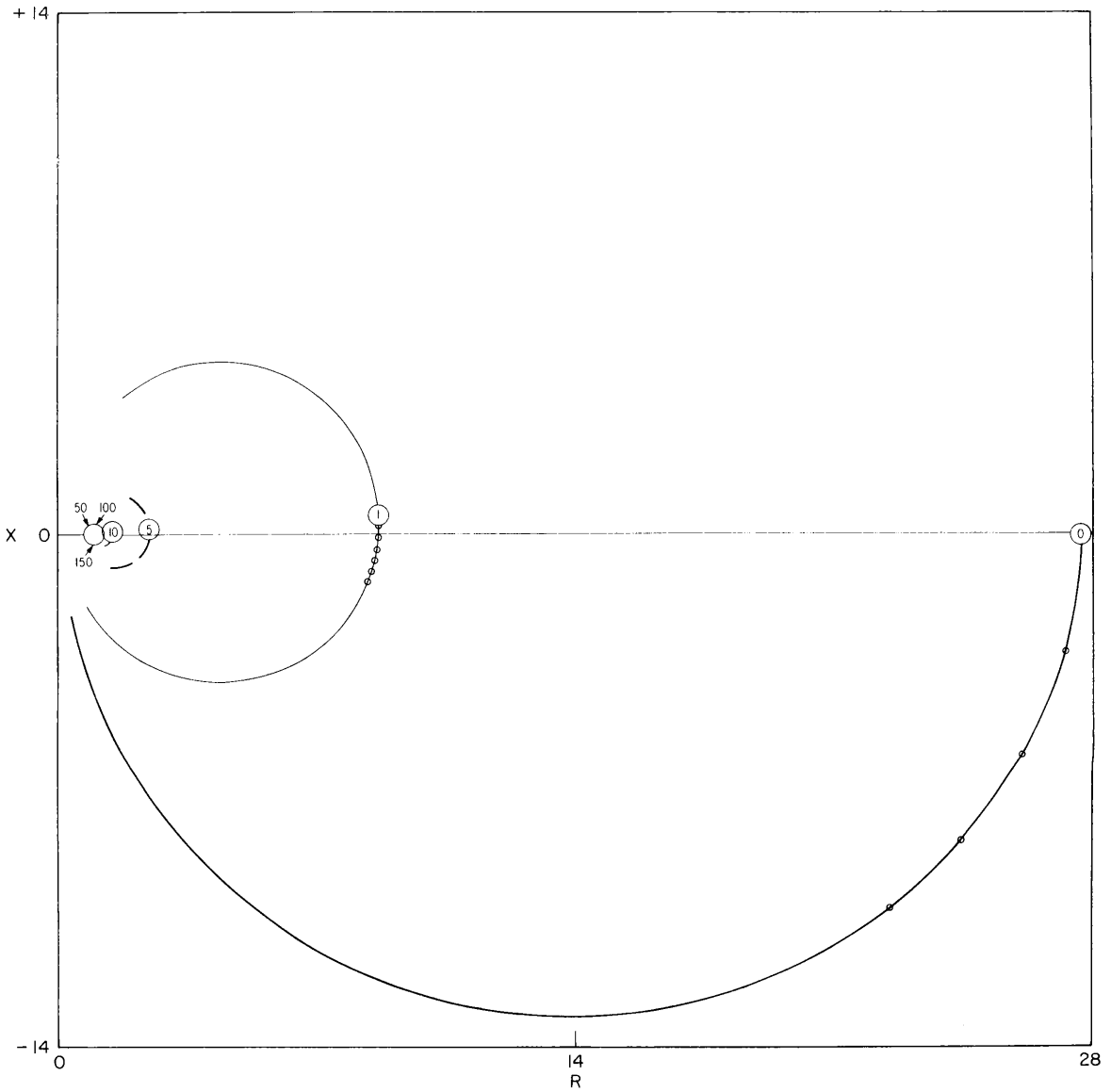

Fig. 36d—R vs X for liquid boundary conditions with $\alpha_3 = 1\ \mathrm{cm}^{-1}$ and $\alpha_3 = 10^{-3}\ \mathrm{cm}^{-1}$ (see Table 74)

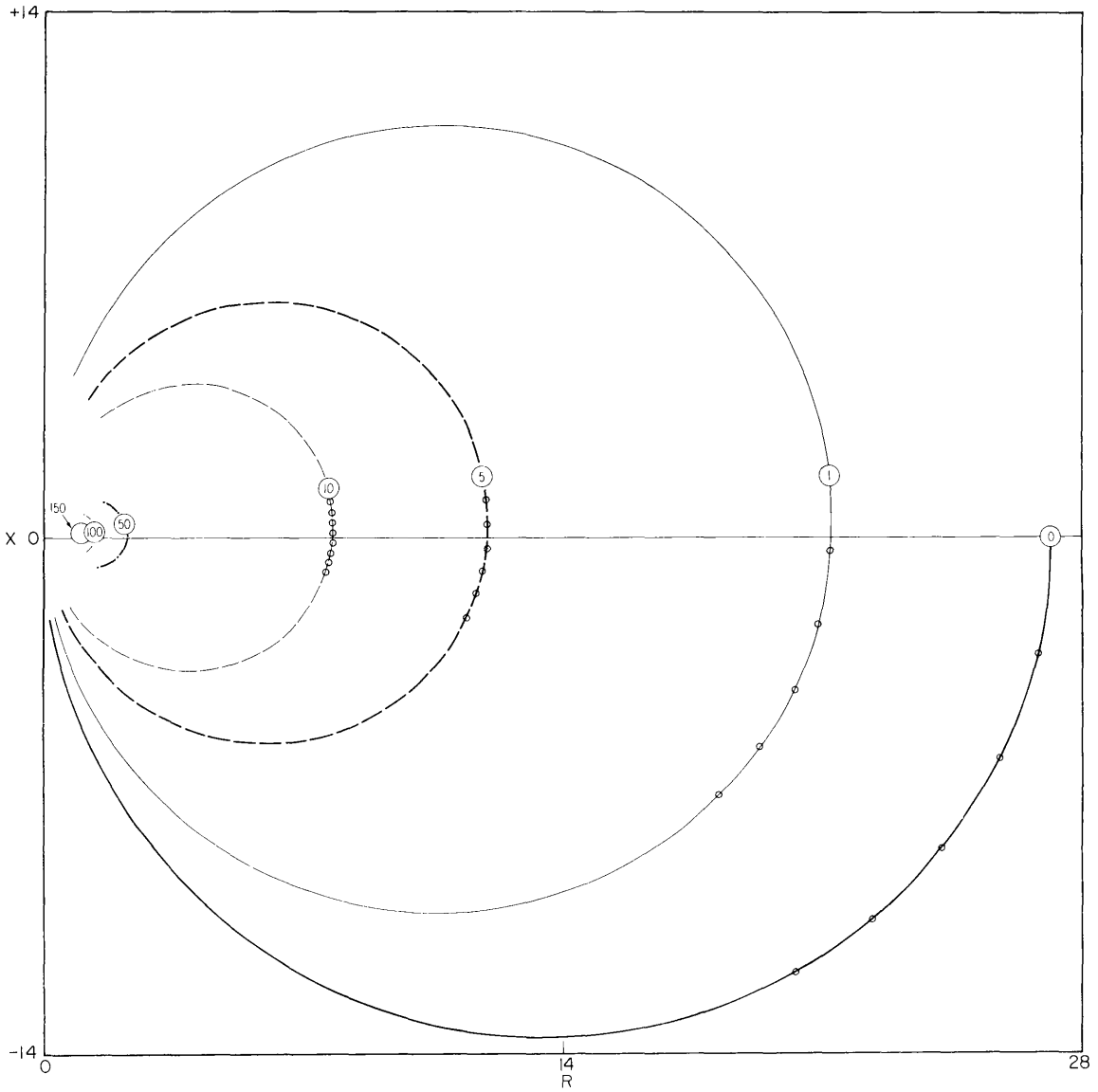

Fig. 37c – R vs X for elastic solid boundary conditions with $\alpha_1 = 10^{-1}$ cm^{-1} and $\alpha_3 = 10^{-3}$ cm^{-1} (see Table 77)

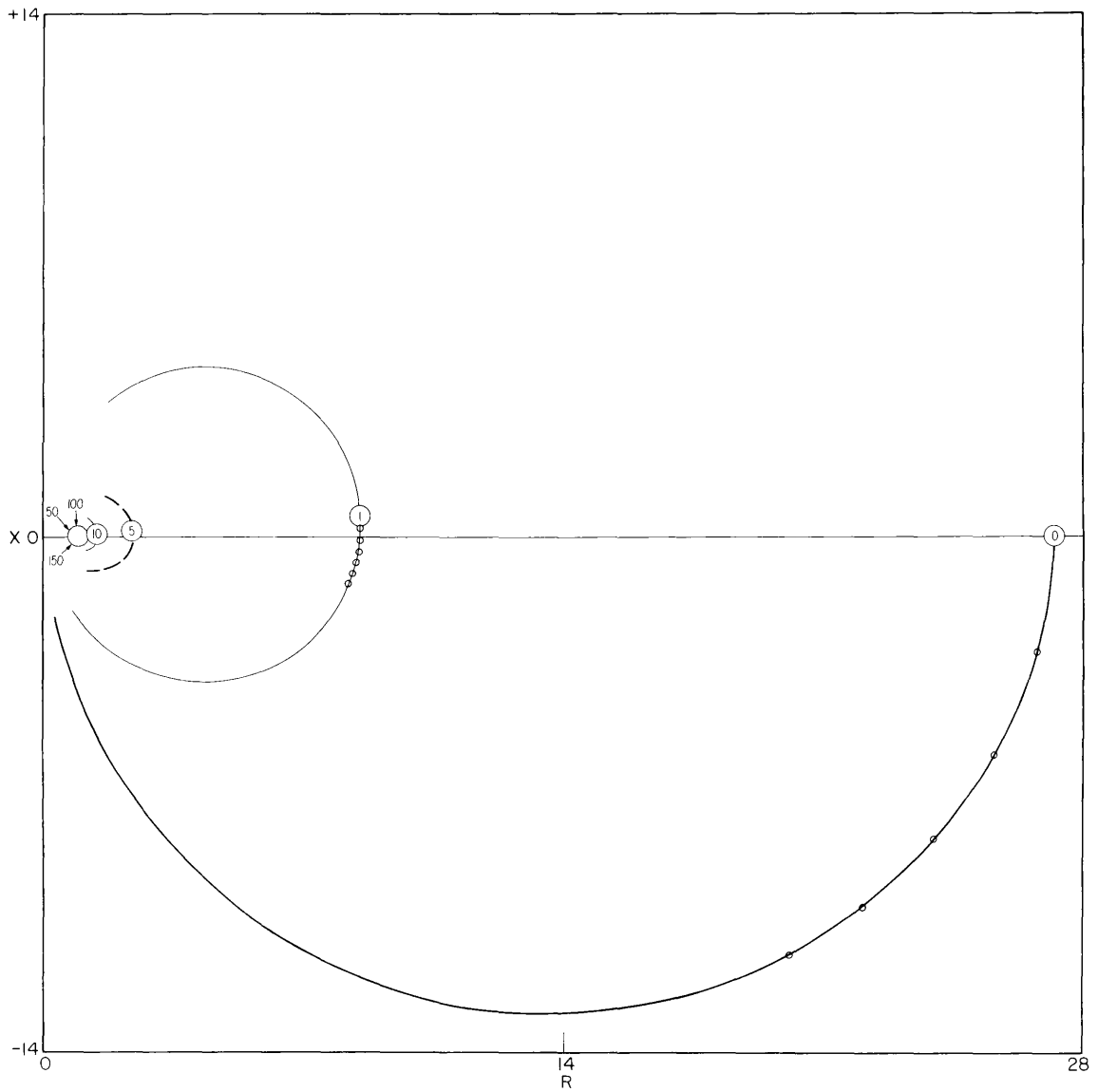

Fig. 37d—R vs X for elastic solid boundary conditions with $\alpha_1 = 1\ \mathrm{cm}^{-1}$ and $\alpha_3 = 10^{-3}\ \mathrm{cm}^{-1}$ (see Table 78)

Table 2

Apparent Sound Speeds C for Successive Intervals Between Indicated Source-to-Reflector Separations ℓ Corresponding to Half Wavelengths n. The Values of ℓ are Read from Fig. 22b for the Imposed Characteristics of Zero Phase, Maximum R, and Maximum Z for the Standard Reference Parameters of Table 1 (Except b/a = 1.1) and Absolutely Rigid Boundary Conditions.

Imposed Characteristic	n	ℓ (cm)	C (m/s)	Error (ppm)
Zero phase	1	0.075050	1501.000	666
	5	0.375039	1499.945	37
	10	0.750029	1501.004	668
	50	3.750003	1499.987	9
	100	7.500002	1500.000	0
	150	11.249998	1499.998	1
Max R	1	0.075025	1500.500	333
	5	0.375007	1499.910	60
	10	0.750006	1499.996	3
	50	3.750002	1499.998	1
	100	7.500001	1500.000	0
	150	11.249999	1499.999	0
Max Z	1	0.075006	1500.120	80
	5	0.374994	1499.994	4
	10	0.749990	1499.984	11
	50	3.749993	1500.002	1
	100	7.499996	1500.001	0
	150	11.250003	1500.003	1

Table 3

Apparent Sound Speeds C for Successive Intervals Between Indicated Source-to-Reflector Separations ℓ Corresponding to Half Wavelengths n. The Values of ℓ are Read from Fig. 22c for the Imposed Characteristics of Zero Phase, Maximum R, and Maximum Z for the Standard Reference Parameters of Table 1 (Except b/a = 2) and Absolutely Rigid Boundary Conditions.

Imposed Characteristic	n	ℓ (cm)	C (m/s)	Error (ppm)
Zero phase	1	0.075071	1501.420	946
	5	0.375179	1500.540	360
	10	0.750290	1500.444	296
	50	3.751593	1500.652	434
	100	7.503399	1500.722	481
	150	11.255169	1500.708	472
Max R	1	0.075052	1501.040	693
	5	0.375145	1500.465	310
	10	0.750259	1500.456	304
	50	3.751708	1500.725	483
	100	7.503469	1500.704	469
	150	11.255222	1500.701	467
Max Z	1	0.075036	1500.720	480
	5	0.375101	1500.325	216
	10	0.750228	1500.508	338
	50	3.751810	1500.791	527
	100	7.503570	1500.704	469
	150	11.255300	1500.692	461

Table 4

Apparent Sound Speeds C for Successive Intervals Between Indicated Source-to-Reflector Separations ℓ Corresponding to Half Wavelengths n. The Values of ℓ are Read from Fig. 22d for the Imposed Characteristics of Zero Phase, Maximum R, and Maximum Z for the Standard Reference Parameters of Table 1 (Except b/a = 5) and Absolutely Rigid Boundary Conditions.

Imposed Characteristic	n	ℓ (cm)	C (m/s)	Error (ppm)
Zero phase	1	0.075071	1501.420	946
	5	0.375179	1500.540	360
	10	0.750289	1500.440	293
	50	3.750987	1500.349	232
	100	7.501770	1500.313	208
	150	11.252723	1500.381	254
Max R	1	0.075058	1501.160	773
	5	0.375148	1500.450	300
	10	0.750225	1500.308	205
	50	3.750778	1500.277	184
	100	7.501784	1500.402	268
	150	11.252769	1500.394	262
Max Z	1	0.075043	1500.860	573
	5	0.375096	1500.265	176
	10	0.750172	1500.304	202
	50	3.750600	1500.214	143
	100	7.500400	1499.920	53
	150	11.250661	1500.104	69

Table 5

Apparent Sound Speeds C for Successive Intervals Between Indicated Source-to-Reflector Separations ℓ Corresponding to Half Wavelengths n. The Values of ℓ are Read from Fig. 22e for the Imposed Characteristics of Zero Phase, Maximum R, and Maximum Z for the Standard Reference Parameters of Table 1 (Except b/a = 10) and Absolutely Rigid Boundary Conditions.

Imposed Characteristic	n	ℓ (cm)	C (m/s)	Error (ppm)
Zero phase	1	0.075071	1501.420	946
	5	0.375180	1500.545	363
	10	0.750289	1500.436	290
	50	3.751001	1500.356	237
	100	7.501687	1500.274	183
	150	11.252416	1500.292	194
Max R	1	0.075053	1501.060	706
	5	0.375144	1500.455	303
	10	0.750242	1500.392	261
	50	3.750761	1500.260	173
	100	7.501048	1500.115	76
	150	11.251400	1500.141	94
Max Z	1	0.075033	1500.660	440
	5	0.375124	1500.455	303
	10	0.750216	1500.368	245
	50	3.750527	1500.155	103
	100	7.500522	1499.998	1
	150	11.250544	1500.009	6

Table 6

Apparent Sound Speeds C for Successive Intervals Between Indicated Source-to-Reflector Separations ℓ Corresponding to Half Wavelengths n. The Values of ℓ are Read from Fig. 23a for the Imposed Characteristics of Zero Phase, Maximum R, and Maximum Z for the Standard Reference Parameters of Table 1 (Except b/a = 1) and Infinitely Flexible Boundary Conditions.

Imposed Characteristic	n	ℓ (cm)	C (m/s)	Error (ppm)
Zero phase	1	0.075147	1502.940	1958
	5	0.375379	1501.160	773
	10	0.750614	1500.940	626
	50	3.752768	1501.077	717
	100	7.505500	1501.093	728
	150	11.258252	1501.101	733
Max R	1	0.075116	1502.320	1545
	5	0.375306	1500.950	633
	10	0.750555	1500.996	663
	50	3.752754	1501.100	732
	100	7.505500	1501.098	731
	150	11.258248	1501.099	732
Max Z	1	0.075086	1501.720	1043
	5	0.375260	1500.870	579
	10	0.750518	1501.032	687
	50	3.752738	1501.110	739
	100	7.505500	1501.105	736
	150	11.258244	1501.098	731

Table 7

Apparent Sound Speeds C for Successive Intervals Between Indicated Source-to-Reflector Separations ℓ Corresponding to Half Wavelengths n. The Values of ℓ are Read from Fig. 23b for the Imposed Characteristics of Zero Phase, Maximum R, and Maximum Z for the Standard Reference Parameters of Table 1 (Except $b/a = 2$) and Infinitely Flexible Boundary Conditions.

Imposed Characteristic	n	ℓ (cm)	C (m/s)	Error (ppm)
Zero phase	1	0.075071	1501.420	946
	5	0.375180	1500.545	363
	10	0.750287	1500.428	285
	50	3.750768	1500.240	160
	100	7.501425	1500.263	175
	150	11.252088	1500.265	177
Max R	1	0.075056	1501.120	746
	5	0.375146	1500.450	300
	10	0.750233	1500.348	232
	50	3.750694	1500.230	153
	100	7.501372	1500.271	180
	150	11.252067	1500.278	185
Max Z	1	0.075050	1501.000	666
	5	0.375106	1500.280	186
	10	0.750193	1500.348	232
	50	3.750628	1500.218	145
	100	7.501318	1500.276	184
	150	11.252029	1500.284	189

Table 8

Apparent Sound Speeds C for Successive Intervals Between Indicated Source-to-Reflector Separations ℓ Corresponding to Half Wavelengths n. The Values of ℓ are Read from Fig. 23c for the Imposed Characteristics of Zero Phase, Maximum R, and Maximum Z for the Standard Reference Parameters of Table 1 (Except b/a = 5) and Infinitely Flexible Boundary Conditions.

Imposed Characteristic	n	ℓ (cm)	C (m/s)	Error (ppm)
Zero phase	1	0.075071	1501.420	946
	5	0.375179	1500.540	360
	10	0.750289	1500.440	293
	50	3.751014	1500.362	241
	100	7.501464	1500.180	120
	150	11.251886	1500.169	112
Max R	1	0.075054	1501.080	719
	5	0.375140	1500.430	286
	10	0.750246	1500.424	282
	50	3.750700	1500.227	151
	100	7.501107	1500.163	108
	150	11.251713	1500.242	161
Max Z	1	0.075046	1500.920	613
	5	0.375100	1500.270	180
	10	0.750189	1500.356	237
	50	3.750454	1500.133	88
	100	7.500964	1500.204	136
	150	11.251636	1500.269	179

Table 9

Apparent Sound Speeds C for Successive Intervals Between Indicated Source-to-Reflector Separations ℓ Corresponding to Half Wavelengths n. The Values of ℓ are Read from Fig. 23d for the Imposed Characteristics of Zero Phase, Maximum R, and Maximum Z for the Standard Reference Parameters of Table 1 (Except b/a = 10) and Infinitely Flexible Boundary Conditions.

Imposed Characteristic	n	ℓ (cm)	C (m/s)	Error (ppm)
Zero phase	1	0.075071	1501.420	946
	5	0.375186	1500.575	383
	10	0.750290	1500.416	277
	50	3.751000	1500.355	236
	100	7.501716	1500.286	191
	150	11.252296	1500.232	155
Max R	1	0.075044	1500.880	586
	5	0.375148	1500.520	346
	10	0.750250	1500.408	272
	50	3.750743	1500.246	164
	100	7.501086	1500.137	91
	150	11.251152	1500.026	18
Max Z	1	0.075013	1500.260	173
	5	0.375096	1500.415	276
	10	0.750200	1500.416	277
	50	3.750492	1500.146	97
	100	7.500547	1500.022	15
	150	11.250600	1500.021	14

Table 10

Apparent Sound Speeds C for Successive Intervals Between Indicated Source-to-Reflector Separations ℓ Corresponding to Half Wavelengths n. The Values of ℓ are Read from Fig. 24a for the Imposed Characteristics of Zero Phase, Maximum R, and Maximum Z for the Standard Reference Parameters of Table 1 (Except b/a = 1) and Liquid Boundary Conditions (Assuming Orthogonal Functions).

Imposed Characteristic	n	ℓ (cm)	C (m/s)	Error (ppm)
Zero phase	1	0.075092	1501.840	1225
	5	0.375297	1501.025	683
	10	0.750494	1500.788	525
	50	3.752208	1500.857	571
	100	7.504480	1500.909	605
	150	11.256601	1500.848	565
Max R	1	0.075095	1501.900	1265
	5	0.375248	1500.765	509
	10	0.750457	1500.836	557
	50	3.752193	1500.868	578
	100	7.504477	1500.914	608
	150	11.256588	1500.844	562
Max Z	1	0.075100	1502.000	1333
	5	0.375225	1500.625	416
	10	0.750393	1500.672	448
	50	3.752182	1500.895	596
	100	7.504469	1500.915	609
	150	11.256583	1500.846	563

Table 11

Apparent Sound Speeds C for Successive Intervals Between Indicated Source-to-Reflector Separations ℓ Corresponding to Half Wavelengths n. The Values of ℓ are Read from Fig. 24b for the Imposed Characteristics of Zero Phase, Maximum R, and Maximum Z for the Standard Reference Parameters of Table 1 (Except b/a = 1) and Liquid Boundary Conditions (Using Actual Functions).

Imposed Characteristic	n	ℓ (cm)	C (m/s)	Error (ppm)
Zero phase	1	0.075094	1501.880	1252
	5	0.375298	1501.020	679
	10	0.750496	1500.792	527
	50	3.752210	1500.857	571
	100	7.504301	1500.836	557
	150	11.256602	1500.920	613
Max R	1	0.075079	1501.580	1052
	5	0.375248	1500.850	563
	10	0.750451	1500.810	541
	50	3.752205	1500.877	584
	100	7.504300	1500.838	558
	150	11.256601	1500.920	613
Max Z	1	0.075062	1501.240	826
	5	0.375220	1500.790	526
	10	0.750415	1500.780	519
	50	3.752202	1500.894	595
	100	7.504300	1500.839	559
	150	11.256600	1500.920	613

Table 12

Apparent Sound Speeds C for Successive Intervals Between Indicated Source-to-Reflector Separations ℓ Corresponding to Half Wavelengths n. The Values of ℓ are Read from Fig. 24c for the Imposed Characteristics of Zero Phase, Maximum R, and Maximum Z for the Standard Reference Parameters of Table 1 (Except b/a = 2) and Liquid Boundary Conditions (Assuming Orthogonal Functions).

Imposed Characteristic	n	ℓ (cm)	C (m/s)	Error (ppm)
Zero phase	1	0.075070	1501.400	932
	5	0.375178	1500.540	360
	10	0.750290	1500.448	298
	50	3.750729	1500.220	147
	100	7.501276	1500.219	146
	150	11.251877	1500.240	160
Max R	1	0.075060	1501.200	799
	5	0.375147	1500.435	290
	10	0.750242	1500.380	253
	50	3.750631	1500.195	130
	100	7.501228	1500.239	159
	150	11.251841	1500.245	163
Max Z	1	0.075054	1501.080	719
	5	0.375128	1500.370	246
	10	0.750191	1500.252	168
	50	3.750539	1500.174	116
	100	7.501165	1500.250	167
	150	11.251803	1500.255	170

Table 13

Apparent Sound Speeds C for Successive Intervals Between Indicated-Source-to-Reflector Separations ℓ Corresponding to Half Wavelengths n. The Values of ℓ are Read from Fig. 24d for the Imposed Characteristics of Zero Phase, Maximum R, and Maximum Z for the Standard Reference Parameters of Table 1 (Except b/a = 2) and Liquid Boundary Conditions (Using Actual Functions).

Imposed Characteristic	n	ℓ (cm)	C (m/s)	Error (ppm)
Zero phase	1	0.075072	1501.440	959
	5	0.375180	1500.540	360
	10	0.750290	1500.440	293
	50	3.750727	1500.219	146
	100	7.501276	1500.220	146
	150	11.251877	1500.240	160
Max R	1	0.075050	1501.000	666
	5	0.375148	1500.490	326
	10	0.750252	1500.416	277
	50	3.750626	1500.187	125
	100	7.501238	1500.245	163
	150	11.251847	1500.244	162
Max Z	1	0.075036	1500.720	480
	5	0.375123	1500.435	290
	10	0.750205	1500.328	218
	50	3.750551	1500.173	115
	100	7.501196	1500.258	172
	150	11.251833	1500.255	170

Table 14

Apparent Sound Speeds C for Successive Intervals Between Indicated Source-to-Reflector Separations ℓ Corresponding to Half Wavelengths n. The Values of ℓ are Read from Fig. 24e for the Imposed Characteristics of Zero Phase, Maximum R, and Maximum Z for the Standard Reference Parameters of Table 1 (Except b/a = 5) and Liquid Boundary Conditions.

Imposed Characteristic	n	ℓ (cm)	C (m/s)	Error (ppm)
Zero phase	1	0.075071	1501.420	946
	5	0.375179	1500.540	360
	10	0.750289	1500.440	293
	50	3.751022	1500.367	244
	100	7.501556	1500.214	142
	150	11.251847	1500.116	77
Max R	1	0.075050	1501.000	666
	5	0.375138	1500.440	293
	10	0.750246	1500.432	288
	50	3.750722	1500.238	159
	100	7.501073	1500.140	94
	150	11.251614	1500.216	144
Max Z	1	0.075043	1500.860	573
	5	0.375100	1500.285	190
	10	0.750184	1500.336	224
	50	3.750463	1500.140	94
	100	7.500889	1500.170	113
	150	11.251537	1500.259	173

Table 15

Apparent Sound Speeds C for Successive Intervals Between Indicated Source-to-Reflector Separations ℓ Corresponding to Half Wavelengths n. The Values of ℓ are Read from Fig. 24f for the Imposed Characteristics of Zero Phase, Maximum R, and Maximum Z for the Standard Reference Parameters of Table 1 (Except b/a = 10) and Liquid Boundary Conditions.

Imposed Characteristic	n	ℓ (cm)	C (m/s)	Error (ppm)
Zero phase	1	0.075071	1501.420	946
	5	0.375180	1500.545	363
	10	0.750289	1500.436	290
	50	3.751000	1500.356	237
	100	7.501705	1500.282	188
	150	11.252350	1500.258	172
Max R	1	0.075061	1501.220	147
	5	0.375145	1500.420	280
	10	0.750242	1500.388	258
	50	3.750758	1500.258	172
	100	7.501148	1500.156	104
	150	11.251200	1500.021	14
Max Z	1	0.075042	1500.840	559
	5	0.375104	1500.310	206
	10	0.750200	1500.384	256
	50	3.750481	1500.140	93
	100	7.500552	1500.028	19
	150	11.250575	1500.009	6

Table 16

Apparent Sound Speeds C for Successive Intervals Between Indicated Source-to-Reflector Separations ℓ Corresponding to Half Wavelengths n. The Values of ℓ are Read from Fig. 25a for the Imposed Characteristics of Zero Phase, Maximum R, and Maximum Z for the Standard Reference Parameters of Table 1 (Except b/a = 1) and Elastic Solid Boundary Conditions (Assuming Orthogonal Functions).

Imposed Characteristic	n	ℓ (cm)	C (m/s)	Error (ppm)
Zero phase	1	0.075140	1502.800	1865
	5	0.375573	1502.165	1442
	10	0.751099	1502.104	1401
	50	3.755415	1502.158	1437
	100	7.510824	1502.164	1441
	150	11.266233	1502.164	1441
Max R	1	0.075132	1502.640	1758
	5	0.375545	1502.065	1375
	10	0.751083	1502.152	1433
	50	3.755422	1502.170	1445
	100	7.510830	1502.163	1440
	150	11.266240	1502.164	1441
Max Z	1	0.075126	1502.520	1665
	5	0.375511	1501.925	1282
	10	0.751063	1502.208	1471
	50	3.755430	1502.184	1454
	100	7.510838	1502.163	1440
	150	11.266248	1502.164	1441

Table 17

Apparent Sound Speeds C for Successive Intervals Between Indicated Source-to-Reflector Separations ℓ Corresponding to Half Wavelengths n. The Values of ℓ are Read from Fig. 25b for the Imposed Characteristics of Zero Phase, Maximum R, and Maximum Z for the Standard Reference Parameters of Table 1 (Except b/a = 1) and Elastic Solid Boundary Conditions (Using Actual Functions).

Imposed Characteristic	n	ℓ (cm)	C (m/s)	Error (ppm)
Zero phase	1	0.075153	1503.060	2038
	5	0.375589	1502.180	1452
	10	0.751084	1501.980	1319
	50	3.755412	1502.164	1441
	100	7.510798	1502.154	1435
	150	11.266235	1502.175	1448
Max R	1	0.075138	1502.760	1838
	5	0.375549	1502.050	1369
	10	0.751082	1502.132	1420
	50	3.755415	1502.167	1443
	100	7.510828	1502.165	1442
	150	11.266231	1502.161	1439
Max Z	1	0.075113	1502.260	1505
	5	0.375500	1501.935	1289
	10	0.751078	1502.312	1540
	50	3.755423	1502.172	1447
	100	7.510864	1502.176	1449
	150	11.266222	1502.143	1427

Table 18

Apparent Sound Speeds C for Successive Intervals Between Indicated Source-to-Reflector Separations ℓ Corresponding to Half Wavelengths n. The Values of ℓ are Read from Fig. 25c for the Imposed Characteristics of Zero Phase, Maximum R, and Maximum Z for the Standard Reference Parameters of Table 1 (Except b/a = 1.1) and Elastic Solid Boundary Conditions (Assuming Orthogonal Functions).

Imposed Characteristic	n	ℓ (cm)	C (m/s)	Error (ppm)
Zero phase	1	0.075265	1505.300	3530
	5	0.375595	1501.650	1099
	10	0.750964	1501.476	983
	50	3.754353	1501.695	1128
	100	7.508696	1501.737	1157
	150	11.263092	1501.758	1171
Max R	1	0.075185	1503.700	2464
	5	0.375465	1501.400	932
	10	0.750876	1501.644	1095
	50	3.754348	1501.736	1156
	100	7.508715	1501.747	1163
	150	11.263100	1501.754	1168
Max Z	1	0.075142	1502.840	1891
	5	0.375379	1501.185	789
	10	0.750820	1501.764	1175
	50	3.754367	1501.774	1181
	100	7.508754	1501.755	1169
	150	11.263100	1501.738	1158

Table 19

Apparent Sound Speeds C for Successive Intervals Between Indicated Source-to-Reflector Separations ℓ Corresponding to Half Wavelengths n. The Values of ℓ are Read from Fig. 25d for the Imposed Characteristics of Zero Phase, Maximum R, and Maximum Z for the Standard Reference Parameters of Table 1 (Except b/a = 1.1) and Elastic Solid Boundary Conditions (Using Actual Functions).

Imposed Characteristic	n	ℓ (cm)	C (m/s)	Error (ppm)
Zero phase	1	0.075266	1505.320	3543
	5	0.375602	1501.680	1119
	10	0.750962	1501.440	959
	50	3.754351	1501.695	1129
	100	7.508693	1501.737	1157
	150	11.263090	1501.759	1171
Max R	1	0.075192	1503.840	2557
	5	0.375457	1501.325	882
	10	0.750874	1501.668	1111
	50	3.754359	1501.743	1161
	100	7.508711	1501.741	1149
	150	11.263100	1501.756	1169
Max Z	1	0.075136	1502.720	1812
	5	0.375409	1501.365	909
	10	0.750825	1501.664	1108
	50	3.754365	1501.770	1179
	100	7.508773	1501.763	1174
	150	11.263129	1501.742	1160

Table 20

Apparent Sound Speeds C for Successive Intervals Between Indicated Source-to-Reflector Separations ℓ Corresponding to Half Wavelengths n. The Values of ℓ are Read from Fig. 25e for the Imposed Characteristics of Zero Phase, Maximum R, and Maximum Z for the Standard Reference Parameters of Table 1 (Except b/a = 2) and Elastic Solid Boundary Conditions (Assuming Orthogonal Functions).

Imposed Characteristic	n	ℓ (cm)	C (m/s)	Error (ppm)
Zero phase	1	0.075073	1501.460	972
	5	0.375185	1500.560	373
	10	0.750286	1500.404	269
	50	3.751114	1500.414	276
	100	7.502202	1500.435	290
	150	11.253295	1500.437	291
Max R	1	0.075045	1500.900	599
	5	0.375150	1500.525	350
	10	0.750242	1500.368	245
	50	3.751096	1500.427	284
	100	7.502200	1500.442	294
	150	11.253300	1500.440	293
Max Z	1	0.075029	1500.580	386
	5	0.375135	1500.530	353
	10	0.750210	1500.300	200
	50	3.751092	1500.441	294
	100	7.502200	1500.443	295
	150	11.253300	1500.440	293

Table 21

Apparent Sound Speeds C for Successive Intervals Between Indicated Source-to-Reflector Separations ℓ Corresponding to Half Wavelengths n. The Values of ℓ are Read from Fig. 25f for the Imposed Characteristics of Zero Phase, Maximum R, and Maximum Z for the Standard Reference Parameters of Table 1 (Except b/a = 2) and Elastic Solid Boundary Conditions (Using Actual Functions).

Imposed Characteristic	n	ℓ (cm)	C (m/s)	Error (ppm)
Zero phase	1	0.075075	1501.500	999
	5	0.375186	1500.555	370
	10	0.750287	1500.404	269
	50	3.751116	1500.415	276
	100	7.502203	1500.435	290
	150	11.253296	1500.437	291
Max R	1	0.075050	1501.000	666
	5	0.375146	1500.480	320
	10	0.750243	1500.388	258
	50	3.751100	1500.429	285
	100	7.502194	1500.438	291
	150	11.253300	1500.442	295
Max Z	1	0.075030	1500.600	400
	5	0.375118	1500.440	293
	10	0.750217	1500.396	264
	50	3.751092	1500.438	291
	100	7.502192	1500.440	293
	150	11.253300	1500.443	295

Table 22

Apparent Sound Speeds C for Successive Intervals Between Indicated Source-to-Reflector Separations ℓ Corresponding to Half Wavelengths n. The Values of ℓ are Read from Fig. 25g for the Imposed Characteristics of Zero Phase, Maximum R, and Maximum Z for the Standard Reference Parameters of Table 1 (Except b/a = 5) and Elastic Solid Boundary Conditions.

Imposed Characteristic	n	ℓ (cm)	C (m/s)	Error (ppm)
Zero phase	1	0.075072	1501.440	959
	5	0.375180	1500.540	360
	10	0.750291	1500.444	296
	50	3.750990	1500.350	233
	100	7.501496	1500.202	135
	150	11.252153	1500.263	175
Max R	1	0.075056	1501.120	746
	5	0.375147	1500.455	303
	10	0.750248	1500.404	269
	50	3.750732	1500.242	161
	100	7.501354	1500.249	166
	150	11.252082	1500.291	194
Max Z	1	0.075044	1500.880	586
	5	0.375119	1500.375	250
	10	0.750225	1500.424	282
	50	3.750543	1500.159	106
	100	7.501300	1500.303	202
	150	11.252034	1500.294	196

Table 23

Apparent Sound Speeds C for Successive Intervals Between Indicated Source-to-Reflector Separations ℓ Corresponding to Half Wavelengths n. The Values of ℓ are Read from Fig. 25h for the Imposed Characteristics of Zero Phase, Maximum R, and Maximum Z for the Standard Reference Parameters of Table 1 (Except b/a = 10) and Elastic Solid Boundary Conditions.

Imposed Characteristic	n	ℓ (cm)	C (m/s)	Error (ppm)
Zero phase	1	0.075070	1501.400	932
	5	0.375179	1500.545	363
	10	0.750288	1500.436	290
	50	3.750996	1500.354	236
	100	7.501680	1500.274	182
	150	11.252276	1500.238	159
Max R	1	0.075046	1500.920	613
	5	0.375141	1500.475	316
	10	0.750242	1500.404	269
	50	3.750765	1500.262	174
	100	7.501175	1500.164	109
	150	11.251271	1500.384	256
Max Z	1	0.075020	1500.400	266
	5	0.375114	1500.470	313
	10	0.750213	1500.396	264
	50	3.750500	1500.144	96
	100	7.500600	1500.040	27
	150	11.250535	1499.974	17

Table 24

Apparent Sound Speeds C for Successive Intervals Between Indicated Source-to-Reflector Separations ℓ Corresponding to Half Wavelengths n. The Values of ℓ are Read from Fig. 25i for the Imposed Characteristics of Zero Phase, Maximum R, and Maximum Z for the Standard Reference Parameters of Table 1 (Except b/a = 20) and Elastic Solid Boundary Conditions.

Imposed Characteristic	n	ℓ (cm)	C (m/s)	Error (ppm)
Zero phase	1	0.075071	1501.420	946
	5	0.375179	1500.540	360
	10	0.750289	1500.440	293
	50	3.751002	1500.357	237
	100	7.501710	1500.283	189
	150	11.252300	1500.236	157
Max R	1	0.075056	1501.120	750
	5	0.375148	1500.460	306
	10	0.750242	1500.376	250
	50	3.750757	1500.258	171
	100	7.501124	1500.147	98
	150	11.251372	1500.099	66
Max Z	1	0.075029	1500.580	386
	5	0.375106	1500.385	256
	10	0.750212	1500.424	282
	50	3.750500	1500.144	96
	100	7.500645	1500.058	39
	150	11.250500	1499.942	39

Table 25

Apparent Sound Speeds C for Successive Intervals Between Indicated Source-to-Reflector Separations ℓ Corresponding to Half Wavelengths n. The Values of ℓ are Read from Fig. 25j for the Imposed Characteristics of Zero Phase, Maximum R, and Maximum Z for the Standard Reference Parameters of Table 1 (Except b/a = 50) and Elastic Solid Boundary Conditions.

Imposed Characteristic	n	ℓ (cm)	C (m/s)	Error (ppm)
Zero phase	1	0.075073	1501.460	972
	5	0.375181	1500.540	360
	10	0.750290	1500.436	290
	50	3.751000	1500.355	336
	100	7.501702	1500.281	187
	150	11.252378	1500.270	180
Max R	1	0.075057	1501.140	759
	5	0.375141	1500.420	280
	10	0.750251	1500.440	293
	50	3.750745	1500.247	165
	100	7.501068	1500.129	86
	150	11.251354	1500.114	76
Max Z	1	0.075030	1500.600	400
	5	0.375112	1500.410	273
	10	0.750218	1500.424	282
	50	3.750500	1500.141	94
	100	7.500560	1500.024	16
	150	11.250559	1499.999	0

Table 26

Apparent Sound Speeds C for Successive Intervals Between Indicated Source-to-Reflector Separations ℓ Corresponding to Half Wavelengths n. The Values of ℓ are Read from Fig. 26a for the Imposed Characteristics of Zero Phase, Maximum R, and Maximum Z for the Standard Reference Parameters of Table 1 (Except $k_1^{III}a = 60\pi$ and $b/a = 1.1$) with Absolutely Rigid Boundary Conditions.

Imposed Characteristic	n	ℓ (cm)	C (m/s)	Error (ppm)
Zero phase	3	0.075014	1500.280	186
	15	0.375017	1500.015	10
	30	0.750015	1499.992	5
	150	3.750007	1499.996	3
	300	7.500002	1499.998	1
	450	11.250003	1500.000	0
Max R	3	0.075009	1500.180	120
	15	0.375006	1499.985	10
	30	0.750005	1499.996	3
	150	3.750001	1499.998	1
	300	7.500000	1500.000	0
	450	11.250000	1500.000	0
Max Z	3	0.075005	1500.100	67
	15	0.375001	1499.980	13
	30	0.749999	1499.992	5
	150	3.749999	1500.000	0
	300	7.499999	1500.000	0
	450	11.249999	1500.000	0

Table 27

Apparent Sound Speeds C for Successive Intervals Between Indicated Source-to-Reflector Separations ℓ Corresponding to Half Wavelengths n. The Values of ℓ are Read from Fig. 26b for the Imposed Characteristics of Zero Phase, Maximum R, and Maximum Z for the Standard Reference Parameters of Table 1 (Except $k_1^{III}a = 60\pi$ and $b/a = 2$) with Absolutely Rigid Boundary Conditions.

Imposed Characteristic	n	ℓ (cm)	C (m/s)	Error (ppm)
Zero phase	3	0.075013	1500.260	173
	15	0.375032	1500.095	63
	30	0.750047	1500.060	40
	150	3.750150	1500.052	34
	300	7.500330	1500.072	48
	450	11.250524	1500.078	52
Max R	3	0.075012	1500.240	160
	15	0.375025	1500.065	43
	30	0.750034	1500.040	27
	150	3.750149	1500.058	38
	300	7.500361	1500.085	56
	450	11.250569	1500.083	55
Max Z	3	0.075011	1500.220	147
	15	0.375019	1500.040	27
	30	0.750033	1500.056	37
	150	3.750148	1500.058	38
	300	7.500395	1500.099	66
	450	11.250600	1500.082	55

Table 28

Apparent Sound Speeds C for Successive Intervals Between Indicated Source-to-Reflector Separations ℓ Corresponding to Half Wavelengths n. The Values of ℓ are Read from Fig. 26c for the Imposed Characteristics of Zero Phase, Maximum R, and Maximum Z for the Standard Reference Parameters of Table 1 (Except $k_1^{III} a = 60\pi$ and $b/a = 5$) with Absolutely Rigid Boundary Conditions.

Imposed Characteristic	n	ℓ (cm)	C (m/s)	Error (ppm)
Zero phase	3	0.075013	1500.260	173
	15	0.375032	1500.095	63
	30	0.750047	1500.060	40
	150	3.750140	1500.047	31
	300	7.500240	1500.040	27
	450	11.250327	1500.035	23
Max R	3	0.075010	1500.200	133
	15	0.375025	1500.075	50
	30	0.750035	1500.040	27
	150	3.750121	1500.043	29
	300	7.500189	1500.027	18
	450	11.250278	1500.036	24
Max Z	3	0.075009	1500.180	120
	15	0.375019	1500.050	33
	30	0.750029	1500.040	27
	150	3.750098	1500.035	23
	300	7.500148	1500.020	13
	450	11.250195	1500.052	34

Table 29

Apparent Sound Speeds C for Successive Intervals Between Indicated Source-to-Reflector Separations ℓ Corresponding to Half Wavelengths n. The Values of ℓ are Read from Fig. 26d for the Imposed Characteristics of Zero Phase, Maximum R, and Maximum Z for the Standard Reference Parameters of Table 1 (Except $k_1^{III}a = 60\pi$ and $b/a = 10$) with Absolutely Rigid Boundary Conditions.

Imposed Characteristic	n	ℓ (cm)	C (m/s)	Error (ppm)
Zero phase	3	0.075013	1500.260	173
	15	0.375032	1500.095	63
	30	0.750047	1500.060	40
	150	3.750143	1500.048	32
	300	7.500244	1500.040	27
	450	11.250332	1500.035	23
Max R	3	0.075010	1500.200	133
	15	0.375023	1500.065	43
	30	0.750039	1500.064	43
	150	3.750119	1500.040	27
	300	7.500197	1500.031	21
	450	11.250249	1500.021	14
Max Z	3	0.075008	1500.160	107
	15	0.375017	1500.045	30
	30	0.750063	1500.184	123
	150	3.750100	1500.019	12
	300	7.500156	1500.022	15
	450	11.250273	1500.047	31

Table 30

Apparent Sound Speeds C for Successive Intervals Between Indicated Source-to-Reflector Separations ℓ Corresponding to Half Wavelengths n. The Values of ℓ are Read from Fig. 27a for the Imposed Characteristics of Zero Phase, Maximum R, and Maximum Z for the Standard Reference Parameters of Table 1 (Except $k_1^{III}a = 60\pi$ and $b/a = 1$) with Infinitely Flexible Boundary Conditions.

Imposed Characteristic	n	ℓ (cm)	C (m/s)	Error (ppm)
Zero phase	3	0.075027	1500.540	360
	15	0.375062	1500.175	117
	30	0.750100	1500.152	101
	150	3.750345	1500.122	82
	300	7.500615	1500.108	72
	450	11.250917	1500.121	80
Max R	3	0.075021	1500.420	280
	15	0.375048	1500.135	90
	30	0.750078	1500.120	80
	150	3.750332	1500.127	85
	300	7.500607	1500.110	73
	450	11.250911	1500.123	82
Max Z	3	0.075013	1500.260	173
	15	0.375039	1500.130	87
	30	0.750060	1500.084	56
	150	3.750330	1500.135	90
	300	7.500602	1500.109	73
	450	11.250906	1500.122	82

Table 31

Apparent Sound Speeds C for Successive Intervals Between Indicated Source-to-Reflector Separations ℓ Corresponding to Half Wavelengths n. The Values of ℓ are Read from Fig. 27b for the Imposed Characteristics of Zero Phase, Maximum R, and Maximum Z for the Standard Reference Parameters of Table 1 (Except $k_1^{III}a = 60\pi$ and $b/a = 2$) with Infinitely Flexible Boundary Conditions.

Imposed Characteristic	n	ℓ (cm)	C (m/s)	Error (ppm)
Zero phase	3	0.075013	1500.260	173
	15	0.375031	1500.090	60
	30	0.750046	1500.060	40
	150	3.750130	1500.042	28
	300	7.500189	1500.024	16
	450	11.250254	1500.026	17
Max R	3	0.075006	1500.120	80
	15	0.375025	1500.095	63
	30	0.750038	1500.052	34
	150	3.750132	1500.047	31
	300	7.500157	1500.010	7
	450	11.250232	1500.030	20
Max Z	3	0.075002	1500.040	27
	15	0.375020	1500.090	60
	30	0.750034	1500.056	37
	150	3.750111	1500.039	26
	300	7.500130	1500.008	5
	450	11.250212	1500.033	22

Table 32

Apparent Sound Speeds C for Successive Intervals Between Indicated Source-to-Reflector Separations ℓ Corresponding to Half Wavelengths n. The Values of ℓ are Read from Fig. 27c for the Imposed Characteristics of Zero Phase, Maximum R, and Maximum Z for the Standard Reference Parameters of Table 1 (Except $k_1^{III} a = 60\pi$ and $b/a = 5$) with Infinitely Flexible Boundary Conditions.

Imposed Characteristic	n	ℓ (cm)	C (m/s)	Error (ppm)
Zero phase	3	0.075013	1500.260	173
	15	0.375031	1500.090	60
	30	0.750047	1500.064	43
	150	3.750139	1500.046	30
	300	7.500242	1500.041	27
	450	11.250273	1500.012	8
Max R	3	0.075015	1500.300	200
	15	0.375029	1500.070	47
	30	0.750042	1500.052	34
	150	3.750122	1500.040	27
	300	7.500202	1500.032	21
	450	11.250230	1500.011	7
Max Z	3	0.075009	1500.180	120
	15	0.375028	1500.095	63
	30	0.750040	1500.048	32
	150	3.750100	1500.030	20
	300	7.500134	1500.014	9
	450	11.250134	1500.000	0

Table 33

Apparent Sound Speeds C for Successive Intervals Between Indicated Source-to-Reflector Separations ℓ Corresponding to Half Wavelengths n. The Values of ℓ are Read from Fig. 27d for the Imposed Characteristics of Zero Phase, Maximum R, and Maximum Z for the Standard Reference Parameters of Table 1 (Except $k_1^{III} a = 60\pi$ and b/a = 10) with Infinitely Flexible Boundary Conditions.

Imposed Characteristic	n	ℓ (cm)	C (m/s)	Error (ppm)
Zero phase	3	0.075014	1500.280	186
	15	0.375032	1500.090	60
	30	0.750047	1500.060	40
	150	3.750143	1500.048	32
	300	7.500244	1500.040	27
	450	11.250333	1500.036	24
Max R	3	0.075010	1500.200	133
	15	0.375023	1500.065	43
	30	0.750035	1500.048	32
	150	3.750121	1500.043	29
	300	7.500195	1500.030	20
	450	11.250246	1500.020	13
Max Z	3	0.075008	1500.160	107
	15	0.375013	1500.025	17
	30	0.750028	1500.060	40
	150	3.750104	1500.038	26
	300	7.500155	1500.020	13
	450	11.250183	1500.011	7

Table 34

Apparent Sound Speeds C for Successive Intervals Between Indicated Source-to-Reflector Separations ℓ Corresponding to Half Wavelengths n. The Values of ℓ are Read from Fig. 28a for the Imposed Characteristics of Zero Phase, Maximum R, and Maximum Z for the Standard Reference Parameters of Table 1 (Except $k_1^{III}a = 60\pi$ and $b/a = 1$) with Liquid Boundary Conditions (Assuming Orthogonal Functions)

Imposed Characteristic	n	ℓ (cm)	C (m/s)	Error (ppm)
Zero phase	3	0.075022	1500.440	293
	15	0.375060	1500.190	127
	30	0.750093	1500.132	88
	150	3.750300	1500.104	69
	300	7.500571	1500.108	72
	450	11.250853	1500.113	75
Max R	3	0.075020	1500.400	266
	15	0.375047	1500.135	90
	30	0.750073	1500.104	69
	150	3.750288	1500.108	72
	300	7.500585	1500.119	79
	450	11.250850	1500.106	71
Max Z	3	0.075019	1500.380	253
	15	0.375039	1500.100	67
	30	0.750057	1500.072	48
	150	3.750276	1500.110	73
	300	7.500584	1500.123	82
	450	11.250849	1500.106	71

Table 35

Apparent Sound Speeds C for Successive Intervals Between Indicated Source-to-Reflector Separations ℓ Corresponding to Half Wavelengths n. The Values of ℓ are Read from Fig. 28b for the Imposed Characteristics of Zero Phase, Maximum R, and Maximum Z for the Standard Reference Parameters of Table 1 (Except $k_1^{III}a = 60\pi$ and $b/a = 1$) with Liquid Boundary Conditions (Using Actual Functions).

Imposed Characteristic	n	ℓ (cm)	C (m/s)	Error (ppm)
Zero phase	3	0.075021	1500.420	280
	15	0.375061	1500.200	133
	30	0.750093	1500.128	85
	150	3.750297	1500.102	68
	300	7.500572	1500.110	73
	450	11.250852	1500.112	75
Max R	3	0.075020	1500.400	266
	15	0.375048	1500.140	93
	30	0.750074	1500.104	69
	150	3.750285	1500.106	70
	300	7.500563	1500.111	74
	450	11.250847	1500.114	76
Max Z	3	0.075018	1500.360	240
	15	0.375035	1500.085	57
	30	0.750057	1500.088	59
	150	3.750271	1500.107	71
	300	7.500556	1500.114	76
	450	11.250844	1500.115	77

Table 36

Apparent Sound Speeds C for Successive Intervals Between Indicated Source-to-Reflector Separations ℓ Corresponding to Half Wavelengths n. The Values of ℓ are Read from Fig. 28c for the Imposed Characteristics of Zero Phase, Maximum R, and Maximum Z for the Standard Reference Parameters of Table 1 (Except $k_1^{III}a = 60\pi$ and $b/a = 2$) with Liquid Boundary Conditions.

Imposed Characteristic	n	ℓ (cm)	C (m/s)	Error (ppm)
Zero phase	3	0.075007	1500.140	93
	15	0.375018	1500.055	37
	30	0.750025	1500.028	17
	150	3.750064	1500.020	13
	300	7.500104	1500.016	11
	450	11.250132	1500.011	7
Max R	3	0.075004	1500.080	53
	15	0.375012	1500.040	27
	30	0.750017	1500.020	13
	150	3.750051	1500.017	11
	300	7.500084	1500.013	8
	450	11.250102	1500.007	5
Max Z	3	0.075002	1500.040	27
	15	0.375004	1500.010	7
	30	0.750008	1500.016	11
	150	3.750039	1500.016	11
	300	7.500066	1500.011	7
	450	11.250076	1500.004	3

Table 37

Apparent Sound Speeds C for Successive Intervals Between Indicated Source-to-Reflector Separations ℓ Corresponding to Half Wavelengths n. The Values of ℓ are Read from Fig. 28d for the Imposed Characteristics of Zero Phase, Maximum R, and Maximum Z for the Standard Reference Parameters of Table 1 (Except $k_1^{III}a = 60\pi$ and $b/a = 5$) with Liquid Boundary Conditions.

Imposed Characteristic	n	ℓ (cm)	C (m/s)	Error (ppm)
Zero phase	3	0.075013	1500.260	173
	15	0.375032	1500.095	63
	30	0.750047	1500.060	40
	150	3.750142	1500.048	32
	300	7.500244	1500.041	27
	450	11.250337	1500.037	25
Max R	3	0.075008	1500.160	107
	15	0.375024	1500.080	53
	30	0.750033	1500.036	24
	150	3.750123	1500.048	32
	300	7.500195	1500.029	19
	450	11.250239	1500.018	12
Max Z	3	0.075003	1500.060	40
	15	0.375016	1500.065	43
	30	0.750024	1500.032	21
	150	3.750113	1500.045	30
	300	7.500167	1500.022	14
	450	11.250167	1500.000	0

Table 38

Apparent Sound Speeds C for Successive Intervals Between Indicated Source-to-Reflector Separations ℓ Corresponding to Half Wavelengths n. The Values of ℓ are Read from Fig. 28e for the Imposed Characteristics of Zero Phase, Maximum R, and Maximum Z for the Standard Reference Parameters of Table 1 (Except $k_1^{III}a = 60\pi$ and $b/a = 10$) with Liquid Boundary Conditions.

Imposed Characteristic	n	ℓ (cm)	C (m/s)	Error (ppm)
Zero phase	3	0.075013	1500.260	173
	15	0.375032	1500.095	63
	30	0.750047	1500.060	40
	150	3.750142	1500.048	32
	300	7.500244	1500.041	27
	450	11.250332	1500.035	23
Max R	3	0.075009	1500.180	120
	15	0.375025	1500.080	53
	30	0.750035	1500.040	27
	150	3.750123	1500.044	29
	300	7.500198	1500.030	20
	450	11.250252	1500.022	14
Max Z	3	0.075002	1500.040	27
	15	0.375021	1500.095	63
	30	0.750030	1500.036	24
	150	3.750102	1500.036	24
	300	7.500150	1500.019	13
	450	11.250183	1500.013	9

Table 39

Apparent Sound Speeds C for Successive Intervals Between Indicated Source-to-Reflector Separations ℓ Corresponding to Half Wavelengths n. The Values of ℓ are Read from Fig. 29a for the Imposed Characteristics of Zero Phase, Maximum R, and Maximum Z for the Standard Reference Parameters of Table 1 (Except $k_1^{III}a = 60\pi$ and $b/a = 1$) with Elastic Solid Boundary Conditions (Assuming Orthogonal Functions).

Imposed Characteristic	n	ℓ (cm)	C (m/s)	Error (ppm)
Zero phase	3	0.075016	1500.320	213
	15	0.375062	1500.230	153
	30	0.750104	1500.168	112
	150	3.750436	1500.166	111
	300	7.500864	1500.171	114
	450	11.251326	1500.185	123
Max R	3	0.075017	1500.340	226
	15	0.375056	1500.195	130
	30	0.750091	1500.140	93
	150	3.750429	1500.169	113
	300	7.500863	1500.174	116
	450	11.251323	1500.184	123
Max Z	3	0.075024	1500.480	320
	15	0.375033	1500.045	30
	30	0.750083	1500.200	133
	150	3.750427	1500.172	115
	300	7.500861	1500.174	116
	450	11.251322	1500.184	123

Table 40

Apparent Sound Speeds C for Successive Intervals Between Indicated Source-to-Reflector Separations ℓ Corresponding to Half Wavelengths n. The Values of ℓ are Read from Fig. 29b for the Imposed Characteristics of Zero Phase, Maximum R, and Maximum Z for the Standard Reference Parameters of Table 1 (Except $k_1^{III} a = 60\pi$ and $b/a = 1$) with Elastic Solid Boundary Conditions (Using Actual Functions).

Imposed Characteristic	n	ℓ (cm)	C (m/s)	Error (ppm)
Zero phase	3	0.075017	1500.340	260
	15	0.375062	1500.225	150
	30	0.750105	1500.172	115
	150	3.750436	1500.166	110
	300	7.500865	1500.172	115
	450	11.251294	1500.172	115
Max R	3	0.075015	1500.300	200
	15	0.375049	1500.170	113
	30	0.750093	1500.176	117
	150	3.750430	1500.169	112
	300	7.500859	1500.172	115
	450	11.251292	1500.173	115
Max Z	3	0.075012	1500.240	160
	15	0.375038	1500.130	87
	30	0.750081	1500.172	115
	150	3.750417	1500.168	112
	300	7.500854	1500.175	116
	450	11.251291	1500.175	116

Table 41

Apparent Sound Speeds C for Successive Intervals Between Indicated Source-to-Reflector Separations ℓ Corresponding to Half Wavelengths n. The Values of ℓ are Read from Fig. 29c for the Imposed Characteristics of Zero Phase, Maximum R, and Maximum Z for the Standard Reference Parameters of Table 1 (Except $k_1^{III}a = 60\pi$ and $b/a = 1.1$) with Elastic Solid Boundary Conditions (Assuming Orthogonal Functions).

Imposed Characteristic	n	ℓ (cm)	C (m/s)	Error (ppm)
Zero phase	3	0.075026	1500.520	346
	15	0.375073	1500.235	157
	30	0.750109	1500.144	96
	150	3.750356	1500.124	82
	300	7.500694	1500.135	90
	450	11.251040	1500.138	92
Max R	3	0.075024	1500.480	320
	15	0.375056	1500.160	107
	30	0.750081	1500.100	67
	150	3.750346	1500.133	88
	300	7.500688	1500.137	91
	450	11.251033	1500.138	92
Max Z	3	0.075022	1500.440	293
	15	0.375047	1500.125	83
	30	0.750067	1500.080	53
	150	3.750338	1500.136	90
	300	7.500687	1500.140	93
	450	11.251033	1500.138	92

Table 42

Apparent Sound Speeds C for Successive Intervals Between Indicated Source-to-Reflector Separations ℓ Corresponding to Half Wavelengths n. The Values of ℓ are Read from Fig. 29d for the Imposed Characteristics of Zero Phase, Maximum R, and Maximum Z for the Standard Reference Parameters of Table 1 (Except k_1^{III} a = 60π and b/a = 1.1) with Elastic Solid Boundary Conditions (Using Actual Functions).

Imposed Characteristic	n	ℓ (cm)	C (m/s)	Error (ppm)
Zero phase	3	0.075026	1500.520	346
	15	0.375073	1500.235	157
	30	0.750110	1500.148	99
	150	3.750359	1500.125	83
	300	7.500698	1500.136	90
	450	11.251041	1500.137	91
Max R	3	0.075022	1500.440	293
	15	0.375057	1500.175	117
	30	0.750084	1500.108	72
	150	3.750347	1500.132	88
	300	7.500693	1500.138	92
	450	11.251038	1500.138	92
Max Z	3	0.075016	1500.320	213
	15	0.375042	1500.130	87
	30	0.750063	1500.084	56
	150	3.750333	1500.135	90
	300	7.500692	1500.144	96
	450	11.251037	1500.138	92

Table 43

Apparent Sound Speeds C for Successive Intervals Between Indicated Source-to-Reflector Separations ℓ Corresponding to Half Wavelengths n. The Values of ℓ are Read from Fig. 29e for the Imposed Characteristics of Zero Phase, Maximum R, and Maximum Z for the Standard Reference Parameters of Table 1 (Except $k_1^{III}a = 60\pi$ and $b/a = 2$) with Elastic Solid Boundary Conditions.

Imposed Characteristic	n	ℓ (cm)	C (m/s)	Error (ppm)
Zero phase	3	0.075014	1500.280	186
	15	0.375032	1500.090	60
	30	0.750047	1500.060	40
	150	3.750125	1500.039	26
	300	7.500204	1500.032	21
	450	11.250290	1500.034	23
Max R	3	0.075007	1500.140	93
	15	0.375029	1500.110	73
	30	0.750035	1500.024	16
	150	3.750100	1500.033	22
	300	7.500187	1500.035	23
	450	11.250275	1500.035	23
Max Z	3	0.075012	1500.240	160
	15	0.375032	1500.100	67
	30	0.750033	1500.004	3
	150	3.750080	1500.024	16
	300	7.500171	1500.036	24
	450	11.250260	1500.036	24

Table 44

Apparent Sound Speeds C for Successive Intervals Between Indicated Source-to-Reflector Separations ℓ Corresponding to Half Wavelengths n. The Values of ℓ are Read from Fig. 29f for the Imposed Characteristics of Zero Phase, Maximum R, and Maximum Z for the Standard Reference Parameters of Table 1 (Except $k_1^{III} a = 60\pi$ and $b/a = 5$) with Elastic Solid Boundary Conditions.

Imposed Characteristic	n	ℓ (cm)	C (m/s)	Error (ppm)
Zero phase	3	0.075013	1500.260	173
	15	0.375031	1500.090	60
	30	0.750047	1500.064	43
	150	3.750143	1500.048	32
	300	7.500245	1500.041	27
	450	11.250337	1500.037	25
Max R	3	0.075010	1500.200	133
	15	0.375026	1500.080	53
	30	0.750037	1500.044	29
	150	3.750122	1500.043	28
	300	7.500193	1500.028	19
	450	11.250230	1500.015	10
Max Z	3	0.075005	1500.100	67
	15	0.375018	1500.065	43
	30	0.750030	1500.048	32
	150	3.750103	1500.037	25
	300	7.500153	1500.020	13
	450	11.250163	1500.004	3

Table 45

Apparent Sound Speeds C for Successive Intervals Between Indicated Source-to-Reflector Separations ℓ Corresponding to Half Wavelengths n. The Values of ℓ are Read from Fig. 29g for the Imposed Characteristics of Zero Phase, Maximum R, and Maximum Z for the Standard Reference Parameters of Table 1 (Except $k_1^{III}a = 60\pi$ and b/a = 10) with Elastic Solid Boundary Conditions.

Imposed Characteristic	n	ℓ (cm)	C (m/s)	Error (ppm)
Zero phase	3	0.075013	1500.260	173
	15	0.375031	1500.090	60
	30	0.750047	1500.064	43
	150	3.750143	1500.048	32
	300	7.500244	1500.040	27
	450	11.250331	1500.035	23
Max R	3	0.075010	1500.200	133
	15	0.375027	1500.085	57
	30	0.750037	1500.040	27
	150	3.750122	1500.043	28
	300	7.500196	1500.030	20
	450	11.250252	1500.022	15
Max Z	3	0.075006	1500.120	80
	15	0.375021	1500.075	50
	30	0.750033	1500.048	32
	150	3.750106	1500.037	24
	300	7.500150	1500.018	12
	450	11.250167	1500.007	5

Table 48

Apparent Sound Speeds C for Successive Intervals Between Indicated Source-to-Reflector Separations ℓ Corresponding to Half Wavelengths n. The Values of ℓ are Read from Fig. 30c for the Imposed Characteristics of Zero Phase, Maximum R, and Maximum Z for the Standard Reference Parameters of Table 1 (Except $k_1^v a = 100\pi$ and $b/a = 5$) with Absolutely Rigid Boundary Conditions.

Imposed Characteristic	n	ℓ (cm)	C (m/s)	Error (ppm)
Zero phase	5	0.075006	1500.120	80
	25	0.375015	1500.045	30
	50	0.750021	1500.024	16
	250	3.750058	1500.019	12
	500	7.500099	1500.016	10
	750	11.250135	1500.014	10
Max R	5	0.075004	1500.080	53
	25	0.375011	1500.035	24
	50	0.750018	1500.028	18
	250	3.750049	1500.016	10
	500	7.500085	1500.014	10
	750	11.250109	1500.010	7
Max Z	5	0.075003	1500.060	40
	25	0.375008	1500.025	16
	50	0.750010	1500.008	6
	250	3.750043	1500.016	10
	500	7.500075	1500.013	8
	750	11.250086	1500.004	3

Table 49

Apparent Sound Speeds C for Successive Intervals Between Indicated Source-to-Reflector Separations ℓ Corresponding to Half Wavelengths n. The Values of ℓ are Read from Fig. 30d for the Imposed Characteristics of Zero Phase, Maximum R, and Maximum Z for the Standard Reference Parameters of Table 1 (Except $k_1^v a = 100\pi$ and $b/a = 10$) with Absolutely Rigid Boundary Conditions.

Imposed Characteristic	n	ℓ (cm)	C (m/s)	Error (ppm)
Zero phase	5	0.075006	1500.120	80
	25	0.375014	1500.040	27
	50	0.750021	1500.028	19
	250	3.750058	1500.019	12
	500	7.500099	1500.016	11
	750	11.250135	1500.014	10
Max R	5	0.075003	1500.060	40
	25	0.375010	1500.035	23
	50	0.750018	1500.032	21
	250	3.750050	1500.016	11
	500	7.500085	1500.014	10
	750	11.250109	1500.010	6
Max Z	5	0.075001	1500.002	1
	25	0.375004	1500.015	10
	50	0.750015	1500.044	29
	250	3.750045	1500.015	10
	500	7.500072	1500.011	7
	750	11.250084	1500.005	3

Table 50

Apparent Sound Speeds C for Successive Intervals Between Indicated Source-to-Reflector Separations ℓ Corresponding to Half Wavelengths n. The Values of ℓ are Read from Fig. 31a for the Imposed Characteristics of Zero Phase, Maximum R, and Maximum Z for the Standard Reference Parameters of Table 1 (Except $k_1^v a = 100\pi$ and $b/a = 1$) with Infinitely Flexible Boundary Conditions.

Imposed Characteristic	n	ℓ (cm)	C (m/s)	Error (ppm)
Zero phase	5	0.075012	1500.240	160
	25	0.375030	1500.090	60
	50	0.750044	1500.056	37
	250	3.750123	1500.040	27
	500	7.500226	1500.041	27
	750	11.250344	1500.047	31
Max R	5	0.075010	1500.200	133
	25	0.375021	1500.055	37
	50	0.750038	1500.068	45
	250	3.750105	1500.034	22
	500	7.500219	1500.046	30
	750	11.250330	1500.044	30
Max Z	5	0.075007	1500.140	93
	25	0.375020	1500.065	43
	50	0.750025	1500.020	13
	250	3.750101	1500.038	25
	500	7.500217	1500.046	30
	750	11.250326	1500.043	29

Table 51

Apparent Sound Speeds C for Successive Intervals Between Indicated Source-to-Reflector Separations ℓ Corresponding to Half Wavelengths n. The Values of ℓ are Read from Fig. 31b for the Imposed Characteristics of Zero Phase, Maximum R, and Maximum Z for the Standard Reference Parameters of Table 1 (Except $k_1^y a = 100\pi$ and $b/a = 2$) with Infinitely Flexible Boundary Conditions.

Imposed Characteristic	n	ℓ (cm)	C (m/s)	Error (ppm)
Zero phase	5	0.075006	1500.120	80
	25	0.375015	1500.045	30
	50	0.750021	1500.024	16
	250	3.750058	1500.019	12
	500	7.500087	1500.012	7
	750	11.250108	1500.008	6
Max R	5	0.075002	1500.040	27
	25	0.375011	1500.045	30
	50	0.750016	1500.020	13
	250	3.750056	1500.020	13
	500	7.500065	1500.004	2
	750	11.250088	1500.009	6
Max Z	5	0.075001	1500.020	13
	25	0.375002	1500.005	3
	50	0.750011	1500.036	24
	250	3.750036	1500.013	8
	500	7.500046	1500.004	2
	750	11.250076	1500.012	7

Table 52

Apparent Sound Speeds C for Successive Intervals Between Indicated Source-to-Reflector Separations ℓ Corresponding to Half Wavelengths n. The Values of ℓ are Read from Fig. 31c for the Imposed Characteristics of Zero Phase, Maximum R, and Maximum Z for the Standard Reference Parameters of Table 1 (Except $k_1^V a = 100\pi$ and $b/a = 5$) with Infinitely Flexible Boundary Conditions.

Imposed Characteristic	n	ℓ (cm)	C (m/s)	Error (ppm)
Zero phase	5	0.075006	1500.120	80
	25	0.375015	1500.045	30
	50	0.750021	1500.024	16
	250	3.750058	1500.019	12
	500	7.500099	1500.016	10
	750	11.250136	1500.015	10
Max R	5	0.075003	1500.600	397
	25	0.375010	1500.035	23
	50	0.750018	1500.032	21
	250	3.750050	1500.016	10
	500	7.500083	1500.013	8
	750	11.250110	1500.011	7
Max Z	5	0.075001	1500.020	13
	25	0.375006	1500.025	17
	50	0.750015	1500.036	24
	250	3.750043	1500.014	9
	500	7.500069	1500.010	7
	750	11.250080	1500.004	3

Table 53

Apparent Sound Speeds C for Successive Intervals Between Indicated Source-to-Reflector Separations ℓ Corresponding to Half Wavelengths n. The Values of ℓ are Read from Fig. 31d for the Imposed Characteristics of Zero Phase, Maximum R, and Maximum Z for the Standard Reference Parameters of Table 1 (Except $k_1^v a = 100\pi$ and $b/a = 10$) with Infinitely Flexible Boundary Conditions.

Imposed Characteristic	n	ℓ (cm)	C (m/s)	Error (ppm)
Zero phase	5	0.075006	1500.120	80
	25	0.375016	1500.050	33
	50	0.750021	1500.020	13
	250	3.750058	1500.019	12
	500	7.500089	1500.012	8
	750	11.250136	1500.019	13
Max R	5	0.075003	1500.060	40
	25	0.375009	1500.030	20
	50	0.750018	1500.036	23
	250	3.750049	1500.016	10
	500	7.500086	1500.015	10
	750	11.250110	1500.010	6
Max Z	5	0.075000	1500.000	0
	25	0.375007	1500.035	23
	50	0.750016	1500.036	24
	250	3.750043	1500.014	9
	500	7.500076	1500.013	9
	750	11.250091	1500.006	4

Table 54

Apparent Sound Speeds C for Successive Intervals Between Indicated Source-to-Reflector Separations ℓ Corresponding to Half Wavelengths n. The Values of ℓ are Read from Fig. 32a for the Imposed Characteristics of Zero Phase, Maximum R, and Maximum Z for the Standard Reference Parameters of Table 1 (Except $k_1^v a = 100\pi$ and $b/a = 1$) with Liquid Boundary Conditions.

Imposed Characteristic	n	ℓ (cm)	C (m/s)	Error (ppm)
Zero phase	5	0.075011	1500.220	147
	25	0.375028	1500.085	57
	50	0.750043	1500.060	40
	250	3.750119	1500.038	25
	500	7.500217	1500.039	26
	750	11.250319	1500.041	27
Max R	5	0.075009	1500.180	120
	25	0.375022	1500.065	43
	50	0.750032	1500.040	27
	250	3.750108	1500.038	25
	500	7.500210	1500.042	28
	750	11.250315	1500.042	28
Max Z	5	0.075008	1500.160	107
	25	0.375019	1500.055	37
	50	0.750027	1500.032	21
	250	3.750103	1500.038	25
	500	7.500205	1500.041	27
	750	11.250314	1500.044	29

Table 55

Apparent Sound Speeds C for Successive Intervals Between Indicated Source-to-Reflector Separations ℓ Corresponding to Half Wavelengths n. The Values of ℓ are Read from Fig. 32b for the Imposed Characteristics of Zero Phase, Maximum R, and Maximum Z for the Standard Reference Parameters of Table 1 (Except $k_1^v a = 100\pi$ and $b/a = 2$) with Liquid Boundary Conditions.

Imposed Characteristic	n	ℓ (cm)	C (m/s)	Error (ppm)
Zero phase	5	0.075006	1500.120	80
	25	0.375015	1500.045	30
	50	0.750021	1500.024	16
	250	3.750058	1500.019	12
	500	7.500086	1500.011	8
	750	11.250108	1500.009	6
Max R	5	0.075005	1500.100	67
	25	0.375010	1500.025	16
	50	0.750018	1500.032	22
	250	3.750048	1500.015	10
	500	7.500065	1500.007	5
	750	11.250086	1500.008	6
Max Z	5	0.075002	1500.040	27
	25	0.375007	1500.025	16
	50	0.750011	1500.016	10
	250	3.750040	1500.015	10
	500	7.500055	1500.006	4
	750	11.250071	1500.006	4

Table 56

Apparent Sound Speeds C for Successive Intervals Between Indicated Source-to-Reflector Separations ℓ Corresponding to Half Wavelengths n. The Values of ℓ are Read from Fig. 32c for the Imposed Characteristics of Zero Phase, Maximum R, and Maximum Z for the Standard Reference Parameters of Table 1 (Except $k_1^v a = 100\pi$ and $b/a = 5$) with Liquid Boundary Conditions.

Imposed Characteristic	n	ℓ (cm)	C (m/s)	Error (ppm)
Zero phase	5	0.075006	1500.120	80
	25	0.375014	1500.040	27
	50	0.750021	1500.028	19
	250	3.750059	1500.019	13
	500	7.500099	1500.016	11
	750	11.250135	1500.014	10
Max R	5	0.075005	1500.100	67
	25	0.375010	1500.025	17
	50	0.750016	1500.024	16
	250	3.750050	1500.017	11
	500	7.500084	1500.014	9
	750	11.250111	1500.011	7
Max Z	5	0.075003	1500.060	40
	25	0.375008	1500.025	17
	50	0.750011	1500.012	8
	250	3.750041	1500.015	10
	500	7.500074	1500.013	9
	750	11.250084	1500.004	3

Table 57

Apparent Sound Speeds C for Successive Intervals Between Indicated Source-to-Reflector Separations ℓ Corresponding to Half Wavelengths n. The Values of ℓ are Read from Fig. 32d for the Imposed Characteristics of Zero Phase, Maximum R, and Maximum Z for the Standard Reference Parameters of Table 1 (Except $k_1^v a = 100\pi$ and $b/a = 10$) with Liquid Boundary Conditions.

Imposed Characteristic	n	ℓ (cm)	C (m/s)	Error (ppm)
Zero phase	5	0.075006	1500.120	80
	25	0.375014	1500.040	27
	50	0.750021	1500.028	19
	250	3.750058	1500.019	13
	500	7.500099	1500.016	11
	750	11.250135	1500.014	10
Max R	5	0.075004	1500.080	53
	25	0.375011	1500.035	23
	50	0.750018	1500.028	19
	250	3.750049	1500.016	10
	500	7.500085	1500.014	10
	750	11.250111	1500.010	7
Max Z	5	0.075002	1500.040	27
	25	0.375006	1500.020	13
	50	0.750017	1500.044	29
	250	3.750043	1500.013	9
	500	7.500070	1500.011	7
	750	11.250085	1500.006	4

Table 58

Apparent Sound Speeds C for Successive Intervals Between Indicated Source-to-Reflector Separations ℓ Corresponding to Half Wavelengths n. The Values of ℓ are Read from Fig. 33a for the Imposed Characteristics of Zero Phase, Maximum R, and Maximum Z for the Standard Reference Parameters of Table 1 (Except $k_1^v a = 100\pi$ and $b/a = 1$) with Elastic Solid Boundary Conditions.

Imposed Characteristic	n	ℓ (cm)	C (m/s)	Error (ppm)
Zero phase	5	0.075007	1500.140	93
	25	0.375026	1500.095	63
	50	0.750043	1500.068	45
	250	3.750145	1500.051	34
	500	7.500277	1500.053	35
	750	11.250412	1500.054	36
Max R	5	0.075008	1500.160	107
	25	0.375023	1500.075	50
	50	0.750035	1500.048	32
	250	3.750138	1500.052	34
	500	7.500271	1500.053	35
	750	11.250411	1500.056	37
Max Z	5	0.075015	1500.300	200
	25	0.375020	1500.025	17
	50	0.750033	1500.052	35
	250	3.750135	1500.051	34
	500	7.500268	1500.053	35
	750	11.250409	1500.056	38

Table 59

Apparent Sound Speeds C for Successive Intervals Between Indicated Source-to-Reflector Separations ℓ Corresponding to Half Wavelengths n. The Values of ℓ are Read from Fig. 33b for the Imposed Characteristics of Zero Phase, Maximum R, and Maximum Z for the Standard Reference Parameters of Table 1 (Except $k_1^v a = 100\pi$ and $b/a = 1.1$) with Elastic Solid Boundary Conditions.

Imposed Characteristic	n	ℓ (cm)	C (m/s)	Error (ppm)
Zero phase	5	0.075009	1500.180	120
	25	0.375029	1500.100	67
	50	0.750044	1500.060	40
	250	3.750124	1500.040	27
	500	7.500228	1500.042	28
	750	11.250337	1500.044	29
Max R	5	0.075006	1500.120	80
	25	0.375023	1500.085	57
	50	0.750035	1500.048	32
	250	3.750110	1500.038	25
	500	7.500221	1500.044	30
	750	11.250330	1500.044	29
Max Z	5	0.075005	1500.100	67
	25	0.375020	1500.075	50
	50	0.750030	1500.040	27
	250	3.750104	1500.037	25
	500	7.500220	1500.046	31
	750	11.250325	1500.042	28

Table 60

Apparent Sound Speeds C for Successive Intervals Between Indicated Source-to-Reflector Separations ℓ Corresponding to Half Wavelengths n. The Values of ℓ are Read from Fig. 33c for the Imposed Characteristics of Zero Phase, Maximum R, and Maximum Z for the Standard Reference Parameters of Table 1 (Except $k_1^v a = 100\pi$ and $b/a = 2$) with Elastic Solid Boundary Conditions.

Imposed Characteristic	n	ℓ (cm)	C (m/s)	Error (ppm)
Zero phase	5	0.075006	1500.120	80
	25	0.375015	1500.045	30
	50	0.750021	1500.024	16
	250	3.750056	1500.018	12
	500	7.500084	1500.011	7
	750	11.250110	1500.010	7
Max R	5	0.075003	1500.060	40
	25	0.375011	1500.040	27
	50	0.750018	1500.028	19
	250	3.750043	1500.013	8
	500	7.500069	1500.010	7
	750	11.250094	1500.010	7
Max Z	5	0.075001	1500.020	13
	25	0.375006	1500.025	17
	50	0.750017	1500.044	29
	250	3.750034	1500.009	6
	500	7.500058	1500.010	6
	750	11.250082	1500.010	6

Table 61

Apparent Sound Speeds C for Successive Intervals Between Indicated Source-to-Reflector Separations ℓ Corresponding to Half Wavelengths n. The Values of ℓ are Read from Fig. 33d for the Imposed Characteristics of Zero Phase, Maximum R, and Maximum Z for the Standard Reference Parameters of Table 1 (Except $k_1^v a = 100\pi$ and $b/a = 5$) with Elastic Solid Boundary Conditions.

Imposed Characteristic	n	ℓ (cm)	C (m/s)	Error (ppm)
Zero phase	5	0.075006	1500.120	80
	25	0.375014	1500.040	27
	50	0.750021	1500.028	19
	250	3.750058	1500.019	12
	500	7.500099	1500.016	11
	750	11.250135	1500.014	10
Max R	5	0.075003	1500.060	40
	25	0.375011	1500.040	27
	50	0.750018	1500.028	19
	250	3.750049	1500.016	10
	500	7.500084	1500.014	10
	750	11.250110	1500.010	7
Max Z	5	0.075001	1500.020	13
	25	0.375008	1500.035	23
	50	0.750011	1500.012	8
	250	3.750040	1500.015	10
	500	7.500064	1500.010	7
	750	11.250090	1500.010	7

Table 62

Apparent Sound Speeds C for Successive Intervals Between Indicated Source-to-Reflector Separations ℓ Corresponding to Half Wavelengths n. The Values of ℓ are Read from Fig. 33e for the Imposed Characteristics of Zero Phase, Maximum R, and Maximum Z for the Standard Reference Parameters of Table 1 (Except $k_1^v a = 100\pi$ and $b/a = 10$) with Elastic Solid Boundary Conditions.

Imposed Characteristic	n	ℓ (cm)	C (m/s)	Error (ppm)
Zero phase	5	0.075006	1500.120	80
	25	0.375014	1500.040	27
	50	0.750021	1500.028	19
	250	3.750058	1500.019	12
	500	7.500099	1500.016	10
	750	11.250135	1500.014	9
Max R	5	0.075004	1500.080	53
	25	0.375011	1500.035	23
	50	0.750015	1500.016	10
	250	3.750050	1500.018	12
	500	7.500084	1500.014	9
	750	11.250109	1500.010	7
Max Z	5	0.075003	1500.060	40
	25	0.375008	1500.025	17
	50	0.750010	1500.008	5
	250	3.750043	1500.017	11
	500	7.500069	1500.010	7
	750	11.250093	1500.010	7

Table 63

Apparent Sound Speeds C for Successive Intervals Between Indicated Source-to-Reflector Separations ℓ Corresponding to Half Wavelengths n. The Values of ℓ are Read from Fig. 34a for the Imposed Characteristics of Zero Phase, Maximum R, and Maximum Z for the Standard Reference Parameters of Table 1 (Except $\alpha_1 = 10^{-3}$ cm^{-1} and $\alpha_3 = 10^{-3}$ cm^{-1}) with Absolutely Rigid Boundary Conditions.

Imposed Characteristic	n	ℓ (cm)	C (m/s)	Error (ppm)
Zero phase	1	0.075072	1501.440	959
	5	0.375180	1500.540	360
	10	0.750292	1500.448	298
	50	3.751567	1500.638	425
	100	7.503360	1500.717	478
	150	11.255131	1500.708	472
Max R	1	0.075055	1501.100	733
	5	0.375145	1500.450	300
	10	0.750262	1500.468	312
	50	3.751692	1500.715	476
	100	7.503469	1500.711	473
	150	11.255200	1500.692	461
Max Z	1	0.075027	1500.540	360
	5	0.375118	1500.455	303
	10	0.750231	1500.452	301
	50	3.751800	1500.785	522
	100	7.503600	1500.720	480
	150	11.255365	1500.706	470

Table 64

Apparent Sound Speeds C for Successive Intervals Between Indicated Source-to-Reflector Separations ℓ Corresponding to Half Wavelengths n. The Values of ℓ are Read from Fig. 34b for the Imposed Characteristics of Zero Phase, Maximum R, and Maximum Z for the Standard Reference Parameters of Table 1 (Except $\alpha_1 = 10^{-2}$ cm^{-1} and $\alpha_3 = 10^{-3}$ cm^{-1}) with Absolutely Rigid Boundary Conditions.

Imposed Characteristic	n	ℓ (cm)	C (m/s)	Error (ppm)
Zero phase	1	0.075072	1501.440	959
	5	0.375186	1500.570	380
	10	0.750303	1500.468	312
	50	3.751402	1500.550	366
	100	7.502900	1500.599	399
	150	11.254512	1500.645	429
Max R	1	0.075058	1501.160	773
	5	0.375153	1500.475	316
	10	0.750251	1500.392	261
	50	3.751552	1500.650	433
	100	7.503252	1501.080	719
	150	11.254949	1500.679	452
Max Z	1	0.075029	1500.580	386
	5	0.375114	1500.425	283
	10	0.750224	1500.440	293
	50	3.751653	1500.715	476
	100	7.503408	1500.702	468
	150	11.255244	1500.734	489

Table 65

Apparent Sound Speeds C for Successive Intervals Between Indicated Source-to-Reflector Separations ℓ Corresponding to Half Wavelengths n. The Values of ℓ are Read from Fig. 34c for the Imposed Characteristics of Zero Phase, Maximum R, and Maximum Z for the Standard Reference Parameters of Table 1 (Except $\alpha_1 = 10^{-1}$ cm^{-1} and $\alpha_3 = 10^{-3}$ cm^{-1}) with Absolutely Rigid Boundary Conditions.

Imposed Characteristic	n	ℓ (cm)	C (m/s)	Error (ppm)
Zero phase	1	0.075078	1501.560	1039
	5	0.375242	1500.820	546
	10	0.750424	1500.728	485
	50	3.751697	1500.637	424
	100	7.502837	1500.456	304
	150	11.254657	1500.728	485
Max R	1	0.075060	1501.200	799
	5	0.375188	1500.640	426
	10	0.750342	1500.616	410
	50	3.751454	1500.556	370
	100	7.502641	1500.875	583
	150	11.254246	1500.642	428
Max Z	1	0.075045	1500.900	599
	5	0.375167	1500.610	406
	10	0.750247	1500.320	213
	50	3.751352	1500.553	368
	100	7.502549	1500.479	319
	150	11.254200	1500.660	440

Table 66

Apparent Sound Speeds C for Successive Intervals Between Indicated Source-to-Reflector Separations ℓ Corresponding to Half Wavelengths n. The Values of ℓ are Read from Fig. 34d for the Imposed Characteristics of Zero Phase, Maximum R, and Maximum Z for the Standard Reference Parameters of Table 1 (Except $\alpha_1 = 1\ \mathrm{cm}^{-1}$ and $\alpha_3 = 10^{-3}\ \mathrm{cm}^{-1}$) with Absolutely Rigid Boundary Conditions.

Imposed Characteristic	n	ℓ (cm)	C (m/s)	Error (ppm)
Zero phase	1	0.075163	1503.260	2171
	5	0.375723	1502.800	1865
	10	0.751514	1503.164	2107
	50	*	*	*
	100	*	*	*
	150	*	*	*
Max R	1	0.075050	1501.000	666
	5	0.375350	1501.500	1000
	10	0.750747	1501.588	1058
	50	*	*	*
	100	*	*	*
	150	*	*	*
Max Z	1	0.074948	1498.960	69
	5	0.375149	1501.005	669
	10	0.750456	1501.228	818
	50	*	*	*
	100	*	*	*
	150	*	*	*

*Values unobtainable because of insufficient reaction on acoustic source.

Table 67

Apparent Sound Speeds C for Successive Intervals Between Indicated Source-to-Reflector Separations ℓ Corresponding to Half Wavelengths n. The Values of ℓ are Read from Fig. 35a for the Imposed Characteristics of Zero Phase, Maximum R, and Maximum Z for the Standard Reference Parameters of Table 1 (Except $\alpha_1 = 10^{-3}$ cm^{-1} and $\alpha_3 = 10^{-3}$ cm^{-1}) with Infinitely Flexible Boundary Conditions.

Imposed Characteristic	n	ℓ (cm)	C (m/s)	Error (ppm)
Zero phase	1	0.075072	1501.440	959
	5	0.375181	1500.545	363
	10	0.750289	1500.432	288
	50	3.750786	1500.249	166
	100	7.501449	1500.265	175
	150	11.252109	1500.264	176
Max R	1	0.075057	1501.140	759
	5	0.375148	1500.455	303
	10	0.750234	1500.344	229
	50	3.750692	1500.229	153
	100	7.501387	1500.278	185
	150	11.252053	1500.266	177
Max Z	1	0.075039	1500.780	519
	5	0.375109	1500.350	233
	10	0.750283	1500.696	463
	50	3.750624	1500.170	113
	100	7.501334	1500.284	189
	150	11.252000	1500.266	177

Table 68

Apparent Sound Speeds C for Successive Intervals Between Indicated Source-to-Reflector Separations ℓ Corresponding to Half Wavelengths n. The Values of ℓ are Read from Fig. 35b for the Imposed Characteristics of Zero Phase, Maximum R, and Maximum Z for the Standard Reference Parameters of Table 1 (Except $\alpha_1 = 10^{-2}$ cm^{-1} and $\alpha_3 = 10^{-3}$ cm^{-1}) with Infinitely Flexible Boundary Conditions.

Imposed Characteristic	n	ℓ (cm)	C (m/s)	Error (ppm)
Zero phase	1	0.075073	1501.460	972
	5	0.375187	1500.570	380
	10	0.750307	1500.480	320
	50	3.750983	1500.338	225
	100	7.501.758	1500.310	206
	150	11.252459	1500.280	187
Max R	1	0.075055	1501.100	733
	5	0.375150	1500.475	316
	10	0.750257	1500.428	285
	50	3.750763	1500.253	168
	100	7.501450	1500.275	183
	150	11.252148	1500.279	186
Max Z	1	0.075032	1500.640	426
	5	0.375115	1500.415	276
	10	0.750182	1500.268	178
	50	3.750618	1500.218	145
	100	7.501255	1500.255	170
	150	11.251849	1500.238	158

Table 69

Apparent Sound Speeds C for Successive Intervals Between Indicated Source-to-Reflector Separations ℓ Corresponding to Half Wavelengths n. The Values of ℓ are Read from Fig. 35c for the Imposed Characteristics of Zero Phase, Maximum R, and Maximum Z for the Standard Reference Parameters of Table 1 (Except $\alpha_1 = 10^{-1}$ cm^{-1} and $\alpha_3 = 10^{-3}$ cm^{-1}) with Infinitely Flexible Boundary Conditions.

Imposed Characteristic	n	ℓ (cm)	C (m/s)	Error (ppm)
Zero phase	1	0.075079	1501.580	1052
	5	0.375240	1500.805	536
	10	0.750426	1500.744	496
	50	3.751753	1500.664	442
	100	7.503126	1500.549	366
	150	11.254126	1500.400	266
Max R	1	0.075056	1501.120	746
	5	0.375167	1500.555	370
	10	0.750344	1500.708	472
	50	3.751494	1500.575	383
	100	7.502858	1500.546	363
	150	11.253882	1500.410	273
Max Z	1	0.075031	1500.620	413
	5	0.375112	1500.405	270
	10	0.750252	1500.560	373
	50	3.751337	1500.543	361
	100	7.502762	1500.570	380
	150	11.253850	1500.435	290

Table 70

Apparent Sound Speeds C for Successive Intervals Between Indicated Source-to-Reflector Separations ℓ Corresponding to Half Wavelengths n. The Values of ℓ are Read from Fig. 35d for the Imposed Characteristics of Zero Phase, Maximum R, and Maximum Z for the Standard Reference Parameters of Table 1 (Except $\alpha_1 = 1\,\mathrm{cm}^{-1}$ and $\alpha_3 = 10^{-3}\,\mathrm{cm}^{-1}$) with Infinitely Flexible Boundary Conditions.

Imposed Characteristic	n	ℓ (cm)	C (m/s)	Error (ppm)
Zero phase	1	0.075163	1503.260	2171
	5	0.375725	1502.810	1871
	10	0.751520	1503.180	2118
	50	*	*	*
	100	*	*	*
	150	*	*	*
Max R	1	0.075058	1501.160	773
	5	0.375344	1501.430	952
	10	0.750746	1501.608	1071
	50	*	*	*
	100	*	*	*
	150	*	*	*
Max Z	1	0.074922	1498.440	1039
	5	0.375143	1501.105	736
	10	0.750400	1501.028	685
	50	*	*	*
	100	*	*	*
	150	*	*	*

*Values unobtainable because of insufficient reaction on acoustic source.

Table 71

Apparent Sound Speeds C for Successive Intervals Between Indicated Source-to-Reflector Separations ℓ Corresponding to Half Wavelengths n. The Values of ℓ are Read from Fig. 36a for the Imposed Characteristics of Zero Phase, Maximum R, and Maximum Z for the Standard Reference Parameters of Table 1 (Except $\alpha_1 = 10^{-3}$ cm^{-1} and $\alpha_3 = 10^{-3}$ cm^{-1}) with Liquid Boundary Conditions.

Imposed Characteristic	n	ℓ (cm)	C (m/s)	Error (ppm)
Zero phase	1	0.075071	1501.420	946
	5	0.375182	1500.555	370
	10	0.750293	1500.444	296
	50	3.750755	1500.231	154
	100	7.501201	1500.178	119
	150	11.251906	1500.282	188
Max R	1	0.075055	1501.100	733
	5	0.375147	1500.460	306
	10	0.750245	1500.392	261
	50	3.750627	1500.191	127
	100	7.501125	1500.199	133
	150	11.251851	1500.290	193
Max Z	1	0.075030	1500.600	400
	5	0.375107	1500.385	256
	10	0.750200	1500.372	248
	50	3.750527	1500.164	109
	100	7.501100	1500.229	153
	150	11.251800	1500.280	186

Table 72

Apparent Sound Speeds C for Successive Intervals Between Indicated Source-to-Reflector Separations ℓ Corresponding to Half Wavelengths n. The Values of ℓ are Read from Fig. 36b for the Imposed Characteristics of Zero Phase, Maximum R, and Maximum Z for the Standard Reference Parameters of Table 1 (Except $\alpha_1 = 10^{-2}$ cm^{-1} and $\alpha_3 = 10^{-3}$ cm^{-1}) with Liquid Boundary Conditions.

Imposed Characteristic	n	ℓ (cm)	C (m/s)	Error (ppm)
Zero phase	1	0.075072	1501.440	959
	5	0.375187	1500.575	383
	10	0.750306	1500.476	317
	50	3.751070	1500.382	254
	100	7.501657	1500.235	156
	150	11.252442	1500.314	209
Max R	1	0.075054	1501.080	719
	5	0.375153	1500.495	330
	10	0.750259	1500.424	282
	50	3.750746	1500.244	162
	100	7.501349	1500.241	161
	150	11.251949	1500.240	160
Max Z	1	0.075034	1500.680	453
	5	0.375118	1500.420	280
	10	0.750200	1500.328	218
	50	3.750550	1500.175	117
	100	7.501045	1500.198	132
	150	11.251554	1500.204	136

Table 73

Apparent Sound Speeds C for Successive Intervals Between Indicated Source-to-Reflector Separations ℓ Corresponding to Half Wavelengths n. The Values of ℓ are Read from Fig. 36c for the Imposed Characteristics of Zero Phase, Maximum R, and Maximum Z for the Standard Reference Parameters of Table 1 (Except $\alpha_1 = 10^{-1}$ cm^{-1} and $\alpha_3 = 10^{-3}$ cm^{-1}) with Liquid Boundary Conditions.

Imposed Characteristic	n	ℓ (cm)	C (m/s)	Error (ppm)
Zero phase	1	0.075078	1501.560	1039
	5	0.375241	1500.815	543
	10	0.750423	1500.728	485
	50	3.751689	1500.633	422
	100	7.502791	1500.441	294
	150	11.254268	1500.591	393
Max R	1	0.075062	1501.240	826
	5	0.375175	1500.565	376
	10	0.750343	1500.672	448
	50	3.751459	1500.558	372
	100	7.502635	1500.470	313
	150	11.254257	1500.649	432
Max Z	1	0.075042	1500.840	559
	5	0.375142	1500.500	333
	10	0.750248	1500.424	282
	50	3.751338	1500.545	363
	100	7.502550	1500.485	323
	150	11.254200	1500.660	440

Table 74

Apparent Sound Speeds C for Successive Intervals Between Indicated Source-to-Reflector Separations ℓ Corresponding to Half Wavelengths n. The Values of ℓ are Read from Fig. 36d for the Imposed Characteristics of Zero Phase, Maximum R, and Maximum Z for the Standard Reference Parameters of Table 1 (Except $\alpha_1 = 1\ \mathrm{cm}^{-1}$ and $\alpha_3 = 10^{-3}\ \mathrm{cm}^{-1}$) with Liquid Boundary Conditions.

Imposed Characteristic	n	ℓ (cm)	C (m/s)	Error (ppm)
Zero phase	1	0.075172	1503.440	2291
	5	0.375710	1502.690	1792
	10	0.751498	1503.152	2099
	50	*	*	*
	100	*	*	*
	150	*	*	*
Max R	1	0.075049	1500.980	653
	5	0.375349	1501.500	1000
	10	0.750746	1501.588	1058
	50	*	*	*
	100	*	*	*
	150	*	*	*
Max Z	1	0.074952	1499.040	64
	5	0.375148	1500.980	653
	10	0.750446	1501.192	794
	50	*	*	*
	100	*	*	*
	150	*	*	*

*Values unobtainable because of insufficient reaction on acoustic source.

Table 75

Apparent Sound Speeds C for Successive Intervals Between Indicated Source-to-Reflector Separations ℓ Corresponding to Half Wavelengths n. The Values of ℓ are Read from Fig. 37a for the Imposed Characteristics of Zero Phase, Maximum R, and Maximum Z for the Standard Reference Parameters of Table 1 (Except $\alpha_1 = 10^{-3}$ cm^{-1} and $\alpha_3 = 10^{-3}$ cm^{-1}) with Elastic Solid Boundary Conditions.

Imposed Characteristic	n	ℓ (cm)	C (m/s)	Error (ppm)
Zero phase	1	0.075074	1501.480	986
	5	0.375186	1500.560	373
	10	0.750288	1500.408	272
	50	3.751120	1500.416	277
	100	7.502205	1500.434	289
	150	11.253297	1500.437	291
Max R	1	0.075049	1500.980	653
	5	0.375148	1500.495	330
	10	0.750243	1500.380	253
	50	3.751087	1500.422	281
	100	7.502185	1500.439	293
	150	11.253307	1500.449	299
Max Z	1	0.075034	1500.680	453
	5	0.375132	1500.490	326
	10	0.750225	1500.372	248
	50	3.751077	1500.426	284
	100	7.502176	1500.440	293
	150	11.253327	1500.460	307

Table 76

Apparent Sound Speeds C for Successive Intervals Between Indicated Source-to-Reflector Separations ℓ Corresponding to Half Wavelengths n. The Values of ℓ are Read from Fig. 37b for the Imposed Characteristics of Zero Phase, Maximum R, and Maximum Z for the Standard Reference Parameters of Table 1 (Except $\alpha_1 = 10^{-2}$ cm^{-1} and $\alpha_3 = 10^{-3}$ cm^{-1}) with Elastic Solid Boundary Conditions.

Imposed Characteristic	n	ℓ (cm)	C (m/s)	Error (ppm)
Zero phase	1	0.075076	1501.520	1012
	5	0.375194	1500.590	393
	10	0.750306	1500.448	298
	50	3.751169	1500.432	287
	100	7.502257	1500.435	290
	150	11.253369	1500.445	296
Max R	1	0.075059	1501.180	786
	5	0.375152	1500.465	310
	10	0.750252	1500.400	266
	50	3.751107	1500.428	285
	100	7.502200	1500.437	291
	150	11.253300	1500.440	293
Max Z	1	0.075036	1500.720	480
	5	0.375109	1500.365	243
	10	0.750195	1500.344	229
	50	3.751065	1500.435	290
	100	7.502160	1500.438	292
	150	11.253263	1500.441	294

Table 77

Apparent Sound Speeds C for Successive Intervals Between Indicated Source-to-Reflector Separations ℓ Corresponding to Half Wavelengths n. The Values of ℓ are Read from Fig. 37c for the Imposed Characteristics of Zero Phase, Maximum R, and Maximum Z for the Standard Reference Parameters of Table 1 (Except $\alpha_1 = 10^{-1}$ cm^{-1} and $\alpha_3 = 10^{-3}$ cm^{-1}) with Elastic Solid Boundary Conditions.

Imposed Characteristic	n	ℓ (cm)	C (m/s)	Error (ppm)
Zero phase	1	0.075082	1501.640	1092
	5	0.375253	1500.855	569
	10	0.750439	1500.744	496
	50	3.751771	1500.666	444
	100	7.503018	1500.499	332
	150	11.254784	1500.706	470
Max R	1	0.075048	1500.960	639
	5	0.375196	1500.740	493
	10	0.750359	1500.652	434
	50	3.751532	1500.587	391
	100	7.502749	1500.487	324
	150	11.254346	1500.639	425
Max Z	1	0.075011	1500.220	147
	5	0.375146	1500.675	450
	10	0.750253	1500.428	285
	50	3.751347	1500.547	364
	100	7.502661	1500.526	350
	150	11.254300	1500.656	437

Table 78

Apparent Sound Speeds C for Successive Intervals Between Indicated Source-to-Reflector Separations ℓ Corresponding to Half Wavelengths n. The Values of ℓ are Read from Fig. 37d for the Imposed Characteristics of Zero Phase, Maximum R, and Maximum Z for the Standard Reference Parameters of Table 1 (Except $\alpha_1 = 1\ \mathrm{cm}^{-1}$ and $\alpha_3 = 10^{-3}\ \mathrm{cm}^{-1}$) with Elastic Solid Boundary Conditions.

Imposed Characteristic	n	ℓ (cm)	C (m/s)	Error (ppm)
Zero phase	1	0.075166	1503.320	2211
	5	0.375731	1502.825	1881
	10	0.751491	1503.040	2025
	50	*	*	*
	100	*	*	*
	150	*	*	*
Max R	1	0.075051	1501.020	679
	5	0.375350	1501.495	996
	10	0.750754	1501.616	1076
	50	*	*	*
	100	*	*	*
	150	*	*	*
Max Z	1	0.074949	1498.980	679
	5	0.375152	1501.015	676
	10	0.750445	1501.172	781
	50	*	*	*
	100	*	*	*
	150	*	*	*

*Values unobtainable because of insufficient reaction on acoustic source.

Table 79

Comparison of Apparent Sound Speed Error in Interval Between Source-to-Reflector Separations ℓ of 0.075 cm to 11.25 cm for Various Boundary Conditions, b/a Ratios, and ka Values as Determined by Imposed Characteristic of Zero Phase. All Other Unspecified Parameters are as Given in Table 1. The Distances Correspond to the Interval Between Nominal Half Wavelengths n of 10 to 150 for $k_1^I a = 20\pi$, 30 to 450 for $k_1^{III} a = 60\pi$, and 50 to 750 for $k_1^V a = 100\pi$, That is, No Closer Than 10 $(\lambda_1/2)$.

Boundary Condition	b/a	20π	60π	100π
RIGID	1	0	0	0
	1.1	3	1	1
	2	463	45	14
	5	231	24	11
	10	205	27	11
FLEXIBLE	1	726	78	28
	2	171	20	8
	5	158	22	11
	10	194	28	11
LIQUID	1 (Orth.)	580	72	26
	1 (Act.)	580	88	-
	2 (Orth.)	151	10	9
	2 (Act.)	151	-	-
	5	154	28	11
	10	199	27	11
ELASTIC	1 (Orth.)	1440	116	35
	1 (Act.)	1441	113	-
	1.1 (Orth.)	1152	88	28
	1.1 (Act.)	1152	88	-
	2 (Orth.)	286	23	9
	2 (Act.)	286	-	-
	5	181	28	11
	10	192	27	11
	20	194	-	-
	50	234	-	-

Table 80

Comparison of Apparent Sound Speed Error in Interval Between Source-to-Reflector Separations ℓ of 0.75 cm to 11.25 cm for Various Boundary Conditions, b/a Ratios, and ka values as Determined by Imposed Characteristics of Maximum R. All Other Unspecified Parameters are as Given in Table 1. The Distances Correspond to the Interval Between Nominal Half Wavelengths n of 10 to 150 for $k_1^I a = 20\pi$, 30 to 450 for $k_1^{III} a = 60\pi$, and 50 to 750 for $k_1^V a = 100\pi$, That is, No Closer Than 10 $(\lambda_1/2)$.

Boundary Condition	b/a	20π	60π	100π
RIGID	1	0	0	0
	1.1	0	0	0
	2	473	50	14
	5	238	24	9
	10	114	21	9
FLEXIBLE	1	732	80	27
	2	173	19	7
	5	140	18	8
	10	91	21	9
LIQUID	1 (Orth.)	583	74	27
	1 (Act.)	585	91	-
	2 (Orth.)	151	8	7
	2 (Act.)	150	-	-
	5	132	21	9
	10	97	21	9
ELASTIC	1 (Orth.)	1442	117	35
	1 (Act.)	1441	114	-
	1.1 (Orth.)	1162	90	28
	1.1 (Act.)	1160	91	-
	2 (Orth.)	290	23	7
	2 (Act.)	290	-	-
	5	174	21	9
	10	180	25	9
	20	112	-	-
	50	90	-	-

Table 81

Comparison of Apparent Sound Speed Error in Interval Between Source-to-Reflector Separations ℓ of 0.75 cm to 11.25 cm for Various Boundary Conditions, b/a Ratios, and ka Values as Determined by Imposed Characteristic of Maximum Z. All Other Unspecified Parameters are as Given in Table 1. The Distances Correspond to the Interval Between Nominal Half Wavelengths n of 10 to 150 for $k_1^I a = 20\pi$, 30 to 450 for $k_1^{III} a = 60\pi$, and 50 to 750 for $k_1^V a = 100\pi$, That is, No Closer Than 10 $(\lambda_1/2)$.

Boundary Condition	b/a	20π	60π	100π
RIGID	1	0	0	0
	1.1	1	0	0
	2	486	53	18
	5	88	23	7
	10	37	19	7
FLEXIBLE	1	735	82	28
	2	173	18	6
	5	134	10	6
	10	42	15	7
LIQUID	1 (orth.)	589	75	27
	1 (Act.)	589	93	-
	2 (Orth.)	151	7	6
	2 (Act.)	152	-	-
	5	127	15	7
	10	39	15	7
ELASTIC	1 (Orth.)	1445	118	36
	1 (Act.)	1441	115	-
	1.1 (Orth.)	1169	92	31
	1.1 (Act.)	1171	93	-
	2 (Orth.)	294	21	6
	2 (Act.)	293	-	-
	5	169	15	7
	10	47	15	7
	20	58	-	-
	50	37	-	-

Table 82

Comparison of Apparent Sound Speed Error in Interval Between Source-to-Reflector Separations ℓ of 0.75 cm to 11.25 cm for Various Boundary Conditions, Liquid Cylinder Medium Absorption Coefficients, and ka Values as Determined by Imposed Characteristics of Zero Phase, Maximum R, and Maximum Z. All Other Unspecified Parameters are as Given in Table 1. The Distances Correspond to the Interval Between Nominal Half Wavelengths n of 10 to 150 for $k_1^I a = 20\pi$, 30 to 450 for $k_1^{III} a = 60\pi$, and 50 to 750 for $k_1^V a = 100\pi$, That is, No Closer Than 10 $(\lambda_1/2)$.

Boundary Condition	b/a (or α_1)	20π (or Zero Phase)	60π (or Max R)	100π (or Max Z)
RIGID	0	463	473	486
	10^{-3}	458	470	491
	10^{-2}	398	535	478
	10^{-1}	404	460	376
FLEXIBLE	0	171	173	173
	10^{-3}	172	172	160
	10^{-2}	206	179	158
	10^{-1}	358	340	344
LIQUID	0	151	151	151
	10^{-3}	154	151	149
	10^{-2}	206	161	128
	10^{-1}	370	372	375
ELASTIC	0	286	290	294
	10^{-3}	286	291	295
	10^{-2}	291	290	292
	10^{-1}	415	380	384

Unclassified
Security Classification

DOCUMENT CONTROL DATA - R&D

(Security classification of title, body of abstract and indexing annotation must be entered when the overall report is classified)

1. ORIGINATING ACTIVITY *(Corporate author)* U.S. NAVAL RESEARCH LABORATORY Washington, D.C. 20390	2a. REPORT SECURITY CLASSIFICATION Unclassified 2b. GROUP —

3. REPORT TITLE
SYSTEMATIC ERRORS IN ULTRASONIC PROPAGATION PARAMETER MEASUREMENTS
Part 3 – Sound Speed by Iterative Reflection – Interferometry

4. DESCRIPTIVE NOTES *(Type of report and inclusive dates)*
An interim report on one phase of the problem.

5. AUTHOR(S) *(Last name, first name, initial)*
Del Grosso, V. A.

6. REPORT DATE	7a. TOTAL NO. OF PAGES	7b. NO. OF REFS
August 9, 1966	246	4

8a. CONTRACT OR GRANT NO. NRL Problem S01-02 b. PROJECT NO. RF 101-03-45-5251 c. d.	9a. ORIGINATOR'S REPORT NUMBER(S) NRL Report 6409 9b. OTHER REPORT NO(S) *(Any other numbers that may be assigned this report)* None

10. AVAILABILITY/LIMITATION NOTICES
Distribution of this document is unlimited. Copies available from the Clearinghouse for Scientific and Technical Information (CFSTI), Springfield, Va. 22151.

11. SUPPLEMENTARY NOTES	12. SPONSORING MILITARY ACTIVITY
None	Department of the Navy (Office of Naval Research)

13. ABSTRACT

This report shows that, although the free-field diffraction and guided mode dispersion errors detailed in Parts 1 and 2 of this series do carry over to the case of iterative reflection (accomplished by adding a termination to the liquid cylinder), the errors for a given geometrical configuration are smaller for interferometry than for nonterminated or pulsing situations. Indeed, the approach with improved parameters is toward plane wave results for interferometry rather than toward free-field results as is the case for pulsing.

Other advantages accruing to interferometry are (a) the use of differential instead of total, acoustic paths, (b) the simplified determination of these paths by the use of parallel source and reflector, (c) the simple measurement of frequency rather than small time intervals, and (d) the suitability of the method for determinations of chemical concentration (salinity) and pressure coefficients, as well as the temperature coefficient.

This report includes many impedance circle plots as well as the more usual reaction plots for ultrasonic interferometers with walls that are either infinitely flexible, absolutely rigid, liquid, or elastic. Various parameters including tube size, source size, source-to-reflector separation, frequency, and attenuation coefficients are included along with several imposed characteristics. The plot readings, and apparent sound speeds calculated from them, are tabulated. Errors may be as large as a few percent or as small as 6 parts per million (0.01 m/s).

DD FORM 1 JAN 64 1473

Unclassified
Security Classification

14. KEY WORDS	LINK A ROLE	LINK A WT	LINK B ROLE	LINK B WT	LINK C ROLE	LINK C WT
Velocity						
Sound Signals						
Ultrasonic Radiation						
Propagation						
Attenuation						
Liquid Cylinder						
Parameter Measurements						
Errors						
Reflection						
Interferometers						
Plane Waves						
Acoustics						
Boundary Conditions – Theory						
Liquid Boundary						
Elastic Solid Boundary						
Infinitely Flexible Boundary						
Absolutely Rigid Boundary						

INSTRUCTIONS

1. ORIGINATING ACTIVITY: Enter the name and address of the contractor, subcontractor, grantee, Department of Defense activity or other organization *(corporate author)* issuing the report.

2*a*. REPORT SECURITY CLASSIFICATION: Enter the overall security classification of the report. Indicate whether "Restricted Data" is included. Marking is to be in accordance with appropriate security regulations.

2*b*. GROUP: Automatic downgrading is specified in DoD Directive 5200.10 and Armed Forces Industrial Manual. Enter the group number. Also, when applicable, show that optional markings have been used for Group 3 and Group 4 as authorized.

3. REPORT TITLE: Enter the complete report title in all capital letters. Titles in all cases should be unclassified. If a meaningful title cannot be selected without classification, show title classification in all capitals in parenthesis immediately following the title.

4. DESCRIPTIVE NOTES: If appropriate, enter the type of report, e.g., interim, progress, summary, annual, or final. Give the inclusive dates when a specific reporting period is covered.

5. AUTHOR(S): Enter the name(s) of author(s) as shown on or in the report. Enter last name, first name, middle initial. If military, show rank and branch of service. The name of the principal author is an absolute minimum requirement.

6. REPORT DATE: Enter the date of the report as day, month, year; or month, year. If more than one date appears on the report, use date of publication.

7*a*. TOTAL NUMBER OF PAGES: The total page count should follow normal pagination procedures, i.e., enter the number of pages containing information.

7*b*. NUMBER OF REFERENCES: Enter the total number of references cited in the report.

8*a*. CONTRACT OR GRANT NUMBER: If appropriate, enter the applicable number of the contract or grant under which the report was written.

8*b*, 8*c*, & 8*d*. PROJECT NUMBER: Enter the appropriate military department identification, such as project number, subproject number, system numbers, task number, etc.

9*a*. ORIGINATOR'S REPORT NUMBER(S): Enter the official report number by which the document will be identified and controlled by the originating activity. This number must be unique to this report.

9*b*. OTHER REPORT NUMBER(S): If the report has been assigned any other report numbers *(either by the originator or by the sponsor)*, also enter this number(s).

10. AVAILABILITY/LIMITATION NOTICES: Enter any limitations on further dissemination of the report, other than those imposed by security classification, using standard statements such as:

(1) "Qualified requesters may obtain copies of this report from DDC."

(2) "Foreign announcement and dissemination of this report by DDC is not authorized."

(3) "U. S. Government agencies may obtain copies of this report directly from DDC. Other qualified DDC users shall request through _____."

(4) "U. S. military agencies may obtain copies of this report directly from DDC. Other qualified users shall request through _____."

(5) "All distribution of this report is controlled. Qualified DDC users shall request through _____."

If the report has been furnished to the Office of Technical Services, Department of Commerce, for sale to the public, indicate this fact and enter the price, if known.

11. SUPPLEMENTARY NOTES: Use for additional explanatory notes.

12. SPONSORING MILITARY ACTIVITY: Enter the name of the departmental project office or laboratory sponsoring *(paying for)* the research and development. Include address.

13. ABSTRACT: Enter an abstract giving a brief and factual summary of the document indicative of the report, even though it may also appear elsewhere in the body of the technical report. If additional space is required, a continuation sheet shall be attached.

It is highly desirable that the abstract of classified reports be unclassified. Each paragraph of the abstract shall end with an indication of the military security classification of the information in the paragraph, represented as *(TS)*, *(S)*, *(C)*, or *(U)*.

There is no limitation on the length of the abstract. However, the suggested length is from 150 to 225 words.

14. KEY WORDS: Key words are technically meaningful terms or short phrases that characterize a report and may be used as index entries for cataloging the report. Key words must be selected so that no security classification is required. Identifiers, such as equipment model designation, trade name, military project code name, geographic location, may be used as key words but will be followed by an indication of technical context. The assignment of links, roles, and weights is optional.